Durham E-Theses

The study of filled rubber composites with rheology and neutron scattering

HART, JAMES,MICHAEL

The study of filled rubber composites with rheology and neutron scattering

James Michael Hart

St. John's College
Department of Chemistry
University of Durham

APRIL 2017

Thesis submitted to Durham University in partial fulfilment of the regulations for the Degree of Doctor of Philosophy.

Declaration

The work reported in this thesis was conducted in the Department of Chemistry at Durham University, at Rutherford Appleton Laboratories, and the Institut Laue-Langevin between October 2013 and December 2016. The work has not been submitted for any other degree in Durham or elsewhere, and unless otherwise stated is the original work of the author.

Data Availability Statement

The data present in this work is open access, and available through the Durham University Collections, doi:10.15128/r1hx11xf24k

Statement of Copyright

Financial Support

Abstract

Polymer nanocomposites represent a growing and important field from academic, environmental, and commercial viewpoints. Filled rubber composites of car tyres are a prime example, as improvement of the material properties and reduction in the carbon footprint are both of interest. However, even with continued research into this subject, questions remain concerning the causes of the observed properties of these composites, namely the non-linear reinforcement and the presence of significant strain softening.

This report documents the examination of polybutadiene rubber composites with multiple techniques to characterise and determine the cause of the non-linear phenomena. The macroscopic material properties were characterised with rheological measurements, while the nanoscale composite structure and polymer dynamics were examined with small angle neutron scattering and quasi-elastic neutron scattering, respectively. Different filler compounds, carbon black, precipitated silica, and Stöber silica, were utilized to provide additional data to build an improved picture of the composite systems. A hydroxyl end functionalised polybutadiene chain known to segregate to silica substrates was used for examination of polymer interfacial dynamics and changes to composite material properties when used as an additive.

Reinforcement of the rubber with the addition of all the fillers was noted and analysed to determine the causes. A significant observation was the change in the mechanical properties of the silica filler composite with the presence of the end functionalised polybutadiene; decreased reinforcement and changes to behaviour under significant strains were noted. Changes to the nanoscale correlations of the silica filler with the presence of the end functionalised polybutadiene was observed with small angle neutron scattering, and determined to be from steric stabilisation of the silica particles. Hindered polymer dynamics near the silica filler surface were noted with quasi elastic neutron scattering. Neither the particle correlations nor the polymer dynamics were found to shift with the application of strain to the composite samples, in contrast to the alterations noted in the mechanical properties.

From the information gathered on the composite microscopic and macroscopic properties a model for the composite behaviour was devised. The reinforcement of the rubber with the addition of filler material was determined to be a result of the networking of the filler particles. The strain softening was found to be caused by the breakages of filler bridging contacts and thus involved only a small fraction of the total material.

Acknowledgements

1 Contents

1.1 Table of contents

1.2 List of terms and abbreviations

DLA	Diffusion limited aggregation
DSC	Differential Scanning Calorimetry
DLS	Dynamic Light Scattering
FCC	Face centred cubic crystal
G'	Storage Modulus
G"	Loss Modulus
IN16B	ILL neutron facility inelastic scattering instrument
IRIS	ISIS neutron facility inelastic scattering instrument
KWW	Kohlrausch Williams Watts stretched exponential function
LOQ	ISIS neutron facility small angle scattering instrument
OFFSPEC	ISIS neutron facility spin echo instrument
4OHPBd	End functional polybutadiene
PBd	Polybutadiene
QENS	Quasi-Elastic Neutron Scattering
RLA	Reaction limited aggregation
SANS	Small Angle Neutron Scattering
SANS2D	ISIS neutron facility small angle scattering instrument
SLD	Neutron scattering length density
TEM	Transmission Electron Microscopy
T_g	Glass transition temperature
VFT	Vogel-Fulcher-Tammann equation
WLF	William-Landel-Ferry equation
A	KWW background term
β	KWW stretching exponent
τ	KWW decay constant
T_0	Vogel-Fulcher-Tammann reference temperature
τ_0	Vogel-Fulcher-Tammann reference time
φ	Volume fraction

η	Viscosity
$[\eta]$	Intrinsic viscosity
B	Mooney and Krieger relation numerical factor
C	Damping constant
U	Potential energy
$B(t)$	Brownian motion term
$G(t)$	Autocorrelation function
γ	Strain
σ	Stress
ω	Radial frequency
δ	Phase shift

1.3 List of Figures

1.4 List of Tables

2 Introduction and literature review

Used for millennia by Mesoamerican peoples, rubber was discovered and utilised by Europeans during the eighteenth century.[1] The development of vulcanisation in 1845 resulted in the growth and development of rubbers as a structural material for both its sealant and elastic properties. The use of rubber for car tyres occurred early in its development with no record of its first use, and the concept of rubber tyres predates the automobile. Similarly, the first addition of solid filler materials, such as carbon black, to strengthen the rubber is not known, however by World War II most tyre rubbers were filled rubber composites and early investigations into the properties occurred at this time.[2] Developments have continued since then, and during the 1990s clay and silica additives were examined for use in such composites while more recent advances involve nanomaterials such as graphene.[3, 4]

With over a billion tyres produced annually, the filled rubber composites used in car tyres are of both commercial and environmental relevance. A tyre's mechanical properties determine its handling and lifetime, and a significant proportion of its carbon foot print is from energy losses during use.[5] As such, these composite systems have been the study of research since the 1940s, and there is a significant pool of literature regarding this subject; however no definitive conclusions have been reached to fully describe and predict composite properties.[4] The complexity of the composites and the associated phenomena are a factor. The two most noteworthy of these phenomena are the reinforcement of the composite to a greater extent than predicted by hydrodynamic theories, and the weakening of the composite modulus when subjected to strains above 0.1%, commonly known as the Payne effect.[2, 6, 7] Disagreement about the causes of these phenomena is common, and no theory put forward has been considered fully acceptable to describe them. This work aims to characterise the properties and illuminate the causes for the observed phenomena by combining rheological studies and neutron scattering. The rheology tests will provide information on the macroscopic behaviour of these filled rubber composites, while the neutron scattering yields information on the nanoscale filler structure and polymer dynamics, both of which are thought to be important.[4]

The report is divided as follows, first an introduction to the concepts and theories of filled rubber composites will be provided, followed by a description of the materials and methods. Then the investigation into linear rheological behaviour of a selection of carbon black and silica polybutadiene composites to determine trends in the reinforcement will be described. The next section will cover the non-linear strain softening behaviour of the same composites, and analyse the results. Following, the small angle neutron scattering on silica composites and the analysis of

the data to determine the filler structure is detailed. The next chapter covers the quasi-elastic neutron scattering work undertaken to examine the polymer dynamics near the filler particles. Finally, the conclusions and data from the previous results will be combined and discussed, and a model for the nature of filled rubber reinforcement and the Payne effect shall be put forward.

The section that follows covers the concepts and theories that are important to the study of polymer composites. Models for polymer and suspensions of particles will be covered as these provide the foundation of understanding the composite systems. Next theories and models for describing composite behaviour are described as well as literature that supports or refutes these models. Where possible, a discussion of the shortcomings of the models will be provided.

2.1 Polymer dynamics

2.1.1 Rouse dynamics

To understand the effect that the filler particles have on the polymer system at both the microscopic and macroscopic level, the unmodified polymer must first be understood and modelled. One of the earliest attempts to define molecular polymer movement was made by Rouse. [8] He proposed that the polymer chain is modelled as a string of beads connected by springs, see Figure 2.1, and this chain is then allowed to oscillate and move in the solvent medium.
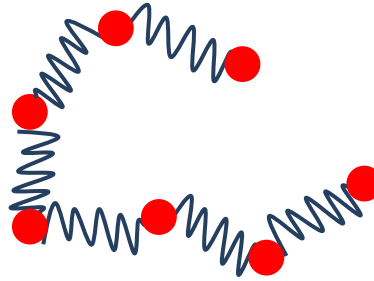
Figure 2.1: Visual image of a Rouse model polymer chain

The movement of the beads is often modelled by the Langevin equation of motion to simulate the viscous solvent medium that the polymer chain is immersed in. This model includes a friction and a Brownian motion term due to the damping and random collisions from the solvent, respectively. [9] The equation for the motion of a bead in this system is

$$m\frac{d^2x}{dt^2} = -C\frac{dx}{dt} + \frac{-\partial U}{\partial x} + B(t) \tag{2.1}$$

where C is the damping constant, m is the bead mass, U is the potential energy of the springs, $g(t)$ is the Brownian motion term. Each bead feels a combined potential from its two attached springs and moves accordingly. The motion of the polymer chain from this method can be

written as a set of harmonic oscillations over the entire chain and general diffusion properties can be predicted.

The Rouse model does not provide accurate predictions for dilute polymer systems due to several overlooked phenomena. The first is excluded volume, since the beads in the Rouse model only feel the potential from the two springs it is possible for the chain to pass through itself, a physical impossibility. Secondly there is the issue of hydrodynamic solvent effects, in real solutions the motion of the polymer chain causes solvent motions leading to additional interactions in the chain, this is lacking in the Rouse model. Thirdly, the conformation of the chain itself is unphysical; the springs are allowed to adopt any 'bond' angle, while in a real system the bond angles are strictly controlled by the molecular structure.

However, the Rouse model is still a useful picture of polymer motion, and is one of the easiest in terms of calculations to implement. Also, it surprisingly predicts correct properties for polymer melts due to the effects of the melt structure cancelling the hydrodynamic effects and allowing for treatment as a solvent.[10, 11] This has allowed its use as the basis for theories of microscopic polymer motion in melts.

2.1.2 Reptation theory

The microscopic nature of a melt is an amorphous polymer network with entanglements and crosslinks that limit motion, something that is unaccounted for in the Rouse model. Therefore a new model is needed to suit the system, the most successful model was first proposed by de Gennes, and is known as reptation theory [12]. The principle method of this is to confine the polymer in a space defined by the surrounding network, normally a tube-like structure, as shown in figure 2.2.

Figure 2.2: Visual of reptation model, polymer chain (red) trapped in a reptation tube (black)

The polymer chain is free to move via the Rouse dynamics but cannot go beyond the sides of the tube; however, the chain is allowed to exit the ends of the tube. When this happens the now vacant segment of the original tube 'vanishes' and a new segment is formed, it is this 'creeping' of the tube that gives the theory its name. Over time the original tube structure will disappear entirely and a new structure will form. Reptation theory has proven to be very useful in the study

of polymer systems and coupled with Rouse motion can explain observed shifts in polymer diffusion rates. [9]
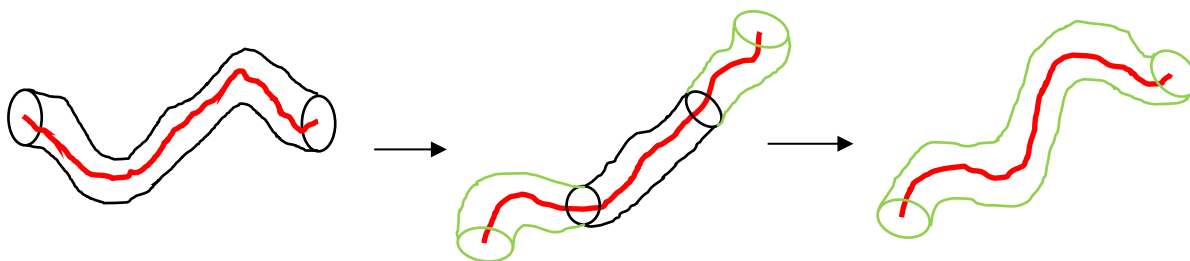
Figure 2.3: Loss of original tube structure with time new tube is in green, left to right

As stated, the combination of Rouse chain motion and reptation theory has proven useful for understanding polymer systems. One of the predictions of this combined approach is several different movement timescales and related relaxation times. At short timescales the polymer chain moves and diffuses via Rouse dynamics unimpeded, as it has not made contact with the reptation barriers. The chain will eventually 'feel' the tube and become confined; however the polymer chain will continue to move via Rouse dynamics inside the tube. Eventually at longer timescales, the fluctuations of the segments will become minimal and the chain will move as a whole, this is known the Rouse relaxation time. However the chain is still confined in the tube and reptation still occurs. Finally as the polymer diffuses out of its initial tube, the reptation process is replaced by standard Fickian diffusion models. These times have importance in the measurement of polymer systems as different analysis methods will probe different timescales. [9]

2.1.3 Glasses and the glass transition

A determining factor of polymer properties is whether the system is in a glass or melt state, as the difference in the behaviour is significant. Firstly it is necessary to define a glass, as an amorphous solid that exhibits a glass transition. Although many polymers can form glasses not all do, and not all glasses are polymeric.

Unlike the standard phase transitions the glass transition is a second order process, and lacks the first order discontinuities in properties such as heat capacity and thermal expansion. Another notable feature is that the properties of the transition depend on the timescale of the measurement used. An easy demonstration of this is through differential scanning calorimetry, where different cooling rates result in different measured glass transition temperatures. [13] These observations have led to discussion and theories on if a glass is a true phase of matter or a kinetically meta-stable state, however as this question is not the primary focus of the work it shall not be covered in detail here. [14]

Theoretically, glass formation has been linked to a decrease in the free volume available to the molecules resulting in reduced conformational changes and segmental relaxation. For the main chain motions, this involves the cooperative motion of several atoms or chain units and is commonly referred to as the α-process or relaxation. This cooperative motion yields a non-Arrhenius temperature dependence for the characteristic timescale of the relaxation, and is commonly modelled by the Vogel-Fulcher-Tammann (VFT) relation, which is

$$\tau = \tau_0 e^{\left(\frac{-H}{T-T_0}\right)} \tag{2.2}$$

where τ is a characteristic time, τ_0 is a reference time, H is a scaling term, and T_0 is a reference temperature. While this relation is stated in terms of timescales it can be used to describe other characteristics in glass forming polymer, in fact it was originally stated in terms of viscosity. This is unsurprising as the α-relaxation is part of the microscopic behaviour that yields macroscopic properties. [15]

By convention, the glass transition temperature is taken as the point where the α-relaxation characteristic timescale reaches 100 seconds in methods like dielectric spectroscopy. [16] It is important to note that the quasi-elastic neutron scattering method used in this study does not measure in this range, instead examining picosecond dynamics. However, work by Zorn *et al.* correlated a fast and slow picosecond timescale polymer dynamics with the β and α-relaxation processes, respectively. [17, 18] From a conceptual viewpoint this is a measurement of the atomic motions that compose the segmental relaxation present above the glass transition. This connection allows a relationship between hindered dynamics and glassy behaviour to be suggested, although it does not provide direct proof. [19]

2.2 Basic composite concepts

2.2.1 Composite hydrodynamic theory

A starting point for understanding reinforcement in polymer systems is the theoretical calculations determining the viscosity of hard sphere suspensions. Although the deviation from these trends in a defining property of the composites, understanding these relations and why they fail is required to make progress in the study of filled rubbers.

The first published relation, Einstein's hard sphere model, only factors in the steric hindrance of the particles on the solution, or in the case of a composite the polymer matrix,

$$G = G_0[1 + 2.5\varphi] \tag{2.3}$$

where G is the material modulus, G_0 is the neat polymer modulus and φ is the volume fraction.[20] From this, extensions have been introduced to account for other interactions in the system. An example is the theory put forth by Guth to describe the reinforcement of carbon black composites via an extension of the Einstein spheres model to include a bound polymer surface layer.[2] Taking the same form as a Virial expansion, the modulus as a function of volume fraction is calculated as

$$G = G_0[1 + 2.5\varphi + 14.1\varphi^2] \tag{2.4}$$

where G_0 is the neat polymer modulus and φ is the volume fraction. This relation was found to hold only below 0.1 volume fraction of carbon black by Guth; who theorised that the formation of particle networks lead to the observed deviation.[2] Other trends to describe the reinforcement of suspensions and composites have been made; Mooney *et al*. derived an exponential function as follows,

$$\eta_r = exp\left(\frac{B\varphi_c}{1 - \frac{\varphi}{\varphi_c}}\right) \tag{2.5}$$

where η_r is the reduced viscosity, B is a numerical factor, φ is the volume fraction of the particles, and φ_c is the maximum obtainable or critical volume fraction.[21] Work by Krieger and Dougherty determined a theoretical relation as,

$$\eta_r = \left(1 - \frac{\varphi}{\varphi_c}\right)^{-B\varphi_c} \tag{2.6}$$

with the same term definitions as for Mooney's relation, equation 2.5. [22, 23] Of importance to both equations is B, which is equivalent to the intrinsic viscosity, $[\eta]$, or the first order coefficient in the viscosity viral relation. Krieger's relation is considered the more theoretically sound, as Mooney's relation deviates to give a combined volume greater than 1 at high filler content. Both equations are empirical, unlike Guth's, and can be fitted to experimental data, though the parameters can also be held at theoretically predicted values. Both relations are defined in terms of viscosity, however the complex viscosity is related to the oscillatory moduli of a material via the oscillation frequency, as

$$\eta' = \frac{G''}{\omega} \qquad \eta'' = \frac{G'}{\omega} \tag{2.7}$$

where ω is the frequency, G' is the storage modulus, G" is the loss modulus, η' is the dynamic viscosity, and η'' is the out of phase viscosity. Through this relation the equations listed above can be used in terms of modulus assuming the frequency is the same.

These equations will be used to examine the rheological reinforcement of a selection of composites in chapter 4. All the models referenced here only hold in semi-dilute regime, once particle contact becomes probable other models have to be employed to examine the rheological properties in the concentrated particle regime. These will be discussed later as part of the composite filler networking section, 2.3.3.

2.2.2 Fractal structure

The behaviour of selected fillers in both dilute and concentrated regime is related in part to the particle structure, deviations from ideal spherical particles result in changes to both the intrinsic viscosity and percolation threshold. [24] As the threshold is the boundary of the concentrated composite behaviour and the intrinsic viscosity factor describes the sample behaviour before this point, understanding the filler structure over different size ranges is important. Both carbon black and precipitated silica are known to have fractally structured primary aggregates and particles, and at greater length scales correlations and aggregation are common with all filler particle types baring repulsive long range interactions.

As a mathematical concept, a fractal is a set which displays self-similarity at every length scale, and is notable for its non-integer scaling properties. Scaling refers to the relation between an object's measured dimensions and properties. In the case of a cube, a three dimensional object, doubling the length of the sides will increase the volume by eight times, so volume scales with length raised to the third. With fractals this scaling is referred to as the fractal dimension, is often a non-integer and different from the topological dimension. An example is the theoretical ideal Gaussian chain used in Debye scattering equations, while the chain is present in three dimensions its pathway results in a fractal dimension of two. Thus increases to the molecular weight or chain length result in the radius of gyration 'volume' increasing to the power 1/2 rather than 1/3, and the chain scatters like a two dimensional surface. It should be noted that for all physical systems; fractal scaling only holds over and can vary within a range of length-scales, with the constituent parts being the lower limit.

Fractal structures of aggregated particles are common in colloidal systems, including polymer composites, and are categorized into two types, diffusion limited and reaction limited. Diffusion limited aggregation (DLA) structures are formed when particle contact results in immediate permanent bonds between the particles, these structures are open and have a fractal dimension of approximately 1.8. Reaction limited aggregation (RLA) results in more compact structures and is caused when particle binding is not immediate or there is an energy barrier present, such aggregates have a fractal dimension of approximately 2.3. These structural formations of the

filler particles are important as theories, like cluster-cluster aggregation, relate the filler fractal dimensions to the measured reinforcement of the polymer matrix.[25]

2.2.3 Percolation of filler particles

Percolation is defined by long range connectivity in a system; with the case of particles in a matrix, networking percolation between the particles results in a continuous pathway of particles that can be 'drawn' through the composite material. The concentration of particles necessary to achieve this is dependent on the particle shape, with anisotropic forms requiring lower concentrations. For hard spheres this value has been calculated as 0.28 volume fraction by computer modelling.[26]

The concept of percolation is related to theories regarding filler networking as the source of the improved reinforcement and other properties such as conductivity, as a network of filler particles is able to support stresses or currents applied to the material. Work with carbon black has found that the point of increased conductivity onset changed with filler type and size, highlighting the importance of particle shape in these systems.[27-31]

2.3 Composite mechanisms and phenomena

Scientific investigations of polymer composites have been ongoing since the 1940s, with initial work examining the greater than predicted reinforcement with filler content observed in these systems.[2] Later in the 1960s, Payne documented the oscillatory strain softening effect that bears his name and hypothesised the cause as a breakdown of the filler network structure.[6, 7] Since then, more theories have been put forward to explain the observed phenomena; the non-linear reinforcement, oscillatory strain softening as the Payne effect, and large strain hysteresis as the Mullins effect. Given the quantity of publications on rubber composites, this section is intended as a brief overview to highlight common trends and theories.[4]

2.3.1 Reinforcement and strain softening

The reinforcement of polymer matrices with filler particles is known to have several properties, the primary of which is the deviation toward greater reinforcement from the predictions of standard hydrodynamic theories for suspended hard particles in a fluid. Literature has often reported the degree of reinforcement follows a power relation with the filler content, and the reinforcement appears to be universal across polymer composite systems. Some differences in behaviour have been noted between composites investigated above and below the respective glass transitions.[4, 32, 33] For this work, composites containing polymer above its glass transition shall be the focus, as it is these filled rubbers that are used in car tyres.

Strain is defined as the deformation a material undergoes with an applied physical force or stress, and is often reported as a percentage change from the unstressed state, further details can be found in section 3.2. The strain softening observed in these filled rubbers is another point of interest and discussion. There are several common features; onset normally occurs between 0.1 and 1% strain, there is a decrease in the storage modulus and an increase in the loss modulus. At greater strains, the loss modulus peaks before decreasing, while the storage modulus continues to decrease. These decreases continue until approximately 15% strain, and the change in the moduli can be several orders of magnitude. It is important to note this process is non-destructive, and a composite can return to the low strain modulus once the strain is removed, although at higher strains, softening hysteresis known as the Mullins effect is observed.[29]

2.3.2 Agglomeration and deagglomeration, Kraus model

Given the importance of these composites in the tyre industry empirical methods describing the reinforcement and strain softening are common, some of which have been developed by implementing concepts from other fields.

Kraus et al. proposed a theory to describe the Payne effect based on reversible reaction kinetic rate equations and an agglomerated filler network.[29, 34] Under oscillatory strain the filler network breaks down, with filler-filler contacts deagglomeration at a rate defined as

$$R_d = k_d \gamma^m N \tag{2.7}$$

where k_d is the rate constant, γ^m is the oscillation strain, and N is the number of filler contacts. Due to random motion, particle contacts associate in the composite, at a rate of

$$R_a = k_a \gamma^{-n} (N_0 - N) \tag{2.8}$$

where N_0 is the number of particle contacts under no strain. As this is a kinetic theory, the lack of time or oscillation frequency dependence is unusual. However this exclusive dependence on strain amplitude is supported by experimental examinations of the Payne effect.[35] Combination and rearrangement of equations (2.7) and (2.8) under the equilibrium conditions yields

$$\frac{N}{N_0} = \frac{1}{1 + \frac{k_d}{k_a} \gamma^{(m+n)}} \tag{2.9}$$

The power exponents for the breaking and formation of contacts would yield a single sum value from fitting this equation, thus it is impossible to determine the exact power dependence of the component from the storage modulus decrease alone. At this stage the N values in equation (2.9) are equated to the composite moduli as a function of amplitude.

$$\frac{G'(\gamma) - G'_{\infty}}{G'_0 - G'_{\infty}} = \frac{N}{N_0} = \frac{1}{1 + \frac{k_d}{k_a}\gamma^{(m+n)}} \tag{2.10}$$

where G'_0 is the zero-strain modulus, and G'_{∞} is the modulus at theoretical infinite strain, if G'_{∞} $\ll G'_0$ than the express can be treated as a normalised modulus. The rate parameters k_d and k_a are often combined to yield a characteristic critical strain, γ_c, defined as,

$$\gamma_c = \left(\frac{k_d}{k_a}\right)^{\frac{1}{m+n}} \tag{2.11}$$

inserted into equation (2.10) this yields,

$$\frac{G'(\gamma)}{G'_0} = \frac{1}{1 + \left(\frac{\gamma}{\gamma_c}\right)^{(m+n)}} \tag{2.12}$$

for the storage modulus behaviour. In the case of the loss modulus, Kraus treats the peak observed in strain softening data as being caused by energy dissipated by the breaking of particle contacts. Thus the loss modulus can be defined as directly related to the rate of deagglomeration,

$$G''(\gamma) - G''_{\infty} = D\,k_d\gamma^m N \tag{2.13}$$

where D is a constant. Equation (2.13) can be combined with equation (2.9) and (2.11) to give,

$$G''(\gamma) - G''_{\infty} = D\,k_d\gamma^m\,\frac{N_0}{1 + \left(\frac{\gamma}{\gamma_c}\right)^{(m+n)}} \tag{2.14}$$

From equation (2.10), N_0 can be equated to $G''_0 - G''_{\infty}$, and can be treated as a constant, and if G'_{∞} and G''_{∞} are insignificant compared with the measured moduli, equation (2.14) be written as

$$\frac{G''(\gamma)}{G''_0} = \frac{E\,\gamma^m}{1 + \left(\frac{\gamma}{\gamma_c}\right)^{(m+n)}} \tag{2.15}$$

where E is a constant composed of k_d, and A. This model can be fitted to experimental data, with a common exponent value of 0.5 - 0.6 for m being reported.[29] However this model is only empirical and does not provide any information on the microscopic phenomena behind the breakdown and reformation or yield any predictive abilities. Of note, it does not provide a relation for the dependence of reinforcement on filler content and assumes a linear relation between the number of filler contacts and modulus reinforcement, which are unlikely given the nature of filler reinforcement. As such, other theories have been developed to describe the polymer composite systems, such as cluster-cluster aggregation and glassy polymer layer effects.

2.3.3　Filler networking, cluster-cluster aggregation

Filler networking has long been thought to be the cause of the non-linear reinforcement observed in polymer nano-composites. Payne himself used this idea to explain the strain softening under deformation as the breakdown of this particle network. [6, 7] The cluster-cluster aggregation (CCA) model is based in this networking concept, and the breakdown of the filler network with strain.

Due to kinetic aggregation, the filler particles form into fractal clusters which aid in the reinforcement of the matrix by providing a stiffer material to store stress. These clusters have a defined size and fractal dimension, illustrated in figure 2.4; above the percolation threshold, these clusters network to bear the stresses applied to the composite. The network is assumed to evenly distribute the stress and be homogeneous above the network's correlation length, as each cluster and its local network can be treated as an average representation of the network. The reinforcement of the composite is taken to be the result of the filler network, and the modulus can be described by a scaling relation dependent on the fractal dimensions of the clusters and cluster network as calculated by Buscall *et al.*,

$$G \propto \varphi^{\frac{3+d_n}{3-d_c}} \tag{2.16}$$

where G is the modulus, φ is the filler volume fraction, d_c is the filler cluster fractal dimension, and d_n is the filler network fractal dimension. [36] The numerator exponential term is defined by the physical response of the filler network, while the denominator exponential term is derived by the scaling of the filler clusters. This relation allows for predictions on the strength of filler reinforcement based on the particle structure. Reports on carbon black rubber composites found agreement from a calculated exponent of 3.5, a cluster dimension of 1.8 and a network dimension of 1.3, with the experimental data, evidencing the viability of the model. Like the Kraus model, strain softening is thought to occur from the breakdown of the cluster network, and utilises the same kinetic approach to explain the Payne effect. [29, 37]
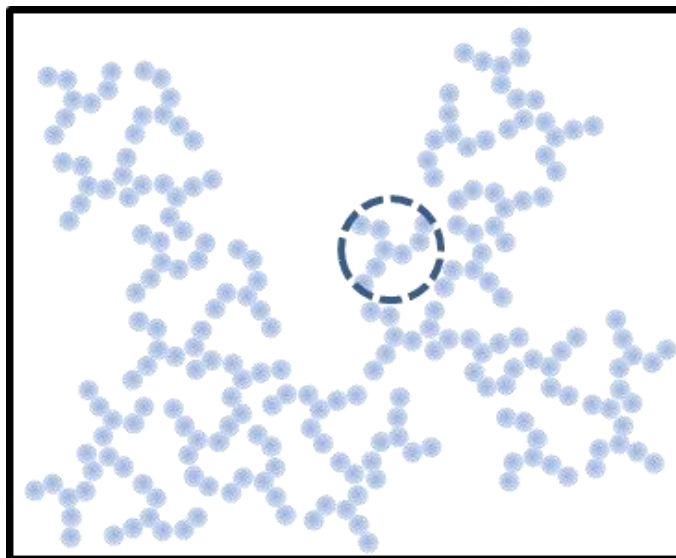
Figure 2.4: Image of cluster-cluster aggregation network, dashed circle represents a single cluster unit

Other models to describe a filler network and its effect on the composite modulus include the van de Walle, Gerspahcher, Tricot (VGT) model which describes a pair of aggregates and the interactions between them and the polymer. There is also the links-nodes-blobs model which utilizes a network of filler agglomerates (blobs), connected by filler bridges (links), to form chains with junctions known as nodes. [38, 39] Although the methodologies differ the principle of the filler network providing reinforcement and its breakdown under strain resulting in material softening remains the same.

Experimentally, there is significant support for the filler network, with x-ray and neutron scattering work corroborating the presence of particle aggregation in filled rubber samples. [40, 41] Other workers have reported that the presence of a percolating particle network provides mechanical reinforcement. [32, 33, 42] The explanation of the filler networking providing reinforcement is not without its criticisms, most notably because the reinforcement is observed at lower volume fractions below threshold required for a percolating network to form; for example, Jouault et al. who reported reinforcement at 0.066 volume fraction of colloidal silica.[43, 44] This lack of networking has been supported with conductivity measurements, as a percolating network will change the electrical properties a composite and this was not observed in work by Yatsuyanagi *et al.*. [45] Others hold that the reinforcement in these filled rubber systems is from filler-matrix interactions and not a percolating network. [46]

Further work needs to be done to characterise if aggregation and percolation of particles in rubbers does lead to increased mechanical reinforcement and strain softening behaviour. In the current work rheology and small angle neutron scattering will be used to examine the mechanical properties and the nanoscale filler structure, respectively.

2.3.4 'Glassy' layers, hindered dynamics

The possible shift in behaviour of polymer near filler surfaces is an important area of composite science, as the inclusion of nanoscale fillers increases the interfacial area. In particular the concept of a dynamically hindered and possibly glassy layer around such filler particles is prevalent.

Several studies of this polymer-surface interface have examined thin polymer films with a variety of experimental techniques. Early work by Forrest *et al.* found decreases in the glass transition temperature for free standing polystyrene films on silica. [47, 48] Since then both decreases and increases in the polymer dynamics have been documented, often through measurements of the glass transition temperature. Reports of decreased glass transition temperature, T_g, in thin films are common [48-50], yet other studies have found the opposite behaviour [51, 52]. These results can be reconciled by examining the dynamic effects based on the preferability of the polymer-substrate interactions, yielding low and high surface energy.[53] As changes to the dynamics of the polymer chains affect the mechanical properties, especially if the polymer is forced into a glassy state, an alteration in reinforcement of a composite may result.

The concept of this possible layer of hindered polymer providing the increased reinforcement was discussed by Berriot *et al.*, who concluded that it was the cause of the phenomena in filled rubber composites. [54] In a composite, each of the filler particles is surrounded by a layer of polymer with hindered dynamics through surface interactions, figure 2.5a, which can be treated as an increase in the glass transition temperature (T_g). This change in T_g is dependent on the proximity to the surface, and can be expressed as,

$$T_g(x) = T_g(\infty)\left(1 + \left(\frac{d}{x}\right)^v\right) \tag{2.17}$$

where x is the distance from the filler surface, d is a characteristic length, and v is an exponent close to unity, figure 2.5b. A polymer melt that is near or below the glass transition will exhibit increased modulus. Therefore the layers of hindered polymer result in a greater volume fraction of the material acting as rigid. This increases the effective volume fraction of the filler material, leading to the observed increase in reinforcement. The removal or reduction of the hindered polymer layer about the sample either from chain desorption or excitation of the dynamics with deformation may result in the strain softening phenomena observed in composites, similar to heating the polymer.[55, 56]
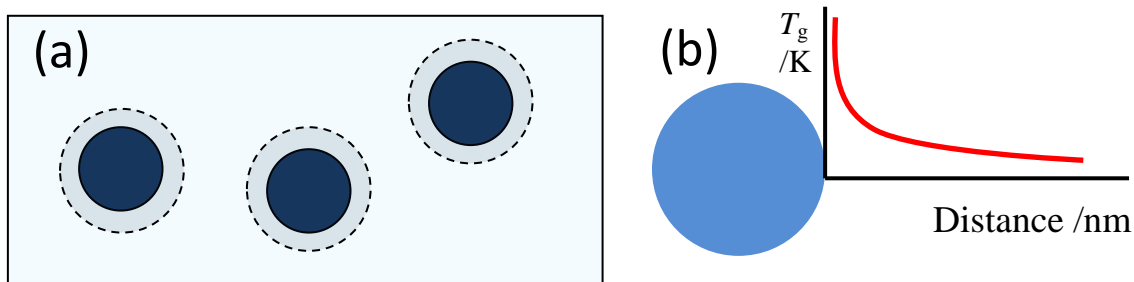
Figure 2.5: (a) Representation of hindered regions about filler particles, (b) glass transition temperature with distance from the particle surface

There is significant support for the presence of a hindered layer in many systems, as can be inferred from the measurements on thin films. Glass transition temperature measurements, dielectric spectroscopy, and NMR studies of different types of filler in bulk composites have also found decreases in the polymer dynamics. [57-62] The hindered layer theory also provides an explanation for the increased reinforcement seen at filler loadings below the percolation threshold, as particle contacts are not necessary for the layer to form.

While there is support for this theory, there are also criticisms. The most common is that hindered dynamics are not present near substrates in all systems, and many find improved dynamics [49, 51, 52, 63], or have found no significant change [64, 65]. Others contend that this layer is not significant enough to produce the reinforcement observed in the composites [44] and that reinforcement is observed in systems tested at 80-100 K above the neat polymer glass transition temperature, where a truly glassy layer should not be present [65-67].

To study the possible presence of changed polymer dynamics, quasi elastic neutron scattering (QENS) will be used in the current work. This technique measures the energy transfers with the sample and correlates it with the dynamic behaviour.

Previous QENS work by Akcora *et al.* on poly-methyl-methacrylate/silica composite and Roh *et al.* on poly-butadiene/carbon black composites found decreased chain motions [68-70], while work by Glomann *et al.* observed no shifts in dynamics for polyethylene-glycol/silica composites [71]. The work undertaken for this report expands on these experimental techniques and was used to obtain additional information about the dynamics in both relaxed and strained composite samples.

2.3.5 Chain bridging

It should be noted that the formation of a particle network and the presence of a hindered polymer layer about the particles are not mutually exclusive. Merabia *et al.* defines a concept of a filler network maintained by glassy bridges, figure 2.6. Unlike the pure filler network, particle-

particle contacts are not needed, and formation of particle bonds is through the overlap of hindered polymer layers to form bridges. These glassy bridges allows for network formation at lower particle concentrations, due to the particle's effective size being increased, and explain the lack of conductively observed in some measurements.
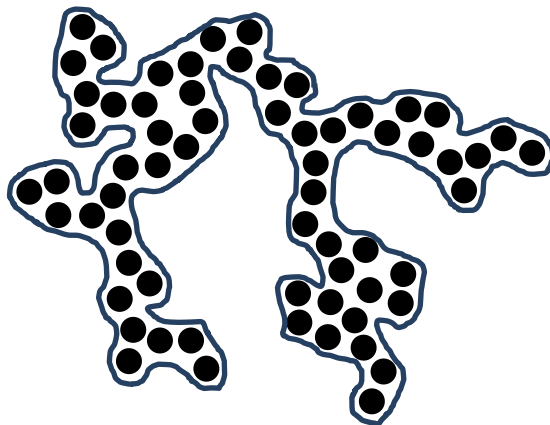
Figure 2.6: Filler network formed by glassy bridging, glassy layer defined by blue outline of the particles

As with the filler networking models, strains to the system break the glassy bridges and decrease the volume of the glassy regions, causing the observed strain softening. The observed loss peak is from the collective energy required to break the glassy bridges. Both molecular dynamics simulations and experiments have reported the presence of glassy bridging and its breakdown leading to the Payne effect. [72-77] Although this model helps remove the issue of low filler volume rubbers displaying reinforcement, it does not completely alleviate it; and it can be argued that the glassy layer would not be significant in some sample systems to provide bridges.[44]

The final concept is that of chain bridging, in which polymer chains bound, physically or chemically, to the particle surface form bridges if bound to two particles. Unlike the previously mentioned glassy bridges, this layer does not need to be dynamically hindered, and can occur over greater ranges. This concept is supported by evidence of three phases of chain dynamics occurring about the filler particles, as illustrated in Figure 2.7. Near the particle surface (<2nm) there is a bound region, the hindered layer, where polymer motion is very restricted. Around this thin layer, there are polymer chains that have segments bound to the surface which restricts the overall motion of the chains but not local dynamics. Finally there is the free polymer layer without any bound chains, the bulk matrix of the melt, which is entangled with the bound chains. [78, 79] This uninhibited but bound layer results in the influence of the filler being much greater than the measured dynamically glassy layer, up to the radius of gyration of the polymer, and this increased influence may explain reinforcement at low filler loadings. [80, 81]
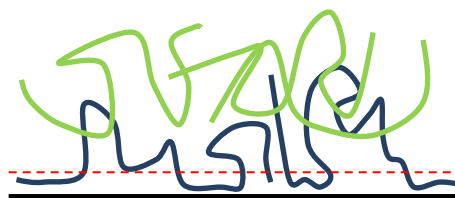
Figure 2.7: Sketch of the polymer layers near a filler surface; red line is the boundary of the restricted layer, blue chains are bound to the surface, green chains are unbound

Under strain, the filler particles rigidity results in the polymer chains bridging the fillers being stretched beyond the applied strain. As this occurs, the chain begin to desorb from the filler surface and the contacts break, causing strain softening; the energy required for chain desorption results in energy dissipation and the formation of a loss peak modulus. [28, 78, 82, 83] Counterarguments of this idea arise from the reinforcement observed with low molecular weight chains unable to form bridges, unfavourable filler-matrix interactions, or where chains capable of bridging are excluded from the surface by a brush layer.

Both the dynamically hindered polymer bridging and chain bridging extend the effective contact range of the fillers in the material in order to explain the reinforcement observed at lower filler concentrations. Neither are exclusive and it may be that filler particle bridging occurs through both mechanisms.[77]

In the current study, examination of the possibility of polymer bridging via either mechanism will be done through rheological and scattering experiments on composites with and without the presence of a particle brush layer. At sufficient density, this layer will exclude matrix chains and provide steric stabilisation to prevent either bridging method. Changes to the composite properties can then be correlated to the lack of these bridging structures.

2.4 Conclusions

While significant progress has been made in the study and classification of filled rubber composites, questions about the origins of the phenomena still remain. Filler networking and inhibited polymer layers are both thought to cause the reinforcement and strain softening effects, and further theories have applied both processes and chain adsorption to provide an explanation. The understanding of the mechanisms will allow for the guided development and control over the material properties and energy dissipation.

By utilising rheology and neutron scattering, this work seeks to provide correlation between the macroscopic material properties and the nanoscale dynamics and structures. Rheological testing

will be used to characterise the reinforcement and strain softening properties of the material. The nanoscale structure of the filled rubber composites will be examined through small angle neutron scattering, and the polymer dynamics through quasi elastic neutron scattering. This information will be analysed together to draw conclusions and to formulate a model of the composite behaviour and link the microscopic and macroscopic behaviour.

3 Experimental

3.1 Materials

3.1.1 Polybutadiene
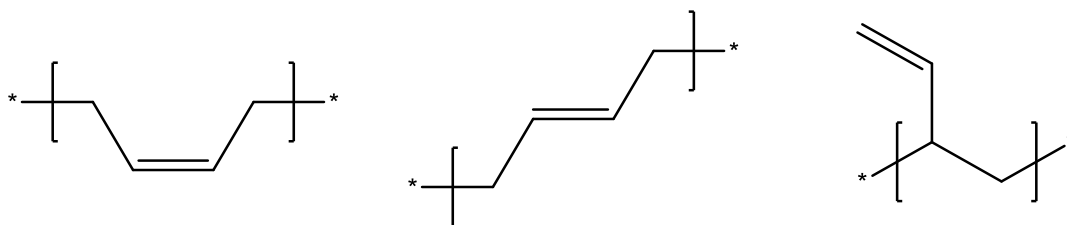
Figure 3.1: Polybutadiene repeat unit structures; from left to right: cis, trans, vinyl

Polybutadiene was first synthesised in 1910 by Sergei Lebedev, and industrial production of the polymer began in the 1930s.[84] The polymer was and is used as a substitute for natural rubber, polyisoprene, often as a copolymer with styrene. Polybutadiene is commonly polymerised from 1,3-butadiene via a Ziegler-Natta reaction with the aid of a metal catalyst. Three distinct chain units form from such reactions, pictured in figure 3.1, the ratios of which depend on the reaction conditions and catalyst used.

The polybutadiene type used for this research was atactic with primarily 1, 4 addition and a molecular weight above the entanglement threshold. This random unit arrangement prevents the formation of crystalline domains, and ensures rubbery behaviour at room temperatures. For rheological tests 310k M_w polybutadiene (Sigma Aldrich, 181382, cis:trans:vinyl 36:55:9) was used in most cases. Deuterated polybutadiene was required for contrast in neutron scattering experiments; this was purchased from Polymer Source in all cases and used as provided.
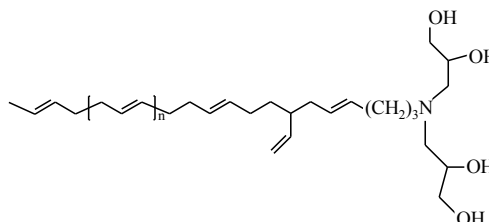
Figure 3.2: Chemical structure of the end functional polybutadiene (4OHPBd)

This work has made use of end hydroxyl functionalised polybutadiene, pictured in figure 3.2, as an additive to affect composite properties. To produce this, 1,3-butadiene was polymerised by living anionic polymerisation, then end capped with the tetrahydroxyl functional group via a click reaction, full details of the process can be found in Kimani et al[85]. The presence of the

hydroxyl group leads to preferential segregation of these polymers toward polar surfaces, such as silica, and the formation of a polymer brush layer. Three different molecular weights were utilized; 10 kDa, 15 kDa, and 20 kDa, each yield a different brush layer thickness. This difference is important to the analysis of the neutron scattering data and will be expanded upon in the results section. A summary of the end functional polymer properties from Kimani et al. and Sigma Aldrich is given in table 3.1. [85]

Table 3.1: Polybutadiene polymer properties

Polymer	M_n / g mol^{-1}	M_w / g mol^{-1}	Degree of end capping	Brush thickness / nm	Surface binding energy / k_bT
4OHPBd-5k	6050	6400	97%	9.4	8.5
4OHPBd-10k	9800	10300	96%	13	10.1
4OHPBd-15k	17400	18500	97%	15.7	9.4
4OHPBd-20k	22500	23600	95%	15.9	7.9
PBd-300k	160000	310000	-	-	-

3.1.2 Crosslinkers

Peroxide radical crosslinking is an alternative to vulcanisation with sulphur, being comparatively simple in both the formulation and reaction mechanisms while still producing a cross-linked polymer network. Peroxides are defined by the presence of an oxygen-oxygen single bond or an O_2^{2-} ion, being further divided into organic and inorganic peroxides. Organic peroxide compounds readily degrade, whether from heat, light, or shock, and often form radical compounds in the process via homolytic cleavage. They are used as an alternative due to lower curing temperatures and the ability to crosslink materials unable to be vulcanised. Benzoyl peroxide was chosen as the crosslinking agent due to its availability, and relative stability at room temperature, ease of handling, solubility in organic compounds, and nontoxicity.

(a)

(b)

(c)
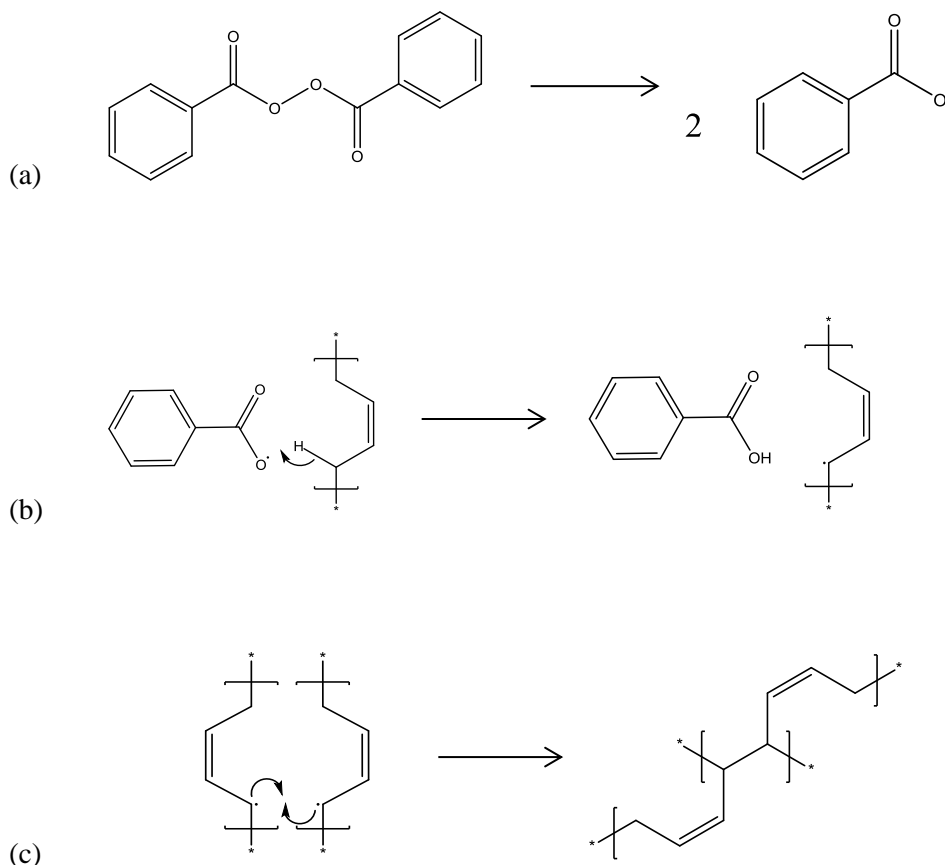
Figure 3.3: Peroxide crosslinking reaction mechanism

Above 70°C benzoyl peroxide degrades into a set of benzoic acid radicals, figure 3.3a, followed by hydrogen abstraction with the polybutadiene, figure 3.3b, yielding benzoic acid and a radical site on the chain. Combination of the radical sites forms the covalent crosslink bond; joining the chains as highlighted in figure 3.3c. This reaction provides a 1:1 relation between peroxide molecules and crosslinks formed assuming perfect efficiency. The effectiveness of the benzoyl peroxide was examined at part of this study, as the crosslink density is known to affect the rubber mechanical properties. Although there is no control over the location of crosslinking sites, the stoichiometric ratio between initial peroxide and produced crosslinks allows for control over the density of the network and corresponding mechanical properties.

Sulphur vulcanisation of natural rubber is the oldest commercial method of polymer crosslinking and the most widely used in commercial applications. Patented independently in both the US and UK in 1845, the development of crosslinking and synthetically elastic material aided in the development of improved machinery and polymer chemistry as a science and industry. The process of vulcanisation has been improved since with the use of initiators, accelerants, and inhibitors to aid in achieving the desired material properties.
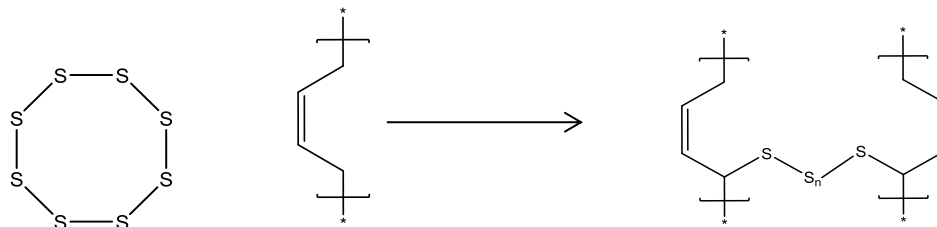
Figure 3.4: Vulcanisation reactants (sulphur and polybutadiene) and product (cross-linked polybutadiene); reaction mechanisms are not shown

In this work, sulphur crosslinking was used under certain circumstances instead of the peroxide system previously mentioned due to its durability; however the theoretical crosslink density is uncertain as bridging sites can contain different numbers of sulphur atoms. Given this uncertainty and the relative complexity of the reaction pathways, a single formulation of vulcanisation reactants was used, as provided by Michelin.[86] The formulation in these experiments was composed of sulphur, zinc oxide, MBTS (2,2'-Dithiobis(benzothiazole)), and stearic acid, solvent casting was performed to ensure proper dispersion.

3.1.3   Types of filler

3.1.3.1   *Precipitated silica*

Precipitated silica is formed from the condensation of silicate salts from solution in an acid-base reaction, with the initial particles aggregating to form bonded clusters. This leads to a porous fractal structure, allowing for greater surface to volume ratios and a lower percolation threshold. For this research silica was purchased from Nanostructured & Amorphous materials (4830HT, SiO2, 99+%, 80nm, CAS# 7631-86-9, lot 4830-012711) and used as provided, from this point onwards this silica will be referred to as precipitated silica.
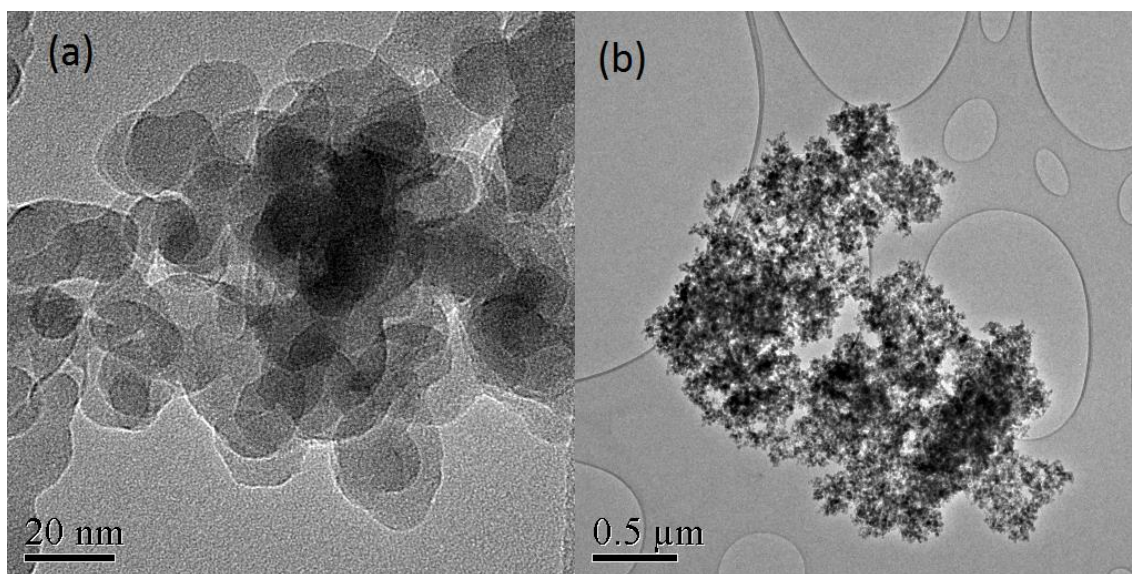
Figure 3.5: TEM images of precipitated silica (a) small scale structure (b) silica agglomerate

Initial structural analysis was carried out with transmission electron microscopy; a quantity of silica nanoparticles were dispersed in acetone with sonication and then deposited on a TEM grid. The images in figure 3.5 show a characteristic precipitated silica structure. In 3.5a the nanoscale structure of the primary aggregates is observed. A visual characterisation of the substructure size was attempted and the mean diameter of the initial unit was determined to be 23 ± 6 nm. Given the non-uniform structure of the silica this measure is an estimate, as evidenced by the uncertainty, and only provides guidance for other methods. All the silica observed was agglomerated into larger structures on the micron scale, seen in figure 3.5b. This aggregation is from the drying effects when the acetone solvent evaporated and is not an accurate representation of the silica when dispersed in a medium.

For determination of particulate size a dynamic light scattering measurement was performed on an aqueous suspension of precipitated silica, the mixture was sonicated to ensure dispersion. Dynamic light scattering utilises the fluctuations in the intensity of scattered light to determine correlations and colloid particulate sizes. A beam of laser light in shone through a suspension, and a detector records the intensity of the light scattered by inhomogeneities, often particles, in the system. Due to the dynamic nature of the particles the intensity fluctuates with time, through the correlator function which compares the intensity at a point to another at a set time interval, an autocorrelation decay can be determined. The transformation is defined as

$$G(\tau) = \lim_{T \to \infty} \frac{1}{T} \int_0^T I(t)I(t + \tau) \, dt \qquad (3.1)$$

where $G(\tau)$ is the autocorrelation function, T is the time integration limit, t is the time variable, and τ represents a time interval. [87] This equation is sometimes normalised to the value obtained by setting the interval to zero.

In the case of monodisperse particles, the normalised autocorrelation decay can be treated as an exponential function,

$$G(\tau) = e^{-2DQ^2\tau} \qquad (3.2)$$

where D is the diffusion constant, and Q is the scattering vector. Through the diffusion constant and the Stokes-Einstein relation, the radius of the scattering particles can be calculated. With polydisperse or multiple particle sizes different approaches must be used. A common method is the CONTIN algorithm, which utilizes inverse Lapace transforms to fit particle sizes to the autocorrelation function. While this does provide values for the sizes, care must be taken as artefacts can be introduced from the quantity of terms and the relative intensity of scattering,

which is known to follow a sixth power trend with particle size. If the intensity difference is great then smaller particles can be lost in the signal of larger particles. This is particularly important if aggregates are present in the solution. [88, 89]

For the precipitated silica, the resulting scattering intensities shown in figure have two distinct sizes with a peak at 300 nm and 3000 nm. Notably, there is no presence of a peak in the 10 to 40 nanometre range. Structures of appropriate length scale were observed on the TEM analysis, thus it is unlikely either of these peaks is an artefact, however, some care must be taken with the comparison of the volume fraction of each peak. The small 20 nm units observed on the TEM are permanently bonded into aggregates of 300 nm average radius, the architecture present in precipitated silica as mentioned previously. The peak at 3000 nm is from agglomerates of the primary aggregate, its presence means that unless hindered the silica nanoparticles will form into larger structures whether in solvent or polymer matrix.
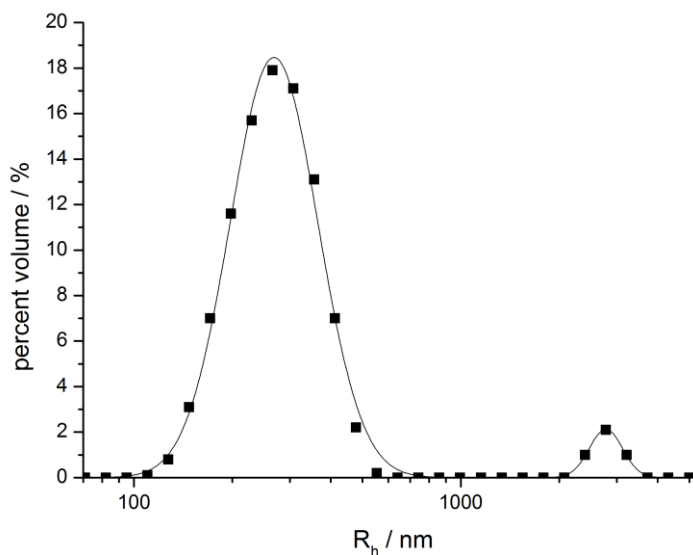
Figure 3.6: Precipitated silica percent volume fraction against hydrodynamic radius, peaks fitted with log-normal distributions

3.1.3.2 *Stöber silica*
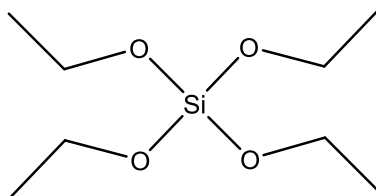
Figure 3.7: Chemical structure of tetraethyl orthosiliate (TEOS)

$$Si(OEt)_4 + 2\,H_2O \rightarrow SiO_2 + 4\,EtOH$$
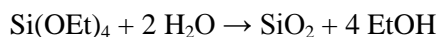
Stöber silica is produced through the hydrolysis and condensation of tetraethyl orthosiliate (TEOS), figure 3.7, in a basic solvent environment. First reported by Stöber in 1968, this technique has been widely studied because of the resulting nanoparticles[90]. Unlike the case with precipitated silica, silica produced by this process is spherical and has low polydispersity, and the final particle radius can be tuned by altering the reaction conditions. As such, these particles are well-defined filler that is useful for both rheological tests and neutron scattering. Although not wide used in industry in favour of precipitated silica, Stöber silica is produced in small commercial quantities, often as an aqueous colloidal dispersion.

The reaction was a single pot process following a procedure by Lindberg et al.[91] The components, ammonium hydroxide solution, deionised water, and TEOS were added to ethanol solvent in a flask. All compounds were used as provided; details and quantities are listed in table 3.2. The flask was sealed and left stirring overnight at room temperature. After completion the solvent was evaporated off and the resultant nanopowder was collected and dried.

Table 3.2: Stöber silica reaction reagents

Compound	Supplier	Product details	Quantity
Ammonia solution	Sigma Aldrich	221228, 28-30% NH_3 basis	1.26 ± 0.01 g
Deionised water	-	-	0.89 ± 0.01 g
Tetraethyl orthosiliate	Sigma Aldrich	86578, ≥99% (GC)	1.88 ± 0.01 g
Ethanol	Fisher Scientific	99.8% purity	50 ± 1 ml

Over the course of the investigation, several batches of Stöber silica were synthesised, each was characterised separately and noted to have a different particle radii. Dynamic light scattering and TEM measurements of the Stöber silica were undertaken to determine average particle size and distribution. Although exact particle size varied slightly between batches, the reaction outlined previously produced particles that are spherical, have an approximately 50 nm radius, and some size distribution, as can be seen in figure 3.8c. While the differences in particle size prevent

direct comparison between different Stöber silica batches, the consistent geometry of the particles allows for the same models of the system to be employed.

Comparison with the precipitated silica yields key differences, although the primary length scale is similar for both, and clustering occurs on drying the Stöber silica is not bonded beyond the initial starting structure. This is evident from the light scattering which yields the same radius as the TEM size characterisation and no further aggregation peaks. The difference between the precipitated and Stöber silica structures stand as a test of the effect of filler morphology on the rheological properties.
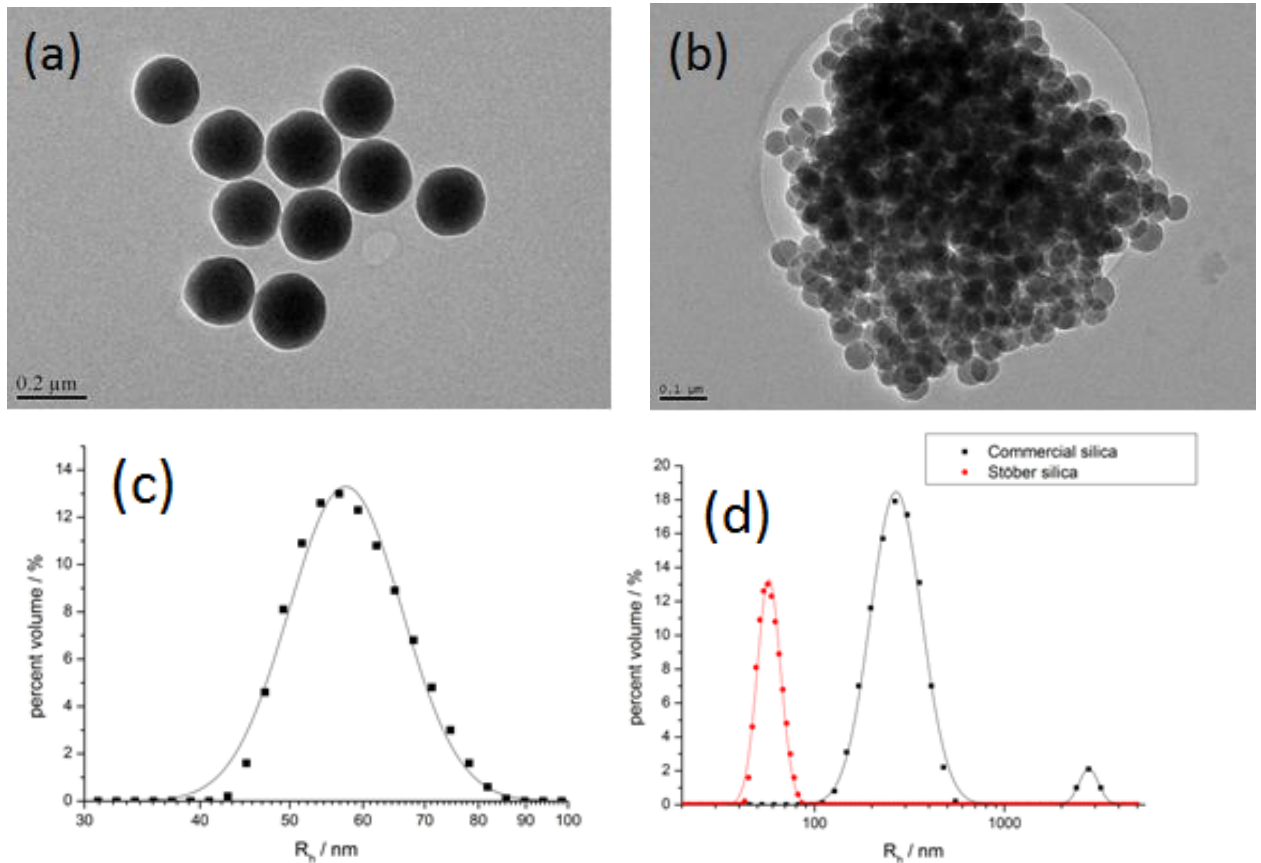
Figure 3.8: Stöber silica (a) example ~100 nm radius, non-standard, spheres TEM image (b) aggregated Stöber silica (~50 nm) cluster, TEM image (c) percent volume fraction against hydrodynamic radius (d) comparison with precipitated silica, peaks fitted with log-normal distributions

3.1.3.3 Carbon black

Carbon based fillers are the oldest used in car tyres systems, with additions to rubber occurring in the 1940s and 50s and continuing to this present day. One of the most common types is carbon black, which is formed from incomplete combustion of tar and petroleum. The microstructure is known to be fractal and slightly porous, resulting in a high surface area to mass ratio of 150-250 m^2/g. Of importance to this research is the difference in surface properties compared with silica, although both contain surface bound oxygen, the required binding energy between carbon black and polybutadiene is smaller than with silica due to the difference in filler polarity[92].

Mesoporous carbon was purchased from Sigma Aldrich (699632, >99.95% trace metals basis, <500 nm particle size) and used without modification. The results of dynamic light scattering measurements, figure 3.9, show a single size peak at 155 nm with some polydispersity. This provides the size for the smallest permanently bonded aggregate, and is of similar size to the precipitated silica primary aggregate. This factor will allow for the examination of the effects of surface properties on composite reinforcement.
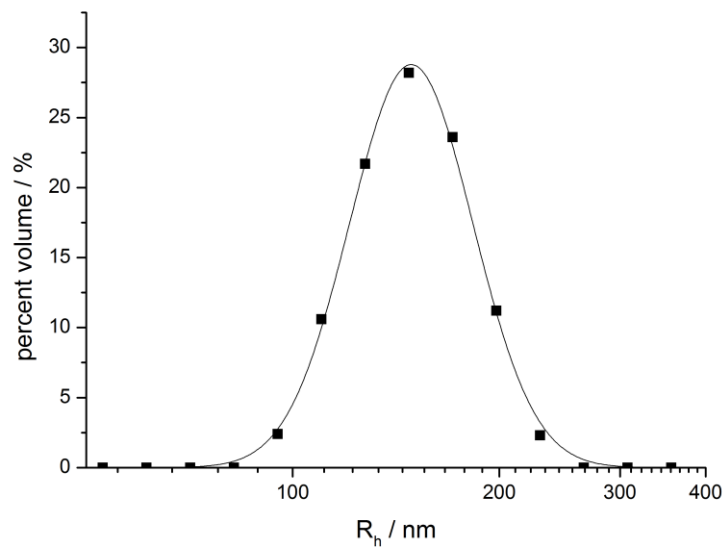
Figure 3.9: Carbon black percent volume fraction against hydrodynamic radius, peak fitted with log-normal distribution

3.2   Rheology

Rheology is defined as the study of a materials mechanical response to an applied force or stress. The response of a substance to physical forces allows for determination and examination of microscopic structures and processes in the material. Material responses can be separated into an elastic (solid) and viscous (fluid) component. The term viscoelastic is used for systems where both components are significant; the composite materials examined in this work fall into this category.
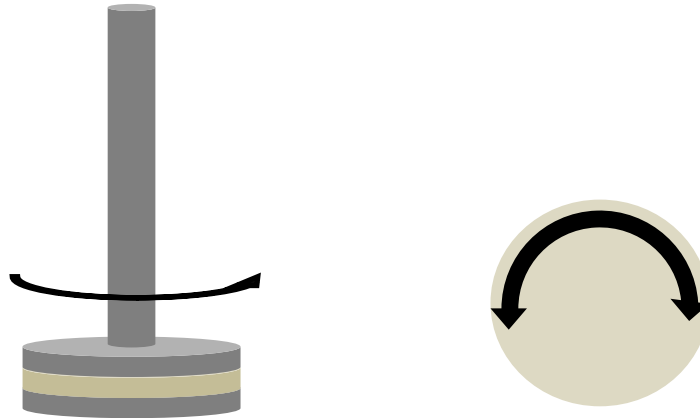
Figure 3.10: Visual of an oscillatory shear setup, sideways on (left) and top down (right). Black arrow denotes the direction of shear

The primary method used in this investigation was an oscillatory shear setup. A sample is held between two parallel plates, as shown in figure 3.10. A continuous sinusoidal stress in the plane of the plate is applied to the sample, resulting in a strain response with a phase difference. The rheometer was held in controlled strain mode for all tests.

Figure 3.11: AR2000 rheometer with peltier stage and 8 mm head attached

The measurement instrument was an AR2000 rheometer, pictured 3.11. Due to the high modulus of the composites, an 8 mm diameter sample geometry was used in all circumstances. All composite samples were solvent cast; the components were dispersed in solvent with sonication then the solvent was evaporated off to form the composite. The dried composite was from into 8 mm diameter discs with 1000 μm thickness using a mould and a heat press. In the case of crosslinked samples, these were then cured in the heat press for a set time and temperature dependent on the type of crosslinker.

For sample measurement below 60 ˚C a peltier stage was used, above 60 ˚C an environmental test chamber (ETC) with an inert nitrogen atmosphere was used so to prevent the oxidation of the samples. A gap of 1000 μm was maintained for all samples as to ensure contact without compression of the disc. The frequency and strain ranges examined were varied depending on the test performed, however unless otherwise noted or required the frequency and strain were held at 1 Hz and 0.1 %, respectively.

For data analysis, the response of the material is separated into in phase and out of phase components, as such,

$$\sigma = \sigma_0 \sin(wt + \delta) = \sigma_0(\cos(\delta)\sin(wt) + \sin(\delta)\cos(wt)) \qquad (3.3)$$

where σ_0 is the magnitude of the stress, w is the oscillation frequency, t is time, and δ is the phase difference. This relation can also be described in terms of strain, yielding

$$\sigma = \gamma_0(G' \sin(wt) + G'' \cos(wt)) \qquad (3.4)$$

where γ_0 in the strain magnitude, G' is the storage modulus, and G'' is the loss modulus. The sine component represents the elastic response of the material with the storage modulus defining the magnitude of the component; likewise the cosine term and loss modulus represents the viscous component and its magnitude. The terms storage and loss refer to the amount of energy stored and dissipated in the structure over an oscillation, with higher moduli corresponding to stiffer and thicker materials respectively. It is the relative magnitude between the components that defines the overall material response, direct comparison is common, however, it is also useful to examine the phase difference, δ. This value provides a dimensionless characterisation of the material properties as elastic (in phase, 0˚) or viscous (out of phase, 90˚).

For polymer systems the storage and loss moduli are known to depend on the probing oscillation frequency. This dependence is due to the reorganisation of the polymer chains either by quick segmental relaxation or slower chain reptation. The behaviour for simple polymer systems has been thoroughly examined, with theories by Rouse and deGennes providing the basis for predictive models, and will not be covered in great detail here.[8, 12]

3.3 Neutron Scattering

Neutron scattering covers a wide variety of experiments that make use of the interaction of a neutron beam with a sample. Many of these techniques are similar to those found in x-ray scattering; however, others make use of properties specific to the neutron and have no such direct analogue.

Neutrons are one of the primary components of atomic nuclei, and are produced for these experiments with nuclear reactions by target spallation from a proton beam or in a research reactor. The produced neutrons are guided and collimated into beams toward the sample environments. Due to wave-particle duality the neutrons that make up the beam can be modelled with the deBroglie wave equation

$$p = \frac{h}{\lambda} = \hbar k \tag{3.5}$$

where p is momentum, λ is wavelength, k is wave vector, and $\hbar$ is the reduced Planck's constant. Interaction with a sample nuclei leads to a change in the neutron wavevector and a divergence from the central beam. The wave-like nature of the neutron results in interference in the scattered beam which then forms scattering patterns as would be seen in an x-ray scattering experiment.

The scattered neutron's position and time at a detector is recorded; this can be converted into the scattering angle or most commonly the scattering vector, Q. This vector is defined as the change in the incident and scattered neutron wavevector, as shown in figure 3.12, and is given in Å^{-1} as convention from neutron scattering. Because the wave-vectors are in reciprocal units, neutron scattering patterns are produced in reciprocal space, as is the case with x-ray scattering, thus smaller Q values relate to greater distances in the material. The exact range observed in an experiment is dependent on the instrument and its setup; however, collectively neutron scattering spans a physical size range from inter-atomic spacing to hundreds of nanometres.
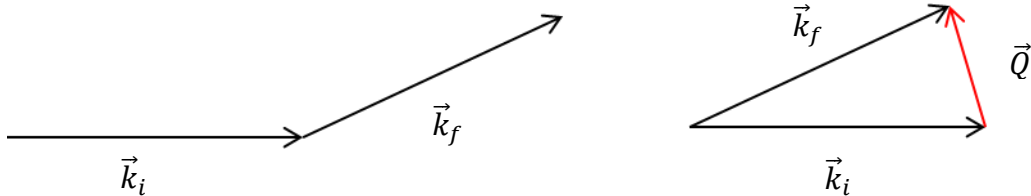
Figure 3.12: Basic scattering diagram, the incident and scattered wave vectors, k_i and k_f, and the scattering vector

In any given sample, the total measured intensity can be written as,

$$I(Q) = I_0 T \eta V_s \Delta\Omega \frac{\partial^2 \Sigma}{\partial\Omega\partial\omega}(Q) \tag{3.6}$$

where I_0 is the incident beam, T is the sample transmission, η is the detector efficiency, V_s is the sample volume, $\Delta\Omega$ is the solid angle formed by the detector position, and $\partial^2\Sigma/\partial\Omega\partial\omega$ is the partial differential cross section which contains information on atomic correlations and interactions in the sample. This term can be defined in by the dynamic structure factors as

$$\frac{\partial^2\Sigma}{\partial\Omega\partial\omega}(Q) = \frac{k_f}{k_i}\bar{b}_c^{\ 2}S_{coh}(Q,\omega) + \frac{k_f}{k_i}(\overline{b_i^2} - \bar{b}_i^{\ 2})S_{inc}(Q,\omega) \tag{3.7}$$

where k_i and k_f are the scattering vectors, b are the nuclear scattering lengths, and $S(Q,\omega)$ are the structure factors. It should be noted there are two factors, the coherent factor is of primary concern for SANS and other measurements of spatial correlations, while the incoherent factor is important to the QENS measurements described later.

A key separation and benefit of neutron scattering over light scattering is the effective nuclear scattering length, b, varies drastically between elements and isotopes, shown in figure 3.13. The differences between isotopes are particularly useful as this allows for isotopic labelling of sections of sample material without significant changes to the chemical properties.

This key concept and experimental technique in small angle neutron scattering is the process of scattering length density (SLD) contrast and its control through isotopic substitution. Above the atomic length scale, the SLD can be determined as a sum of the component nuclei scattering lengths over the molar volume, written as

$$\rho = \frac{\sum b_c}{V_m} \tag{3.8}$$

where ρ is the scattering length density, b_c is the coherent scattering length, and V_m is the molar volume. As mentioned previously different atomic nuclei yield drastically different scattering properties, shown in figure 3.13. For soft matter systems, of particular note is the difference between hydrogen and its isotope deuterium, details in table 3.3.
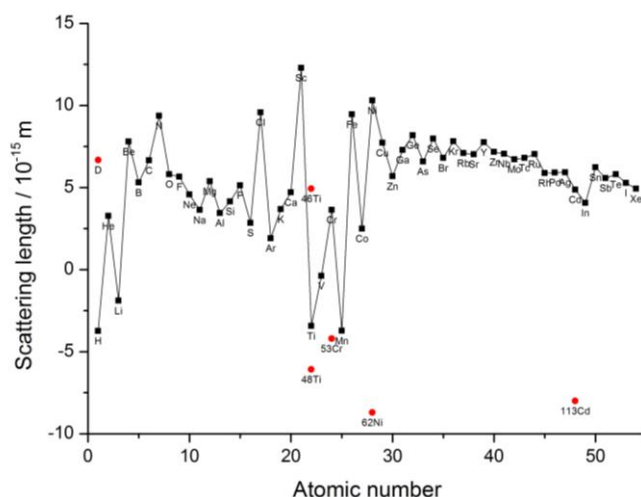
Figure 3.13: Real coherent neutron scattering length vs atomic number, red points indicate isotopes with notable scattering differences, values from NIST database[93]

Table 3.3: Bound scattering data for common nuclei in examined samples (NIST database)[93]

Nuclei	Coherent scattering length / m^{-15}	Incoherent scattering length / m^{-15}	Coherent cross section / 10^{-24} cm^2	Incoherent cross section / 10^{-24} cm^2	Absorbance cross section / 10^{-24} cm^2
H	-3.7406	25.274	1.7583	80.27	0.3326
D (^{2}H)	6.671	4.04	5.592	2.05	0.000519
C	6.646	0	5.551	0.001	0.0035
N	9.36	2.0	11.01	0.5	1.9
O	5.803	0	4.232	0.0008	0.00019
Si	4.1491	0	2.163	0.004	0.171

The difference in coherent scattering length between the isotopes allows for controlled variation of the SLD of hydrogenous molecules, through the substitution of hydrogen with deuterium, without major changes to the chemical nature of the molecule. As the scattering is defined by the scattering length density contrast, this is useful as a tool to screen out components or gain additional information about particular molecular formations in a sample.

3.3.1 Small angle neutron scattering

Small angle neutron scattering are elastic scattering measurements consisting of Q values below 0.1 $Å^{-1}$. This corresponds to a distance of 62.8 Angstroms and greater in real space, allowing for the examination of nanoscale structures by this method. Spatial measurements focus on elastic neutron collisions, where no kinetic energy is exchanged. In regards to equation (3.7), possible ω differences are averaged or assumed insignificant to give the expression as the differential cross section, $\partial\Sigma/\partial\Omega$. The method also requires coherence, a single wavelength and constant phase angle between the neutrons, in order to produce a scattering pattern through interference. Incoherent scattering results in a flat noise background in the measurements, most clearly seen at higher Q values. Thus, for these experiments, the coherent scattering length is of primary

concern. The magnitude of the incident and scattering neutron wavevectors are equal in these collisions, allowing for simplifications of the scattering equations to determine Q. With elastic collisions Q is defined as

$$Q = \frac{4\pi}{\lambda} \sin\left(\frac{\theta}{2}\right)$$

(3.9)

where λ is the neutron wavelength and θ is the scattering angle. Both variables can be determined from the experimental setup and measurement, allowing for the determination of Q. Due to spatial correlations and changes of the scattering properties in the sample, the intensity of the scattered beam will vary with Q to produce a scattering pattern. These scattering patterns can be modelled from the theoretical real space distribution of SLD to characterise and define the distribution of the components.

In regards to this series of experiments, the samples contained a mixture of the chemicals listed earlier, as well as per-deuterated polybutadiene purchased from Polymer Source and used as provided. This deuterated polymer was to provide the scattering contrast needed for informative SANS results, details of each component's scattering properties are listed in table 3.4. The details of the sample composition will be covered in the results of each experiment.

Table 3.4: Calculated scattering data for components in examined samples

Component	Coherent scattering length density / 10^{-6} Å^2	Incoherent scattering length density / 10^{-6} Å^2	Coherent cross-section (1/cm)	Incoherent cross-section (1/cm)
SiO$_2$	3.791	0.074	0.25	0
dPBd	6.674	3.134	0.559	0.123
hPBd	0.416	19.615	0.002	4.825
4OH-PBd-20k	0.416	19.615	0.002	4.825
4OH-PBd-15k	0.416	19.615	0.002	4.825
4OH-PBd-10k	0.416	19.615	0.002	4.825
4OH-PBd-5k	0.416	19.615	0.002	4.825

The small angle neutron scattering experiments were conducted on three different SANS instruments for the project, LOQ and SANS2D at ISIS, and D11 at the Institut Laue-Langevin (ILL). The overall experimental design is simple, with an incident neutron beam scattering off of the sample and onto the detectors, though care has to be taken to avoid multiple scattering and sample absorbance. In all cases, the samples were 1 mm thick and had a diameter greater or equal to 8 mm. This was to ensure reasonable scattering intensity and to compare the results with

the rheological tests. Data reduction and fitting was performed by Mantid software and SASview, respectively[94, 95].

For initial scattering experiments on LOQ, samples were prepared from per-deuterated polybutadiene (Polymer Source, M_w 138,000, PDI 1.06, P4016-dPBd), 20k 4OHPBd, and Stöber silica (R_h: 51 nm, DLS) by solvent casting; filler loadings of 0, 2, 4, 8, 12, 16, 20, and 24 were chosen, samples are summarised in table 6.1. In addition, samples contained benzoyl peroxide (Sigma Aldrich, 517909, Luperox A75) for 100 monomers per crosslink density, to be cured in situ to examine possible changes to the microstructure. The composites were pressed into disks and placed in 20 mm diameter and 1mm thick quartz cells. Pre-cured samples containing 0, 4, 12, and 24 percent filler loading were placed in a stretching rig, figure 3.14, to examine the effect of deformation on the composite structure. The 2% and 24% silica weight fraction samples were also examined on SANS2D using the express sample service at ISIS, with the rear detector set at 12 m to examine low Q values.

Figure 3.14: Manual stretching rig, LOQ sample environment

Further analysis of the filler behaviour with the addition of end functional polybutadiene was performed on data gathered on D11. Samples of this experiment were composed of perdeuterated polybutadiene (M_n:88000, M_w: 90600, linear) from anionic polymerisation, end functional polymer (5k, 10k, 15k, and 20k) and the precipitated silica from nanostructured and amorphous materials mentioned previously. 20mm diameter, 1 mm thick quartz window cells were used to house the samples. Two silica concentrations, 5 and 20% w/w, were chosen and the concentration of the end functional polymer was varied between 1 and 16 percent weight across the samples. Three detector distances, 1.2, 8, and 39 m, were used to cover the entire range of available Q space, 8.59 x 10^{-4} – 0.31 Å^{-1}. The different scattering curves were stitched together to form a single curve for analysis.

For the examination of the effect of strain, the SANS2D instrument at ISIS was used. The rear detector was set at 12 m, 0.8 mm diameter collimation was used, and samples were strips of 30 mm x 13 mm x 1 mm. The components of the samples were 15k 4OHPBd, per-deuterated PBd

(Polymer Source, M_w 95,000, PDI 1.05, P5899-dPBd), and Stöber silica (19.4 nm, DLS). All samples were crosslinked with sulphur by the method detailed in the experimental; curing was done at 160 ˚C for one hour. The sample strips were clamped with a set of clips attached to a mobile stage as shown in figure 3.15. The position of upper clip section (in figure) was controllable by a lead screw mechanism, driven by a computer controlled stepper motor. Strain on the samples was induced by separation of the clips; the strain was taken as the engineering definition, determined from the initial clip separation and relative movement as

$$\gamma_e = \frac{\Delta L}{L_0} \tag{3.10}$$

where L_0 is the initial sample length. Strains between 0 and 40% were attempted on the samples over the course of these experiments. Angular cross sections of the reduced scattering data were analysed to search for anisotropy due to strain.
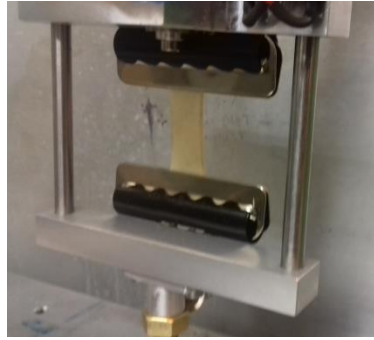
Figure 3.15: Image of neutron scattering strain rig, the sample environment on SANS2D

3.3.2 Spin echo small angle neutron scattering

To examine the filler structure at greater length scales than possible on small angle neutron scattering instruments, non-cross-linked Stöber silica composite samples were subjected to measurements on the OFFSPEC instrument at ISIS. Samples contained different ratios of Stöber silica (R_h: 49 nm, DLS), 15k 4OHPBd, and 310k polybutadiene; samples are summarised in table 6.6. The Offspec instrument was run at magnet angles of 55 and 75 with a magnetic field strength of 18.13 mT, yielding a measurement range from 50 to 800 nm.
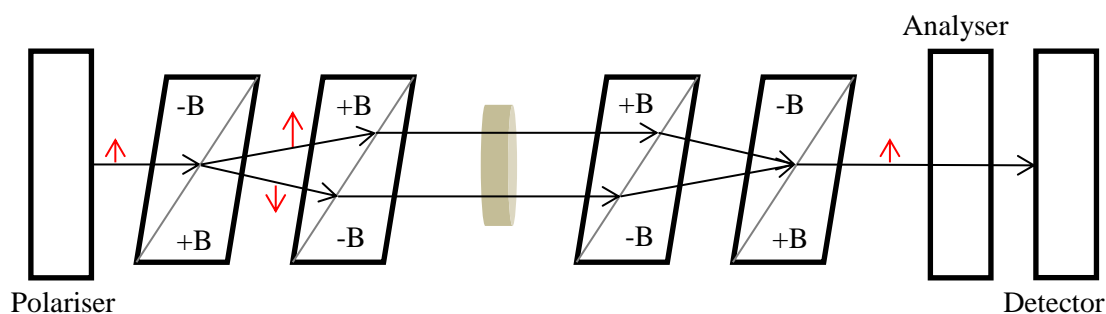
Figure 3.16: Schematic of SESANS theoretical setup

Spin echo small angle neutron scattering (SESANS) utilizes the spin properties of neutrons and Larmor precession to investigate material structure. Developed in the 1970s by Mezei for the measurement of dynamics, the technique has been adapted for structural measurements. A simplified diagram of the OFFSPEC theoretical setup is shown in figure 3.16. A beam of neutrons is filtered with a polariser setup to preferentially transmit either the spin up or down state. This net polarised beam is then passed through a set of magnetic fields before and after the sample. These serve to invert the neutron spin state via the spin echo process, yielding the formation of a spin echo peak at the analyser which transmits the selected neutron spin state to be detected. The magnetic fields also serve to separate the neutron's spin up and down eigenstates, visible in the figure; although the beam is polarised quantum effects result in the beam sampling both paths and interfering with itself. The theoretical physical separation of the eigenstates as they pass through the sample is the measured length scale of the scattering. [96]

Without interactions with a sample material, this measured neutron intensity does not vary with magnetic field strength as both paths are identical. With the presence of a sample, neutron interaction and scattering results in a net depolarisation of the neutron beam. This is treated as measurement of the correlation with respect to length scale in the sample, as the probed distance in the sample is controlled by the strength of the magnetic field. By varying the field intensity a spectrum of correlation against distance can be built up and analysed. This is a real space measurement of the correlations and can be extended to micron length scales, significantly above the range of SANS.

3.3.3 Quasi elastic neutron scattering
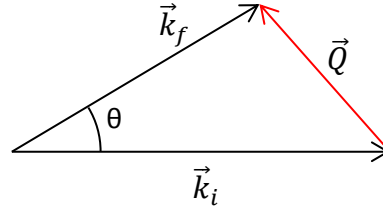
Figure 3.17: Basic inelastic scattering diagram, the incident and scattered wave vectors, k_i and k_f, and the scattering vector.

Quasi elastic neutron scattering (QENS) is part of the regime of experiments known as inelastic neutron scattering. As the name suggests these tests examine the collisions in which kinetic energy transfer does occur between the neutron and the sample, resulting in a change in the magnitude of the neutron wave vector, figure 3.17. This change prevents the simplifications of the scattering equations often used in elastic scattering; however the energy transfer provides information about the dynamics of the measured system. The energy exchange can be determined from the change in wave vector magnitude,

$$\Delta E = \frac{\hbar^2}{2m}\left(k_f^2 - k_i^2\right) \tag{3.11}$$

where m is the neutron mass, $\hbar$ is the reduced Planck constant and k_i and k_f are the incident and scattered wave vectors. The scattering vector, Q, can be determined with an application of the law of cosines,

$$Q^2 = |k_i|^2 + \left|k_f\right|^2 - 2|k_i|\left|k_f\right|\cos(\theta) \tag{3.12}$$

where θ is the scattering angle. However, the magnitude of the wave vector cannot be directly obtained by the detector, as the reaction required to detect the neutron prevents measurement of its kinetic energy. For this reason time of flight measurements are required for these experiments, with knowledge of distances between the sample and the detectors, and arrival time of the neutrons at the detector the velocity and wave vector of the neutron can be calculated.

The inelastic scattering of neutrons from a sample is often partitioned into distinct types depending on the nature and energy of the observed motions. Large energy transfers with clear peaks are the result of collective motions in the sample, such as phonons and lattice vibrations. These scattering events are coherent as the energy transfer and length scale is consistent across the sample, resulting in defined peaks. However, both IRIS and IN16B were not setup in these

experiments to probe the energy transfer levels associated with this scattering, instead observing the incoherent inelastic scattering of the quasi-elastic peak.

Small energy transfers are the result of atomic translational motions and diffusion, as these motions are random there is no distinct energy transfer and they serve to broaden the elastic peak. Experiments that probe this area about the elastic peak are known as quasi-elastic. Given the lack of a specific length scale and random motion, these scattering events are incoherent, thus the incoherent scattering terms dominate the response. It is these experiments that were used to examine the diffusion dynamics of the rubber samples.

Two spectrometer instruments were used to examine the sample dynamics, IRIS at ISIS and IN16B at the ILL. IRIS is configured in an indirect geometry, meaning it measures the energy transfer to a known energy rather than from a set energy. The spallation source at ISIS produces neutron pulses with a range of velocities which is refined with collimation and beam choppers on the IRIS instrument. These pulses impact and scatter from the sample in the chamber toward a graphite analyser which reflects neutron of 6.67 Å wavelength toward the detector; this provides a single k_f magnitude to be detected. As the position and arrival time of the neutrons is recorded, k_i, the energy transfer, and Q can be calculated. With the standard graphite analyser (002) used for these experiments, an energy transfer range of ± 0.4 meV is observable with a resolution of 17.5 μeV and a Q range of 0.42-1.85 Å^{-1}. A total of four experiments were performed on the IRIS spectrometer, and in all cases samples were 65 x 30 x 0.1 mm dimensional sheets. In the case of poorly scattering samples two identical layered sheets were used to achieve the required thickness for scattering.

For the examination of strain on the dynamics, a simple extensional stretching rig was devised, figure 3.18, clamp position was adjusted by a lead screw mechanism. Crosslinked polymer composite sheets were fixed and strained in the rig, strain was treated with the engineering definition as for the SANS experiment. This rig was designed to attach to a CCR sample stick at IRIS, allowing for some temperature control of the sample.

Figure 3.18: Simple extensional stretching rig, without shielding

For further examination of the strain on the polymer dynamics, a second rig was designed to allow for deformation of the sample in situ, figure 3.19. The system used a lead screw mechanism and was controlled through a stepper motor; this device was also used to apply strain for a SANS experiment, mentioned previously. Due to the motorised components the CCR setup could not be used on IRIS, as such, only the evacuated chamber was used.
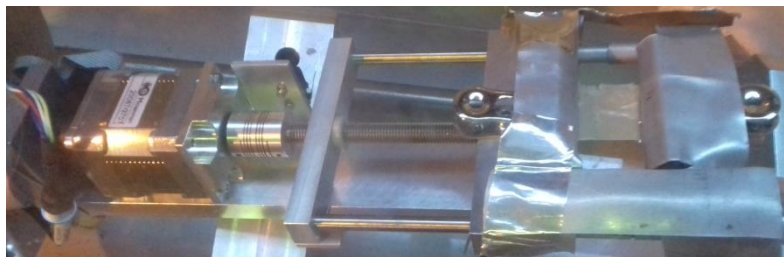
Figure 3.19: Image of neutron scattering strain rig including driving motor and cadmium shielding, IRIS workstation

IN16B is a backscattering spectrometer that is also an indirect geometry. The initial neutron flux from the reactor is refined and pulsed by velocity selectors and choppers. This beam is directed into the instrument where it reflects off of an oscillating silicon monochromator, known as the Doppler drive. This drive selects neutrons with an incident wavelength of 6.271 Å, however due to the oscillations a well-defined spread of wavelengths is achieved through the Doppler Effect. These reflected neutrons pass through the sample and scatter, after which they reflect off of silicon analysers into the detector. As with IRIS the final wavelength of the scattered neutrons is known, and the incident wavelength can be determined by time of flight.

Scattering differences between nuclei play an important role in these QENS experiments. As hydrogen has significantly greater incoherent scattering than other nuclei, see table 3.3, the detected inelasticity scattered neutrons primarily come from hydrogen. Thus the measured dynamics in these experiments are from hydrogenous polymer. This factor combined with deuteration of the polymer and the surface selectivity of the 4OH polybutadiene allows for spatial control of the measured dynamics though the segregation of the deuterated and hydrogenous polymer. The segregation of the hydrogenous polymer to a selected region results in dynamics measurements specific to that area rather than an average over the whole system. This selection allows for a spatial analysis of the dynamics and can serve to highlight different dynamic environments.

The product of these quasi elastic scattering experiments is an energy transfer distribution, an example is shown in figure 3.20a, where the intensity describes the relative frequency of such energy transitions and the related motion. The peaks shown can be analysed by the fitting of

Lorentzian functions, however for this work analysis was performed via transformation of these peaks into time-dependent autocorrelation functions. As shown earlier, equation 3.1, autocorrelation curve are often determined by comparing the fluctuations in a value over time. For a stationary random process, such as Brownian motion, the time-dependent autocorrelation function can be treated as a Fourier transform pair with the frequency spectrum. [97] Coupled with the deBroglie relation between frequency and energy, this allows for the conversion of the energy distribution into an autocorrelation function. Thus a correlation was achieved by fast Fourier transformation of the data; a sample resultant autocorrelation is shown in figure 3.20b. An autocorrelation represents a system's similarity with its initial state, and examining its decay is a method to determine the dynamics in a system.
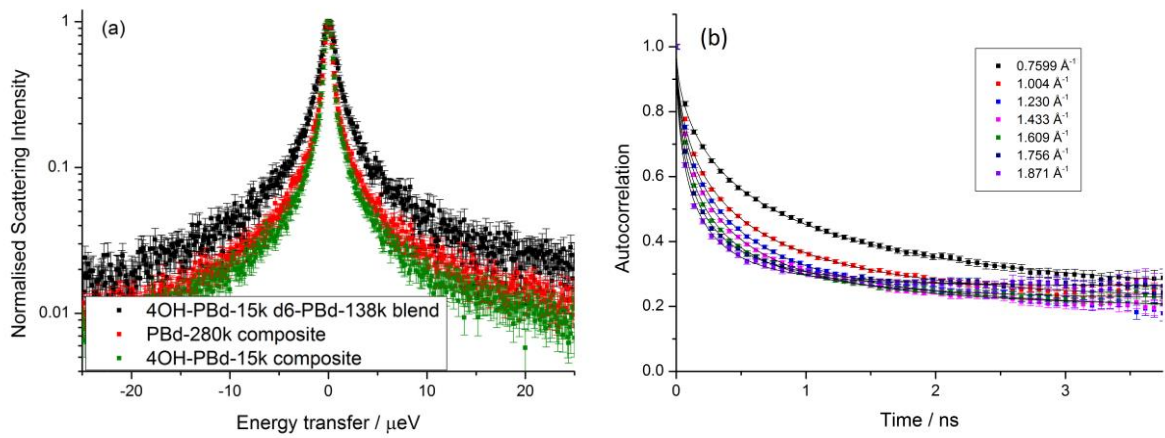
Figure 3.20: (a) Sample energy distributions, IN16B spectrometer, 280 K, Q: 1.23Å^{-1} (b) sample autocorrelation functions IN16B spectrometer 310 K

The primary tool used for analysis here was a fitted stretched exponential function, defined with a background term here as

$$I(Q,t) = A + (1 - A)e^{-\left(\frac{t}{\tau}\right)^{\beta}} \tag{3.13}$$

where I is the autocorrelation value, A is the background intensity, t is time, τ is the characteristic decay time, and β is the stretching exponent, beta. The background intensity is a measure of the proportion of the observed material that does not measurably move over the experimental timeframe. The characteristic decay time represents the average of the measured decay times in the system, inversely proportional to the rate at which components are moving. The stretching exponent defines the heterogeneity or distribution of the decay times and can take a value between 0 and 1. At a value of 1, a single decay time is present and the equation reduces to a standard exponential decay; as the beta value decreases toward zero, the distribution of decay times increases.

In polymer systems, this relation is referred to as a Kohlrausch-Williams-Watts or KWW function, and is useful due to the nature of amorphous polymer relaxation and motion. In an amorphous polymer melt there is no single characteristic decay time as each section is in a slightly different local environment, instead a distribution of relaxations is present. For most polymer systems above the glass transition the distribution is experimentally known to yield a beta value between 0.4 and 0.6. The KWW relation was fitted in Origin to the autocorrelation functions with least squares regression with the Levenberg Marquardt algorithm. The results of this fitting will be discussed in the quasi-elastic neutron scattering chapter.

4 Rheology of polybutadiene composites

4.1 Comparison of vulcanisation and peroxide crosslinking

Crosslinking was first patented by Charles Goodyear (US) and Thomas Hancock (UK) in 1845, using sulphur mixed into rubber gum then applying heat to cure the material, a method known as vulcanization. It was the discovery of vulcanization that led to the use of rubber as a structural material, and the development of accelerants in 1905 by George Oenslager only increased rubbers use. Further discoveries led to crosslinking of other polymers and the development of other crosslinking reagents, such as peroxides. Today many polymer systems are cross-linked, and it is a continually studied and vital area of polymer systems. Although industrially well-developed, scientific understanding of the microscopic processes is poor, and information on how crosslinking may interact with filler materials is limited; as such the micro and macroscopic effects of crosslinking need to be well characterised for the development and practical application of composite theory.

4.1.1 Benzoyl peroxide crosslinking

To examine the rate of the crosslinking reaction a sample containing PBd-300k (Sigma Aldrich) and benzoyl peroxide (Sigma Aldrich) was cured at 80˚C under nitrogen in an AR2000 rheometer environmental test chamber for five and a half hours. A stoichiometric ratio to achieve 100 monomer units per crosslink was used to ensure a measurable change in material properties with time. Figure 4.1 shows an increase of the storage modulus along with a decrease in the loss modulus over the course of the experiment, as expected from a crosslinking reaction. The reaction itself shows no incubation time as the storage modulus rapidly increases but slows with time, this implies the rate of the reaction is dependent on the concentration of benzoyl peroxide remaining and that the radical states are short-lived.
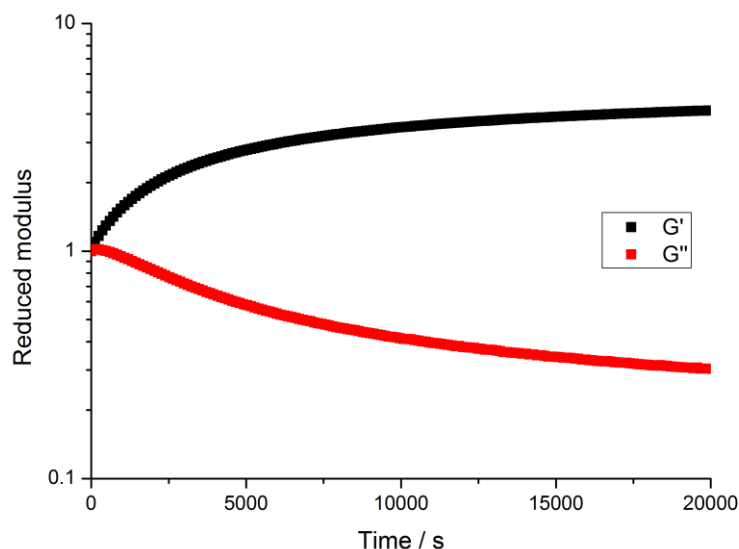
Figure 4.1: Curing of 100 monomer unit per xlink polybutadiene sample at 80˚C in nitrogen atmosphere, 1 rad/s

To examine the effect of network density on the rheological properties of long chain polybutadiene, samples containing various concentrations of benzoyl peroxide were prepared by solvent casting and curing in inert atmosphere for 3 hours at 80˚C. The concentrations were chosen to encompass crosslink densities ranging from a light network to the average entanglement length of the polymer. These benzoyl peroxide concentrations are given in the molar ratio of polybutadiene chain units to benzoyl peroxide.

The crosslinking yields a general increase of the storage modulus at low frequencies and a drop in the storage modulus at higher frequencies, shown in Figure 4.2. The increase can be attributed to the networked polymer matrix being unable to completely relax strains by reptation leading to an extended storage modulus plateau. The drop in modulus observed at high frequencies is from the benzoic acid products providing a plasticizing or diluent effect to the matrix. [11] What is notable is that even fairly light crosslinking yields large changes in the rheological properties as the largest modulus shift that occurs is between the linear (black) and 950 monomers per crosslink (red) polybutadiene samples. This is not unexpected as even this crosslink density still yields approximately four crosslinks per chain, enough to form a continuous network and prevent chain migration, with higher crosslink densities hindering relaxations to a greater extent.
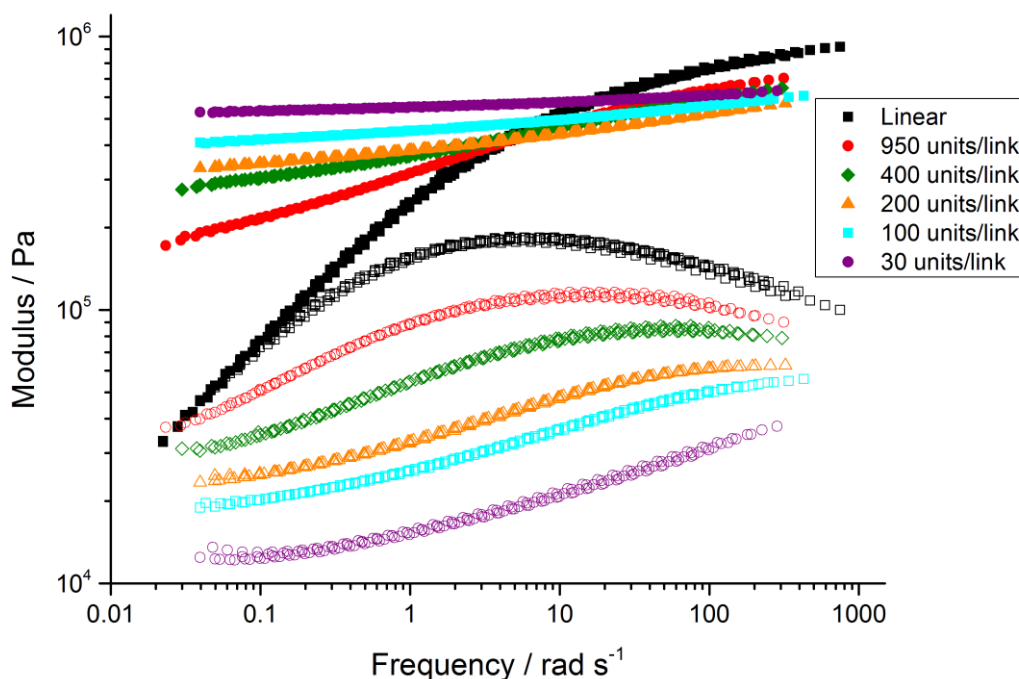
Figure 4.2: Cross-linked and linear PBd (M_w 310,000) modulus, G' (closed), G'' (open); listed in monomer units per crosslink ratio in legend, temperatures 273-303 K WLF shifted to 293 K reference temperature

Crosslinking also affects the loss modulus; the decrease in modulus with the increase in crosslink density is clearly visible, figure 4.2 (open), along with an apparent shift in the maximum to higher frequencies. The overall decrease in loss modulus is unsurprising as crosslinking prevents the dissipation of stored elastic energy via vicious flow; however the observed loss modulus peak shift requires more explanation. With light crosslinking the polymer matrix will contain a number of free chain segments which are able to dissipate energy. As the chain segments are shorter than the linear chains the time needed to fully relax the segment is less, hence the maxima occur at higher frequencies. This is supported by the relation between a calculated average chain end molecular weight and the maxima frequency, which is in agreement with theory for branches on star polymers and chain ends on cross-linked networks. [98]

Figure 4.3 shows a steady decrease in the phase angle, delta, with increasing crosslinking as polymer chain relaxation is hindered. The other notable feature is the presence of a peak in the angle at low crosslink densities; again this is from the effects of free chain segments or ends being able to reptate and release entanglements. At higher crosslink densities the maxima are not visible due to being outside the measurement range and decreasing in intensity as the quantity and average length of free chain segments decreases.
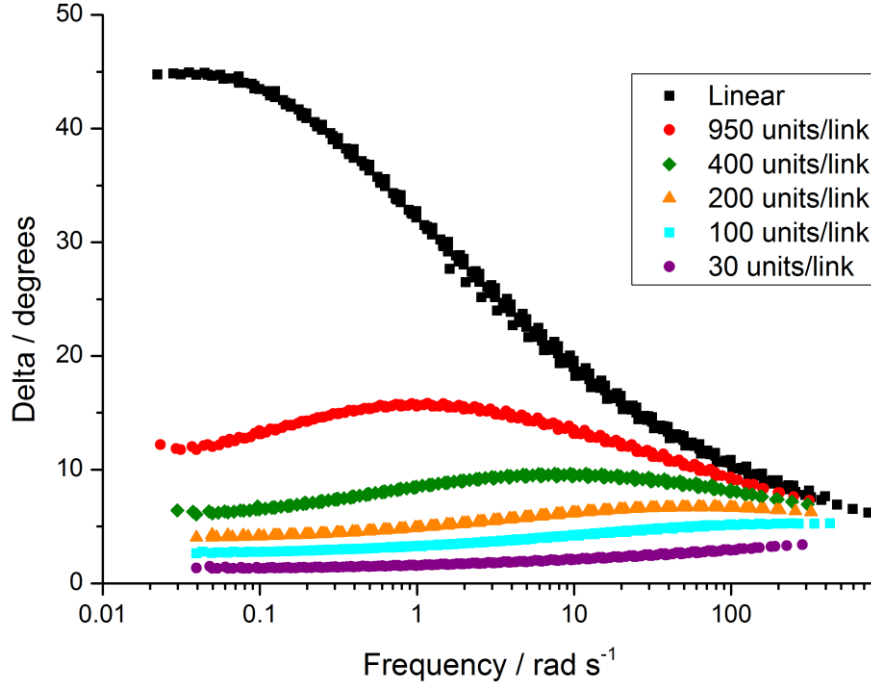
Figure 4.3: Delta vs frequency for different degrees of crosslinking, listed in monomer units per crosslink ratio in legend, temperatures 273-303 K WLF shifted to 293 K reference temperature

4.1.2 Solvent swelling tests of cross-linked rubber

Solvent swelling is a technique to measure the density of the permanent crosslinks in a polymer sample and remove small free chains from the matrix. The theory was derived from statistical mechanics by Flory and Rehner[99], who related the average molecular mass between crosslink sites to the polymer volume fraction, as shown below

$$-[\ln(1-v_2) + v_2 + \chi^2 v_2{}^2] = \frac{V_1}{\bar{v}M_c}\left(1 - \frac{2M_c}{M}\right)\left(v_2^{\frac{1}{3}} - \frac{v_2}{2}\right) \qquad (4.1)$$

Where v_2 is the polymer volume fraction, $\bar{v}$ is the polymer specific volume, V_1 is the solvent molar volume, χ is the Flory Huggins parameter, M is the uncross-linked molar mass, and M_c is the average molar mass between crosslinks [100]. This can be rearranged to

$$M_c = \left[\frac{-[\ln(1-v_2) + v_2 + \chi^2 v_2{}^2]}{\left(v_2^{\frac{1}{3}} - \frac{v_2}{2}\right)\frac{V_1}{\bar{v}}} + \frac{2}{M}\right]^{-1} \qquad (4.2)$$

This relation is sensitive to the solvent-polymer interaction parameter and the uncross-linked molar mass of the polymer; as such accurate values are required for readings.

Cross-linked polybutadiene samples were weighed and placed in a toluene bath for 24 hours, after which they were removed and weighed again. The samples were weighed after drying to

check for material loss. From the difference in mass the amount of solvent absorbed by the sample and the polymer volume fraction was calculated.

From equation (5.2) the number of repeat units per crosslink can be calculated; the results are shown in figure 4.4. The data suggest a good correlation between the predicted crosslink density from peroxide content and the value determined by solvent swelling with no major deviations from a linear trend. Linear regression of the points yields a slope of 1.14 ± 0.06 and an intercept of 2 ± 37. An intercept of zero is expected from theory, and the slope can be interpreted as a measurement of the peroxide reaction yield, in this case $88 \pm 5\%$ yield. It is difficult to say if this yield is due to uninitiated peroxide or side reactions, however there is still a clear relation between the quantity of peroxide and crosslink density that can be controlled and used as a guide for other systems.
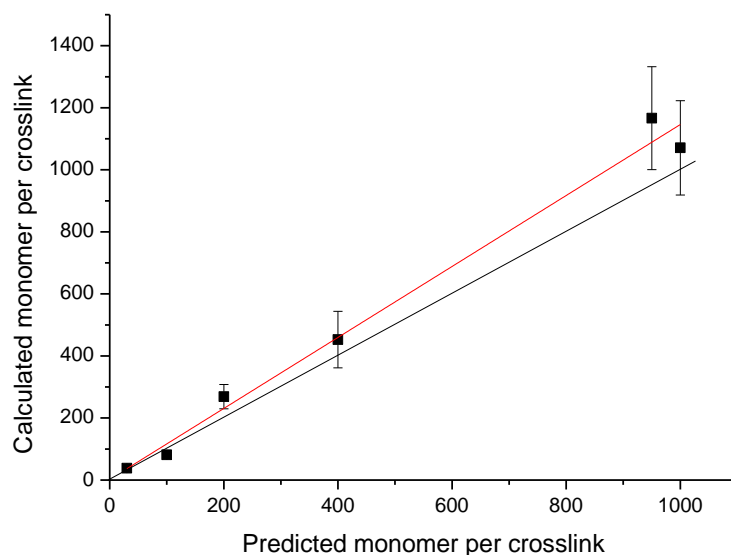
Figure 4.4: Predicted monomer units between chains against calculated swelling test number for different peroxide concentrations, red line is a line of best fit determined by least squares regression, black line is 100% yield of peroxide crosslink reaction

4.1.3 Sulphur crosslinking

A reaction was performed at 160° C in an AR2000 environmental test chamber under nitrogen atmosphere, the formulation of the vulcanisation mixture was as detailed in the experimental with 300k polybutadiene.

Similar to the peroxide cross-linking for the sulphur sample there is a visible increase and decrease in the storage and loss moduli, respectively, shown in figure 4.5. However there is an incubation period until 1000-1500 seconds where the moduli do not rapidly change, this is in

agreement with reports for accelerated vulcanisation systems[101, 102] as the induction period of the reaction. Also, the presence of a plateau in the moduli at the end of the experiment suggests the reaction is completed over the course of an hour.
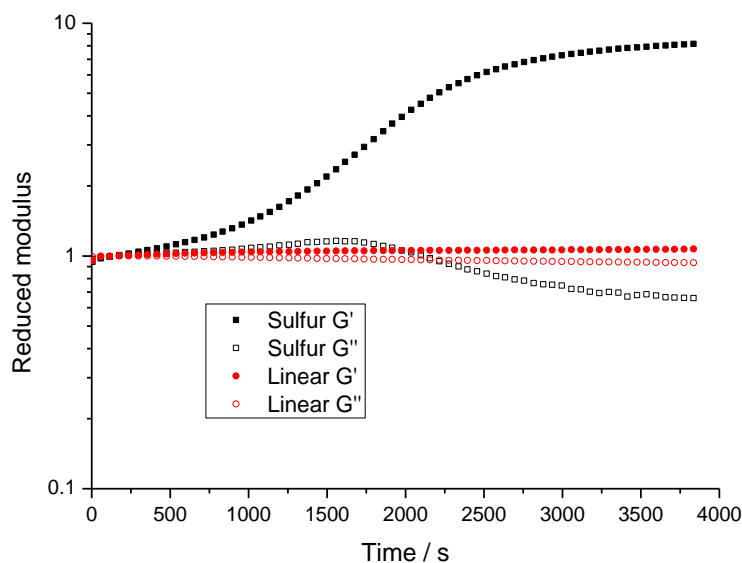
Figure 4.5: Curing of sulphur sample (black) and pure linear PBd-300k (red) at 160 ˚C in nitrogen atmosphere, 1 Hz, storage and loss moduli (full and hollow) have been reduced for ease of comparison

A control sample of pure 200k polybutadiene was also run to quantify if there was any uninitiated crosslinking occurring at these temperatures as polybutadiene is known to oxidize over time at and above room temperatures. There is a minor shift in the samples rheological properties with time suggesting the presence of some changes, possibly auto crosslinking, however this change is negligible compared with the shift seen with the sulphur containing sample. Given this data it is reasonable to assume that the crosslinking in the vulcanised sample is due to sulphur bridging and not self-crosslinking.

Rheological test results of the sulphur cross-linked matrix were compared with the data gathered on the peroxide based networks. Equivalent properties were found between the 200 monomer units per crosslink peroxide and the sulphur sample, evidencing a similar network density. This result is backed by solvent swelling tests, from which the monomer units per crosslink was determined to be 211 ± 30 for the sulphur bonded network. Together these indicate that the chemical nature of these permanent crosslinks has little to no effect on the rheological properties over the range observed and that samples prepared by both methods are comparable. The behaviour independent of crosslink type suggests that it is the inhibition of the chain motion that yields the greatest effect on the material properties.
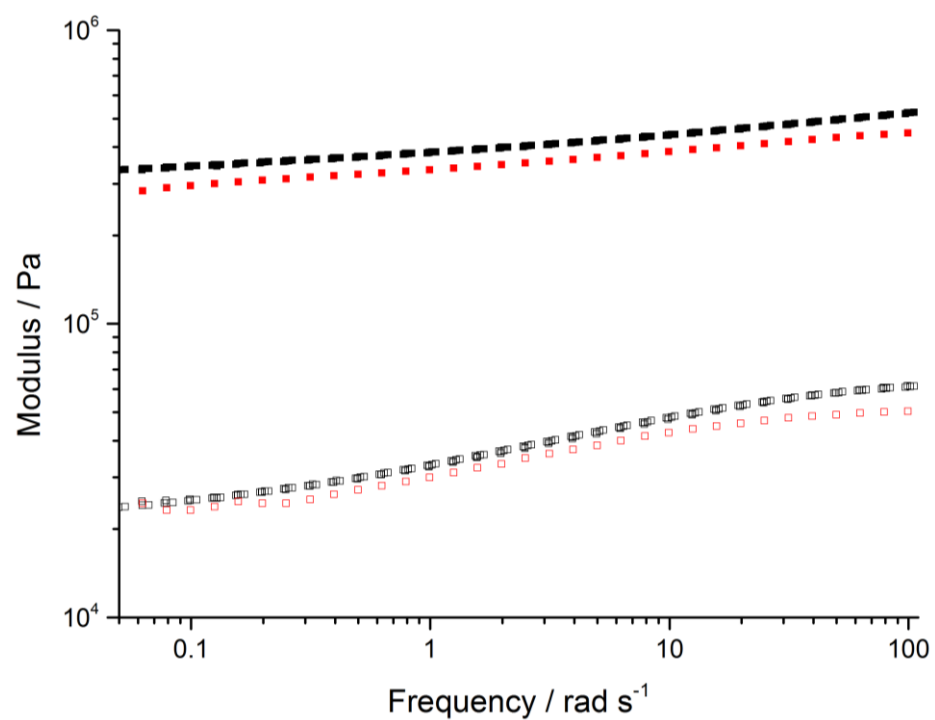
Figure 4.6: Storage (full) and loss (hollow) moduli of 200m per xlink peroxide (black) and sulphur (red) cross-linked samples

4.2 Reinforcement of neat polybutadiene with filler

The addition of inorganic and carbon fillers to rubber matrices is a common but poorly understood technique in materials science. In relation to tyre manufacture, the addition of filler began with carbon black in the 1940s, with silica and clay coming as an alternative in the 1990s. Used to improve modulus and wear resistance, the presence of the particles leads to emergent rheological phenomena such as the Payne and Mullins effects. As the proposed explanations of the macroscopic phenomena rely on microscopic interactions, it is important to fully characterise the nature of the filler material at both length-scales.

4.2.1 Filler comparison

To compare the rheological properties of the various fillers, sample sets containing different fractions of filler were formed. The fillers chosen were carbon black, precipitated silica, and Stöber silica with 50 nm radius determined by DLS. To disperse the filler particles, solvent casting along with sonication was performed. The solvent was allowed to evaporate off and the composite was pressed into disks for testing. The AR2000 rheometer with peltier stage was used, the temperature was set to 20˚C, strain was held at 0.1%, and a frequency sweep from 0.05 to 10 Hz was performed.

Unsurprisingly there is an increase in the storage modulus with the addition of filler particles in all samples tested. Of note is that higher concentrations of the fillers in all the composites yield a shift in the shape of the modulus toward what would be expected of an elastic solid. This implies that at these concentrations a filler network is controlling the rheological properties. The other notable observation involves the loss moduli; for the carbon black and Stöber silica samples the loss modulus continues to increase with filler concentration while in the precipitated silica, figure 4.7a, the modulus plateaus at 10% volume fraction. The presence of a strong network could be the cause of the plateau by preventing relaxation through structural rearrangement in the case of the precipitated silica filler.
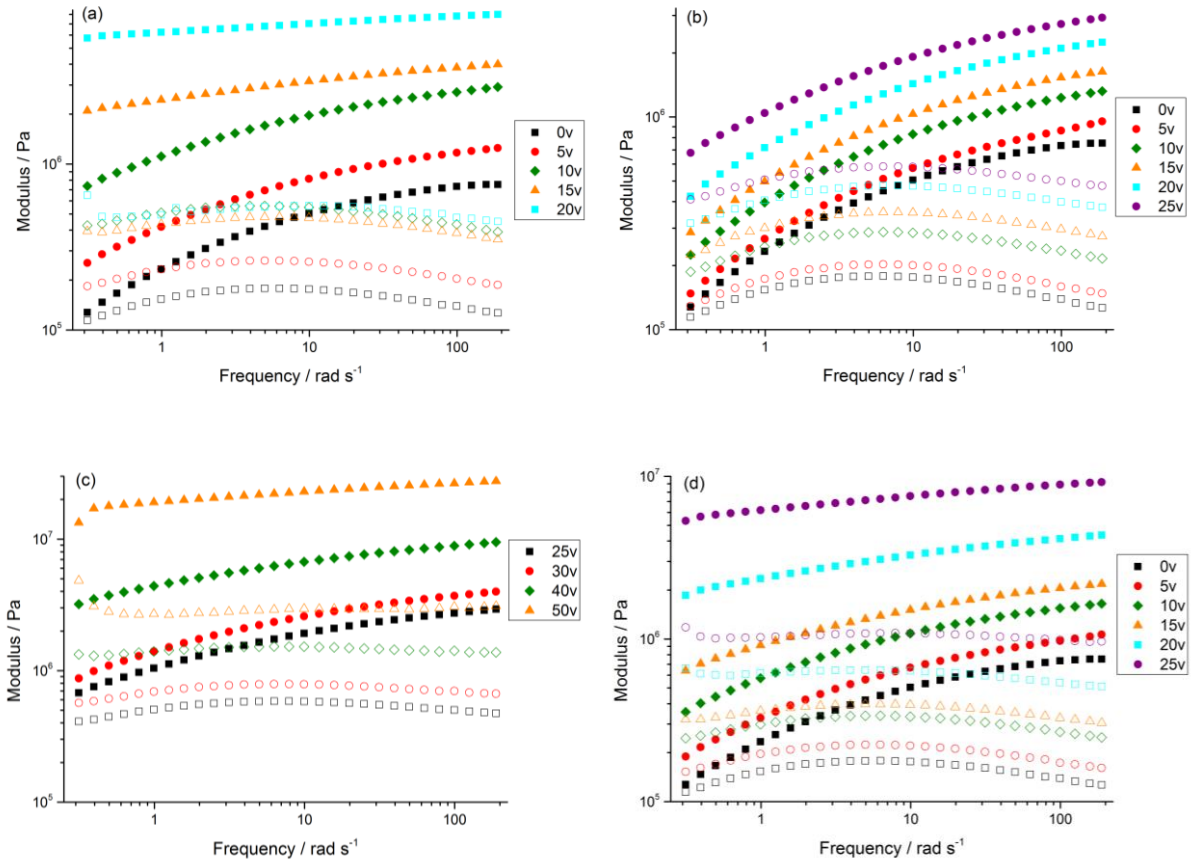
Figure 4.7: Storage (full) and loss (hollow) moduli for precipitated silica (a), Stöber silica (b, c), and carbon black (d) at various volume percents given in the legend, neat linear 200k polybutadiene is included on each graph as a baseline

The presence of the filler network controlling the physical properties of the material may be the result of a percolation phenomenon for the particles. If this is similar to the gel point, such as for sol-gel materials, then the frequency dependence of the storage and loss moduli should be equal, and the viscoelastic nature of the material independent of the probe frequency with an ideal system. From the $\tan(\delta)$ plots in figure 4.8, there is a clear shift in behaviour toward frequency independence for both the precipitated and Stöber silica at 0.15 and 0.3 volume fraction respectively. This shift akin to a gel transition suggests the possible presence of a percolating network at higher volume fractions. For the Stöber silica this is in agreement with the finding of a percolation threshold of 0.28 for hard spheres. [26] In the case of the carbon black no clear point is visible although a shift is present, which suggests there is no single threshold for this filler. This may be attributed to the greater compatibility of the carbon black and the polybutadiene matrix, which should aid in the dispersal of the filler. In relation to the cluster-cluster aggregation theory mentioned in the literature, after percolation of the filler material the moduli should follow power law dependence. To examine this, plots of the reduced moduli were formed

and plotted with expected power law relations above this shift in tan(δ), it is important to note that these relation were not fit to the data given the lack of points at high volume fractions.
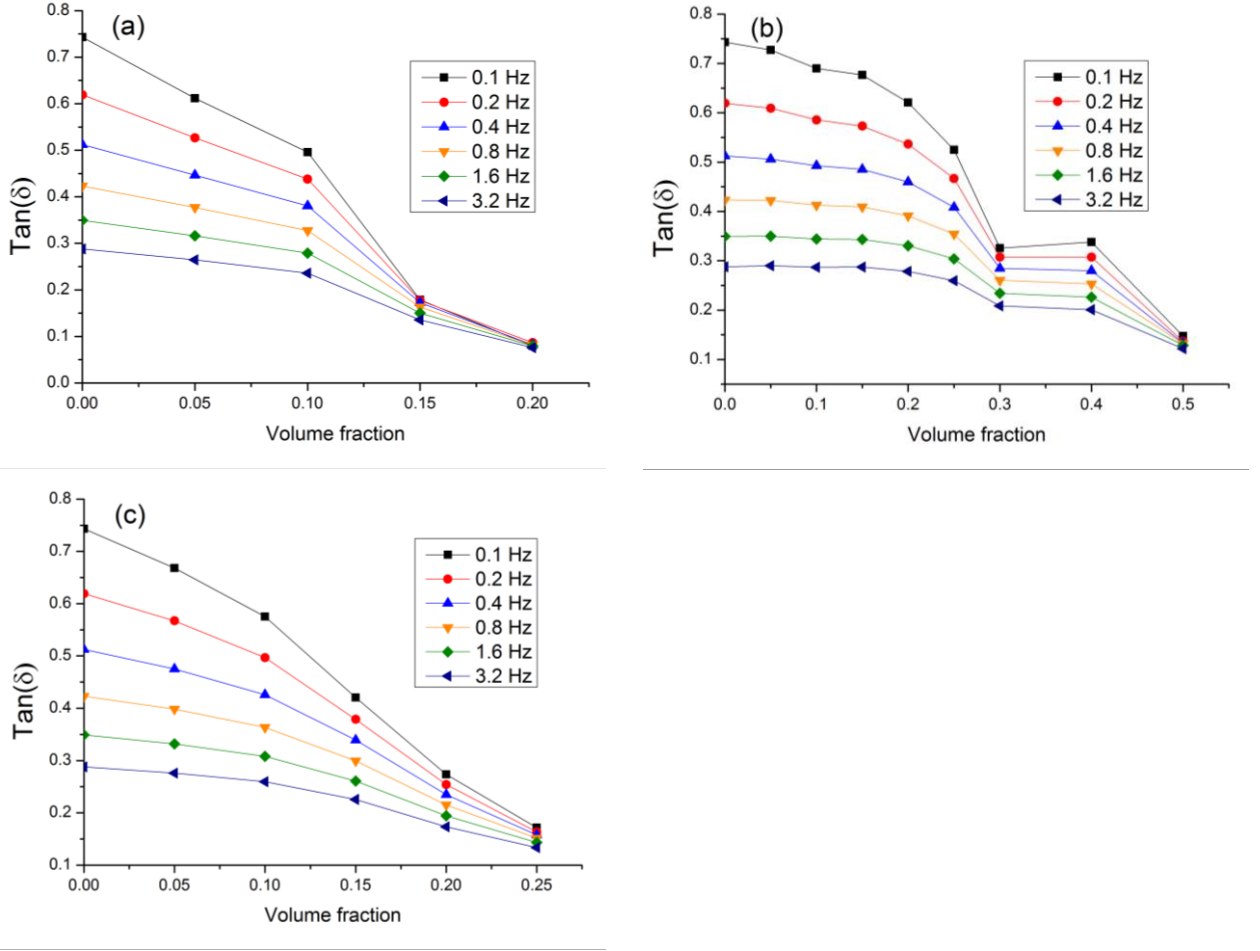
Figure 4.8: Tan(δ) against volume fraction at different sample frequencies for precipitated silica (a), Stöber silica (b), and carbon black (d)

The plots of the reduced moduli G_r; defined as

$$G_r = \frac{G_v}{G_n} \tag{4.4}$$

where G_v is composite modulus, and G_n is the neat matrix modulus; allow for comparison with Guth's (section 2.2) theory, moduli values were taken at 1 Hz for all cases. Plotted as the green points on figure 4.9, it is clear that beyond 0.05 volume fraction of filler samples diverge from this theory. This is not completely unexpected, Guth himself noted that the relation only held in regions before significant networking developed above approximately 0.1 volume fraction. However even Stöber silica, which is the most physically similar the Guth model, shows divergence at 0.1 volume fraction. The increasing nature of the divergence in all cases suggests additional sources of reinforcement, a possibility being the formation of filler networks. With the fractally structured fillers, carbon black and precipitated silica, this is probable as other works

have found that the percolation threshold is lower for more anisotropic particle shapes, with reported experimental values of 0.03 and 0.15 for precipitated silica and carbon black respectively [30, 103]. There appears to be rough agreement with these findings, as there is a notable change in gradient about 0.15 volume fraction for the carbon black, although no effect is seen in the tan(δ) plot. But long range percolation is not possible for Stöber silica where the particle concentrations are lower than the percolation threshold of 0.28, which suggests the presence of another mechanism such as glassy layers or polymer bridges[26]. A single chain polymer bridge is unlikely at lower concentrations as calculations place the mean inter-particle distances to be greater than the mean 200k polybutadiene end to end length until 0.18 volume fraction. It is worth noting that the reinforcement of the moduli appears to be independent of frequency, figure 4.9c/d, thus in future sections only 1 Hz values will be examined.
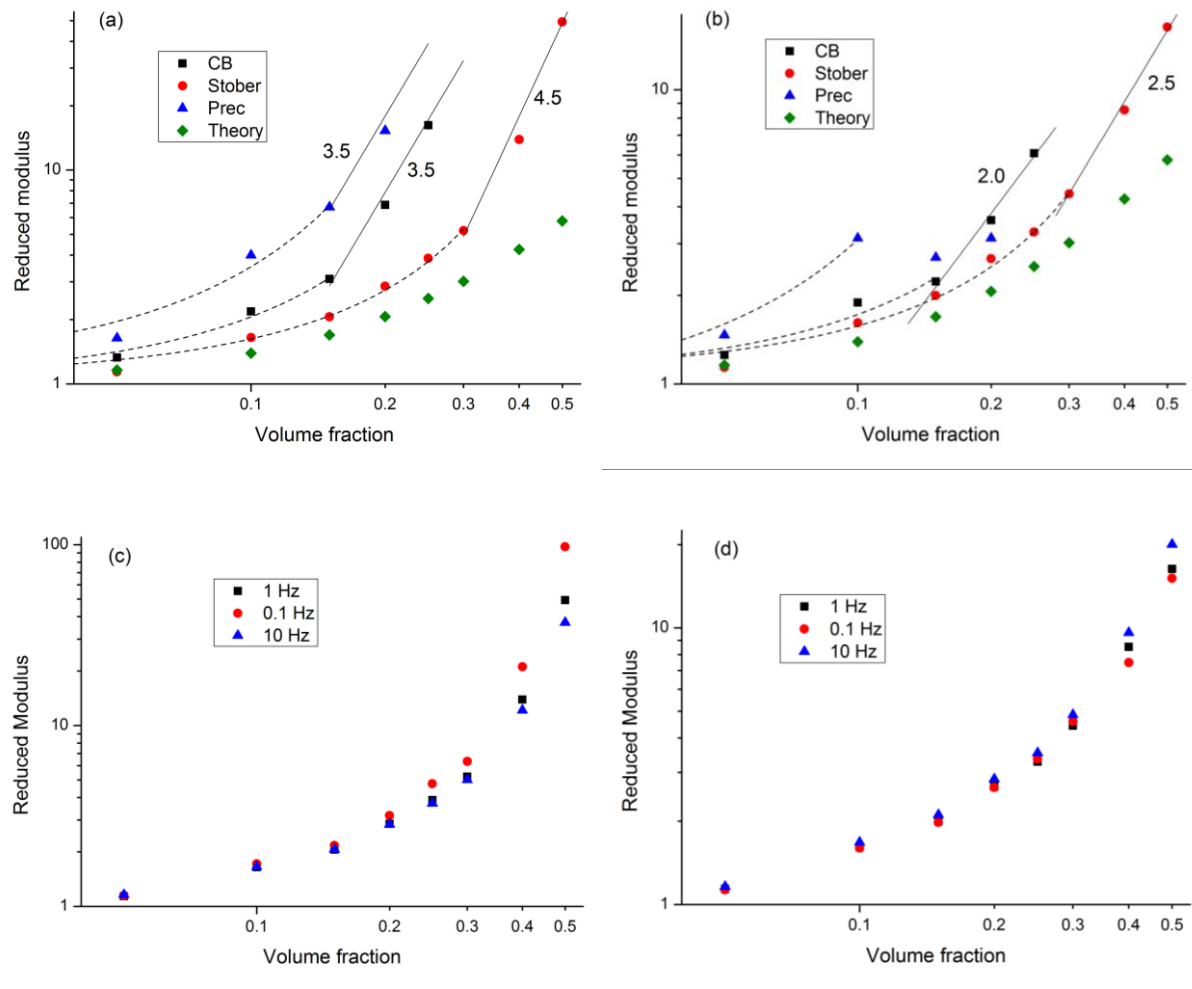
Figure 4.9: Reduced storage (a) and loss (b) moduli at 1 Hz for the various fillers and for Guth hydrodynamic theory, figures include fitted Krieger relations (dashed), possible power law relations (solid) for selected portions of the data; Reduced storage (c) and loss (d) moduli at different frequencies for Stöber silica

Another notable and striking feature of the data is the presence of what appears to be an exponential relation between reinforcement and volume fraction before a shift in slope. It is difficult to say with certainty for the carbon black and precipitated silica fillers whether this trend is truly exponential in nature due to limited points and onset of possible percolation; however it is apparent this is the case with the Stöber silica due to the range of volume fractions testable. Such trends are not unprecedented in previous rheological experiments, in particular work on particle suspensions outside the dilute regime. Mooney noted these trends and derived an exponential function as follows,

$$\eta_r = exp\left(\frac{B\varphi_c}{1 - \frac{\varphi}{\varphi_c}}\right) \qquad (4.5)$$

where η_r is the reduced viscosity, B is a numerical factor, φ is the volume fraction, and φ_c is the maximum obtainable or critical volume fraction.[21] Other work by Krieger and Dougherty determined a theoretical relation as

$$\eta_r = \left(1 - \frac{\varphi}{\varphi_c}\right)^{-B\varphi_c} \qquad (4.6)$$

with the same term definitions as for Mooney's relation, equation 4.5. [22] Of importance to both equations is B, which is equivalent to the intrinsic viscosity, $[\eta]$, or the first order coefficient in a viral relation. Einstein predicted a value of 2.5 for a dispersion of freely moving hard spheres, a value supported by Guth's and others work. These expressions are in terms of the viscosity, however as with Guth's predictions, these terms can be applied to the moduli as the two properties are analogous.[2] Below the percolation threshold, these predictions can be tested; fitting of the Krieger relation with a numerical prefactor, C, was performed on the moduli values at and below percolation for the carbon black and Stöber silica, the critical volume fraction was held at 0.64 as for random close packing. The parameters are in appendix 10.1, and fits are shown on figure 4.9. For the Stöber silica, a B value of 4.00 ± 0.14 was found, this is in disagreement with Einstein's prediction. However, inhibition of the sphere's rotation yields a value of 4 as calculated by Brenner, and would be applicable given the nature of the polybutadiene as a rubber.[104]

Fitting of the carbon black data yielded a B value of 6.68 ± 0.47, the fractal structure of the carbon black material is the cause of this greater power value. Modifying the volume fraction to take account of a reaction limited aggregation structure (D = 2.23) using fractal scaling properties to give an effective volume fraction results in a B value of 4.10 ± 0.29, which agrees with Brenner's predictions. A similar effect is noted for the precipitated silica, with an unmodified B value of 14.2 ± 1.7, but with effective volume modification from diffusion limited

aggregates (D = 1.8), B is 4.91 ± 0.58. This is higher than the non-rotating sphere predictions, which suggests further reinforcement from other sources or inclusion of part of the networked filler regime in the fits.

Above the percolation threshold direct continuous particle networking is possible for the fillers and is evidenced by the greater increase of the storage modulus at higher filler concentrations as well as a possible change in trend to a power relation, figure 4.9a. For the carbon black and precipitated silica samples, a power trend predicted by cluster-cluster aggregation theory for diffusion limited aggregation. For the carbon black this is at odds with the observation of the reaction limited aggregation below the percolation limit, however this discrepancy may be from the difference in the local aggregate structure compared with the network structure, and the lack of percolation as defined by the model.

For the Stöber silica systems the case is different; the modulus trend observed is approximately a $\varphi^{4.5}$ dependence.[36] This has been observed before by Cassagnau et al. with fumed silica systems and was attributed to a non-fluctuating fractal structure over the experimental timescale.[30, 105] In this case, however, we assume fluctuations are still able to occur as nothing is binding the silica spheres, and the greater dependence is instead due to the increased compactness of the network structure.[35] A reaction limited network structure yields power dependences of approximately 4.5 as observed with the Stöber silica, evidencing the presence of compact aggregates of the silica spheres in the matrix.

4.2.2 Effect of end functionalised polybutadiene

The hydroxyl end functional polybutadiene used in this experiment is known to segregate toward polar surfaces when placed into a blend, and is thought to aid in the dispersion of silica filler through steric stabilisation.[85] To examine the effect of this polymer on the rheological properties of the composites, samples composed of equal amounts (50:50) of linear 200k polybutadiene and 15k OH-polybutadiene in matrix were rheologically tested. As before, volume fractions of the fillers ranged from 0 to 25%, samples were solvent cast, and the test parameters were kept constant.

The blend of 15k 4OH and 310k linear PBd yields a modulus lower than that of a simple combination. As both polymers are above the molecular entanglement length no definite theoretical relation can be determined. However, it has been noted that combination of liquid viscosities to form a blend can be treated empirically by a cubic average, given as

$$\eta_r^{1/3} = \eta_1^{1/3} + \eta_2^{1/3} \qquad (4.7)$$

where the η_r is the resultant viscosity, and η_1 and η_2 are the viscosities of the components. [106] From figure 4.10, this appears to provide a reasonable approximation for the resultant behaviour; as such, there does not appear to be any additional interactions between the two polymer components and blend can be treated as a constant for these tests.
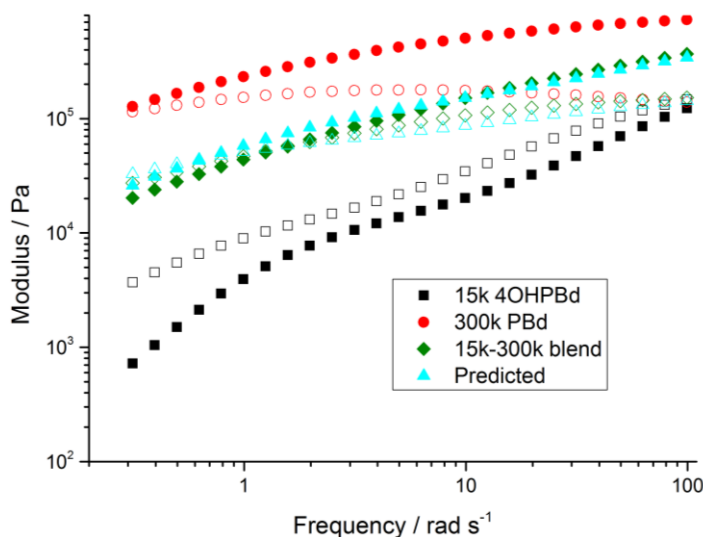
Figure 4.10: Measured 310k PBd, 15k 4OHPBd, and 50:50 blend along with calculated cubic power combination, solid G', hollow G''

A standard increasing plateau modulus with filler concentration is observed in all the sets, however important differences and phenomena are observed when these results are compared to those from samples without end-functionalised polymer. In the carbon black samples there is a changeover between 15 and 20 percent filler volume, with the higher carbon black content samples yielding similar moduli to the non-functionalised counterparts, shown in figure 4.11a. Again this represents a shift from polymer to filler defining the material characteristics, and is due to the percolation of the filler network through the material. The loss moduli do show minor differences however, suggesting the polymer matrix still affects the properties. The relative similarity of the carbon black is evidence of non-binding of the end functional polymer, which would be expected given the non-polar nature of the carbon surface.
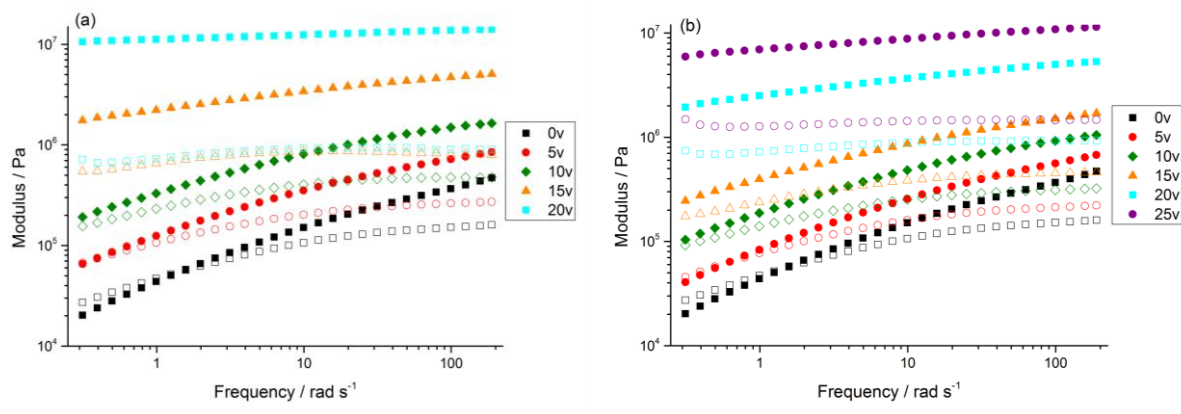
Figure 4.11: Storage (full) and loss (hollow) moduli for precipitated silica (a), and carbon black (b), linear 310k polybutadiene/15k 4OHPBd (50:50) is included on each graph as a baseline
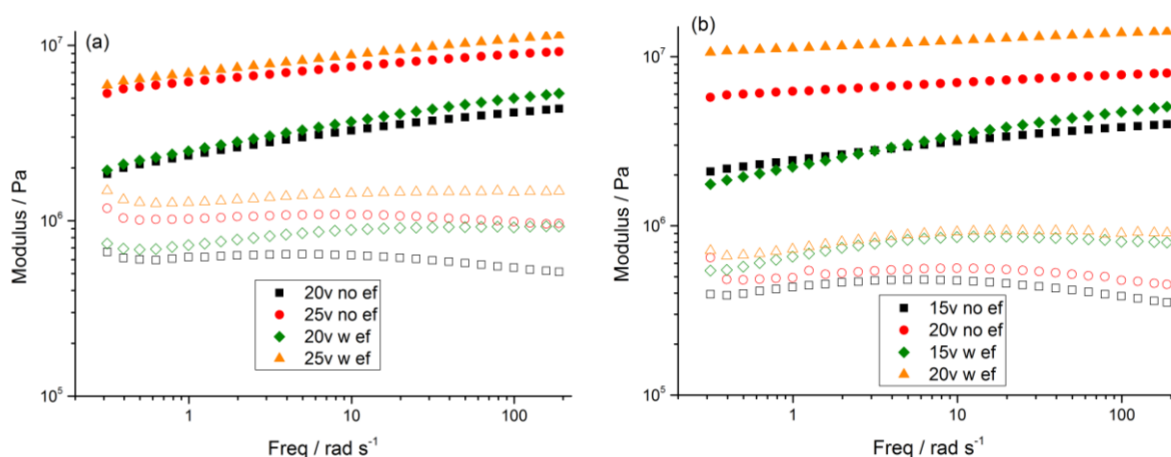
Figure 4.12: Comparison of carbon black (a) and precipitated silica (b) fillers with and without hydroxyl end functional polybutadiene

The precipitated silica also yields the conversion between polymer and filler controlled properties between 10 and 15% filler volume. However there is less similarity in the moduli of the samples, figure 4.12b, which hints that the end functional polybutadiene does aid in the dispersion of the filler. Of note, at 20% volume the storage modulus is higher in the composite with end functional polymer. A reasonable explanation is that the dispersion of the filler by the polymer yields an improved network at high concentrations by breaking apart dense agglomerates into a more open space filling structure; however the polymer brush layer cannot completely sterically stabilise the filler, yielding increased networking contacts. The increased contacts between the fillers in this scenario would improve the storage modulus of the material, but would only be possible at higher filler concentrations as the brush density decreases. An open structure would also have fewer barriers to contact breakages as the bridges between aggregates are thinner, as well as the end functional polymer decreasing the energy cost of the break, yielding the increased loss modulus observed.
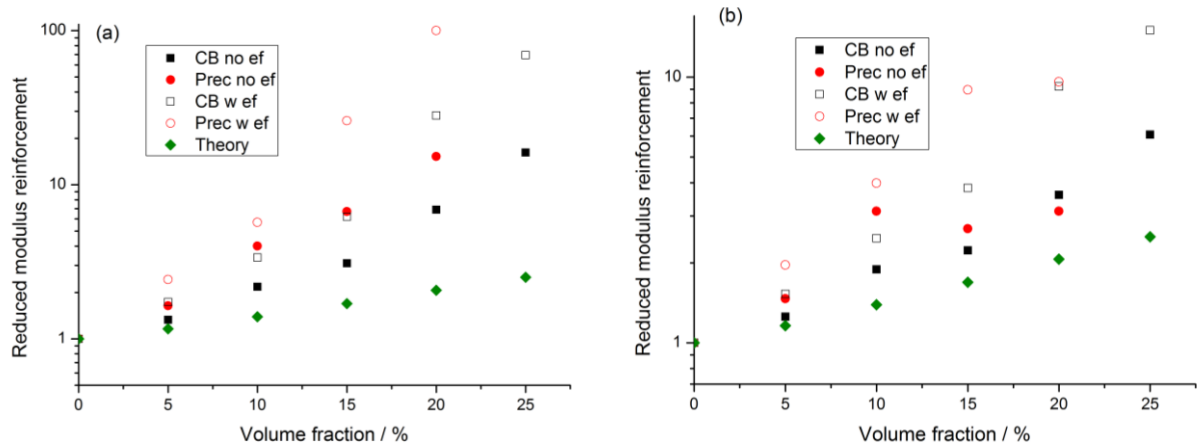
Figure 4.13: Reduced storage and loss moduli for carbon black and precipitated silica composites with and without 15k end functional polybutadiene, sample frequency 1 Hz
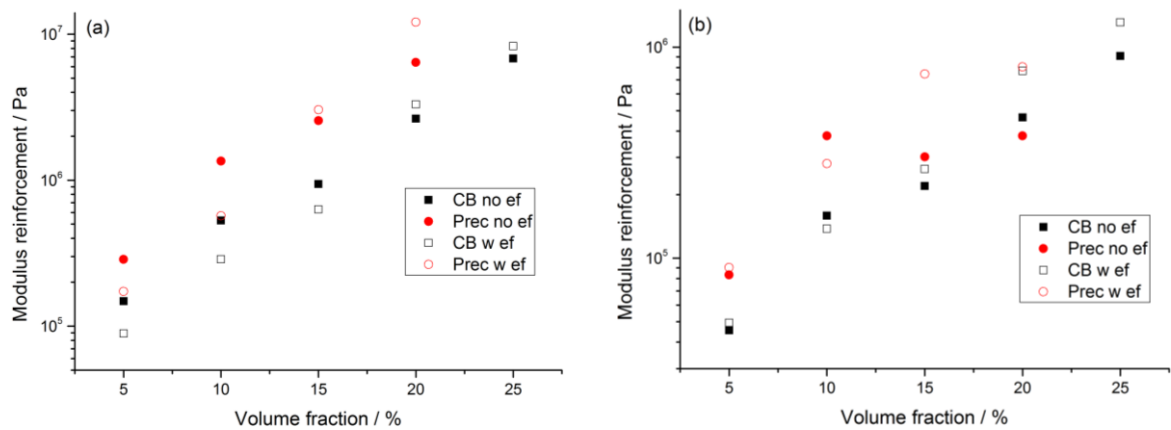
Figure 4.14: Storage (a) and loss (b) modulus reinforcement for carbon black and precipitated silica, sample frequency 1 Hz

With the reduction of the moduli there appears to be a general trend of greater modulus growth with the inclusion of the hydroxylated polymer. An argument can be made that this is an artefact of the calculations; greater relative reinforcement would be expected as the initial polymer blend modulus is lower. This is partly backed by the relative modulus increases, shown in figure 4.14. Comparison of the moduli difference finds that below 15% filler concentrations, the non-functionalised composites yield greater reinforcement in both moduli. At higher concentrations the trend is no longer present and samples have similar moduli shifts, as previously noted with the non-functionalised silica sample.

However, standard theories on composites state that a proportional percentage modulus growth dependent on the starting neat matrix is expected rather than the trend shown here. The observed behaviour can be explained with the filler network dominating the composite response.

The general increase of the moduli with Stöber silica content is similar to the trend with the other fillers, but there is a key difference. Although the magnitude of the reinforcement diverges from hydrodynamic theory, the moduli growth is related to the neat matrix modulus, as can be seen in figure 4.16. There is also no clear shift in rheological behaviour with higher filler content in frequency sweeps of the composites in figure 4.15. Considering the precipitated silica samples this would imply that the observed difference is a result of the differences filler structure rather than the surface properties. The spherical Stöber silica does not form a percolating network until approximately 28% volume fraction and its shape prevents the possibility of sterically induced jamming, while fractal structure of the precipitated silica causes network formation at lower concentrations and the possibility of jammed aggregates.
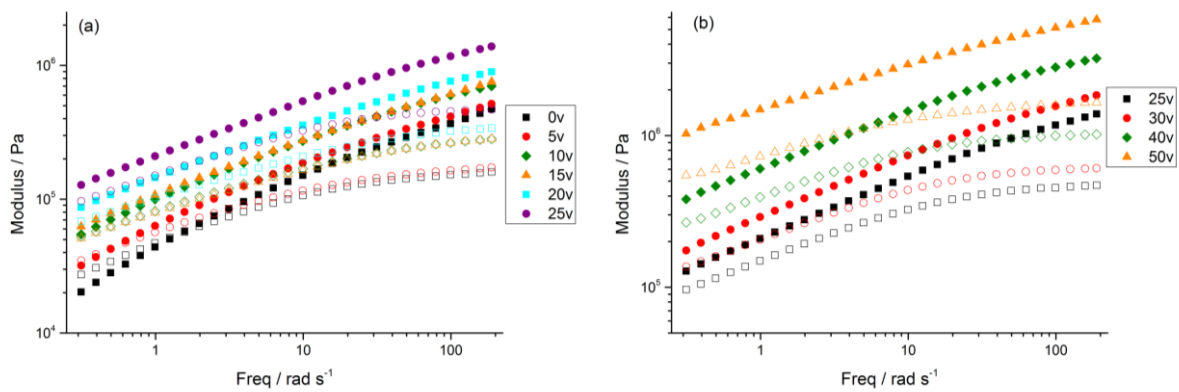
Figure 4.15: Frequency sweeps of Stöber silica composites at low (a) and high (b) loading with 15k 4OHPBd blend
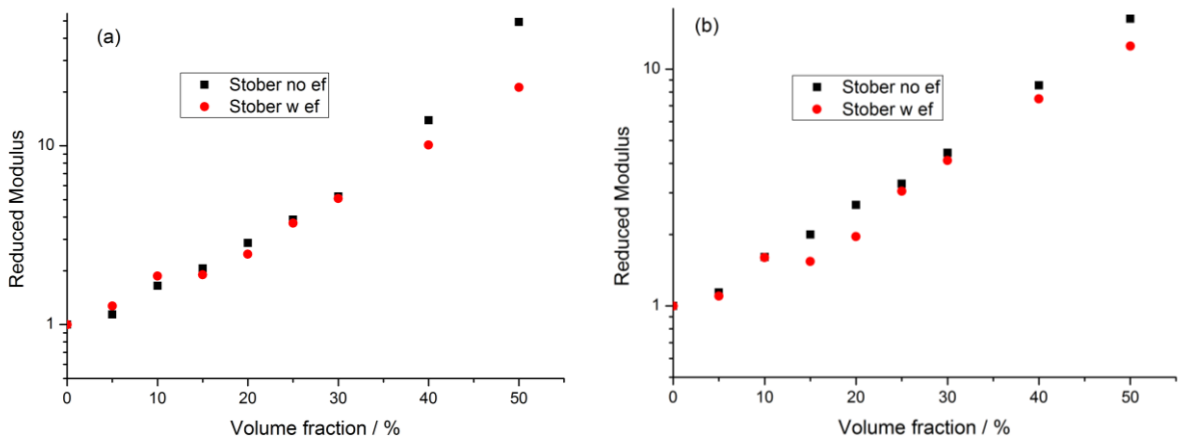
Figure 4.16: Comparison of (a) reduced storage moduli at 1 Hz for Stöber silica (b) reduced loss moduli at 1 Hz for Stöber silica

There is also divergence compared with the non-end functional samples, figure 4.16a, and this indicates the prevention of network formation that was found in the unmodified case. This is the opposite of the behaviour for the precipitated silica composite samples, where it was suggested

that the end functional polybutadiene aided in the formation of a network at high filler content. But unlike the precipitated silica, the Stöber silica does not have a primary fractal structure which aids percolation, and the relative particle surface area is lower, which means the possibility of an inadequate polymer brush forming is unlikely. Thus the end functional polymer still fully disperses the Stöber silica and prevents network formation.
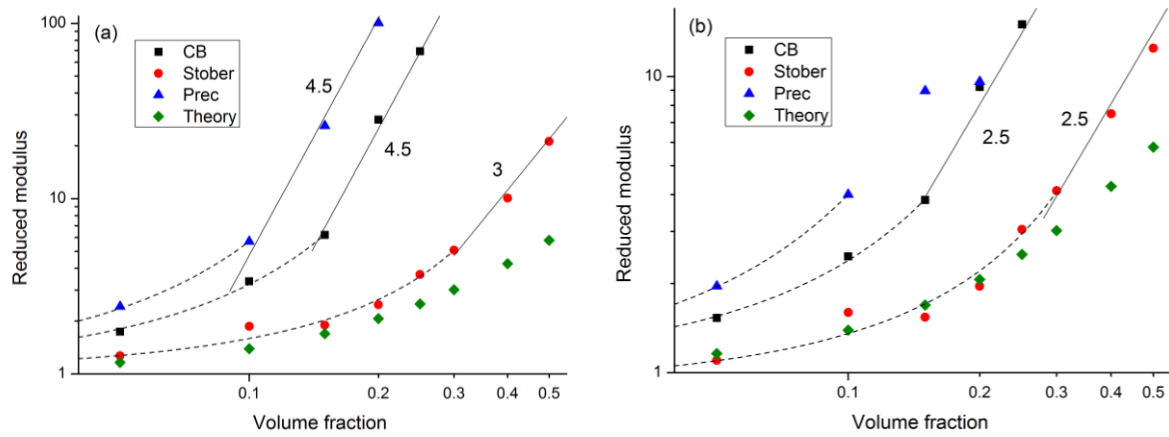
Figure 4.17: Reduced storage (a) and loss (b) modulus at 1 Hz, includes fitted Krieger relations and possible power law trend lines for portions of the linear 310k polybutadiene/15k 4OHPBd data

As with the unmodified samples, the two regimes before and after percolation have been fitted with a Krieger and power law relation, respectively. The B value in the Krieger relation was determined as 3.9 ± 0.2, 15.2 ± 0.5, and 10.4 ± 0.3; for Stöber silica, precipitated silica, and carbon black, respectively. The addition of the 15k 4OHPBd does not appear to have affected the nature of the Stöber silica interactions before percolation given the similarity in the constants, 4.00 ± 0.14 and 3.9 ± 0.2; as such the model devised by Brenner for non-rotating particles holds.

Conversion of the values using the fractal scaling concept yields a B value of 5.17 ± 0.16 for precipitated silica and a value of 5.71 ± 0.18 for the carbon black. As with the Stöber silica, the precipitated silica bonding nature does not appear to have been affected by the additive. This hints that the trend of increased reinforcement, figure 4.13, below percolation is due to numerical methods. In the case of the carbon black, however, there does appear to be a significant shift in behaviour with the additive. This may be considered unusual, as the polar group on the chain should not bind with the carbon black surface, but the presence of these polar hydroxyl groups in the matrix may force the carbon black particles into locally aggregated structures yielding a fractal formation that would increase the power dependence. The effect of matrix polarity on filler dispersion has been documented before by Stöckelhuber et al., and the phenomenon seen here is in agreement with their findings.[92]

After the percolation threshold is reached, power law behaviour is observed in all three samples. The increase of the exponential from 3.5 to 4.5 with the end functional polybutadiene is present in the precipitated silica and carbon black, while the Stöber silica relation decreases from 4.5 to 3.0. For the carbon black this is a continuation of the trend seen before percolation, with the present polar groups forcing the filler into a denser structure with a similar fractal dimension to reaction limited aggregation, ~2.2, which yields greater power dependence. This is not the case with the precipitated silica, as the increased loss modulus growth mentioned earlier suggests a more open network capable of rearrangement. While this open network allows for easier contact breakages in the structure it may prevent large scale fluctuations due to steric hindrances. A non-fluctuating fractal structure would result in the 4.5 power dependence observed in the system[30].

The decrease in the Stöber silica exponent is from the prevention of a larger network structure forming in the matrix. Calculations with CCA theory yield an expected power trend of 3 in the case of no contact between reaction limited aggregate structures. This supports the theory of the dispersal of the silica by steric stabilisation.

4.3   Reinforcement of cross-linked polybutadiene with filler

As many polymer products are cross-linked and contain filler materials, it is important to examine the interplay, if any, between the two modifications. The sulphur crosslinking method (4.2.3) was chosen for all composite samples due to its repeatability and production of durable samples. Filler and crosslinking components were dispersed by sonication and solvent casting from toluene, curing was performed at 160˚ C within a heat press. Filler material concentrations to complement the non-crosslinked samples were chosen, and the effect of the addition of end functional polybutadiene was also investigated.

4.3.1   Study of sulphur cross linked samples without end functional polybutadiene

Frequency sweeps of the cross-linked composites are visible in figure 4.18, along with a neat vulcanised polybutadiene baseline. The changes in material response with increasing filler concentration are subtle compared with those seen in the uncured samples, figure 4.7. In part, this is due to the cross-linked polymer being elastic and the moduli being almost independent of the oscillation frequency in the range measured.
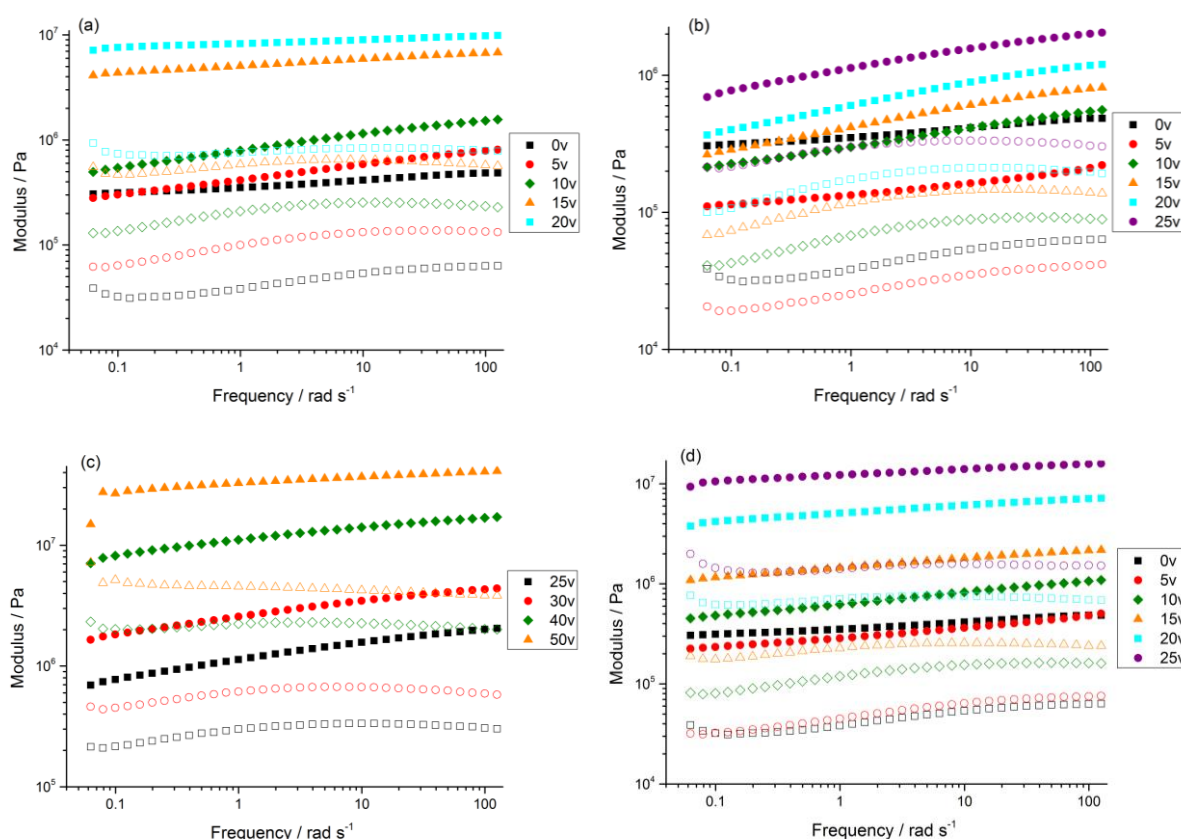
Figure 4.18: Storage (full) and loss (hollow) moduli for precipitated silica (a), Stöber silica (b, c), and carbon black (d) at various volume fractions, crosslinked linear 200k polybutadiene is included on each graph as a baseline

The shift in the curve structure at higher filler concentrations is present, although less pronounced than in the non-cross-linked samples as previously mentioned. Therefore the filler network still dominates the rheological response with full percolation in the material at higher filler concentrations. The overall trend in the samples of reinforcement with addition of filler particles occurs, however there are notable differences related to the crosslinking and low filler concentrations.
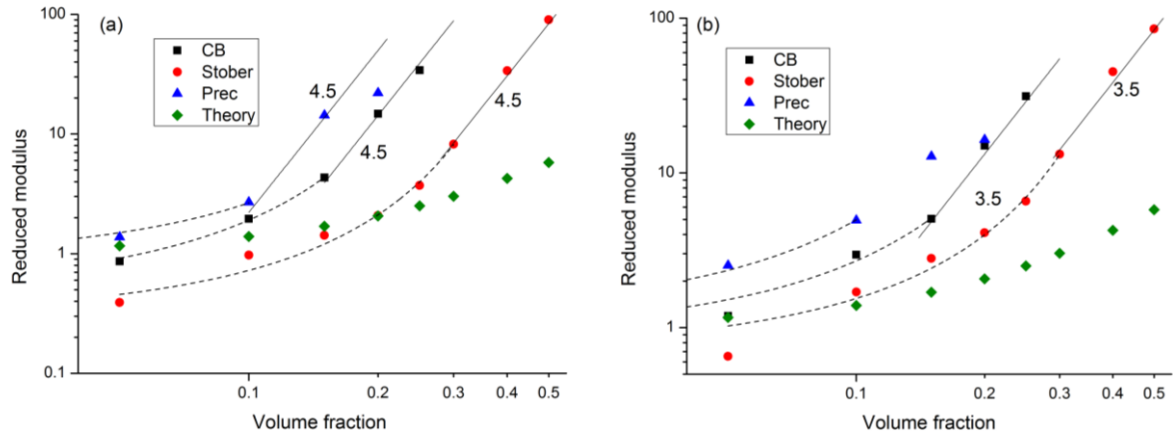
Figure 4.19: Reduced storage (a) and loss (b) moduli at 1Hz for cross linked composite samples, figures include fitted Krieger relations (dashed) and possible power law trends (solid) for selected portions of the data

A major difference with cross linked composite samples is the visibly discernible drop in moduli present in the carbon black and Stöber silica samples at low volume fractions. This decrease is also comparatively less severe with the loss modulus, implying a net fluidity increase in the composites. This could be the result of the filler interfering with the crosslinking network, weakening the material by preventing uniform stress distribution in the rubber matrix. This was investigated further and will be reported later in section 4.2.3.

Fits of the Krieger relation, shown in figure 4.19 (dashed), for carbon black yield a value of 13.2 ± 0.4, and conversion using the reaction limited aggregation fractal dimension, defined previously, results in a value of 6.79 ± 0.21; this is much greater than those seen in the non-cross-linked carbon black samples. For precipitated silica the B value was determined to be 9.9 ± 1.5, with diffusion limited aggregation fractal dimension adjustment giving a value of 4.0 ± 0.62. This is in agreement with Brenner's predictions of non-rotating particles, however the uncertainty and difference from the non-cross-linked samples suggest this may not be accurate. The Stöber silica yields the greatest change in behaviour from the non-vulcanised samples with a calculated B value of 8.2 ± 0.4. The cross linked matrix provides an explanation of this change with the immobility of the filler material resulting in a permanent fractal structure. Treatment of

the *B* value with a reaction limited aggregation fractal dimension, 2.23, yields a new *B* value of 4.8 ± 0.2, which is similar to the value found for the non-cross-linked precipitated silica samples, filler which has a permanent fractal structure.
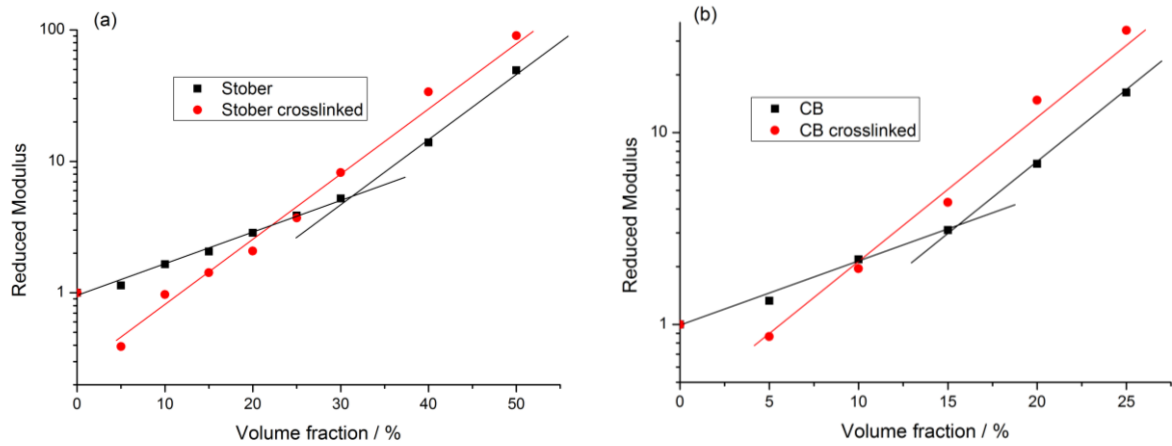
Figure 4.20: Reduced storage moduli for Stöber silica and carbon black composite samples, lines are to guide the eye, sample frequency 1 Hz

Supporting this idea of a permanent filler structure is the lack of a crossover at critical filler concentrations for the cross-linked data if plotted as an exponential trend seen in figure 4.20 as the red points; and a rate similar to the percolated growth rate in the non-cross-linked samples, shown as the black data. The crosslinks preventing reorganisation of the particles and constant particle aggregation above the percolation threshold would both result in permanent structures in the matrix and explain the similar trends. Power fits after the percolation thresholds found in the non-cross-linked samples yield a power value of 4.5 for all filler types. This is an increase from 3.5 for both the carbon black and precipitated silica with the formation of crosslinks, and can be explained by the loss of the fluctuations in the filler network due to the crosslinks hindering rearrangement, resulting in a power value of 4.5 as predicted for non-fluctuating fractal networks[107]. For Stöber silica, there is no shift in the power value from the non-cross-linked equivalent; however the cause of the power has changed from a reaction limited to a non-fluctuating diffusion limited network, implying that the vulcanisation process aids dispersion somehow.

4.3.2 Filler material effect on vulcanisation process
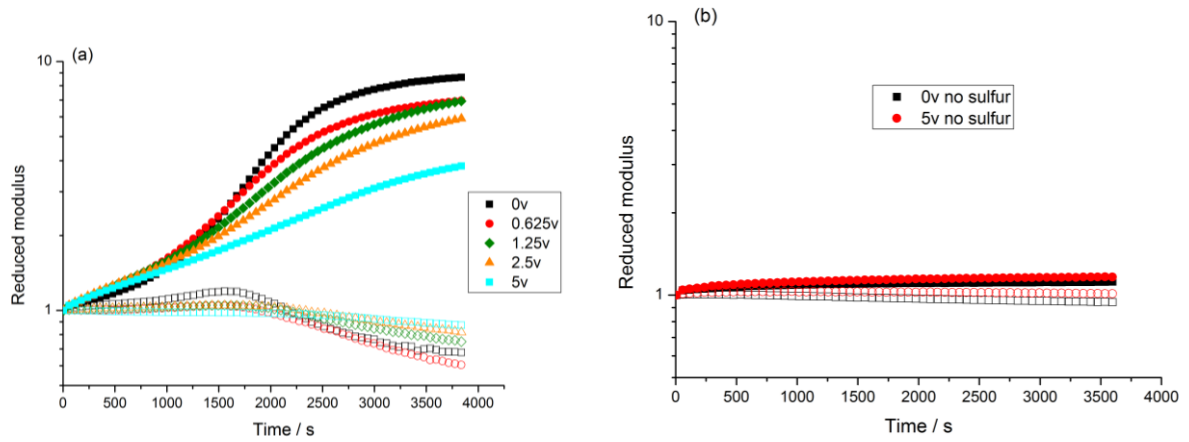
Figure 4.21: Normalised storage and loss moduli for (a) low Stöber silica content samples with sulphur crosslinking (b) neat and 5% volume Stöber silica samples without sulphur, during cross linking curing conditions; temperature: 160 ˚C, frequency: 1 Hz, strain: 0.1%, filler content given in legend

Samples containing low volumes of Stöber silica were cross-linked with sulphur in inert atmosphere in the AR2000 rheometer to examine the effect of the filler on the cross linking process. The decrease in storage modulus growth with increasing silica content confirms the trend observed with cross-linked composite samples. The data in figure 4.21b demonstrate that this change is not due to filler rearrangement, and although there is a minor difference between the neat and filled samples during curing it cannot explain the shift in trends seen in figure 4.21a. With this taken into account, the change in moduli growth must be caused by the filler affecting the crosslinking in some form.
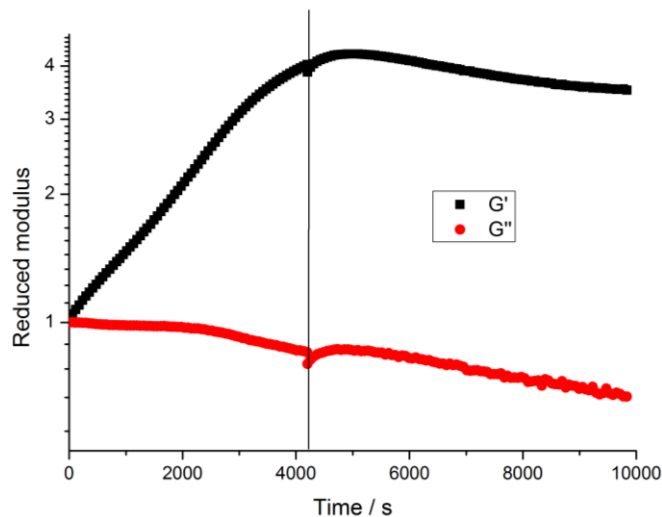
Figure 4.22: Continued curing of the 5% volume Stöber silica sample, black line represents initial time sweep end point, it was decided to continue curing the sample for this investigation; moduli have been scaled to unity

The filler may be retarding the formation of the crosslinks, thus the potential network is not fully realized. The formation of plateaus in the storage modulus in the continued vulcanisation of the Stöber silica sample, figure 4.22, indicates that is not the case. The other possibility is that the filler particles disrupt the network itself, as previously mentioned, and weaken the overall material.
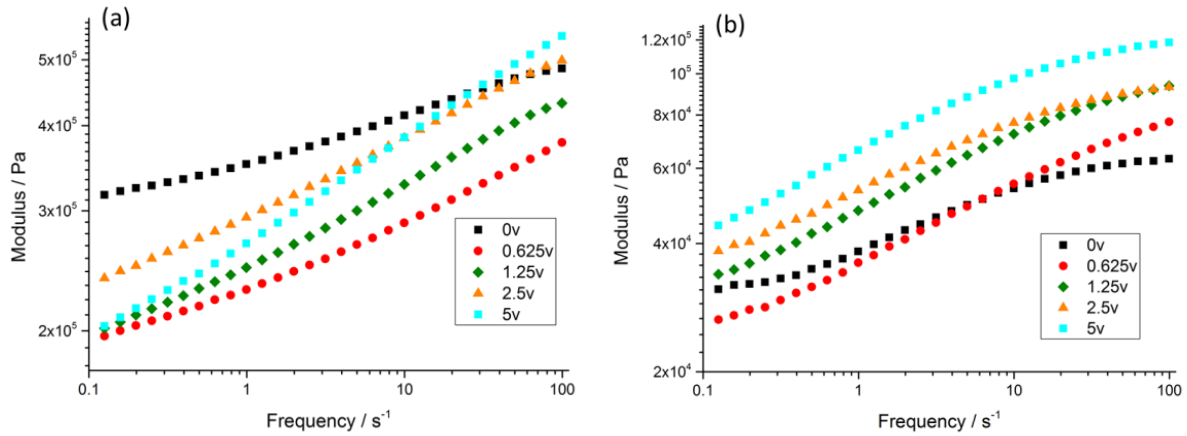
Figure 4.23: Low Stöber silica content sample frequency sweeps (a) storage modulus (b) loss modulus; filler content (% volume) is given in the legend

The rheological behaviour of these cross-linked low silica content samples was also examined. Apart from the 5% Stöber silica content sample, there do not appear to be significant shifts in the storage modulus (a) dependence with frequency, however, there is a clear decrease of the modulus even with the smallest fraction of Stöber silica filler. This suggests the disruption is more than a steric effect, as a low filler volume fraction should not disrupt a crosslink network greatly. The effective decrease appears to be constant among the samples, or at least offset by increased filler reinforcement to provide such a trend.

Strain magnification by the particle presence is a possibility and is supported by molecular dynamics simulations on cross-linked composites, which have found defects and cavities occur near the filler particles when under strain[108]. It is difficult to discern whether this is the cause of this effect from the rheology alone, and unfortunately due to time constraints this line of investigation was not able to be continued in this work; however this phenomenon demonstrates the need for understanding and studying the composite microstructure.

4.3.3 Effect of end functional presence and crosslinking

To examine both end functionalization and crosslinking, a blend with a 50:50 ratio of 15k 4OHPBd to PBd-300k with filler material was used, vulcanisation was performed with the same conditions.
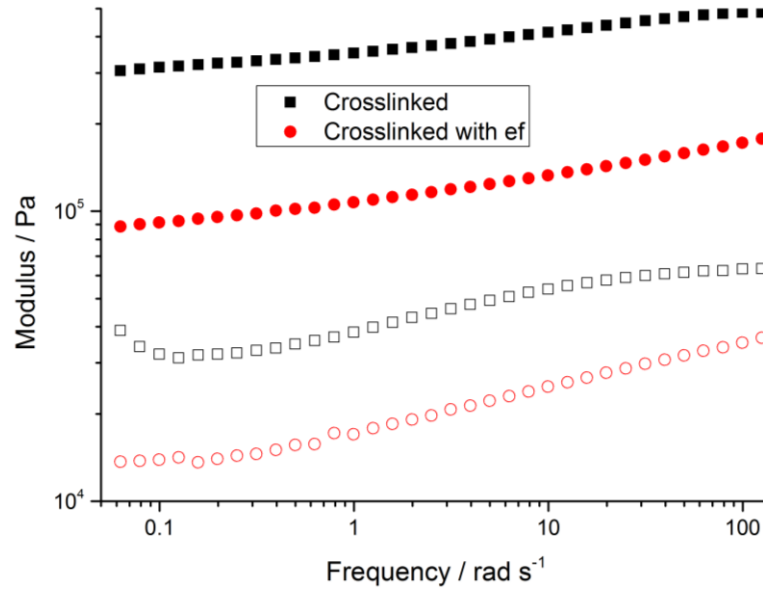
Figure 4.24: Neat sulphur crosslinked polybutadiene storage (closed) and loss (open) moduli, pure 310k PBd starter (black), 50:50 15k 4OHPBd blend (red)

Comparison of the neat cross-linked samples yields a clear difference in moduli, similar to the case for the blends. Diluent effects of the 15k polymer chains are a probable cause. As the sulphur crosslinking in the sample achieves ~10800 g/mol between sites, on par with the 4OHPBd chain length, it is probable that a significant number of 15k chains remain unlinked in the network and act as diluents.
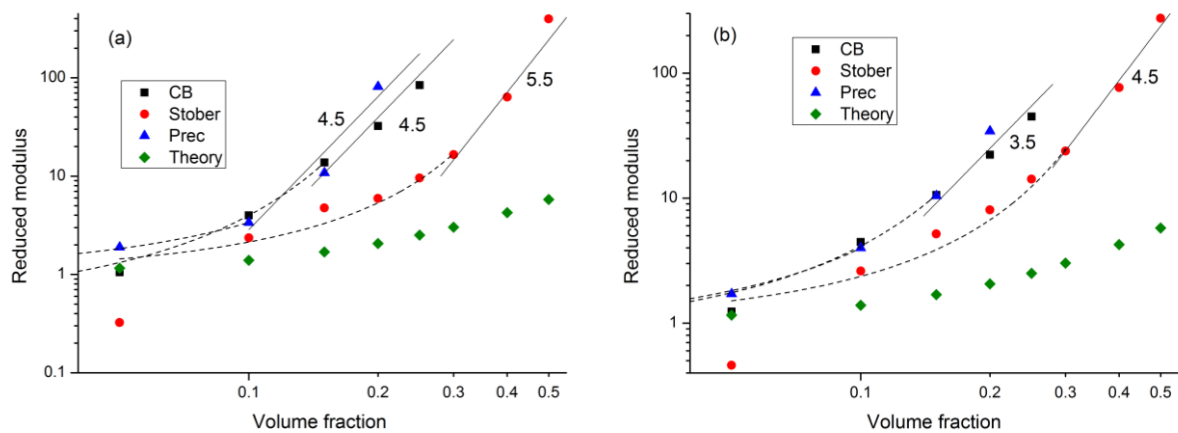
Figure 4.25: Reduced storage (a) and loss (b) moduli at 1 Hz for cross linked composite samples, figures include fitted Krieger relations and possible power law trends for selected portions of the data

As with the non-end functional cross-linked samples, there is a notable decrease in moduli with the low levels of the filler particles at 5% volume fraction, in figure 4.25 this is most visible with the Stöber silica (red). A steady increase in modulus after this point is observed here as with the non-functionalised cross-linked samples with no obvious shift in slope with any of the fillers.

Fits of the pre-percolation data with the Krieger relation result in *B* values of 19.81 ± 1.41, 10.6 ± 0.6, and 6.4 ± 0.6 for carbon black, precipitated silica, and Stöber silica samples, respectively; conversion of the values with the fractal dimension calculation results in values of 9.2 ± 0.7 (RLA), 4.16 ± 0.21(DLA), and 3.96 ± 0.35 (RLA), respectively. For carbon black the determined *B* value is higher than both the only end functional (5.71) or cross-linked equivalents (6.79); however the change with the addition of the end functional additive is similar to that seen in the non-vulcanised samples. This hints that the cause is similar in both cases, theorised to be the polar end functional heads by flocculation of the network due to increased surface interaction energy.

The precipitated silica shows little change with the addition of the end functional polymer, hinting at similar structure besides the dispersive effects of the additive. The converted Stöber silica value is similar to what is expected for fixed particles, and in agreement with the non-cross-linked results. This indicates that the additive does help to break up the silica spheres in this instance, compared with the possible permanent structures found in the cross-linked sample set.

Power relations are observed above percolation for the samples. The 4.5 value for both the carbon black and precipitated silica is equal to the non-end functional cross-linked sets, suggesting that the end functional polymer does not make a great difference these composite systems. For Stöber silica the 5.5 power value is greater than observed for the non-functionalised equivalent, which hints at a change in structure. This change would be derived from a shift from a diffusion limited to reaction limited aggregation due to the steric hindrance from a bound surface layer. Counter intuitively, the addition of the 4OHPBd appears to result in a more aggregated structure in this case; however, these structures are smaller clusters as contact does not always lead to bond formation. As such dispersion may still be occurring in the sample.
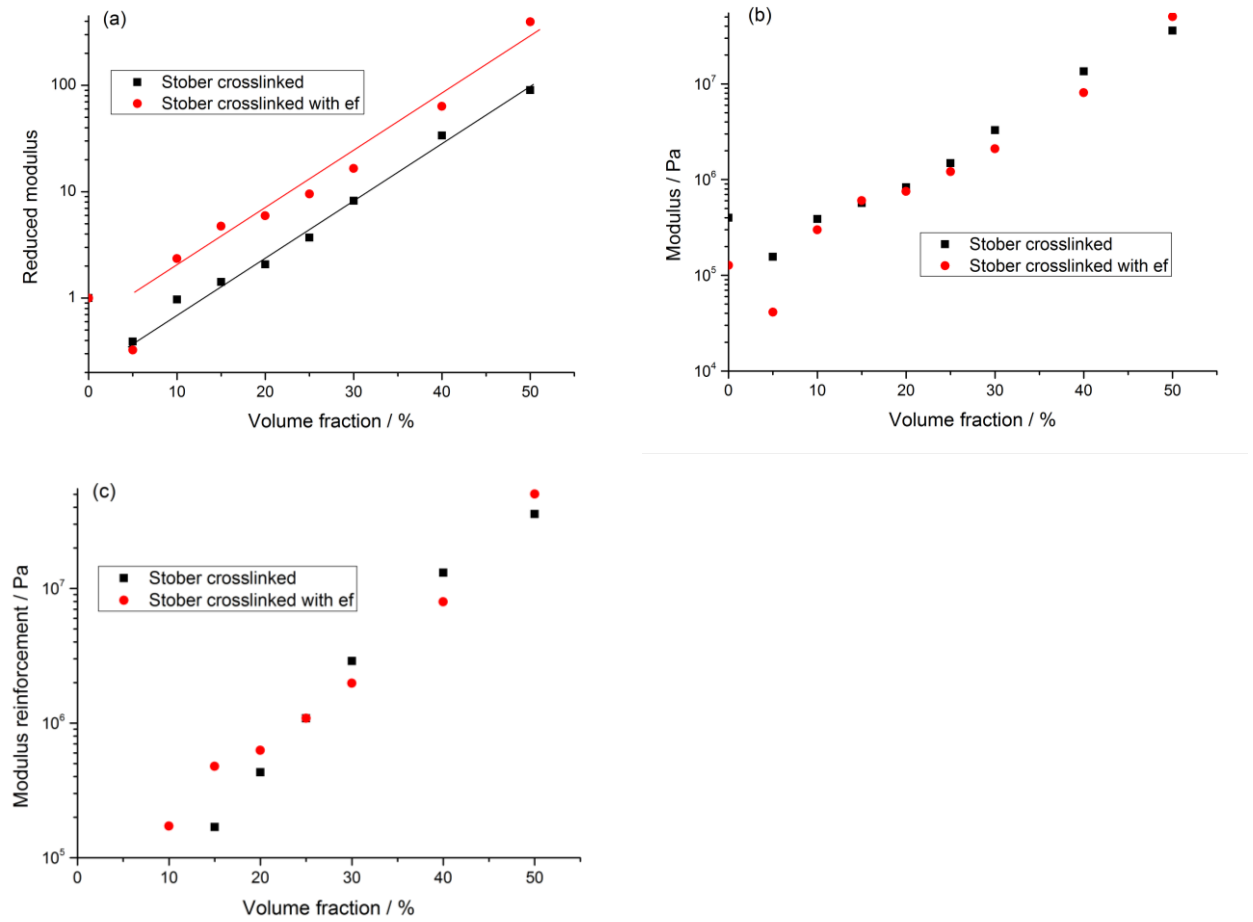
Figure 4.26: Reduced (a), measured (b), and reinforcement in (c) storage moduli for cross-linked Stöber silica composite samples, sample frequency 1 Hz

Unlike the case with the non-vulcanised Stöber silica samples, there is a clear difference in the reduced moduli, figure 4.26a, with and without the presence of end functional polymer over most of the volume range. From the data in figure 4.26b, the moduli for the Stöber silica composites are comparable after 10% volume fraction. This, along with the relative difference in neat matrix modulus, provides a mathematical explanation the difference in the reduced measures. The physical cause of this change may be from the binding of the end functional polybutadiene to the silica surface, once removed from the bulk it no longer affects the matrix modulus, resulting in an increased modulus similar to the non-additive sample's.

Interestingly, this trend is the opposite behaviour to that observed in the non-cross-linked Stöber silica samples, where the reduced modulus growth was similar. It was previously mentioned that the permanent particle fractal structure found in the carbon black and precipitated silica may be related to the growth in modulus being independent of initial neat modulus. With crosslinking preventing the movement of the silica, the overall structure would behave as a rigid body and would not deagglomerate with deformation, yielding modulus reinforcement behaviour closer to that observed in the precipitated silica and carbon black.
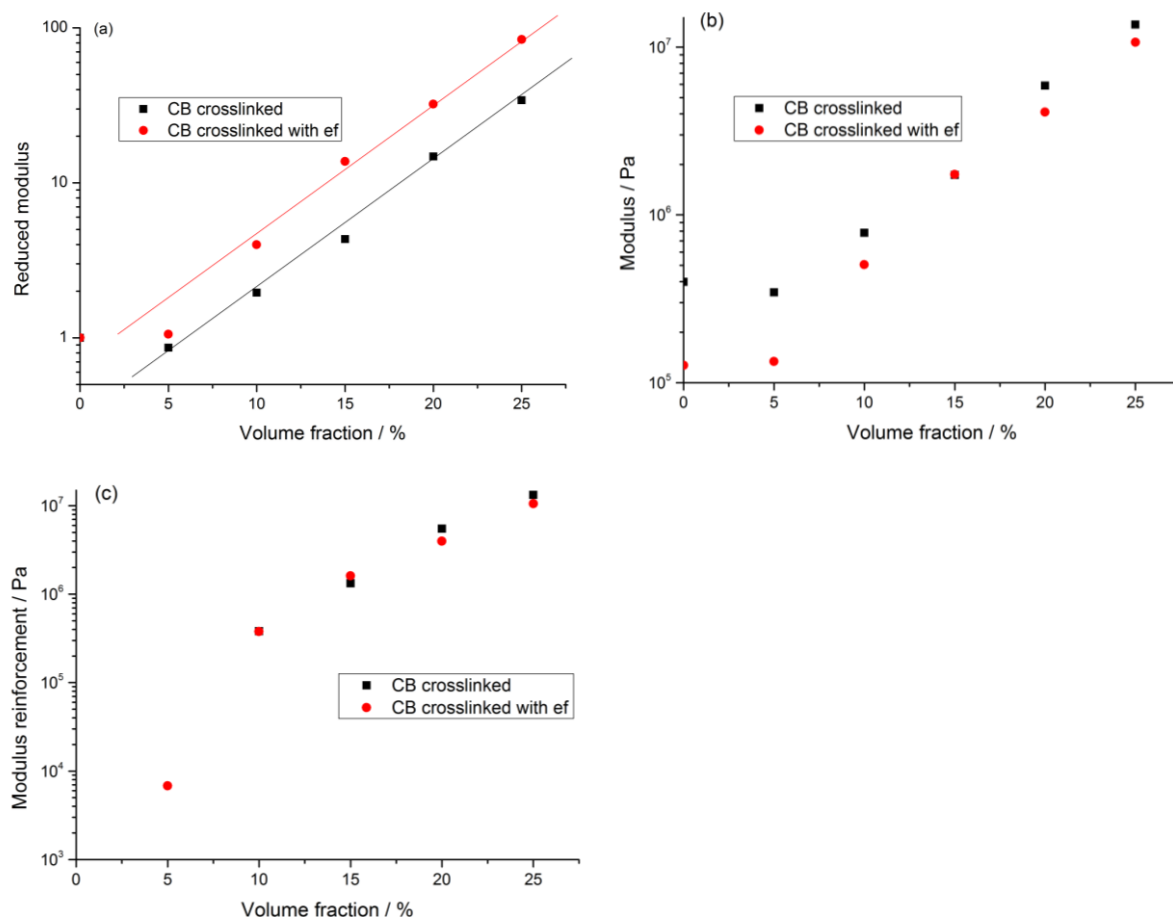
Figure 4.27: Reduced (a), measured (b), and reinforcement in (c) storage moduli at 1 Hz carbon black cross-linked composite samples

For the cross-linked carbon black composites, the addition of the end functional polybutadiene to the matrix does not appear to have greatly affected the nature of the reinforcement, as with the non-vulcanised samples. The same trend seen in the non-end functional cross-linked equivalent samples, of greater reduced modulus but equal gained reinforcement, is observed here. This can be attributed to the lack of attractive interactions between the hydroxyl functional groups and the carbon black surface. As such the addition of the polymer does not affect the matrix-filler interactions and little change outside of diluent effects is seen. In comparison with the non-cross-linked carbon black materials, this behaviour is similar, suggesting that matrix-filler interactions do not change with vulcanisation for carbon black.
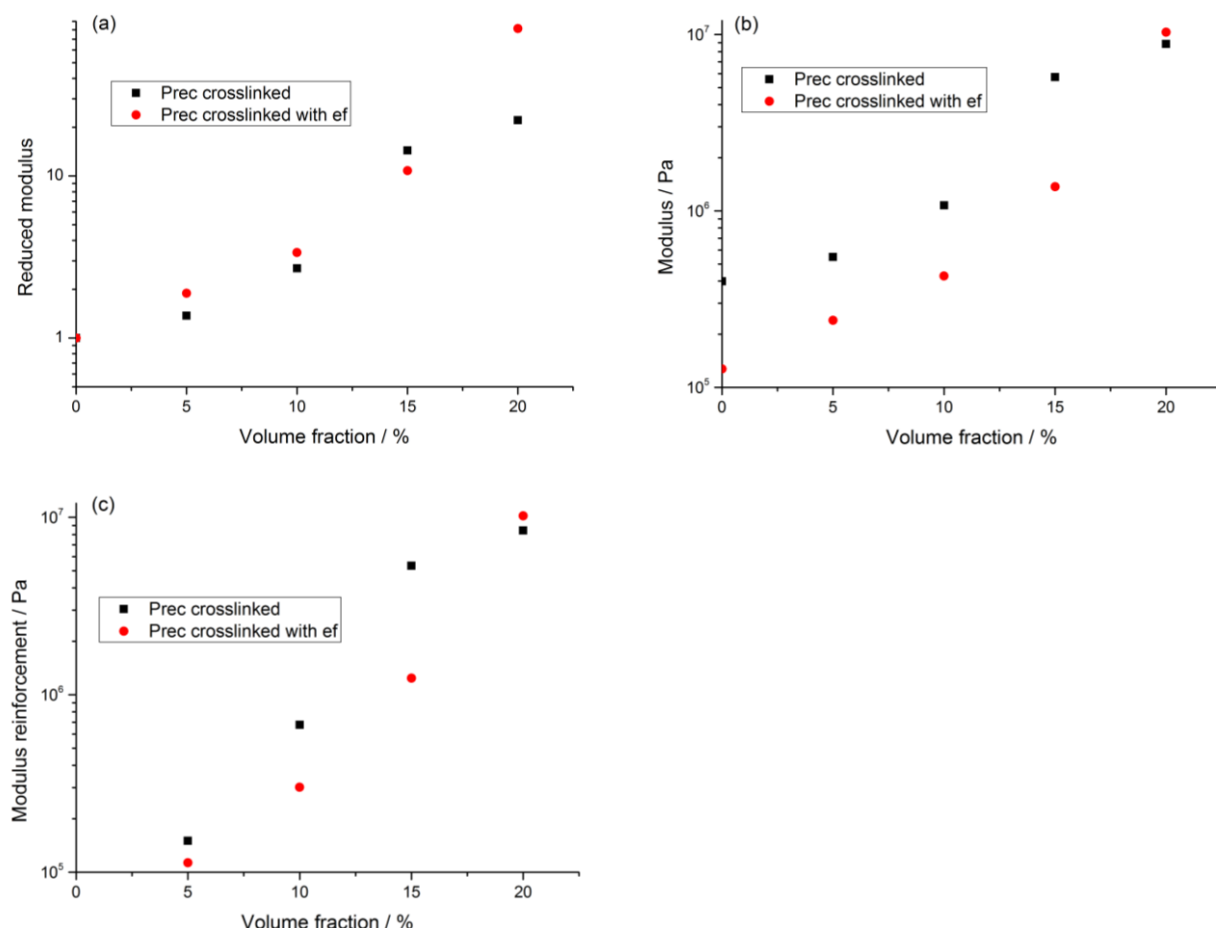
Figure 4.28: Reduced (a), measured (b), and reinforcement in (c) storage moduli for precipitated silica cross-linked composite samples, sample frequency 1 Hz

For the precipitated silica, the reduced moduli show behaviour independent of the presence of the functional polymer. This is in contrast with the non-cross-linked samples which demonstrated a clear difference with and without the 15k 4OHPBd. This may be a result of mathematical chance, as the modulus reinforcement demonstrates the same trend observed in the non-cross-linked precipitated silica fillers, suggesting there is no observable difference in the filler matrix interactions.

4.4 Rheology of composites examined in neutron scattering experiments

Filled rubbers and other composites are complex systems, and cannot be characterised by a single technique. By examining samples with both macroscopic and microscopic techniques, changes at either length scale can be correlated with those in the other. This combined information allows for further conclusions to be drawn about the system in question. As the rheology of these composites is thought to be influenced by the microscopic filler arrangement and interactions, samples of composites used in neutron scattering were also subjected to mechanical testing.

4.4.1 Silica dispersion via 4OHPBd sample rheology

As part of examination of the effective surface concentration on filler dispersion, several samples from the D11 experiment (section 6.3) were rheologically tested. The bulk matrix was deuterated polybutadiene purchased from Polymer source, precipitated silica was the filler material, and 20k 4OHPBd was the additive. When included a 16% weight fraction of 20k 4OHPBd was used independently of the remaining sample composition. Sweeps from 0.1-5 Hz at various temperatures were performed and WLF shifted to 20˚C. The time temperature superposition was developed from the relation between the timescale of polymer motion and the sample temperature during the measurement. The storage and loss moduli of a polymer melt are dependent on the frequency of the probe oscillation as several relaxations are present in the matrix over standard measurement ranges. Increased kinetic energy results in quicker relaxations of the polymer chains and a shift in the frequency of the measured relaxations and moduli. This shift is constant, and can be modelled with the William-Landel-Ferry equation,

$$\ln(a) = \frac{-C_1(T - T_0)}{C_2 + (T - T_0)}$$

(4.8)

where a is the shift factor, C_1 and C_2 are constants, T_0 is the reference temperature, and T is the temperature of the measurement. [109] By performing frequency sweeps at different temperatures, then using the WLF relation an increased frequency range can be determined at the reference temperature. For this work, the curves were superimposed with RepTate software to yield the observed frequency curves.[11, 110]
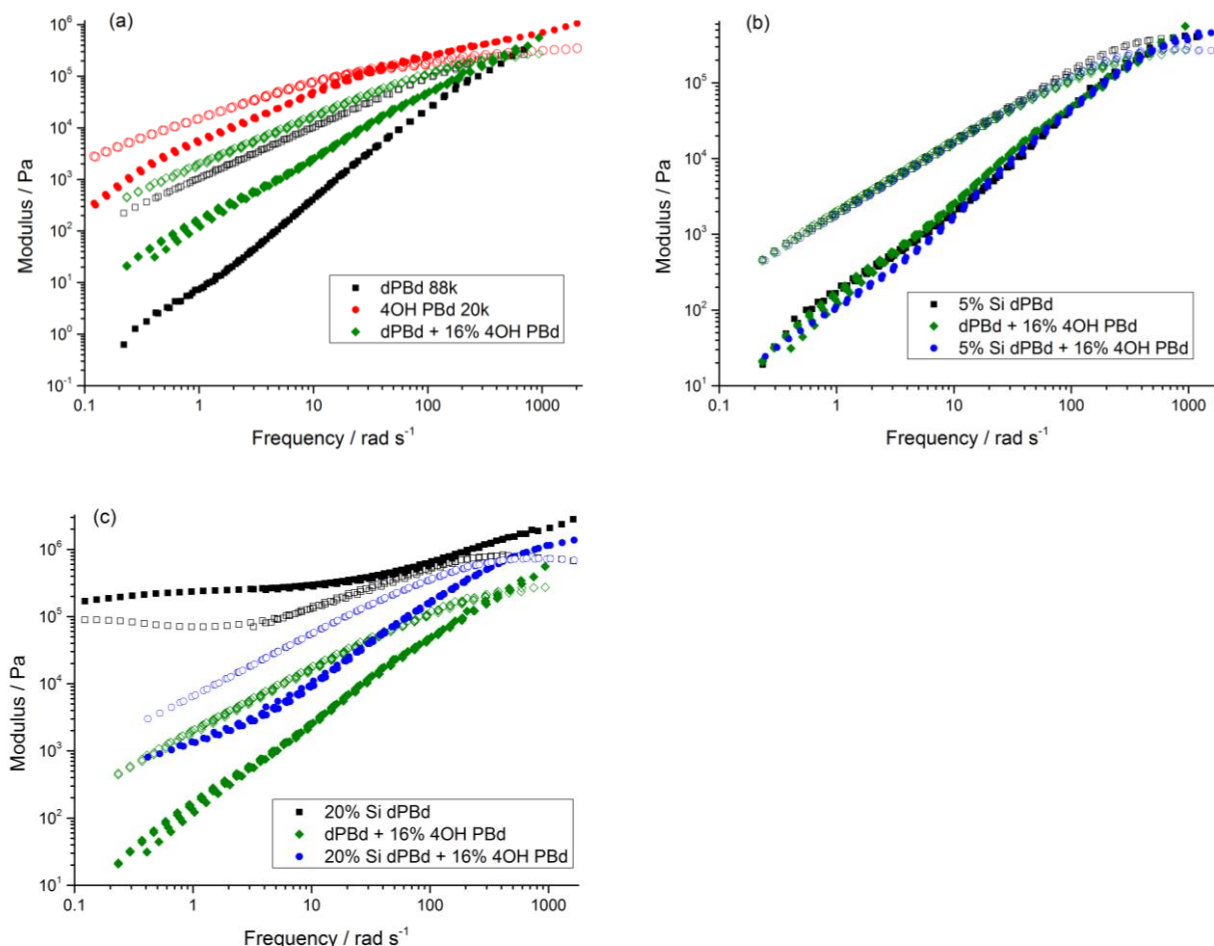
Figure 4.29: Storage (solid) and loss (open) moduli of WLF shifted frequency sweeps of blends, percentages are weight fraction of the component

The blend of 20k 4OHPBd and 88k deuterated polybutadiene yields an averaged modulus, figure 4.29a. Addition of the precipitated silica at both 5% and 20% weight fraction results in reinforcement without the presence of the end functional polymer. This is especially noticeable with 20% silica loading as at low frequencies the moduli are independent. The presence of the 4OHPBd decreases the moduli in the composite samples and restores the viscous behaviour at the higher silica concentration. This is in agreement with the results for precipitated silica discussed earlier, and may be caused by polymer brush layers forming about the silica particles and preventing percolation.

4.4.2 Glassy layer characterisation sample rheology

Rheological testing of the samples used to examine glassy layer dynamics was performed to examine possible correlations between the molecular dynamics, different additive chain lengths, and rheological properties.
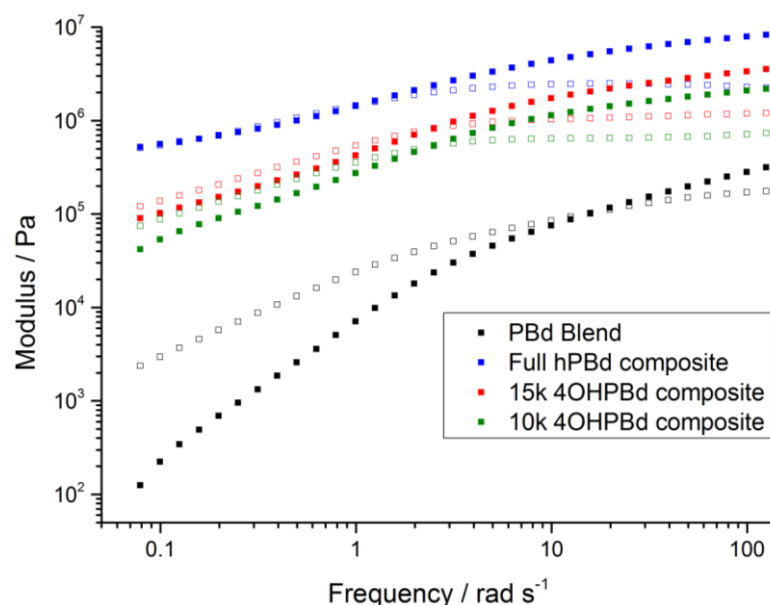
Figure 4.30: Frequency sweeps of IRIS GLASSY samples at 20 °C, storage (solid) and loss (open) moduli are displayed

The addition of the Stöber silica reinforces the polymer matrix, as seen with the difference between the polybutadiene blend and composites. The presence of the end functional polymer results in a decrease in modulus; with a similar value for both the 10k and 15k polybutadiene chains and no visible change in the moduli curve. This suggests that the different end functional polymers behave similarly even on a molecular level, and the only notable difference is the length of the chain. This allows for the composites with different end functional polymers to be compared.

4.5   Conclusions

From the rheological properties of the composites the effects of the end functional additive and crosslinking have been investigated. Investigations of peroxide and sulphur crosslink were able to determine that crosslink density affects the rheological properties; however the chemistry of the crosslinks does not and the behaviour observed is from the hindrance of reptation. The studies of carbon black, precipitated silica, and Stöber silica composites were useful in elucidating the effect of filler surface chemistry and morphology on the material properties. Comparison of the reinforcement with different filler content highlighted the importance of the filler morphology, with fractally structured precipitated silica and carbon black yielding greater reinforcement and earlier percolation thresholds than the spherical Stöber silica. The addition of hydroxyl end functional polybutadiene did affect the composite behaviours; carbon black composites demonstrated little change or increased reinforcement, while the silica composites showed decreased reinforcement. These changes were attributed to the possible flocculation and

dispersion of the particles for the carbon black and silica fillers, respectively, and is evidence supporting the idea of a filler network structure providing reinforcement. Some interaction was also noted between the filler materials and the sulphur crosslinking in the form of a modulus lower than the neat polymer below 10% volume fraction for Stöber silica and carbon black. It was postulated that this is the result of the filler particles disrupting the crosslink network and weakening the material. These results will be discussed in further detail with the neutron scattering data in chapter 8.

5 Composite strain softening studies

The exhibition of strain softening in filled rubbers has been well documented since Payne's article[6, 7] on the phenomenon which bears his name. Even with this documentation, however, the cause of this softening under continuous oscillatory strain is still a point of contention and discussion. Any complete model of the composite system needs to address and describe the phenomenon to the extent of providing predictive capacity. Filler networking and breakdown is the most considered model for the strain softening observed. In this model, the reinforcement observed in filled rubbers in from a filler network that supports the polymer matrix by bearing stress. With sufficient deformation this network breaks down and cannot support the stress applied to the material, resulting in a decrease in the storage modulus. The breakdown of this network also requires energy to break the particle contacts; this energy is dissipated into the matrix and results in an increase in the loss modulus until higher strains where the overall material softening dominates and a decrease is observed. [29]

From SANS results, section 6.3, the surface segregation of the 4OHPBd used in this study is thought to prevent silica contacts from forming; study of samples with and without this additive will provide insight into the accuracy of this model.

The softening phenomena observed is dependent on the strain experienced by the sample and not the stress applied, and as the composites contain different fillers and additives, the moduli with vary between the samples as will the stresses each sample is subjected to during the measurement. The use of the strain as a variable allows for some measure of comparison between the samples both experimentally and theoretically.

Strain sweeps for the silica and carbon black composite samples, from linear rheology section 4.2-3, were also performed as part of the rheological testing along with the rubber baselines. An AR2000 rheometer with Peltier stage was used, the temperature was set to 20˚C, strain was varied from 0.01 to 30%, and frequency was held at 1 Hz for all tests performed.

5.1 Strain softening of neat polybutadiene with fillers

The strain sweeps for the composites with only carbon black filler are shown in figure 5.1. At 5% filler loading (red), the carbon black composite sample does not demonstrate any visible strain softening, however at all greater loadings the Payne effect is present. The decrease with strain appears to be minor for the 10% (green) sample, while it is more pronounced at higher loadings with the development of a peak in the loss modulus at 20% and 25% carbon black volume (blue/purple). Taking into account the changes in reinforcement behaviour from section 4.2 and decreased percolation threshold due to the filler fractal structure, this development in the

effect may correspond to the formation of a percolating filler network in the rubber. This supports the theory that network breakdown is responsible for strain softening in these circumstances. [34]
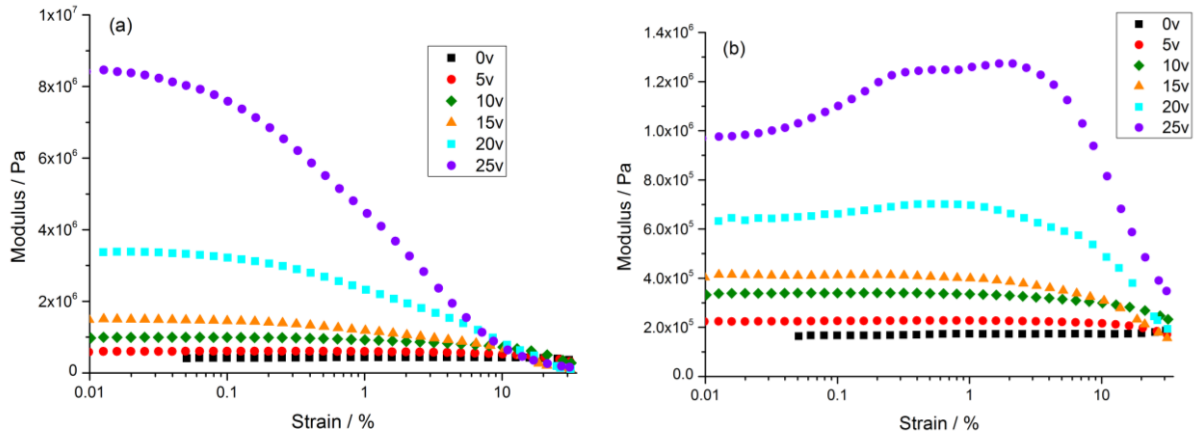
Figure 5.1: Carbon black sample modulus vs strain; (a) storage, and (b) loss, 1 Hz, concentration (% volume) of filler is given in the legend

Other notable observations of this system include the decrease of the storage and loss moduli at high strains, and the presence of two features in the loss modulus peak. The decrease of the moduli is predicted by theory and in agreement with previous experimental reports [6, 7]; however, care needs to be taken with the data above 10% strain as wall slip in the shear setup is a significant possibility. Indeed, the presence of wall slip may be responsible for the two features seen in the loss moduli rather than two separate processes. Wall slip occurs primarily in shearing measurements, comparison of the data with that from a bending sample experiment could be used to clarify this issue; unfortunately the samples were unable to be tested with such equipment.

In the silica sample strain sweeps, figure 5.2, there is a decrease in the moduli above 10% strain for the 5% volume silica sample (red) in contrast to the equivalent carbon black sample with did not show such a change. While this could be the result of strain softening it is possible to be the result of wall slip, which confirms mentioned issues and caution with the analysis of higher strain data. As with the carbon black the higher silica loadings, 15% and 20% silica (orange/blue), display a peak in the loss modulus. The presence of a fully percolating filler structure and its breakdown may be the cause of this. Unlike the carbon black filler there is only a single feature present and at a higher strain, hinting at either decreased wall slip or differences in the filler interaction. In combination with the observation that the onset of the strain softening occurs at greater strain, ~0.51 % rather than 0.13 %, implies there is a difference in the

networking behaviour of the precipitated silica. Given the structural similarity of the fillers, a difference in surface properties or arrangement in the matrix is the cause.
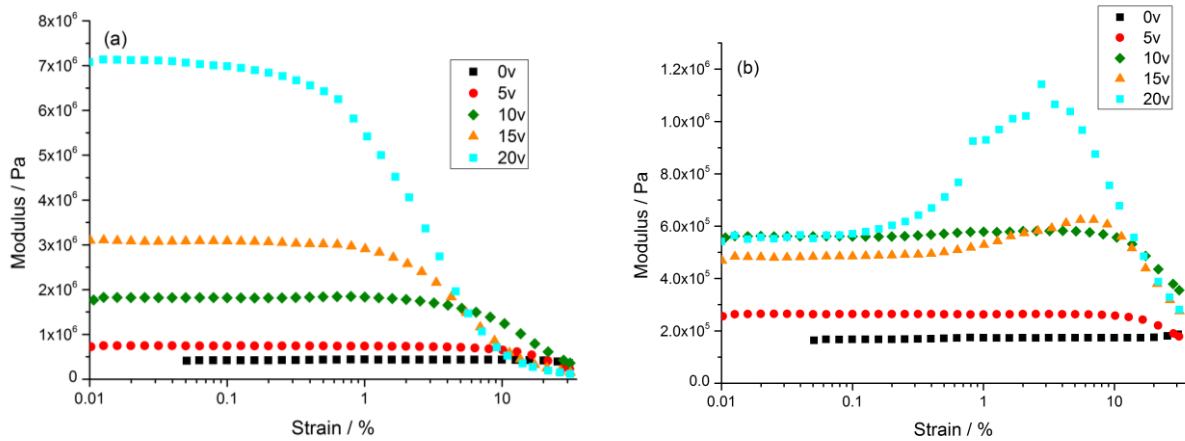
Figure 5.2: Precipitated silica modulus vs strain; (a) storage, and (b) loss, concentration (% volume) of filler is given in the legend

Another interesting observation is that the 10% silica sample (green) yields a clear decrease in the storage modulus as theory would predict, but no notable peak in the loss modulus, figure 5.2b; and while not discussed previously there is also a no loss peak in the 15% carbon black data. This implies that there are several regimes in relation to filler loading and composite response, possibly corresponding to a dilute, semi-dilute, and concentrated regime. In the dilute regime no strain softening occurs, while in the semi-dilute regime decreases in the moduli are found but no loss peak feature, and in the concentrated regime the feature of a loss peak is present.

Now considering Stöber silica nanoparticles, at lower filler loadings of Stöber silica figure 5.3a, 10% through 30%, strain softening at high strain with the onset decreasing with filler concentration is found; at 5% loading, it is uncertain if this trend is from softening because of the onset's proximity to the maximum strain tested. None of these samples yield a peak in the loss modulus, with it instead decreasing rapidly between 10% and 30% strain. At 40% and 50% silica concentration the peak in the loss tangent in present, along with the trend of decreasing strain non-linearity onset in the storage modulus. The loss modulus increase observed at very low strain in the 50% volume is of unknown origin, but suggests some additional dissipation mechanism at high filler loadings. As previously noted, the appearance of the peak occurs in both the carbon black and precipitated silica data, and was attributed to different regimes of filler behaviour. Of the filler materials studied, the Stöber silica has the most easily defined percolation threshold, 0.28 for hard spheres [26]; as the loss peak appears after this point it is reasonable to assume that it is related to a filler network. The loss peak itself is postulated to be

caused by the increased dissipation of energy from the breaking of network contacts. This viewpoint is supported by finding the peak only above percolation; however this observation implies that different models or parameters are required to model the strain softening above and below percolation.

The nature of the onset of strain softening in the Stöber silica appears to be similar to that seen in the precipitated silica, with a visible plateau and sudden shift in slope rather than the gradual shift observed in the carbon black. Silica has higher surface interaction energy than carbon black for polybutadiene, resulting in more aggregation and stronger filler-filler contacts in the composite.[92] Greater deformation would be required to break silica contacts consistent with the observed plateau and delayed softening onset point.

Figure 5.3: Stöber silica modulus vs strain, loadings split for clarity; (a) storage, (b) loss, (c) high loading storage, (d) high loading loss, concentration (% volume) of filler is given in the legend

5.2 Effect of the addition of 4OHPBd polymer on strain softening

The same samples as used for linear rheological testing were used here. The polymer matrix is composed a 50:50 blend of 15k 4OHPBd and 300k PBd (Sigma Aldrich).
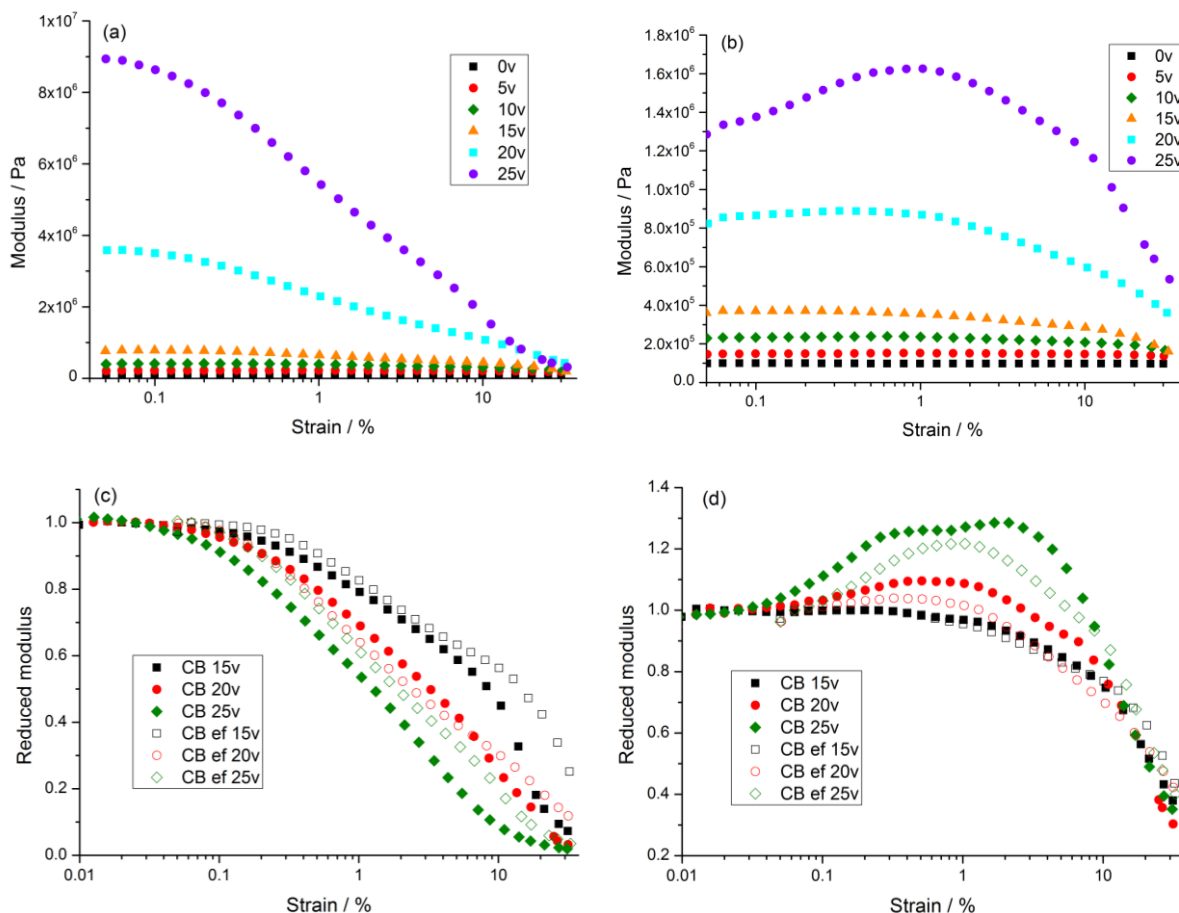
Figure 5.4: Carbon black with 15k 4OHPBd modulus vs strain; (a) storage, and (b) loss; reduced (c) storage and (d) loss modulus comparison of carbon black and carbon black with end functional polybutadiene composites, both samples contain 25% volume carbon black; concentration (% volume) of filler is given in the legend

Strain softening only appears to be present at and above 15% carbon black content, with few noteworthy changes with the addition of 15k 4OHPBd polymer. The most visible change is in the shape of the loss peak in figure 5.4b (purple), which contains a single feature compared with the two features found in the equivalent unmodified sample, figure 5.4d. Overall, the addition of the end functional polymer does not appear to greatly affect the strain properties of the carbon black composite, implying limited interaction between the filler and additive.

For the precipitated silica, only the 15% and 20% silica content samples undergo strain softening with the addition of the 15k 4OHPBd, in contrast to the unmodified equivalent where softening was seen at 10% silica, figure 5.5c/d (black). The onset of softening occurs at similar

deformations at higher filler concentrations. The additive does not appear to reduce the present loss peak seen in the data at 20% silica (green); thus energy dissipation caused by breakages is still present and appears to be increased. Perhaps particle contacts are able to form despite the layer due to insufficient coverage. If the silica was semi-dispersed but still able to network, the resultant structures would open and similar to diffusion limited aggregation structures. Such a structure may contain more numerous smaller network bridges, which then break under strain to yield the greater loss peak.
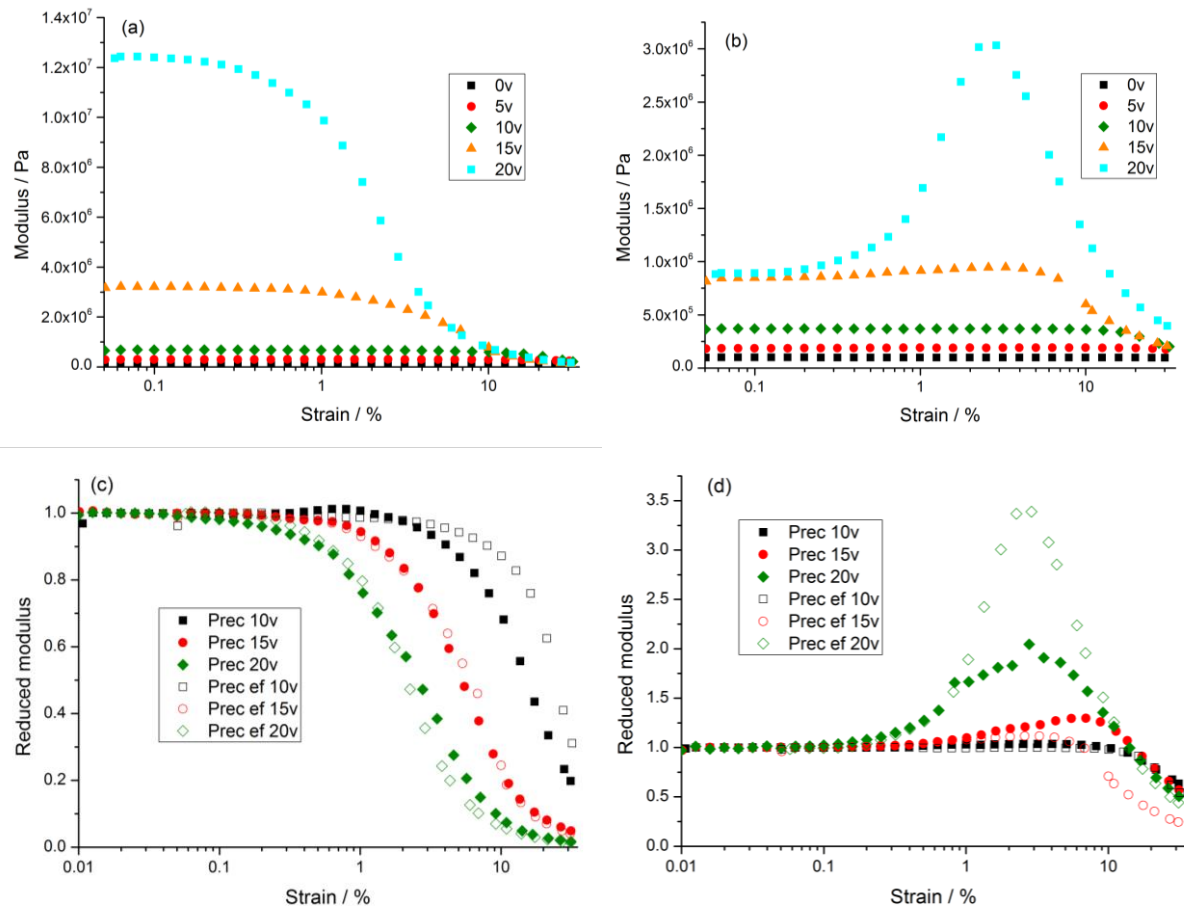
Figure 5.5: Precipitated silica with additive modulus vs strain; (a) storage, and (b) loss; reduced (c) storage and (d) loss modulus comparison of precipitated silica and precipitated silica with end functional polybutadiene composites; concentration (% volume) of filler is given in the legend

Supporting the lack of coverage is the minor loss peak at 15% silica, figure 5.5b (orange), and the finding of silica dispersal at lower concentrations. If the change in surface coverage is correct, then it can be postulated that the loss peak is the result of energy loss through network breakages, and its disappearance with 4OHPBd presence is from the lack of filler contacts to break.

As was the case in the Stöber silica samples without 4OHPBd, strain softening occurs at and above 10% silica volume fraction and increases in magnitude with filler loadings. The location of the softening onset has shifted to higher strains and the transition is more gradual, figure 5.7c, compared with the unmodified samples. The other notable feature of the data is the complete lack of a loss peak at any filler content with the 4OHPBd, figure 5.6d. As previously stated this peak arises from the breakages of filler contacts during deformation, thus the lack of the peaks implies the absence of such contacts through dispersion and steric hindrance or that the contacts are not broken with applied strain due to decreased network rigidity. This finding confirms the results from the precipitated silica; that the silica is dispersed by the polymer brush layer and that the loss peak observed from the Payne effect is due to energy dissipation from network breakages.
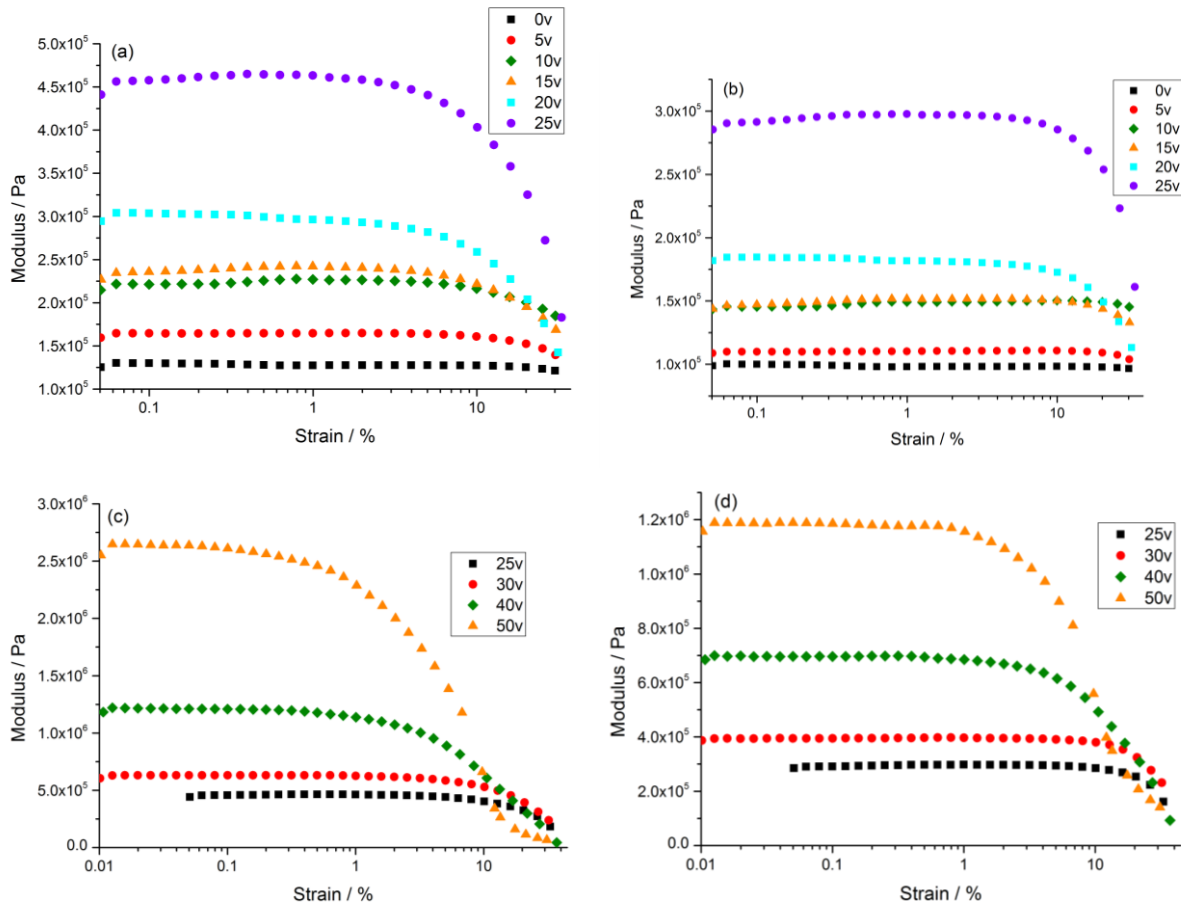
Figure 5.6: Modulus of Stöber silica with 15k 4OHPBd composites vs strain, loadings split for clarity; (a) storage, (b) loss, (c) high loading storage, (d) high loading loss; concentration (% volume) of filler is given in the legend
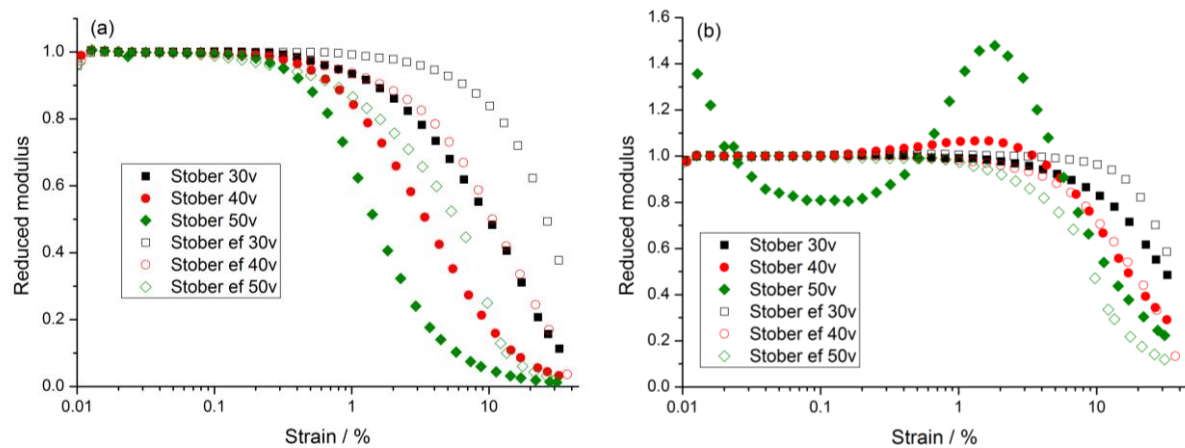
Figure 5.7: Reduced (a) storage and (b) loss modulus comparison of Stöber silica and Stöber silica with end functional polybutadiene composites; concentration (% volume) of filler is given in the legend

Overall, the addition of the end functional polybutadiene was found to have different effects on the silica and carbon black filled composites. There was little change observed in the carbon black sample behaviour, while for the silica particles a reduction of the loss modulus peak was noted in most cases. It was theorised this reduction is from the lack of filler network breakdown either by a lack of contacts or greater flexibility in the network.

5.3 Studies of cross-linked polybutadiene composites

As crosslinking of the rubber matrix is common in commercial rubbers, understanding if the process affects the material behaviour under significant strain is relevant. Samples of each filler type were examined and differences with the equivalent non-cross-linked samples are discussed to determine their origins. The carbon black composite samples are displayed first.
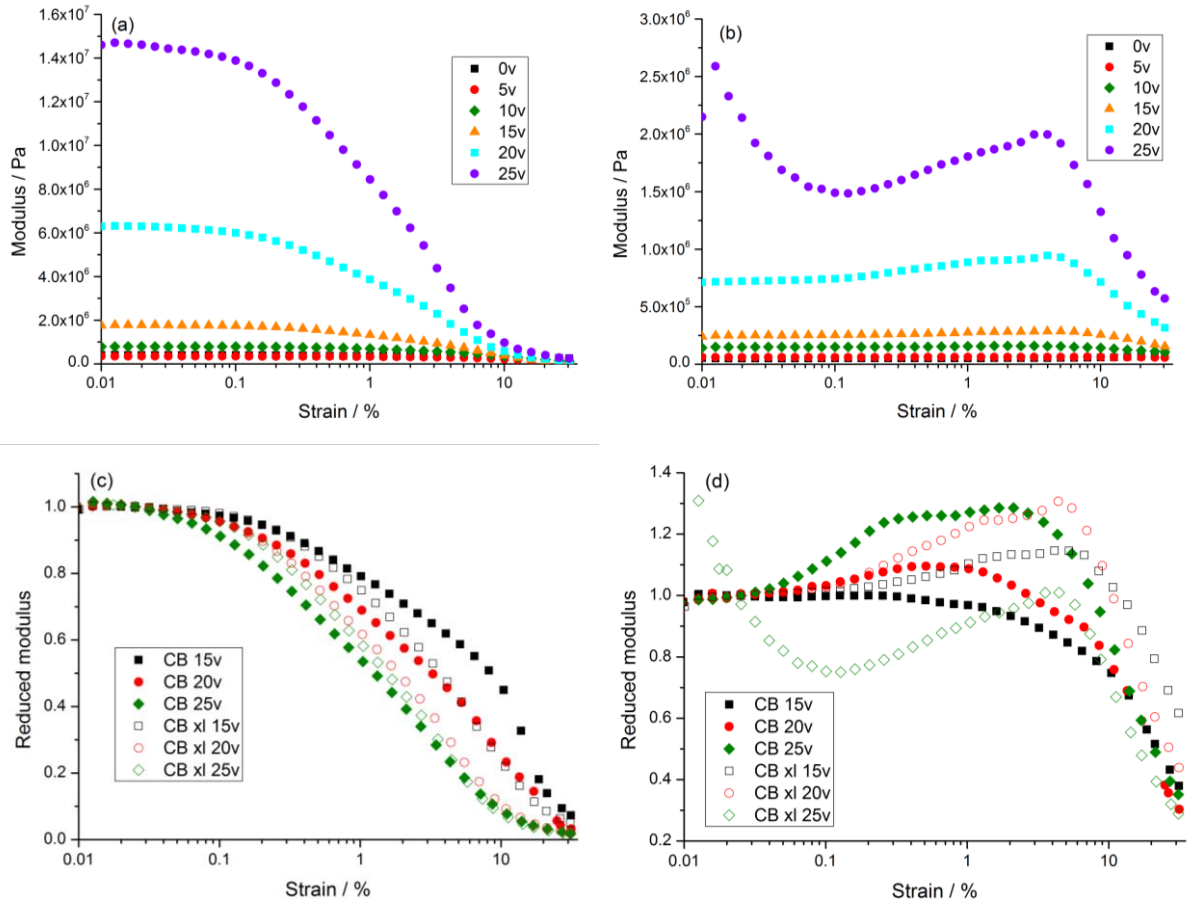
Figure 5.8: Carbon black cross-linked composite modulus vs strain; (a) storage, and (b) loss; reduced (c) storage and (d) loss modulus comparison of carbon black and cross-linked carbon black composites; concentration (% volume) of filler is given in the legend

The vulcanisation of the polybutadiene rubber with sulfur does appear to affect the strain related properties of the carbon black composites. With the storage moduli, figure 5.8a, the change in modulus at most loadings, figure 5.8c (black/red), is quicker compared with the non-cross-linked sample data. This implies that the inter-particle contacts require less energy or deformation to yield with crosslinking, though this effect is subtle and suggests only a minor change. A possible source of this development is the lack of mobility or rearrangement of the filler in the cross-linked polymer, which decreases toughness by forcing the contacts to be broken at bridging sites.

In the loss modulus there is single peak at greater strain compared with the non-cross-linked samples, shown in figure 5.8d. The steady increase in the loss modulus suggests a range of network contact strengths rather than a consistent bonding interaction which would produce a single peak.

For the cross-linked precipitated silica; qualitatively the trends in the samples appear to be similar to those found in the non-vulcanised precipitated silica samples. The onset of strain softening is abrupt and there is a visible presence of a loss modulus peak above 5% silica content, figure 5.9b. The shift in both the onset point of strain softening and the location of the loss peak is notable. Assuming the filler networking model, these observations imply that the network contacts are more easily broken for precipitated silica in a cross-linked matrix.
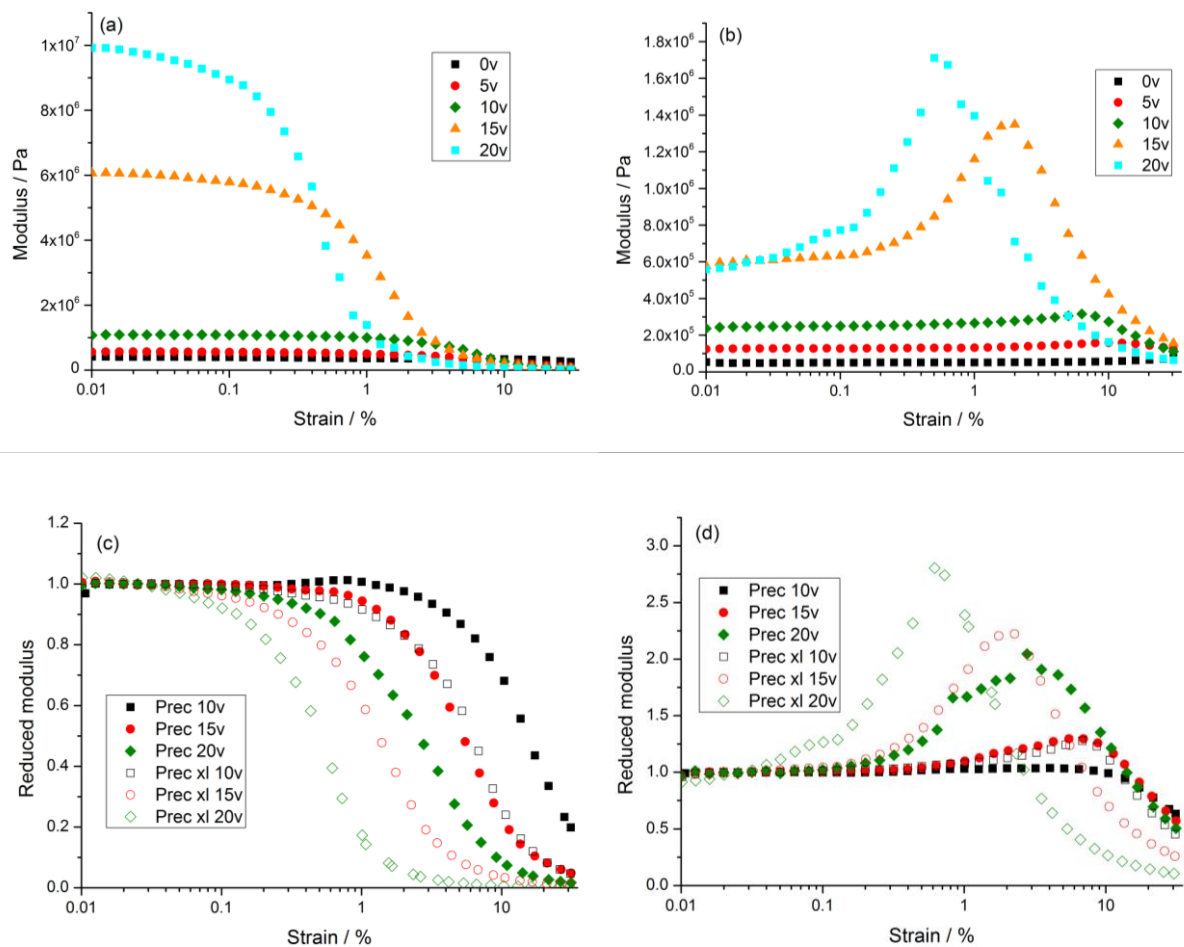
Figure 5.9: Precipitated silica cross-linked composite modulus vs strain; (a) storage, and (b) loss; reduced (c) storage and (d) loss modulus comparison of precipitated silica and cross-linked precipitated silica composites; concentration (% volume) of filler is given in the legend

As with the unvulcanised samples, strain softening occurs with any composition of Stöber silica. Unusually, the Payne effect appears at greater strains with increased silica content from 5% to 20%, figure 5.10a (red/green/orange), in contrast with other trends of decreasing onset point with

filler volume fraction. This may be related to the decrease in modulus seen at low filler fractions and is thought to be caused by the particles disrupting the crosslink network.
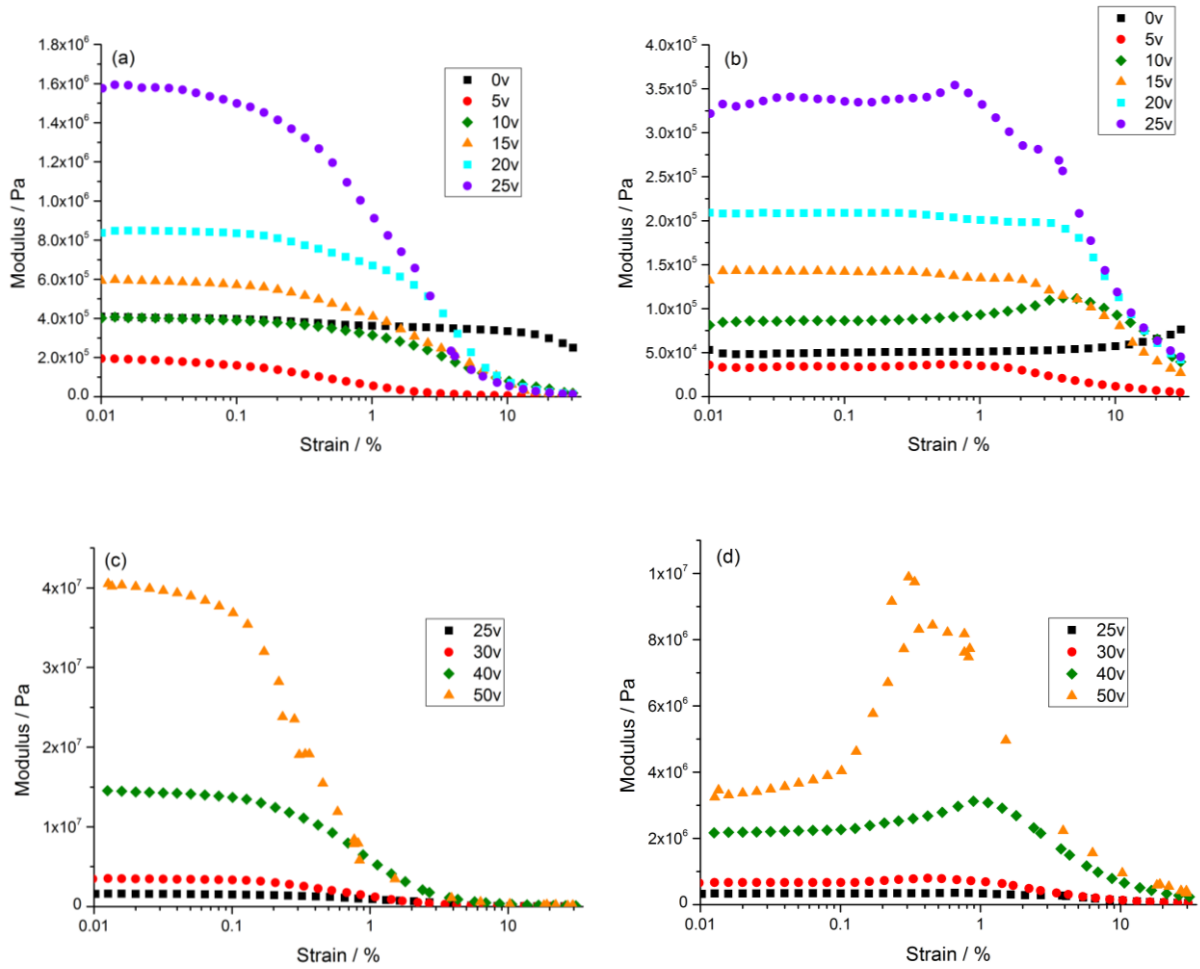
Figure 5.10: Stöber silica cross-linked composite vs strain, loadings split for clarity; (a) storage, (b) loss, (c) high loading storage, (d) high loading loss

The observed trends in the cross-linked precipitated silica, of net decreased onset point with respect to the non-cross-linked samples and the shift in the loss peak position, are also seen here in figure 5.11. The precipitated and Stöber silica have different particle structures, this implies that the strain softening behaviour is independent of the structure beyond its effect on the effective volume fraction and filler spacing. It should be noted that the precipitated silica fractal structure is isotropic without preference to a specific axis, and this result should not be applied to anisotropic particles.
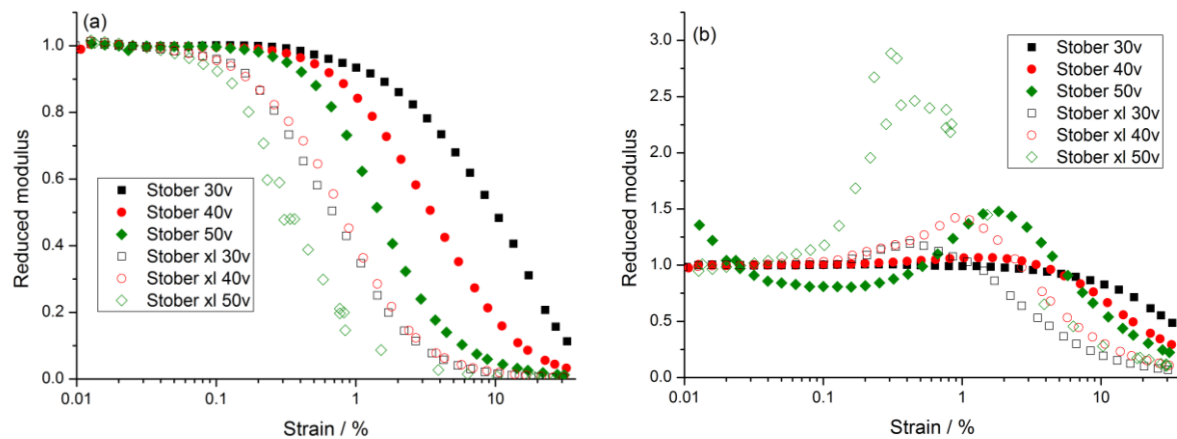
Figure 5.11: Reduced (a) storage and (b) loss modulus comparison of Stöber silica and cross-linked Stöber silica composites; concentration (% volume) of filler is given in the legend

The sulfur crosslinking of the filler composites yielded different behaviours for the carbon black and silica fillers. Upon examination, carbon black composites show only a minor increase in strain softening behaviour and no shift in the onset strain, while the silica composites yield greater strain softening with a visibly decreased onset point. The general behaviour of the earlier and increased strain softening for the composites indicates a more fragile filler network; similar results have been reported for clay reinforced composites.[111, 112] We postulate that the fragility is from the cross-links increasing the rigidity of the filler structure, preventing it from deforming to bear the applied stress and instead breaking down to yield strain softening.

The difference between the carbon black and silica fillers may be the result of the surface interactions and chemistry of the filler in question. Vulcanisation forms sulphur bridges between carbon atoms, see section 3.1.2, thus bonding between the carbon on the surface and the matrix should be possible, and is thought to contribute in the reinforcement of such systems.[113] The effective crosslink bridges between the carbon black particles would increase filler contact toughness, resulting in the observed strain behaviour. In the case of the silica particles, the Si-OH functional groups on the surface do not readily form the sulphur bridges with the polymer chains, preventing filler-filler bond reinforcement by the method described. Further investigation to examine this topic would require in-situ small angle scattering techniques; x-ray scattering may provide additional information given the speed of data acquisition.

5.4 Cross-linked polybutadiene samples with 4OHPBd additive

The presence of the 4OHPBd does not appear to greatly influence the cross-linked carbon black composite behaviour. In comparison with the unmodified equivalent, figure 5.12d, the only notable change is an increase in the magnitude of the loss peak. This implies that the end functional polymer aids in the energy dissipation during filler contact breakages. As was the case with the non-cross-linked carbon black samples, the additive has not greatly affected the properties due to the lack of favourable interactions with the filler particles.
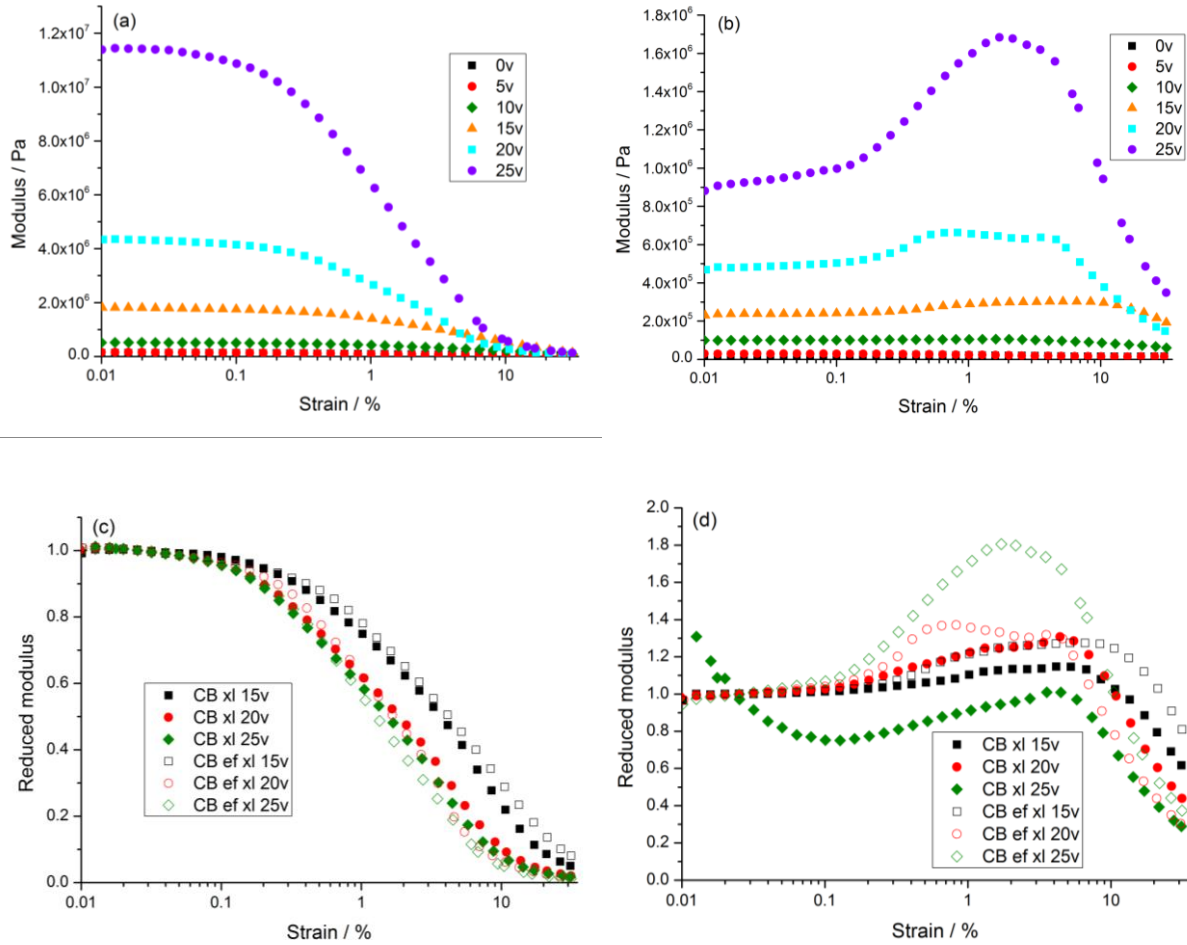
Figure 5.12: Carbon black and additive cross-linked composite modulus vs strain; (a) storage, and (b) loss; reduced (c) storage and (d) loss modulus comparison of cross-linked carbon black composites with and without 15k 4OHPBd; concentration (% volume) of filler is given in the legend

With the presence of the 4OHPBd in the precipitated silica, the presence of the peak in the loss modulus is reduced compared with the equivalent samples strain curves, figure 5.13d, while the difference caused by the 4OHPBd is minor at 20% precipitated silica volume fraction (blue), for the other compositions the effect is clear. This is in agreement with the non-vulcanised precipitated silica findings, and is caused by the lack of filler-filler contacts breaking with strain.

For the storage modulus, figure 5.13c, the onset point of strain softening does not appear to have changed.
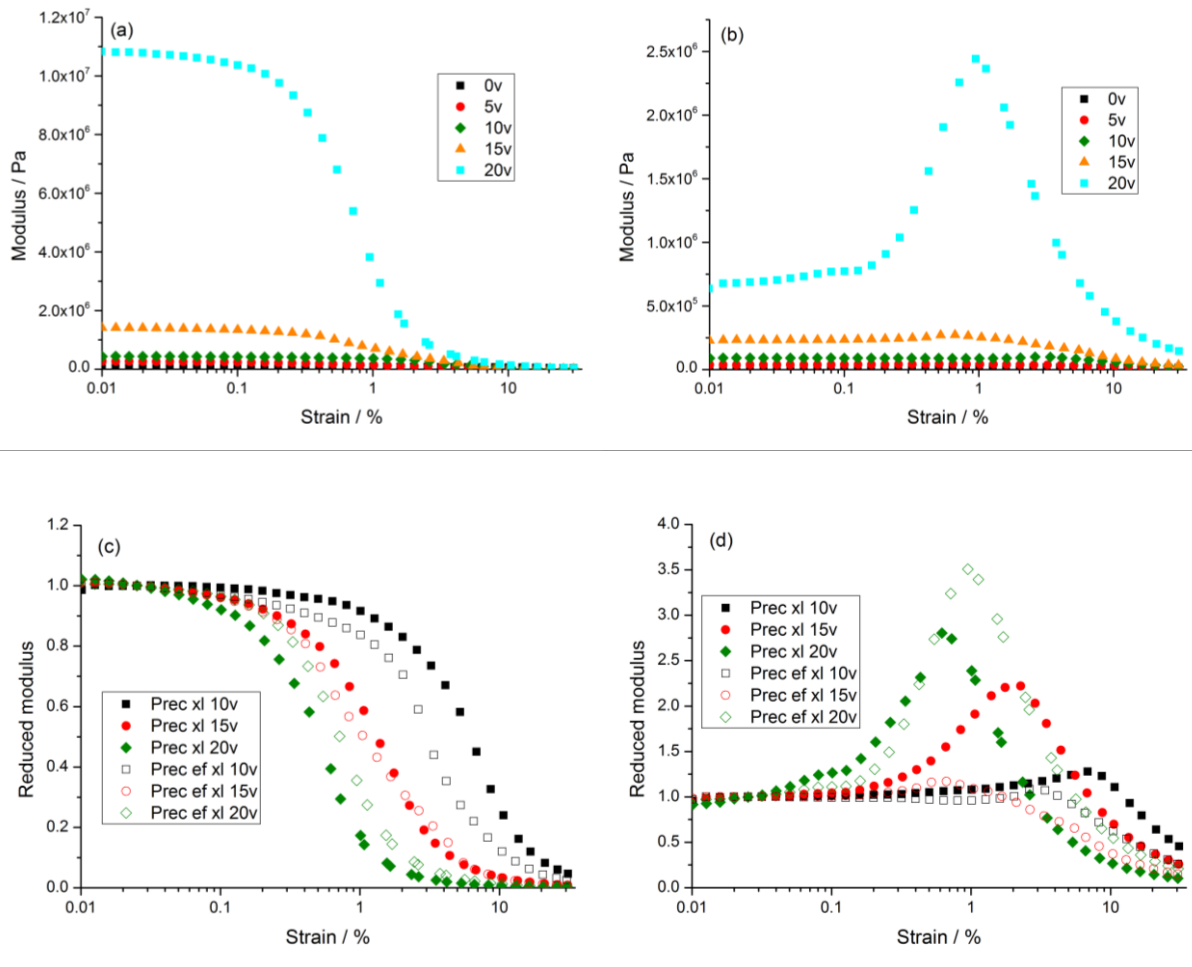
Figure 5.13: Precipitated silica and additive cross-linked composite modulus vs strain; (a) storage, and (b) loss; reduced (c) storage and (d) loss modulus comparison of cross-linked precipitated silica composites with and without 15k 4OHPBd; concentration (% volume) of filler is given in the legend

The lack of filler contact breakages is interesting when considered with the finding of increased filler network rigidity due to cross-linking. Together these suggest that even with the increased stiffness and lack of reorganisation which should lead to stress amplification and filler network bonds breaking, no breakdown is observed. This serves to highlight the importance of the particle-matrix interface and interactions in these composites.

The Stöber silica composite trends are in agreement with the trend observed in the precipitated silica; there is a removal or decreased presence of the loss peak, figure 5.14d, with the presence of the end functional polybutadiene. The onset of strain softening is also higher and more gradual, figure 5.15a, than without the presence of the 4OHPBd as seen in the non-cross-linked equivalents. This gradual onset implies the increase of network breakages with strain is less

severe and the network may be able to deform to a greater extend with the presence of the end functional polymer.

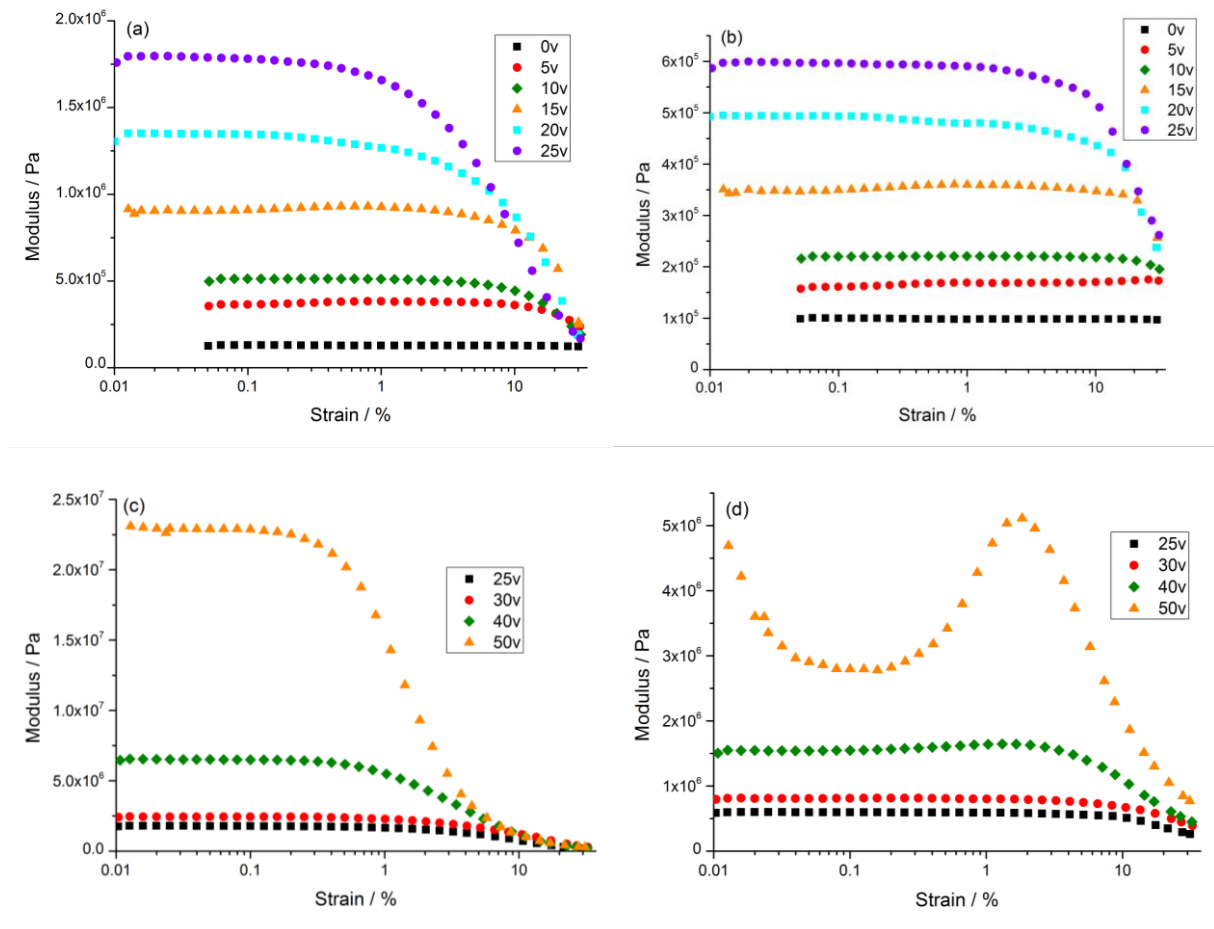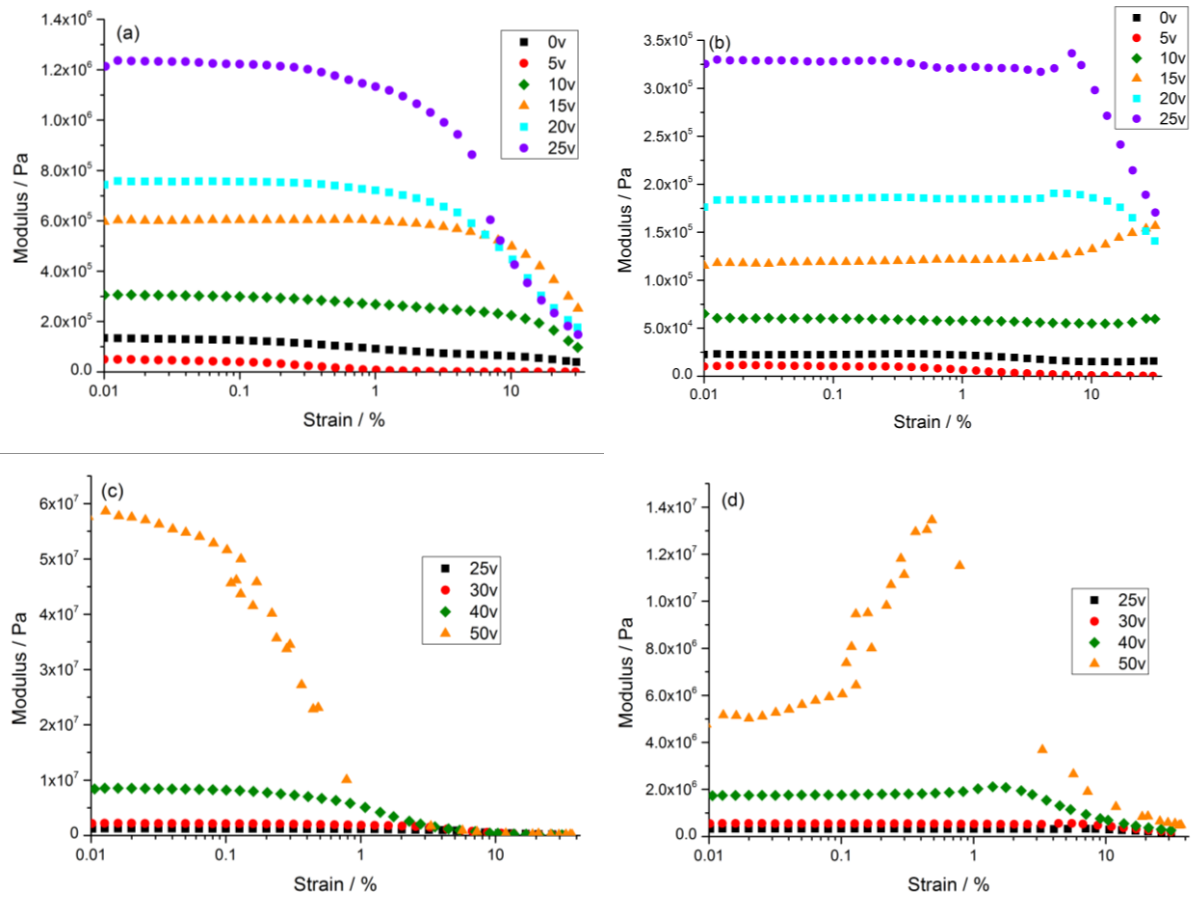Figure 5.14: Stöber silica cross-linked and additive composite modulus vs strain, loadings split for clarity; (a) storage, (b) loss, (c) high loading storage, (d) high loading loss; concentration (% volume) of filler is given in the legend
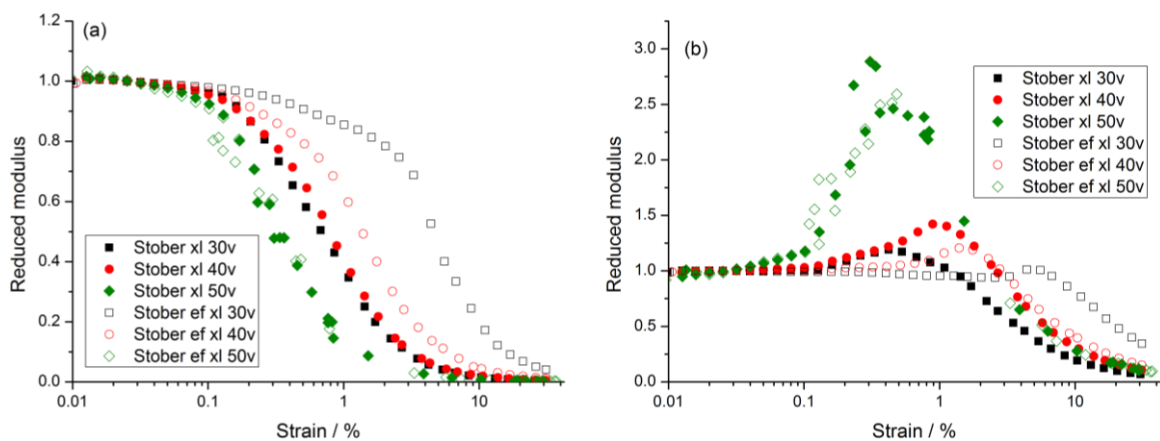
Figure 5.15: Reduced (a) storage and (b) loss modulus comparison of Stöber silica and Stöber silica with end functional polybutadiene cross-linked composites; concentration (% volume) of filler is given in the legend

102

Unlike the case in the non-cross-linked 15k 4OHPBd Stöber silica composites, figure 5.6d, the loss peak is still visible at 40 and 50 percent volume fraction, figure 5.15b, suggesting that there is a filler network breaks to dissipate energy, and the difference that may arise from the hindrance of filler reorganisation. Regardless of crosslinking, in both the end-functionalised Stöber silica systems there is a presence of a correlated filler network; however the Stöber silica particles have weak interactions due to the brush layer. Without the crosslinking sites, little energy is required to break apart networks and reorganise the filler as strain is applied, resulting in no increase in energy loss to these factors. With the cross-linked polymer, however, the percolating networks are fixed in position and energy is required to break and deform the aggregates when sufficient strain is applied, yielding the loss peak. As a related note, the loss peak is only prominent in the 50% Stöber silica sample, figure 5.12d (orange), which means that insufficient surface coverage, mentioned before with the precipitated silica, may be responsible for the peak.

5.5   Analysis with fitted Kraus strain softening model

To establish numerical measures of the softening data, the kinetic agglomeration and de-agglomeration model devised by Kraus was employed. [34] Although completely empirical in the determination of the parameters, its relative simplicity prevents over-parameterisation and provides values that can be examined to for insight into the composite material behaviour. The equations, 2.12 and 2.15, were fit simultaneously to both the storage and loss modulus respectively. The parameters for the two rate exponents and critical strain were allowed to vary to determine both their value and the associated uncertainty.

Results of the fitting were mixed, appendix 10.2 with failure of the loss peak location due to the conjoined fit being the most visible deviation. The option of separately fitting the storage and loss modulus curves was entertained, but it was concluded this would lead to over-parameterisation and irrelevant data and was dropped. The strain softening onset is first examined, and then the rate constant exponents, and finally the parameters are discussed as a whole.

5.5.1 Strain softening onset

The onset of strain softening was treated as the critical strain value in the storage modulus Kraus fitting. Softening was observed for most samples; though in the case of higher strains applied the neat or low filler volume fraction samples this phenomenon may indicate presence of sample wall slip instead of physical softening.

Table 5.1: Modulus critical strain point, % strain

	Volume fraction							
Filler type	0.05	0.1	0.15	0.2	0.25	0.3	0.4	0.5
CB	52.9 ± 3.6	31.6 ± 2.9	6.96 ± 0.56	3.34 ± 0.29	1.43 ± 0.17	-	-	-
Prec.	30.3 ± 1.5	22.3 ± 1.6	5.92 ± 0.65	2.75 ± 0.19	-	-	-	-
Stöber	76 ± 21	47.8 ± 6.8	31.2 ± 1.7	17.8 ± 1.3	10.59 ± 0.94	12.55 ± 0.99	4.58 ± 0.44	1.66 ± 0.08
CB ef	180 ± 24	53.2 ± 3.4	12.80 ± 0.72	3.19 ± 0.19	2.31 ± 0.16	-	-	-
Prec. ef	76 ± 9	28.4 ± 0.9	6.70 ± 0.44	2.51 ± 0.11	-	-	-	-
Stöber ef	114 ± 18	119 ± 30	72 ± 8	38.1 ± 1.7	33.4 ± 1.0	32.4 ± 1.3	11.87 ± 0.47	5.57 ± 0.26
CB xl	33 ± 6	11.9 ± 1.3	4.44 ± 0.67	2.20 ± 0.36	1.51 ± 0.13	-	-	-
Prec. xl	19.1 ± 4.5	8.79 ± 1.25	1.81 ± 0.18	0.60 ± 0.03	-	-	-	-
Stöber xl	0.57 ± 0.07	4.61 ± 0.82	2.55 ± 0.24	3.57 ± 0.38	1.52 ± 0.15	0.86 ± 0.08	0.88 ± 0.06	0.39 ± 0.01
CB ef xl	3.07 ± 0.25	8.42 ± 0.70	5.89 ± 0.95	2.15 ± 0.29	1.59 ± 0.16	-	-	-
Prec. ef xl	1.43 ± 0.14	3.94 ± 0.48	1.36 ± 0.13	0.86 ± 0.03	-	-	-	-
Stöber ef xl	0.37 ± 0.02	74 ± 21	360 ± 300	23.8 ± 3.2	11.0 ± 1.3	5.78 ± 0.74	1.73 ± 0.21	0.38 ± 0.01

With exception of lower filler volume fractions in the cross-linked samples, there is a trend of decreasing softening onset point with increasing filler content, in agreement with the qualitative observations. Assuming network reinforcement, this counter intuitively implies weaker network bonds with increased filler networking; however, with greater interconnectedness the rigidity of the structure will increase, preventing even distribution of stress and forcing breakages of the particle contacts at lower strains through strain amplification. This is similar to reported literature results for clay composite systems. [111, 112]
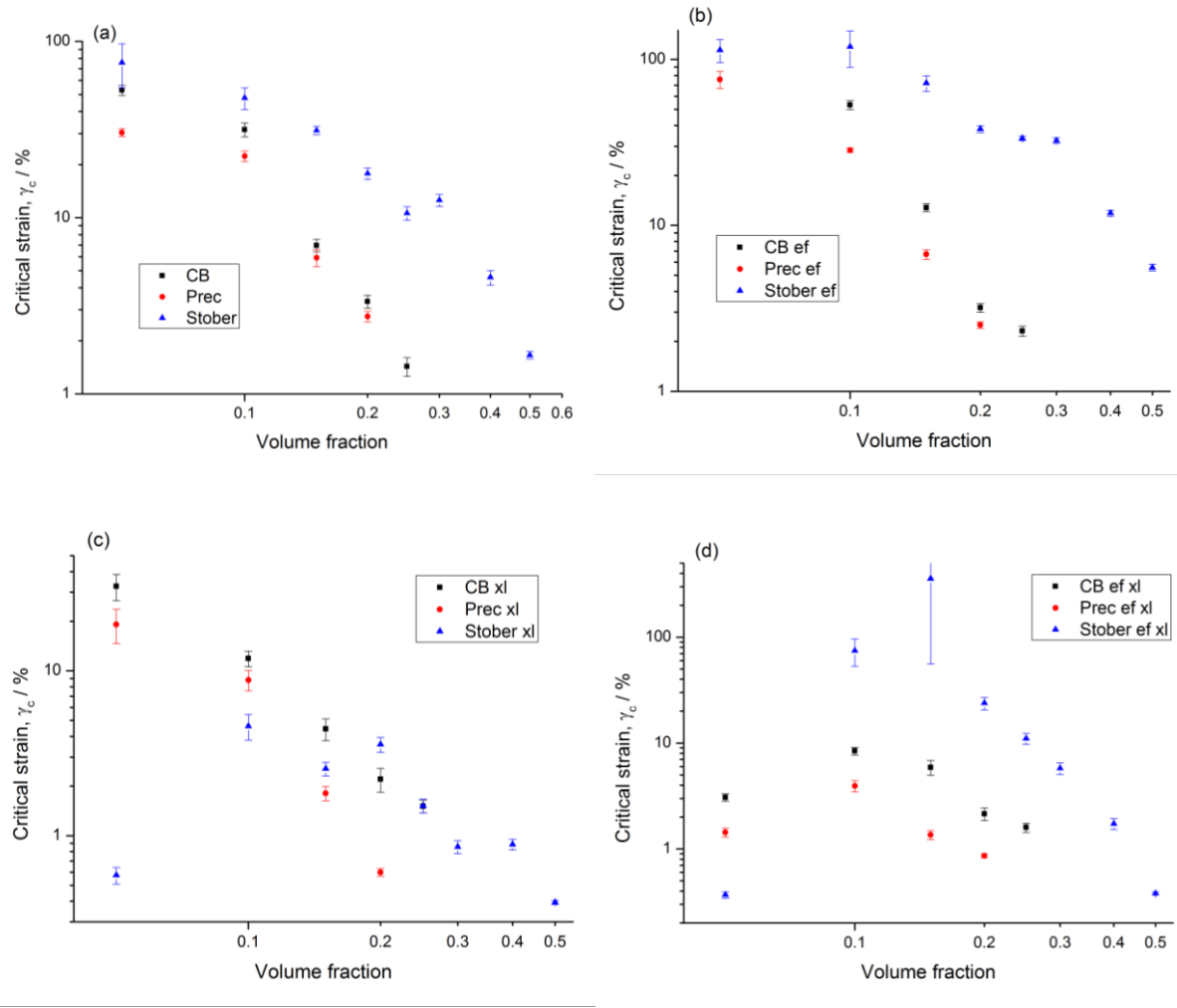
Figure 5.16: strain softening onset values against filler content for all composite samples

For the Stöber silica non-vulcanised samples, figure 5.13a/b, the onset of the softening occurs at a high strain before 20% volume fraction is reached and is often beyond the measurement range of the experiment, a case of no observed softening. There is a notable increase in the rate of change after this concentration, suggesting strain softening only occurs after this point. Although 20% volume fraction is before the percolation threshold, this lack of softening and the change of slope imply that some filler-filler interactions are required for the Payne effect and support the concept that the reinforcement and strain softening come from filler networking.

Without crosslinking, the high volume fraction composites yield at approximately 5-10% strain, however with cross-linking this value is reduced by about an order of magnitude. Differences in structural rigidity may also explain the difference in onset at lower filler fractions between non-cross-linked and cross-linked samples. In the absence of crosslinks, filler aggregates are able to distort to evenly distribute the applied stress. The crosslink network inhibits polymer flow, resulting in strain amplification about particle contacts and breakages at lower strains.

The early strain onset observed with 5% filler fraction for the Stöber silica cross-linked composite samples is a clear outlier from the mentioned trends. This may be related to the decreases in modulus seen in the frequency sweeps, with the common cause of interference between the crosslinks and filler weakening the material.

5.5.2 Rate exponents in the Kraus model

There are two exponents in the formulation of Kraus' empirical model used to describe the order of the filler contacts breakdown and reformation as dependent on strain. Kraus assumed that these exponents were equal and summed them into a single exponent; however, here they have been kept separate to analyse both processes. While the Kraus model does not have predictive capacities, previous works have often reported an exponent value of 0.6 for both processes. [29] Changes in the bond reformation exponent will be discussed first.

Table 5.2: Bond reformation rate exponent, *n,* for all composites

Filler type	Volume fraction							
	0.05	0.1	0.15	0.2	0.25	0.3	0.4	0.5
CB	1.14 ± 0.07	0.68 ± 0.04	0.65 ± 0.03	0.59 ± 0.03	0.48 ± 0.03	-	-	-
Prec.	1.75 ± 0.18	1.16 ± 0.11	0.73 ± 0.06	0.76 ± 0.03	-	-	-	-
Stöber	1.57 ± 0.41	0.96 ± 0.13	1.89 ± 0.23	1.02 ± 0.08	0.82 ± 0.06	0.81 ± 0.05	0.79 ± 0.05	0.83 ± 0.03
CB ef	0.91 ± 0.06	0.62 ± 0.02	0.61 ± 0.02	0.54 ± 0.02	0.55 ± 0.02	-	-	-
Prec. ef	1.88 ± 0.21	2.09 ± 0.15	1.21 ± 0.08	1.09 ± 0.04	-	-	-	-
Stöber ef	1.53 ± 0.16	1.42 ± 0.23	1.37 ± 0.13	1.27 ± 0.07	1.87 ± 0.12	1.51 ± 0.10	1.25 ± 0.06	1.31 ± 0.07
CB xl	0.52 ± 0.06	0.56 ± 0.04	0.45 ± 0.04	0.46 ± 0.04	0.51 ± 0.03	-	-	-
Prec. xl	0.37 ± 0.05	0.75 ± 0.08	0.92 ± 0.06	1.05 ± 0.04	-	-	-	-
Stöber xl	0.57 ± 0.03	0.50 ± 0.05	0.69 ± 0.04	0.81 ± 0.06	0.74 ± 0.04	0.84 ± 0.04	0.80 ± 0.03	0.85 ± 0.02
CB ef xl	0.48 ± 0.02	0.53 ± 0.03	0.39 ± 0.03	0.61 ± 0.04	0.62 ± 0.03	-	-	-
Prec. ef xl	0.48 ± 0.02	0.75 ± 0.06	0.73 ± 0.04	1.01 ± 0.03	-	-	-	-
Stöber ef xl	0.86 ± 0.04	0.40 ± 0.04	0.38 ± 0.09	0.63 ± 0.06	0.72 ± 0.06	0.71 ± 0.06	0.76 ± 0.05	0.86 ± 0.02

The rate exponent of reformation is initially decreases with increasing filler fraction in the non-cross-linked samples, figure 5.17a/b, and then plateaus to a constant value. For carbon black, this value is close to that observed in literature, 0.5 - 0.6.[29] The consistency of the exponent at the higher filler loadings implies the nature of the filler network, if present, does not vary in this regime. For the silica filler samples the calculated exponent is greater; however given the

differences in the materials this is unsurprising, and a higher exponent suggests a more rapid loss of contact reformation with increasing strain possibly from shorter range interactions. This is supported by the further increased exponent in the end functionalised silica where the brush layer prevents particle contacts from forming.
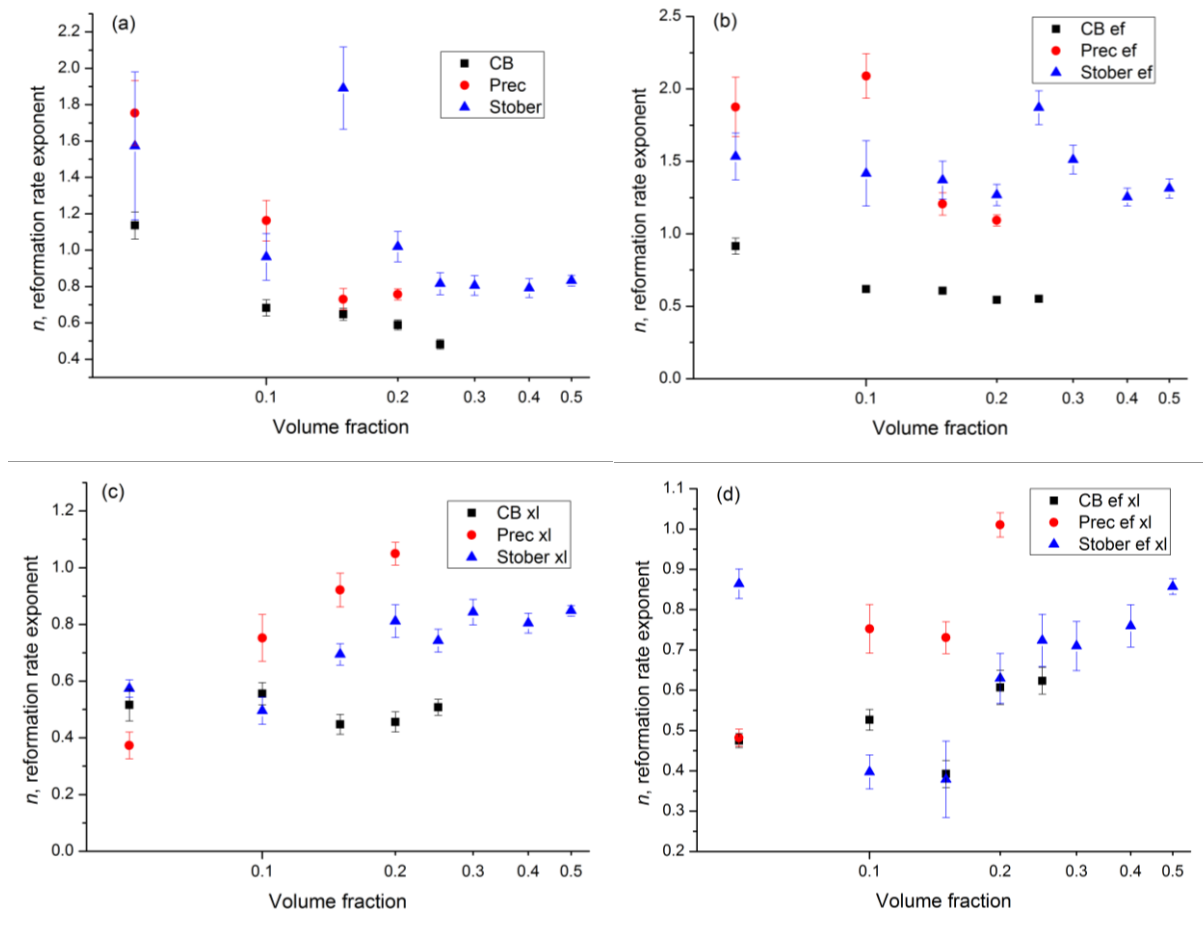
Figure 5.17: Reformation rate exponent, n, against filler content for all composite samples

For the cross-linked samples, figure 5.17c/d, there is a trend of increasing reformation rate exponent value with filler content in the silica samples. A rapid decrease in the network reformation rate implies weaker filler-filler interactions with increased filler content, however this does not take into account the crosslinks which may prevent the structures from reorganising to reform contacts. The lack of this increase with the carbon black may be the result of higher flexibility in the filler aggregates, or improved rebinding between the particles by polymer bridging.

The polymer-carbon black surface interaction is requires less energy when compared with the silica surface interactions.[92] This smaller energy difference would allow for the polymer in the matrix to aid in the reformation of polymer bridges and result in a lower exponent and less dependence on the volume fraction for the carbon black compared with the silica samples.

Table 5.3: Bond breaking rate exponent, *m,* for all composites

Filler type	Volume fraction							
	0.05	0.1	0.15	0.2	0.25	0.3	0.4	0.5
CB	0.017 ± 0.002	0.037 ± 0.004	0.072 ± 0.007	0.131 ± 0.008	0.233 ± 0.014	-	-	-
Prec.	0.020 ± 0.005	0.047 ± 0.007	0.345 ± 0.029	0.583 ± 0.028	-	-	-	-
Stöber	0.031 ± 0.005	0.048 ± 0.008	0.024 ± 0.005	0.037 ± 0.007	0.066 ± 0.008	0.058 ± 0.007	0.113 ± 0.011	0.707 ± 0.031
CB ef	0.013 ± 0.001	0.034 ± 0.003	0.057 ± 0.005	0.148 ± 0.008	0.245 ± 0.012	-	-	-
Prec. ef	0.013 ± 0.002	0.022 ± 0.005	0.136 ± 0.013	1.178 ± 0.050	-	-	-	-
Stöber ef	0.009 ± 0.001	0.017 ± 0.002	0.021 ± 0.003	0.020 ± 0.003	0.021 ± 0.003	0.018 ± 0.003	0.028 ± 0.005	0.041 ± 0.007
CB xl	0.073 ± 0.008	0.094 ± 0.008	0.156 ± 0.012	0.213 ± 0.017	0.452 ± 0.031	-	-	-
Prec. xl	0.118 ± 0.011	0.125 ± 0.014	0.654 ± 0.048	1.026 ± 0.056	-	-	-	-
Stöber xl	0.230 ± 0.019	0.167 ± 0.016	0.115 ± 0.011	0.102 ± 0.013	0.147 ± 0.013	0.206 ± 0.017	0.483 ± 0.031	1.111 ± 0.037
CB ef xl	0.054 ± 0.006	0.094 ± 0.006	0.172 ± 0.012	0.230 ± 0.017	0.509 ± 0.031	-	-	-
Prec. ef xl	0.181 ± 0.011	0.114 ± 0.014	0.179 ± 0.014	1.183 ± 0.046	-	-	-	-
Stöber ef xl	0.183 ± 0.016	0.042 ± 0.006	0.061 ± 0.008	0.069 ± 0.008	0.076 ± 0.010	0.096 ± 0.013	0.173 ± 0.017	1.173 ± 0.0038

The breaking rate exponent was found to increase with filler concentration for most samples after 0.1 volume fraction, figure 5.18, with a few notable exceptions. The lack of a change at low filler concentrations suggests that it is percolating network bonds that break during sample deformation. For the non-cross-linked carbon black samples, figure 5.18a/b, this growth increases steadily towards 0.3 with less growth than for the precipitated silica samples. This low exponent value implies that the rate of bond severance does not change rapidly with increasing strain, and alludes to the greater flexibility in the carbon black aggregates mentioned before. There also appears to be little change with the presence of 4OHPBd, as expected due to the lack of surface binding to the carbon black. In regards to theories attributing the strain softening to the presence of chain ends, the significant increase in the number of chains and chain ends from molecular weight differences does not appear to have an effect.
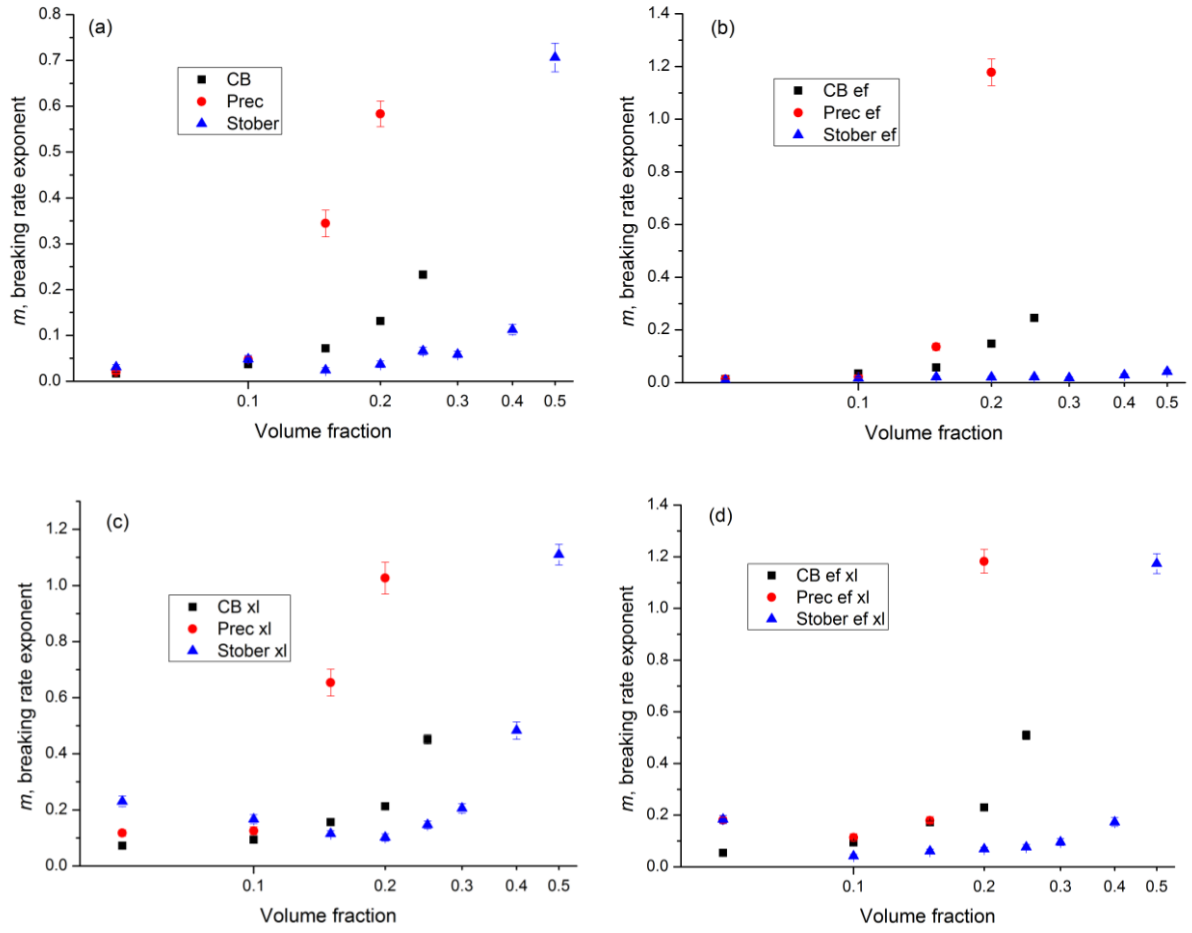
Figure 5.18: Breaking rate exponent, *m,* against filler content for all composite samples

For the non-cross-linked silica samples, the growth in the exponent, *m*, is greater than for the carbon black and results in larger exponential values at high filler content. These larger exponents suggest the filler network breaks down rapidly with increasing strain, which may be from the rigidity of the network leading to strain amplification at contact points. For the Stöber silica the increase occurs at and above 0.3 volume fraction, suggesting a percolating network is required for this effect.

Comparing the samples with and without end functional polybutadiene, figure 5.18a and b, the presence of the polymer removes or delays the growth of the exponent. This is in agreement with the removal of the loss peak in the data and the interpretation of its cause. The presence of a significant polymer brush layer prevents the formation of particle contacts, thus these non-present contacts cannot be broken with strain and the exponent is effectively zero. There is a large increase seen in the end functional precipitated silica composite at 0.2 filler volume fraction, as mentioned before in section 5.2 this may be due to the polymer brush failing to provide full steric hindrance without this particle contacts forming.

From comparison of figures 5.18a/b and 5.18c/d there appear to be some changes to the nature of the strain softening. The calculated exponents for the composites have approximately doubled without the end functional polybutadiene, with the carbon black filler achieving a value close to that seen in literature.[29] The crosslinking preventing reorganisation of the filler clusters and increasing the rigidity of the network may be the cause of this effect. Also of note is the presence of a decreasing Stöber silica composite exponent between 0.05 and 0.2 volume fraction, figure 5.18c; at this filler concentration a full percolating network has not formed, so the significant presence of this exponent is unusual. This observation is related to the decrease in matrix reinforcement found in these samples, section 4.3, with is theorised to be caused by the filler particles affecting the polymer crosslink network.

The presence of end functional polybutadiene in the cross-linked matrix did not affect the carbon black sample exponents as the polymer does not form a brush layer on this filler. For the silica samples, the trend of removal of the exponent baring high filler content, as was seen in the non-cross-linked samples, is observed. Overall, the breaking rate exponent was found to increase with filler content and was greater in systems with rigid filler aggregates.

5.5.3   Kraus fit conclusions

From qualitative analysis of the fit parameters, several conclusions can be made about the Payne effect and its causes. The shifts in the exponents and onset point with filler concentration allude to the importance of filler contacts and networking in the reinforcement and softening, while the also highlighting the effect of the filler network properties on the composite, and in particular, the concept of the rigidity of the filler network. Under stress, the filler network can either deform or break; deformations allow for the storage of elastic energy in the network should not result in strain softening behaviour while breakages in the network structure prevent the bearing of the stress by the filler and yield softening behaviour. Flexible aggregate structures result in few breakages and strain softening, observed in the comparison of the carbon black and silica composites. The stronger surface-matrix interaction energy and material modulus of the silica should result in a stiffer network compared with the carbon black. This network would yield a higher breakdown rate exponent and a lower critical strain point, both of which are observed for the precipitated silica. Change in the softening onset point and breakdown exponent in the samples with cross-linking also evidence the importance of the filler network flexibility and reorganisation.

With the end functionalised Stöber silica samples, the breakdown rate exponent was found to be almost zero in most cases; this would correspond to a network breakdown that is independent of

strain amplitude, with the observed softening behaviour due to the prevention of contact reformation. While this fit does agree with the data and support the concept that the loss peak is due to network breakages, it is at odds with the physical picture of the Kraus model where the applied strain breaks the network bonds to cause softening behaviour. The implication is that although the Kraus kinetic approach can empirically describe the softening, it lacks molecular level conceptual understanding of the processes involved in the Payne effect.

5.6   Conclusions

Examining the differences of strain softening has elucidated how a filler network and its nature affect a composite's mechanical properties. The addition of the 15k 4OHPBd polymer to the silica samples resulted in the reduction or removal of the loss peak in the strain softening. The end functional polymer is known to disperse silica particles, thus the observation supports theory that the loss peak is due to energy dissipation from filler contact breakages. This implies that a percolation, including particle contacts, is required for the full Payne effect to be observed, and highlights the importance of filler networks in these composites. Notably, the strain softening of the storage modulus is still seen, hinting that the contact breakages are not solely responsible for the Payne effect.

Differences in the strain onset behaviour between the carbon black and silica samples, as well as the effect of the end functional polymer, point to how the relative strength of the filler-filler interactions affects the nature of the strain softening. For the silica, interaction with the polybutadiene matrix is unfavourable, yielding particle-particle contacts that are not easily broken at smaller strains. When the applied stress overcomes the contact strength, the aggregates rapidly break resulting in a sharp transition. In contrast, the carbon black/polybutadiene interactions are more favourable, with comparatively weaker particle-particle contacts where present. Small strains result in some of these bonds breaking while others remain intact, resulting in a disperse onset of softening behaviour. This hypothesis is supported with the strain sweeps of the silica composites with end functional polymer, the transition to softening behaviour is gradual and the additive is known to form a surface layer to limit filler interaction and contacts.

Crosslinking also provides insight into how filler reorientations affect the composite behaviour. Preventing filler reorientation via crosslinking the polymer matrix was found to decrease the onset of strain softening by an order of magnitude. It is hypothesised that the lack of reorientation prevented even distribution of stress in the filler network with strain amplification and breakages occurring at filler contact sites, yielding the observed change in onset behaviour.

These results are supported by the numerical analysis of the strain softening, which found that the rigidity of the filler network is involved in the behaviour. Stiffer networks that could not support deformation resulted in contact breakages and softening at lower strains; in agreement with the onset behaviour of the silica and the effect of crosslinking on the strain onset point. Furthermore, it was concluded that while the Kraus model provides a decent empirical fit to the data, it does not adequately describe the microscopic properties that yield the softening behaviour.

6 Small angle neutron scattering

The analysis of small angle neutron scattering (SANS) allows for the examination of the structure of a material at the nanoscale. From this, important conclusions can be drawn about a material's macroscopic properties and how they arise. Theories for describing the rubber reinforcement seen with the addition of filler particles rely on phenomenon and structures present at this nanometer length scale. SANS and SESANS were used to examine the filler structure of precipitated and Stöber silica samples, and the data was analysed to determine the filler and polymer structure. First the individual filler particle structure and the presence of an end functional polybutadiene brush layer are examined. Further work is then done to analyse the filler aggregate networks and the effect of the presence of the polybutadiene brush layer on these networks at several length-scales. Finally, scattering performed on strained samples is examined to determine the impact of strain on the filler aggregates.

6.1 Stöber silica/4OHPBd core-shell particle structure

Initial small angle experiments were performed on the samples listed in table 6.1 by the LOQ instrument, data was collected before, during, and after a 3 hour period at 75˚C. The beam was collimated to an 8mm diameter circle, detectors were in standard position, and a temperature controlled scaffold was used to hold the cells. Unfortunately for the stretched Stöber silica composite samples, creep over the timescale of the measurements prevented the acquisition of useful data.

Table 6.1: LOQ sample name and weight percent composition

Sample	20k 4OHPBd w/w percent (± 0.2)	per-deuterated PBd w/w percent (± 0.2)	Stöber silica w/w percent (± 0.2)
LOQ 0% Si dPBd composite	0.0	100.0	0.0
LOQ 2% Si dPBd composite	1.6	96.5	1.9
LOQ 4% Si dPBd composite	3.2	92.7	4.1
LOQ 8% Si dPBd composite	6.3	85.7	8.0
LOQ 12% Si dPBd composite	10.0	78.3	11.7
LOQ 16% Si dPBd composite	12.7	71.0	16.3
LOQ 20% Si dPBd composite	16.0	64.0	20.0
LOQ 24% Si dPBd composite	19.2	56.8	24.0
LOQ 0% Si dPBd composite stretch	0.0	100.0	0.0
LOQ 4% Si dPBd composite stretch	3.2	92.8	4.0
LOQ 12% Si dPBd composite stretch	9.8	78.2	12.0
LOQ 24% Si dPBd composite stretch	19.2	56.8	24.0

The pre and post cure data shows clear differences in the scattering intensity, with the data displayed providing a representative sample; therefore some structural change has occurred during the curing process. As the shift does not involve drastic changes to the curve intensity and shape, with implies variations on the same structural type, model fitting is required. As the end functional polymer is known to form surface layers on silica, the data was fitted to a two part function composed of a core shell term and a Debye polymer term for any unbound polymer, visualised in figure 6.1b. [85] Given the Q range observed by the instrument the decision was made to not include a term with an inter-particle structure factor. The core shell form factor, $P(Q)$, is given by

$$P(Q) = \frac{1}{V_s}\left[3V_c(\rho_c - \rho_s)\frac{(\sin(Qr_c) - Qr_c\cos(Qr_c))}{(Qr_c)^3} + 3V_s(\rho_s - \rho_{solv})\frac{(\sin(Qr_s) - Qr\cos(Qr_s))}{(Qr_s)^3}\right]^2$$

(6.1)

where r_c is the core radius, r_s is the combined core and shell radius, V_s is the total particle volume, V_c is the core volume. ρ_s, ρ_c, and ρ_{solv} are the shell, core, and solvent scattering length densities, respectively; these were constrained to 0.5 x 10^{-6} Å^{-2}, 3.7 x 10^{-6} Å^{-2}, and 6.61 x 10^{-6} Å^{-2} for the fitting. In the fitting process, a polydispersity term was included for both the particle radius and brush layer thickness, and was held as 1.15 and 1.05 respectively. This value is factored into the uncertainty in the given values.

The Debye scattering relation for Gaussian polymer chains is in its standard form,

$$D(Q) = \frac{2(e^{-(QR_g)^2} + (QR_g)^2 - 1)}{(QR_g)^4} \tag{6.2}$$

where R_g is the polymer radius of gyration. A scaling factor was included on both terms along with a background term. The combined scattering function is,

$$I(Q) = B + C_1 P(Q) + C_3 D(Q) \tag{6.3}$$

where B is the incoherent background intensity and C is the scaling factor for each term. Resulting fit parameters are shown in table 6.2; fitted curves are included on figures 6.1c and 6.1d.
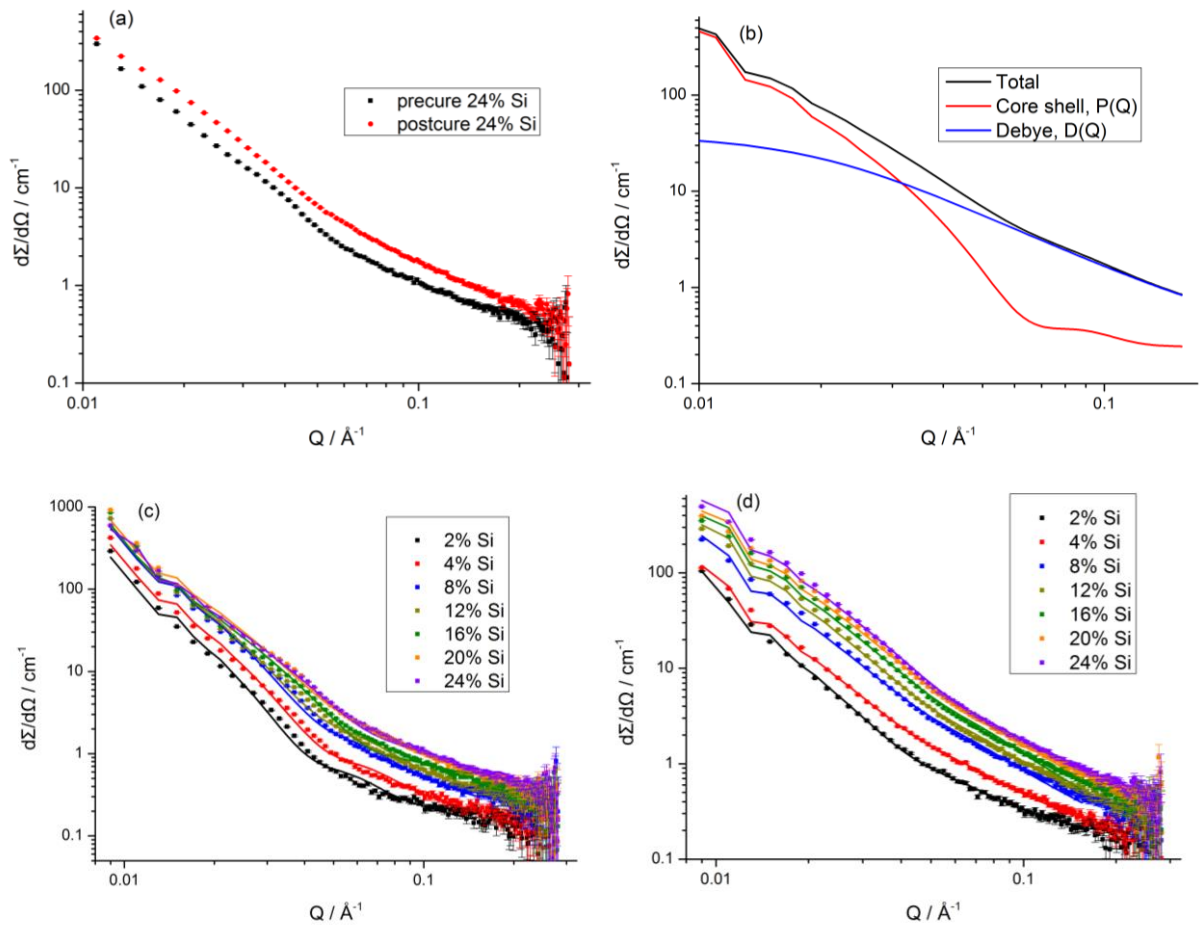
Figure 6.1: SANS data for (a) high silica fraction curing comparison (b) components of the fit (c) collective pre-cure data and fits (d) collective post-cure data and fits

Table 6.2: Fit parameters for LOQ scattering results, before and after 3 hour cure at 75 ˚C

Sample	Radius / Å	Thickness / Å	Background / cm⁻¹	R_g / Å	Core shell scaling, C_1	Debye scaling, C_3
Precure						
2% Si	433 ± 65	139 ± 7	0.106 ± 0.004	49.6 ± 0.1	0.0107 ± 0.0001	1.40 ± 0.02
4% Si	448 ± 67	122 ± 6	0.095 ± 0.003	38.5 ± 0.1	0.0175 ± 0.0002	1.63 ± 0.02
8% Si	445 ± 67	127 ± 6	0.140 ± 0.005	55.2 ± 0.1	0.0271 ± 0.0004	5.79 ± 0.06
12% Si	444 ± 67	126 ± 6	0.117 ± 0.004	57.2 ± 0.1	0.0285 ± 0.0004	8.09 ± 0.09
16% Si	448 ± 67	125 ± 6	0.272 ± 0.009	63.8 ± 0.1	0.0310 ± 0.0004	11.00 ± 0.12
20% Si	461 ± 69	108 ± 5	0.201 ± 0.007	59.7 ± 0.1	0.0388 ± 0.0005	14.02 ± 0.16
24% Si	448 ± 96	96 ± 5	0.384 ± 0.013	77.6 ± 0.1	0.0370 ± 0.0005	20.00 ± 0.22
Postcure						
2% Si	438 ± 66	123 ± 6	0.136 ± 0.005	63.6 ± 0.1	0.0051 ± 0.0001	3.90 ± 0.04
4% Si	424 ± 64	119 ± 6	0.117 ± 0.004	64.3 ± 0.1	0.0065 ± 0.0001	7.58 ± 0.08
8% Si	425 ± 64	114 ± 6	0.066 ± 0.002	65.0 ± 0.1	0.0140 ± 0.0002	16.43 ± 0.18
12% Si	418 ± 63	109 ± 5	0.090 ± 0.003	67.2 ± 0.1	0.0210 ± 0.0003	21.01 ± 0.24
16% Si	418 ± 63	105 ± 5	0.001 ± 0.0001	67.9 ± 0.1	0.0273 ± 0.0004	28.97 ± 0.32
20% Si	419 ± 63	102 ± 5	0.045 ± 0.0016	68.9 ± 0.1	0.0318 ± 0.0004	36.88 ± 0.41
24% Si	430 ± 65	91 ± 5	0.231 ± 0.008	73.8 ± 0.1	0.0465 ± 0.0006	39.71 ± 0.44

The calculated scattering is in good agreement with the data; figure 6.1 c/d, suggesting that the model chosen is accurate for this system. The average particle radius, 436 ± 17 Å, is in rough agreement with the DLS measurement on the Stöber silica. Similarly most of the layer thicknesses are in reasonable agreement with previous neutron reflectivity measurements, which found a surface layer of 159 Å thickness[85]. The polymer radius of gyration is in the expected range for the 20k 4OHPBd, the calculated value from molecular weight is 58.7 angstroms.
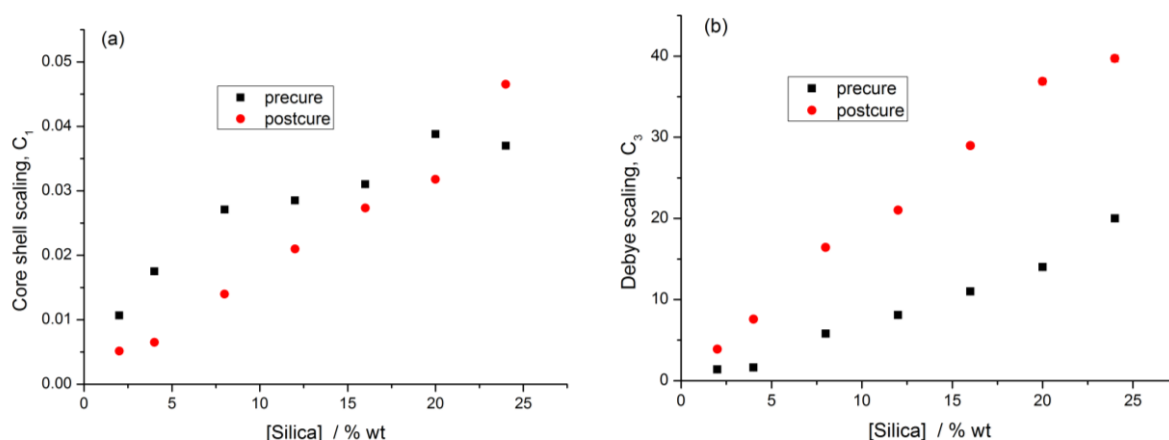
Figure 6.2: The core shell particle and Debye scattering scaling terms against silica concentration

Both the pre and post cure core shell scaling factors show, figure 6.2a, an approximately linear trend with similar magnitudes, suggesting little change in the core shell nature with the concentration of particles. Data variance has decreased after sample annealing; this suggests rearrangement of the system toward a general equilibrium state shared by the samples. This is further supported by the increase in the free polymer Debye term with the curing process, shown in figure 6.2b. Interestingly, this does appear to have affected the hydroxyl end functional surface layer as its value decreases slightly with the annealing process, table 6.2.

A possibility for the increased Debye factor is the improved dispersion of the free hydroxyl capped and deuterated polybutadiene during the annealing process. The separation of deuterated and hydrogenous polymers is well known and documented, however the increased temperature would overcome the minor enthalpic incompatibility between the polymers and lead to improved chain interpenetration and greater Debye scattering. [114]

This chain mixing does not explain the minor decrease seen in the brush layer thickness; however the increased temperature during the curing process would remove 4OHPBd chains from the silica surfaces through thermal motions decreasing the layer thickness and moving the bulk ratio of hydrogenous and deuterated polymer closer to unity. This change is polymer concentrations would increase Debye scattering; thus increased thermal motions causing improved chain interpenetration and removal of adsorbed polymer can explain the trends observed in the samples.

The formation of the core shell particle structure is confirmation of the surface segregation found by Kimani et al, and this brush layer provides steric hindrance to allow for silica dispersion in the matrix.[85]

6.2   Stöber silica/4OHPBd network structure

Several of the LOQ samples were also examined on SANS2D. The same core shell particle form factor and Debye scattering term used previously for the LOQ fits were also applied here, labelled as *P(Q)* and *D(Q)* respectively. As greater length scales can be probed by the SANS2D instrument an additional term containing an inter-particle structure factor was included and a generic fractal term was chosen for this purpose. Calculated by Teixeira[115], the structure term in relation to scattering vector is

$$S(Q) = \left[\frac{D\Gamma(D-1)\sin((D-1)\tan^{-1}(Q\xi))}{(Qr_c)^D(1+\frac{1}{Q^2\xi^2})^{\frac{D-1}{2}}} \right] \qquad (6.4)$$

where D is the fractal dimension, ξ is the correlation length, r_c is the length scale of the primary component, and Γ is the gamma function.

The complete scattering function is

$$I(Q) = B + C_1 P(Q) + C_2 P(Q)S(Q) + C_3 D(Q) \qquad (6.5)$$

where B is the background intensity and C represents a scaling factor for each term. This function is representative of a system with dispersed and aggregated core shell particles. Scattering length densities and core radius dimension were tied for the fitting process, a polydispersity term was included for both the particle radius and brush layer thickness, and was held as 1.15 and 1.05 respectively and factored into the uncertainty; fractal dimension, correlation length, shell thickness, and the scale factor were allowed to vary within physically possible limits.
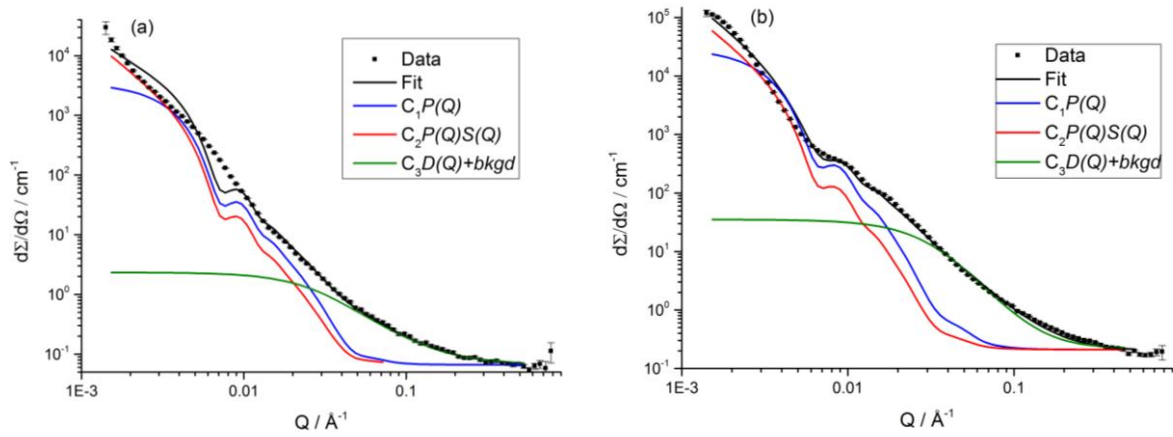
Figure 6.3: Scattering intensity and fits of (a) 2% and (b) 24% silica weight fraction composite samples

High Q scattering ($Q > 0.04$ Å^{-1}) is dominated by the Debye term, figure 6.3, its significant presence suggests a number of unbound end functional polymer in the matrix and a saturated surface layer, or significant penetration of the hydrogenous bulk into the brush layer. The difference in scaling terms between the samples is roughly proportional to the change in the concentration of 20k 4OHPBd as seen the LOQ data; as such there is little change in the nature of the coating layer or free polymer with the shift in polymer concentration. Low Q scattering is controlled by the particle core shell terms, fitting yielded similar relative proportions for both samples. As with the Debye term this suggests there is no major shift in the nature of the particle dispersion between 2% and 24% weight fraction. The relative stability of the proportions of free and aggregated particles is interesting as independence of the large scale structure from particle concentration may not be expected. Correlation lengths for both the samples are outside the measurement range of the instrument, hence the large associated error and evidence that the

networking in the system is long range even at low particle concentrations. The fractal dimension value, 2.20, corresponds to a reaction limited aggregate network.[116] Given the bound polymer layer about each particle this result is reasonable as lasting contacts would not form immediately.

Divergence of the fits from the data in the low Q region does suggest the presence of unaccounted phenomena. The 2% data the lack of a local minima at 0.008 Å^{-1} in comparison with the fit is a notable example, though this feature is not observed in the 24% sample. The other divergence is the lack of a predicted core shell peak in the data at 0.004 Å^{-1} in both samples. Given the known and regular shape of the Stöber silica nanospheres and the well documented binding of the end functional polymer, only the nature of the network remains tentative. The equation used for fit assumes a fractal structure, including self-similarity on different length scales; however it is possible that the nature of the clustering cannot be described as self-similar due to aggregates of specific sizes forming in the matrix. Unfortunately the limitations of the equipment prevent analysis at higher length scales and determination of the network structure. But the fractal model does provide a reasonable representation of the system in question, and will be applied to other systems.

Table 6.3: Fit parameters for 2% and 24% weight fraction composite samples

Parameter	2% silica	24% silica
Radius, r_s / Å	405 ± 61	405 ± 61
Shell thickness r_c-r_s / Å	120 ± 15	173 ± 24
Fractal dimension D	2.20 ± 0.02	2.20 ± 0.02
Correlation length ξ / Å	33000 ± 32000	4400 ± 3100
C_1 Free particle scale	$(2.14 \pm 0.7) \times 10^{-3}$	$(11.0 \pm 0.05) \times 10^{-3}$
C_2 Aggregate scale	$(1.10 \pm 0.7) \times 10^{-3}$	$(4.13 \pm 0.03) \times 10^{-3}$
C_3 Debye scale	2.27 ± 0.05	35.5 ± 0.6
4OH-PBd-20k R_g / Å	58 ± 1	58 ± 1
d6-PBd-140k R_g / Å	134 ± 1	134 ± 1

6.3   Silica dispersion via 4OHPBd

The core shell aggregate model devised in section 6.2 was applied to data gathered by Richard Thompson, Nigel Clarke, and Solomon Kimani on D11 at ILL, to determine the effect of the end functional polymer on silica dispersion, samples listed in table 6.4.

Table 6.4: D11 sample name and weight percent composition

Sample	4OHPBd w/w percent ($\pm$ 0.2)	per-deuterated PBd w/w percent ($\pm$ 0.2)	Precipitated silica w/w percent ($\pm$ 0.2)
D11 20Si 0 4OH-PBd	0.0	80.0	20.0
D11 20Si 2 4OH-PBd-5k	2.0	78.0	20.0
D11 20Si 4 4OH-PBd-5k	4.0	76.0	20.0
D11 20Si 8 4OH-PBd-5k	8.0	72.0	20.0
D11 20Si 16 4OH-PBd-5k	16.0	64.0	20.0
D11 20Si 4 4OH-PBd-10k	4.0	76.0	20.0
D11 20Si 8 4OH-PBd-10k	8.0	72.0	20.0
D11 20Si 16 4OH-PBd-10k	16.0	64.0	20.0
D11 20Si 2 4OH-PBd-15k	2.0	78.0	20.0
D11 20Si 4 4OH-PBd-15k	4.0	76.0	20.0
D11 20Si 8 4OH-PBd-15k	8.0	72.0	20.0
D11 20Si 16 4OH-PBd-15k	16.0	64.0	20.0
D11 20Si 4 4OH-PBd-20k	4.0	76.0	20.0
D11 20Si 16 4OH-PBd-20k	16.0	64.0	20.0
D11 5Si 2 4OH-PBd-5k	2.0	93.0	5.0
D11 5Si 4 4OH-PBd-5k	4.0	91.0	5.0
D11 5Si 8 4OH-PBd-5k	8.0	87.0	5.0
D11 5Si 16 4OH-PBd-5k	16.0	79.0	5.0
D11 5Si 2 4OH-PBd-10k	2.0	93.0	5.0
D11 5Si 4 4OH-PBd-10k	4.0	91.0	5.0
D11 5Si 8 4OH-PBd-10k	8.0	87.0	5.0
D11 5Si 16 4OH-PBd-10k	16.0	79.0	5.0
D11 5Si 2 4OH-PBd-15k	2.0	93.0	5.0
D11 5Si 4 4OH-PBd-15k	4.0	91.0	5.0
D11 5Si 8 4OH-PBd-15k	8.0	87.0	5.0
D11 5Si 16 4OH-PBd-15k	16.0	79.0	5.0
D11 5Si 1 4OH-PBd-20k	1.0	94.0	5.0
D11 5Si 2 4OH-PBd-20k	2.0	93.0	5.0

Qualitatively there is a clear increase in the Debye polymer scattering (0.04 Å^{-1}) in the samples with end functional polymer concentration, most visible in figure 6.4a. Although less noticeable the shift in slope at low Q values in both samples indicates the changes to the long range structure with the addition of the end functional polymer regardless of filler concentration.
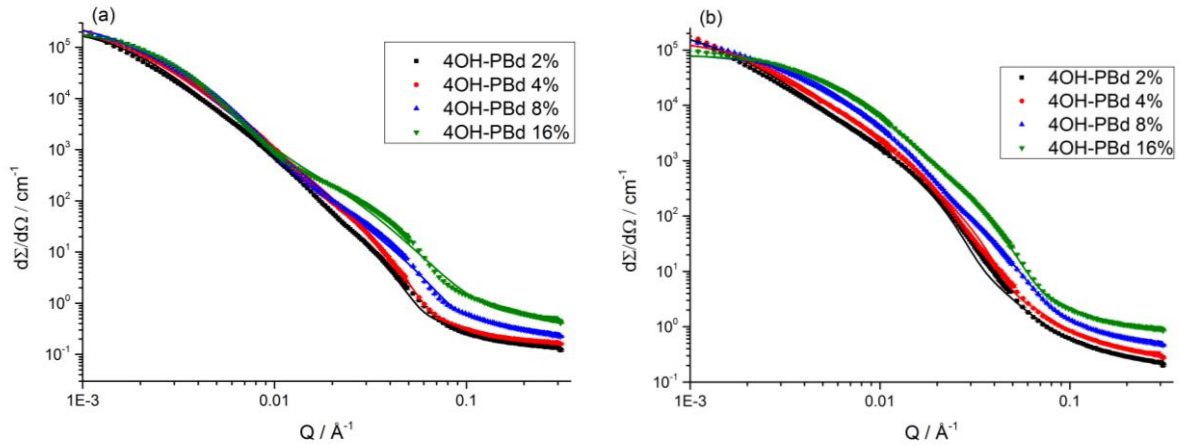
Figure 6.4: SANS data and fits for (a) 5% w/w precipitated silica (b) 20% w/w precipitated silica samples with various 5k 4OHPBd loadings, polymer content (% weight) is given in the legend.

The scattering model described in sections 6.1 and 6.2 was used here to fit the data. Scattering length densities for the shell, core, and matrix were held at 0.5 x 10^{-6} Å^{-2}, 3.7 x 10^{-6} Å^{-2}, and 6.61 x 10^{-6} Å^{-2}, respectively; and the free polymer R_g was fixed at the value calculated from end functional chain length. The other descriptive parameters and scaling factors were allowed to vary within physical limits.

Table 6.5: Fitted parameters for the D11 samples, free particles and aggregates model

Sample code	r_s / Å	$r_c\text{-}r_s$ / Å	ξ / Å	D	C_1	C_2	C_3	Debye Rg / Å
20Si 0 4OHPBd	51	0.0	1160	2.20	0	0.133	0	-
20Si 2 4OHPBd-5k	68	12	810	2.24	1.51E-6	0.0605	6.13E-6	30
20Si 4 4OHPBd-5k	38	22	430	2.45	6.94E-8	0.0306	8.68E-4	30
20Si 8 4OHPBd-5k	23	25	180	2.85	5.16E-3	0.0138	3.19	30
20Si 16 4OHPBd-5k	29	13	200	2.69	0.0147	0.0394	1.99	30
20Si 4 4OHPBd-10k	66	20	790	2.14	4.90E-7	0.0719	0	-
20Si 8 4OHPBd-10k	34	28	200	2.85	2.23E-3	0.0198	5.15	38
20Si 16 4OHPBd-10k	29	20	180	2.79	6.11E-3	0.0519	2.27	38
20Si 2 4OHPBd-15k	74	16	880	2.29	2.54E-3	0.0394	0.933	47
20Si 4 4OHPBd-15k	66	27	760	2.23	9.78E-6	0.031	0.002	47
20Si 8 4OHPBd-15k	46	50	390	2.36	4.67E-3	0.0251	6.12	47
20Si 16 4OHPBd-15k	34	27	150	2.98	8.79E-3	0.0197	11.99	47
20Si 4 4OHPBd-20k	65	35	720	2.22	1.95E-6	0.0249	3.74	58
20Si 16 4OHPBd-20k	33	21	160	3.00	8.59E-8	0.0467	13.2	58
5Si 2 4OHPBd-5k	29	24	550	2.80	1.31E-3	4.95E-3	0.169	30
5Si 4 4OHPBd-5k	18	34	560	2.69	1.70E-3	2.08E-3	0.252	30
5Si 8 4OHPBd-5k	21	10	550	2.77	0.0200	6.82E-3	0.2	30
5Si 16 4OHPBd-5k	30	76	390	3.00	0.0258	5.12E-3	8.06	30
5Si 2 4OHPBd-10k	30	23	620	2.76	5.62E-9	4.75E-3	0.0294	38
5Si 4 4OHPBd-10k	36	34	570	2.66	1.31E-4	7.04E-3	0.246	38
5Si 8 4OHPBd-10k	27	14	430	2.83	9.87E-3	5.49E-3	0.306	38
5Si 16 4OHPBd-10k	32	12	540	2.78	0.0512	8.25E-6	1.15	38
5Si 2 4OHPBd-15k	27	33	650	2.77	1.69E-7	1.67E-3	1.03	47
5Si 4 4OHPBd-15k	31	45	540	2.73	3.12E-4	2.27E-3	2.04	47
5Si 8 4OHPBd-15k	34	33	330	2.93	3.25E-3	6.56E-3	1.15	47
5Si 16 4OHPBd-15k	29	29	420	2.82	0.0336	5.42E-3	6.64	47
5Si 1 4OHPBd-20k	49	33	1050	2.56	2.53E-6	3.73E-3	0.60	58
5Si 2 4OHPBd-20k	31	41	610	2.79	1.02E-4	1.55E-3	2.34	58

Although there are minor variations in the trends from sample to sample, the same general features were found throughout; an exemplar set is shown in figure 6.5. Decreasing correlation length and increasing fractal dimension were found with increasing 4OHPBd concentration. Also the free particle (C_1) and Debye scaling factors increased while the particle aggregate scaling factor (C_2) decreased with the increased presence of end functional polymer. The shift in the Debye scaling is expected with the increased mixing of hydrogenous and deuterated polymer and in agreement with the qualitative trend seen in the scattered intensity.
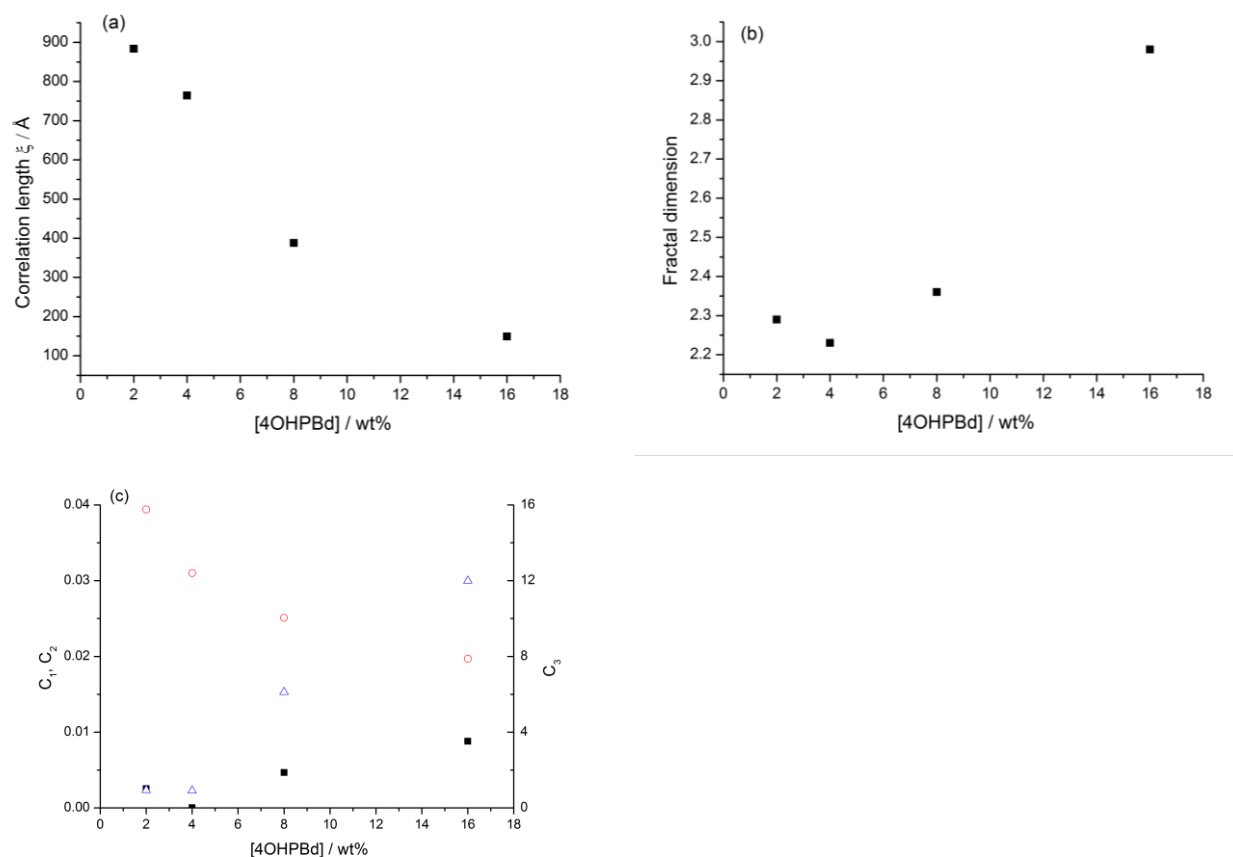
Figure 6.5: Dependence of fitted parameters for 20% silica composite at different concentrations of 15k 4OHPBd additive (a) Correlation length, (b) fractal dimension and (c) scaling factors, C_1 (black solid squares), C_2 (red open circles) and C_3 (blue open triangles).

The changes in correlation length, free particle scale, and particle aggregate scale all suggest the dispersion of the precipitated silica aggregates by the hydroxyl end functional polymer. The shift in fractal dimension from 2.20 towards 3 seems to be at odds with the other observations; however this trend needs to be understood in terms of the changing correlation length and aggregation level. The dispersal of large loosely bound agglomerates by the end functional polymer produces small compact aggregates which are composed of a number of well bonded primary silica particles, as seen with TEM. A small compact structure results in a higher fractal dimension along with a decreased correlation length and aggregate scaling term, as observed in the data.

For further analysis the surface area of the silica was calculated by treating the particles as ideal spheres with a set radius. From this average chain surface area was determined for each sample, and the fitted parameters were examined. A step in correlation length is visible at ~1000 Å^2 per chain in the 20% silica samples, figure 6.6b. Although this change is not visible in the 5% samples, figure 6.6a, there is insufficient data in the region for certainty. The correlation length

plateau in the 20% silica at high chain surface area, and the point at 2000 Å^2 in the 5% silica, are in agreement with the measured bare silica aggregate size. This step and the value of the correlation length at low chain density suggest a critical surface concentration of 4OHPBd must be reached to achieve dispersion of the precipitated silica, which does not depend on chain length.
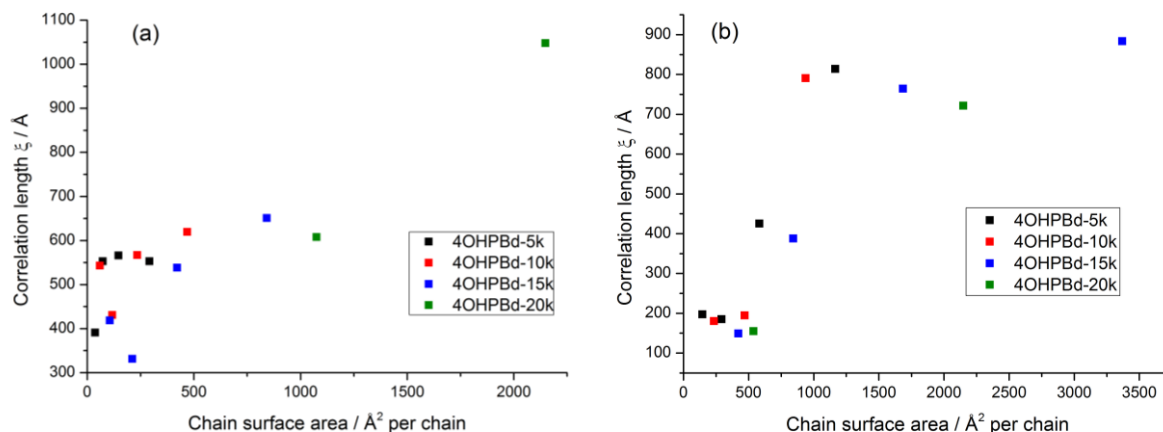
Figure 6.6: Correlation length against chain surface area for (a) 5% and (b) 20% silica weight fraction samples

Another important feature is the difference in the value of the correlation length between the 5% and 20% samples below the step, with the 20% samples having a consistently lower value. The difference is due to the nature of the fractal model, the correlation length defines the distance over which the fractal approximation holds. With agglomerates this is the average cluster diameter, however in the case of dispersed particulate systems the value is related to the average particle spacing. The higher concentration of silica in the 20% system yields smaller particle distances and the lower correlation length observed. That some correlation between the particles is present even after dispersion suggests that the particle interactions are still important and these filled rubbers may still possess long range correlations even without percolation or agglomeration.

Normalised grafting density was determined from molecular weight (M_w) and chain surface area using the method described by Aubouy *et al*. The variable σ is the number of bound chains per unit area, which is defined as the chain statistical step length squared. The step length has been reported as 9.6 Å for 1,4 polybutadiene by Aharoni and this value was used for the calculation. [117, 118]
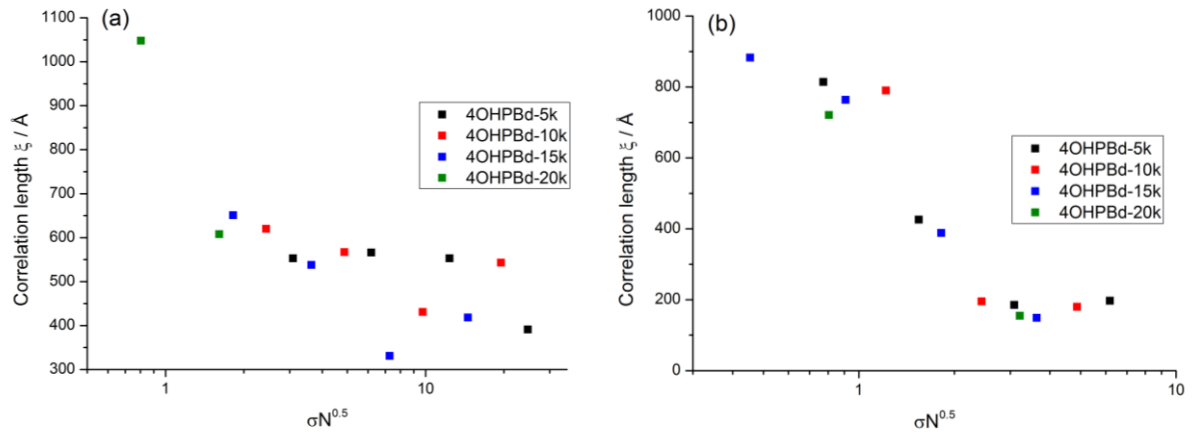
Figure 6.7: Normalised grafting density against correlation length for 5% (a) and 20% (b) silica concentrations

When the correlation length data are plotted against the normalised graft density, figure 6.7, the critical point for silica dispersion is at approximately $\sigma N^{0.5}$ equals 1. Aubouy noted when the matrix chain length exceeds that of the brush chains, there is no change in the brush layer thickness until σ approximately equals $N^{-0.5}$. This point is when the surface bound chains begin to be constrained and affected by other bound chains. In regards to the data, before the critical point the bound end functional polymer density is low and can be increased without incurring an entropy penalty, such as the case of particles in close contact. Once bound chain density is above this point any further increase is entropically unfavourable and the brush acts to sterically stabilise the silica, yielding the observed change in correlation length.
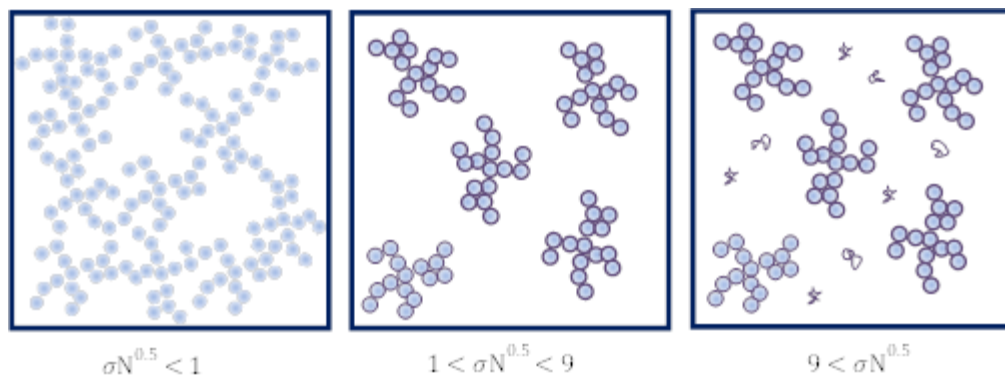
Figure 6.8: Depiction of a composite sample structure with increasing 4OHPBd additive concentration, left to right.

Three different regions of composite behavior dependent on end functional polymer concentration are visible from the SANS results, shown in figure 6.8. At low concentrations of end functional polymer, $\sigma N^{0.5} < 1$, the brush layer cannot provide steric stabilisation, and the silica forms agglomerated structures, evidenced by the fractal dimension and higher correlation

length. Once the brush concentration is significant enough to perturb the chains the silica is dispersed into individual aggregate structures, decreasing the correlation length. After surface saturation of the polymer brush is reached, approximately $9 < \sigma N^{0.5}$, further end functional polymer remains in the matrix resulting in the increase in Debye scattering visible in figure 6.4a and 6.5c. Evidence of the different filler aggregation regimes dependent on the end functional polymer concentration highlights the importance of these additives in filled rubber systems.

6.4   Long range Stöber silica network

To examine possible larger scale filler fractal structure that was implied from the analysis of the dispersion experiment, an SESANS experiment of silica filled compounds was undertaken.

Table 6.6: OFFSPEC sample composition

Sample	15k 4OHPBd / wt%	300k PBd / wt%	Stöber silica / wt%
OFFSPEC 5% Si	0.0	94.8	5.2
OFFSPEC 10% Si	0.0	90.2	9.8
OFFSPEC 25% Si	0.0	75.2	24.8
OFFSPEC 50% Si	0.0	50.0	50.0
OFFSPEC 5% Si with 4OHPBd	3.8	91.0	5.2
OFFSPEC 25% Si with 4OHPBd	20.1	55.0	24.9

The natural logarithm of the normalised polarisation can be treated as $G(z)$ with an offset and is related to the correlations in the sample. There are two major observations, firstly the change in slope with concentration, and secondly the lack of a shift in the slope at any point. In the low silica samples there is little change in the polarisation with path length, figure 6.9, which would be observed in a dilute system of free particles and no spatial heterogeneity. This presents the fact that the silica is dispersed without correlation throughout the matrix on length scales from 100 to 800 nm, either as individual particles or small clusters with small local correlation.
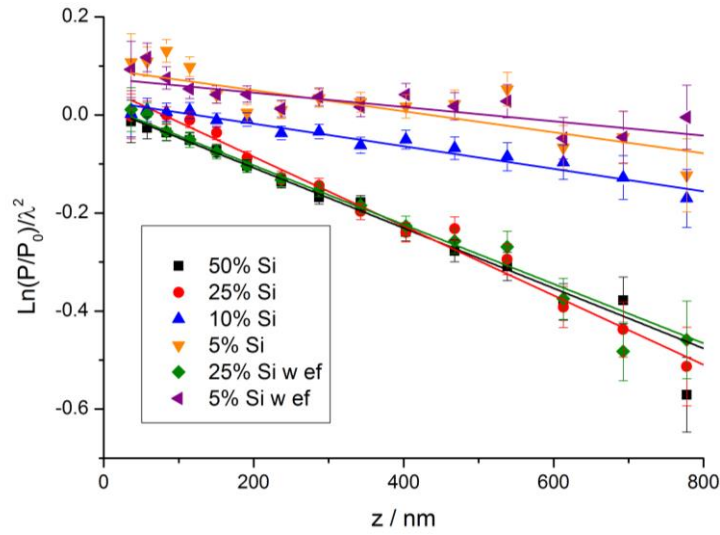
Figure 6.9: Normalised polarisation over wavelength against spin echo path length for Offspec composite samples, linear least squares regression fits

The increase in the magnitude of the slope is due to greater heterogeneity and clustering at higher particle loadings. There appears to be no apparent difference after 25% weight silica loading is reached, and the end functional polymer does not appear to have an effect on the dispersion at these length scales. The lack of change at higher silica loadings suggests a presence of a critical shift in the nature of the dispersion between 10 and 25 percent weight silica, and whatever clusters form are consistent in nature over the range measured. Interestingly this is not the percolation threshold, as this would occur at approximately 51 percent weight for the silica spheres, determined from the volume fraction required for percolation. Therefore presence of particle clustering or correlation before percolation is therefore likely. This is not unusual, as the percolation threshold is defined as the point where continuous paths can be made through the material, and does not exclude localised clustering at lower filler concentrations. The lack of a clear shift in slope implies that the present correlated structure does not cease over the length scale of the probed and there is heterogeneity in the system toward the micron length scales.

The lack of shift with the end functional polymer presence for both measured silica concentrations is explainable by the nature of the dispersion. Although the 4OHPBd is known to separate the silica spheres it does not provide any long range repulsive forces, thus the spheres remain in relatively close proximity to one another to yield a similar dispersion. Combined with the findings from the D11 experiment, this suggests that even though separated by end functional polymer the silica tends to form correlated arrangements in the matrix and create a heterogeneous dispersion.

Table 6.7: Parameters of linear least squared regression for SESANS data, figure 6.9

Sample code	Intercept	Slope / (x 10^{-4}) nm^{-1}
OFFSPEC 5% Si	0.093 ± 0.016	-2.1 ± 0.5
OFFSPEC 10% Si	0.028 ± 0.006	-2.3 ± 0.2
OFFSPEC 25% Si	0.056 ± 0.009	-7.1 ± 0.3
OFFSPEC 50% Si	0.015 ± 0.006	-6.2 ± 0.2
OFFSPEC 5% Si with 4OHPBd	0.075 ± 0.009	-1.5 ± 0.3
OFFSPEC 25% Si with 4OHPBd	0.018 ± 0.006	-6.0 ± 0.2

6.5 Study of strain on the Stöber silica network

Measurements on strained polybutadiene composite samples were performed on SANS2D at ISIS. The scattering data was analysed by comparing the relative intensities over a range of defined strains, and in certain cases by examining set cross sections of the scattering data.

Table 6.8: Name and weight percent composition of SAN2D strain test samples

Sample	15k 4OHPBd	95k dPBd	Stöber silica
SANS2D polymer blend	9.9	90.1	-
SANS2D 5% Si dPBd composite	2.0	93.0	5.0
SANS2D 5% Si hPBd composite	2.0	92.9	5.1
SANS2D 24% Si dPBd composite	9.6	66.3	24.1
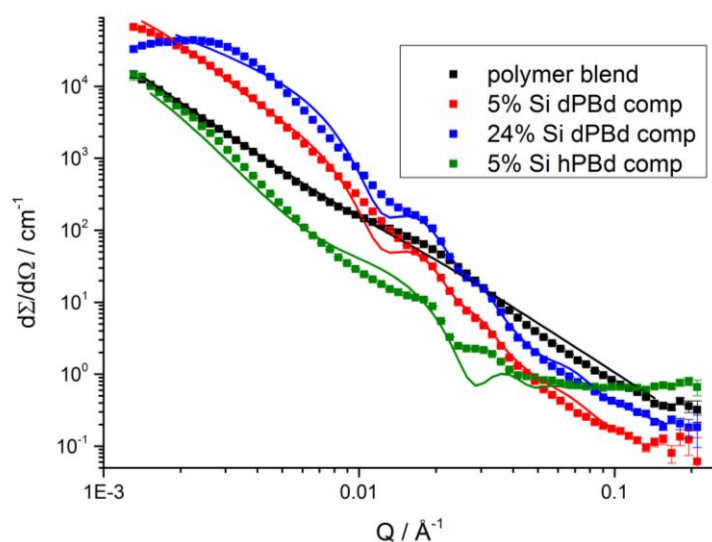
Figure 6.10: SANS2D strain experiment sample, no strain, trendlines are fitted functions

The 15k 4OHPBd/dPBd blend scattering, figure 6.10a, was fitted to a combined scattering function defined by a power scattering term and a Debye chain scattering term (equation 6.2) along with a background,

$$I(Q) = \frac{A}{Q^n} + CD(Q) + B \qquad (6.6)$$

where A and C are scaling terms, B is the incoherent background, n is the power scattering exponent. The power term defines the low Q scattering from clusters while the chain scattering term defines the chain correlations at higher Q values. Fitting to the blend sample yielded values summarized in table 6.9. The presence of the low Q scattering implies long range ordering or structures on this length scale. The polymer blend itself should not exhibit this behaviour, thus the cause is the chemicals used in the crosslinking process, such as the zinc oxide which may have aggregated into clusters after the curing of the sample. This result may need to be taken into consideration in the analysis of the other data sets. For the Debye scattering, the radius of gyration was calculated as 108.43 ± 1.34 Å, this value is similar to the calculated R_g for the 95k dPBd, 115 Å, which suggests it is this component that is the primary scattering source.

For the composite samples the combined scattering equation used for the SAN2D express and D11 analysis was again employed here. Reasonable fits were achieved for the deuterated composites, the only notable deviations occurring at low Q values (~0.002 Å^{-1}) and at 0.01- 0.02 Å^{-1}; parameters for the fits can be found in table 6.10. The deviation at low Q is clearly visible in the 24% silica data and is caused by the plateau in the scattering, a sign that the fractal structure ends at that length scale and implies localised clusters of Stöber silica aggregates. This was not observed in the SAN2D express samples, and may be due to increased brush chain density as a result of the shorter 4OHPBd chains in this experiment compared with those in the express samples. The other deviation seen in the data at 0.01 Å^{-1} is the lack of a defined trough as predicted from scattering theory, likely from some unaccounted polydispersity or structure in the samples.

The 5% hPBd composite fit contains a substantial deviation as one of the scattering peaks is not properly modelled with the correct intensity. The converted distance of approximately 200 Å suggests that the smaller individual silica particles of 100 Å radii are underrepresented in this fit.

Overall, the previously described model does fit the scattering results and the proposed filler formation of a mixture of free and aggregated particles is present in the samples. This suggests that the crosslinking of the matrix with sulphur bridges has not drastically changed the silica filler dispersion.

Table 6.9: Correlation length function fit parameters for the SANS2D polymer blend

Sample code	A ($\times 10^{-4}$) / cm^{-1}	C / cm^{-1}	n	R_g / Å	B / cm^{-1}
0% strain	15.86 ± 0.41	52.05 ± 0.55	2.435 ± 0.005	108.34 ± 1.34	0.000 ± 0.007

Table 6.10: Fitted parameters for the SANS2D samples, free particle and aggregate model

Sample code	r_s / Å	r_c-r_s / Å	ξ / Å	D	C_1	C_2	C_3	Debye Rg / Å
SANS2D 5% Si dPBd composite	155 ± 8	127.3 ± 0.5	650 ± 20	3.00 ± 0.02	(8.34 ± 0.07) x 10^{-3}	(1.55 ± 0.02) x 10^{-3}	2.53 ± 0.05	47
SANS2D 5% Si hPBd composite	155 ± 8	-	900 ± 5	3.00 ± 0.02	(0 ± 1.5) x 10^{-5}	(3.51 ± 0.01) x 10^{-3}	-	-
SANS2D 24% Si dPBd composite	155 ± 8	127.3 ± 0.5	1000 ± 10	2.00 ± 0.05	(24.9 ± 0.03) x 10^{-3}	(5.62 ± 0.04) x 10^{-3}	5.00 ± 0.03	47

As a control the cross-linked polymer blend was strained in the rig to search for possible shifts in the scattered intensity. The complete small angle scattering of both the relaxed and strained sample are shown in figure 6.11a, visually there is a slight decrease in the scattered intensity with strain. This would be expected as the extensional strain will decrease the thickness of sample material in the neutron beam. There does not appear to be significant discrepancy between the horizontal and vertical cross-sections of the data either. This would indicate that there is no shift in the polymer chain orientation with the strain, or that the shift relaxed faster than the neutron scattering window can measure. The result of no change barring a minor decrease in intensity allows for the direct analysis of any other shifts in scattering seen with the composite samples.
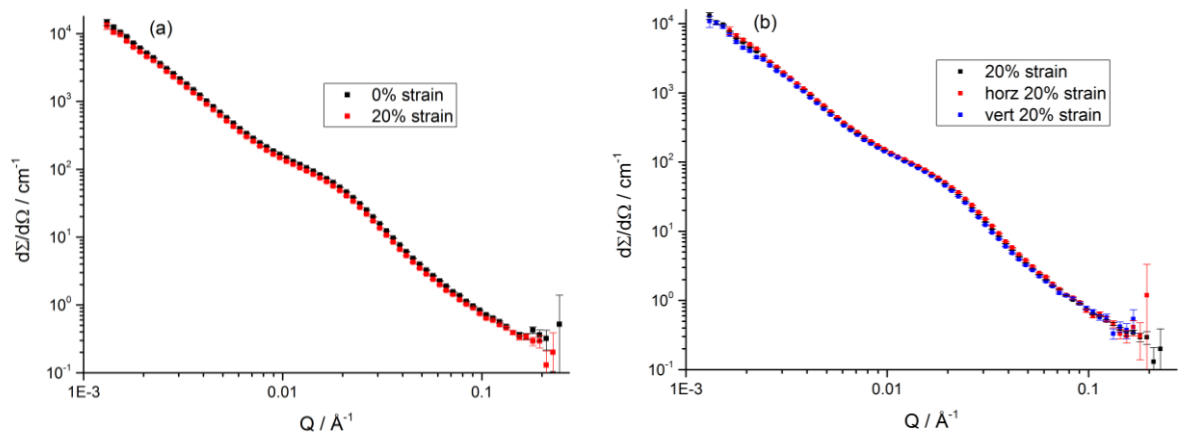
Figure 6.11: SANS2D blend sample, comparison of (a) the radial average scattering 0 and 20% strain (b) horizontal and vertical scattering slices of the data

Examination of the deuterated 5% Stöber silica composite complete small angle scattering, figure 12a, finds a minor decrease of scattering intensity, as was the case with previous examination of the polymer blend scattering. The horizontal cross-section, seen in figure 6.12b, has a slightly greater scattered intensity compared with the vertical cross-section, and complete scattering below 0.01 Å^{-1}. This suggests that the fractal filler network is broken down in the vertical direction, as would be expected from the strain on the sample. The break down does not appear to be drastic as the change is slight, and is too small to note in the fitted model with any certainty.
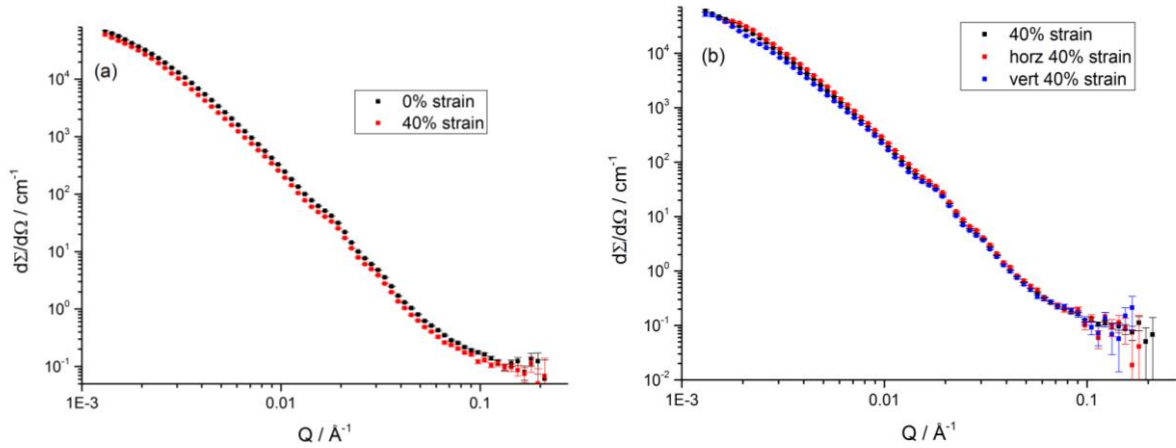
Figure 6.12: SANS2D 5% dPBd composite sample, comparison of (a) the radial average scattering 0 and 40% strain (b) horizontal and vertical scattering slices of the data
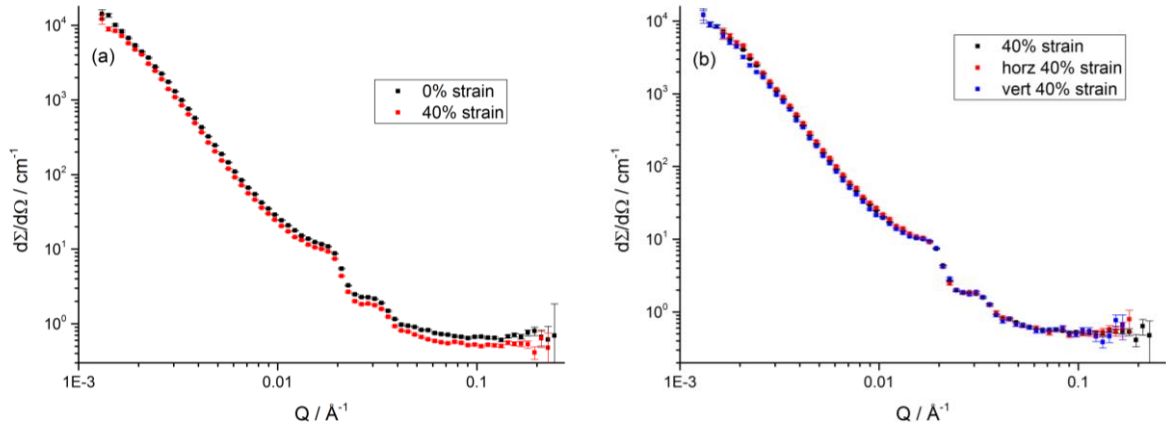
Figure 6.13: SANS2D 5% hPBd composite sample, comparison of (a) the radial average scattering 0 and 40% strain (b) horizontal and vertical scattering slices of the data

As seen before with the deuterated composite and polymer blend samples, there is a small drop in scattering intensity with the strain on the sample. The slight separation of the horizontal and vertical cross section scattering is also present. As this sample does not contain deuterated polymer, it is possible to ascribe this shift to the silica filler rather than a change in the polymer

chains. This confirms the result found with the deuterated 5% silica sample, that the fractal network is broken slightly by the strain on the rubber composite.

Unlike the case with the blend and 5% composite samples, figure 6.12 and 13, there is no visible shift in the scattering intensity with the 24% silica sample, figure 6.14. The relatively low strain may be the cause of this difference, as the sample rubber tore under further elongation and greater strains could not be reached. The lack of change suggests that the filler material does not undergo any reorganization. This is supported by the results of the low silica concentration composites which only demonstrate minimal change in the direction of the strain up to 40% strain.
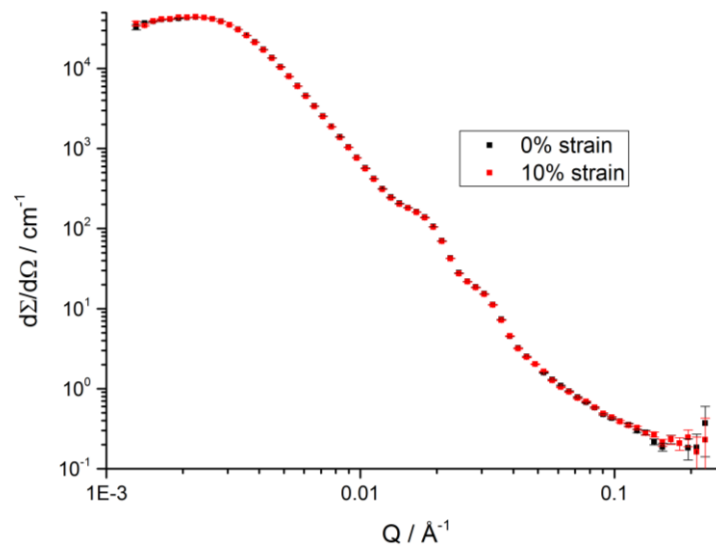
Figure 6.14: SANS2D 24% dPBd composite sample, comparison of the radial average scattering 0 and 10% strain

The minor shift in intensity and corresponding structure with strain is noteworthy, as 10% strain is still within the bounds of nonlinear rheological behaviour such as the Payne effect. Overall, there is no large scale change to the filler network with applied strain in these samples, in contrast to the change in rheological properties. There is a possibility that the change are occurring outside the experimental window, 5-600 nm, at the micron length scale, however some change in the scattering should be present here if this was the case. If filler networking and its loss with strain is responsible for the phenomena in these composites, it can be concluded that the breakdown of the network does not appear to affect the overall network correlations. As reorganisation does not occur, network breakdown and prevention from load bearing may be caused by loss of rigidity the cluster contacts, a volumetrically small effect that would not be seen with scattering techniques.

6.6 Conclusions

Study of the small angle scattering has found several notable features of the silica filler and its interaction with the end functional polymer. Results from neutron scattering studies on LOQ and SANS2D express were able to verify surface segregation of the end functional polymer and the formation of a core shell system, and noted the presence of minor desorption of the surface segregated layer with curing. Further work on D11 was able to determine the cause for the dispersion of silica by the 4OHPBd as steric stability by the polymer brush layer, evidenced by the shift in correlation length and fractal dimension at a critical brush density. The noted presence of correlations even after dispersal is interesting, and suggests that although the filler material is not strictly percolating; clustering of the filler material is still present. As models such as cluster-cluster aggregation require filler contacts and networks to explain the composite properties, analysis of systems with these filler material will provide insight into the accuracy of the models.

The SESANS work found correlations and heterogeneity occurs in these systems regardless of steric stabilisation and is present to the micron length scale, explained by the lack of long range repulsion interactions. The continued fractal correlations in the samples evidences that filler networking and aggregation is present before percolation, as has been noted before in other reports. This implies that network reinforcement theories may be valid below the percolation threshold. The observation that the end functional polymer does not drastically change the filler correlations provides a route for simple comparisons between these systems and highlights the importance of understanding factors occurring at the nanoscale, in particular the filler-filler bridging and contacts. [43, 44, 107]

Straining of the samples in the SANS2D has led to the conclusion that deformation does not greatly affect the structure of the filler network at these length scales. This implies that in the case of cross-linked samples, strain softening phenomena are not the result of large scale reorganisation of the filler materials; thus it is changes that involve a small fraction of the material, such as the breaking of cluster contacts, which are the most probable cause.

7 Quasi-elastic neutron scattering

Quasi-elastic neutron scattering provides a way to probe short-range molecular motions in composite materials. This is useful as many theories regarding the reinforcement in composites involve the effect of the filler on the polymer matrix dynamics. In particular, the hindered polymer layer about filler particles is thought to aid in both directly reinforcing the matrix and providing bonding interactions between particles. Hence characterising a possible glassy dynamics layer is important to develop the understanding and theories for composite reinforcement.

In this the end functional polybutadiene and its known surface segregation to silica was used to label different regimes in the composites and explore the dynamics. First, the influence of crosslinks on the polymer chain dynamics was investigated to establish its significance in the composite systems. Secondly, Stöber silica composite samples containing different molecular weights of 4OHPBd chain where examined to probe the dynamics about the filler surfaces at two different dynamic timescale windows. Finally the effect of strain on the polymer dynamics in these polymers was examined as changes to the glassy layer dynamics are theorised to cause the Payne effect. [119]

7.1 Effect of cross-linking on polymer dynamics

Crosslinking is thought to have some effect on the polymer dynamics, as rheology has already shown relaxation times and rheological properties are altered. To investigate this samples of various crosslink densities were examined over 3-310K with elastic window scans and fixed temperature QENS scans at 130, 160, 190, 220, 250, 280, 310, and 363K. Cross-linking was performed with benzoyl peroxide (Sigma Aldrich, 517909, Luperox A75), at 80˚C in inert atmosphere for 3 hours which was found to take the reaction to completion, see section 4.1.1. The cross-link density was controlled by the concentration of the benzoyl peroxide, the chosen sample concentrations are listed in table 7.1. For each sample, the number of polybutadiene repeat units per crosslink site was calculated and used for the notation, N cross-linked, where N equals the number of repeat units. Cylindrical aluminium cans were used to house the samples, and the temperature was regulated with the CCR system.

Table 7.1: Composition of crosslinking IRIS samples by percent weight

Sample	Benzoyl Peroxide / %wt	200k PBd / %wt	Monomers per crosslink
IRIS XLINK linear	-	100	n/a
IRIS XLINK 25 cross-linked	19.2	80.8	25.1
IRIS XLINK 50 cross-linked	10.7	89.3	50.2
IRIS XLINK 100 cross-linked	5.4	94.6	106
IRIS XLINK 1000 cross-linked	0.56	99.44	1040

Due to time constraints and loss of beam, only the linear and 25 cross-linked samples were run to completion. The general elastic peak scattering is similar for both samples, figure 7.1, with the increase in gradient occurring at 180-200K in agreement with the known glass transition temperature for 1,4 polybutadiene. The similarity confirms that the crosslinking does not drastically change the nature of the polymer dynamics and means that the same theoretical models and analysis can be used for both samples. There is a notable increase in the elastic intensity for the cross-linked polymer system, in line with hindered dynamics. Although not clearly visible in figure 7.1, this separation increases until 310K reaching an average value of 0.034 ± 0.005 across all Q values. At the highest temperature considered, 363K, the difference in elastic intensity due the cross-links appears to have diminished, suggesting a limit to the effect. The lack of dependence on Q suggests that the phenomenon does not have a characteristic length scale over the range measured.
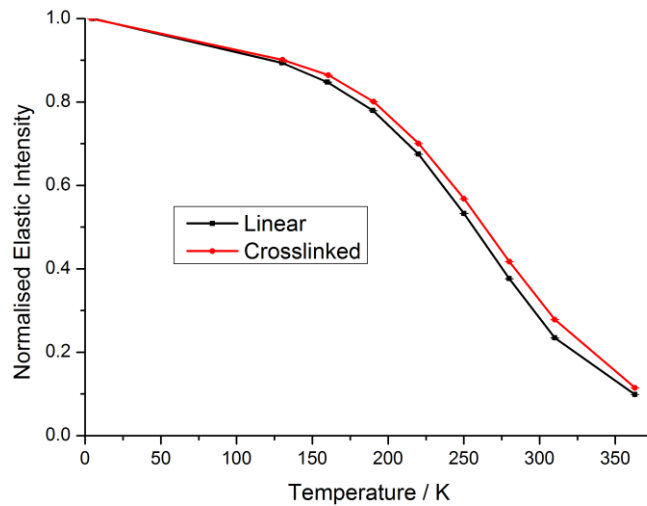
Figure 7.1: Comparison of elastic intensity for linear and highly cross-linked polybutadiene, 25 cross-linked, Q: 1.42 Å^{-1}

For the 250K, 280K, 310K, and 363K measurements, conversion of the quasielastic peaks into autocorrelations was performed by fast Fourier transforms. As mentioned in the experimental

section, a stretched exponential function know as a KWW function was used to fit the autocorrelations, defined with a background term here as

$$I(Q,t) = A + (1-A)e^{-\left(\frac{t}{\tau}\right)^{\beta}} \qquad (7.1)$$

where I is the autocorrelation value, A is the background intensity, t is time, τ is the characteristic decay time, and β is the stretching exponent, beta. The KWW function was fitted to these trends; β was allowed to vary for the first fit, since no trend was noted an average beta value was taken and fixed for a secondary fit of the function. The 310K data is plotted, figure 7.2, as an example of the observed trends. Although tau is similar between the samples, there is a clear difference in the background. The consistently higher background intensity with crosslinking is the result of inhibited kinetic movement by the crosslinks, consistent with the elastic scans. Given the difference seen in the background, the inhibition must be severe enough as to be outside the experimental window. In this quasi-elastic neutron scattering experiment, there is not a measured change in the dynamics of the sample, as would be expected, but the change is noted in the proportion of the material that undergoes discernible motion.
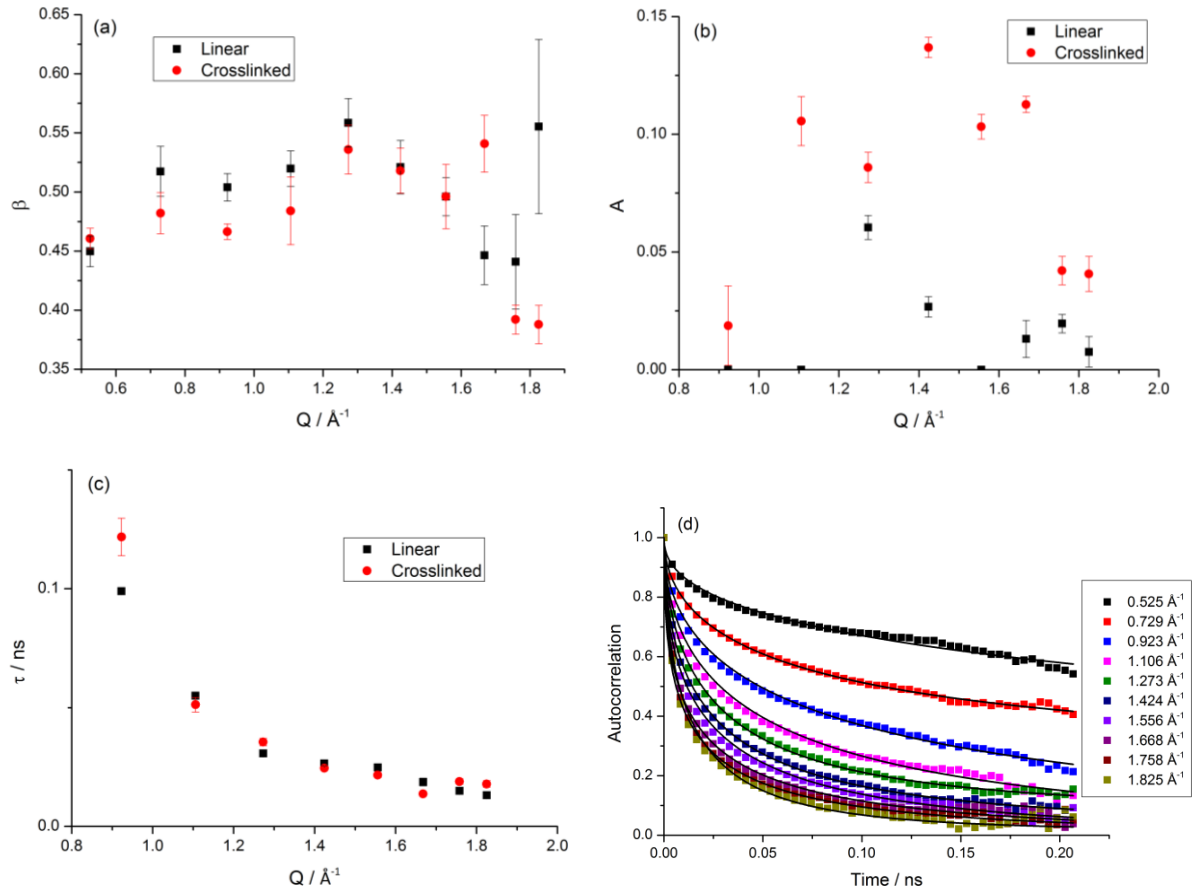
Figure 7.2: (a) Initial fitted β, (b) second fit background, A, and (c) τ for linear and highly cross-linked PBd, 310K (d) Linear PBd at 310k autocorrelation functions, lines are fitted stretched exponential functions

This increase in background with crosslinking is visible across most of the temperature range, as shown in figure 7.3. For lower temperatures the size of the increase is between 0.05 and 0.1, values which equate to approximately one or two polybutadiene monomer units per cross-link. Thus only the units involved in the crosslink are slowed, and bulk polymer dynamics is rapidly recovered on further chain segments.
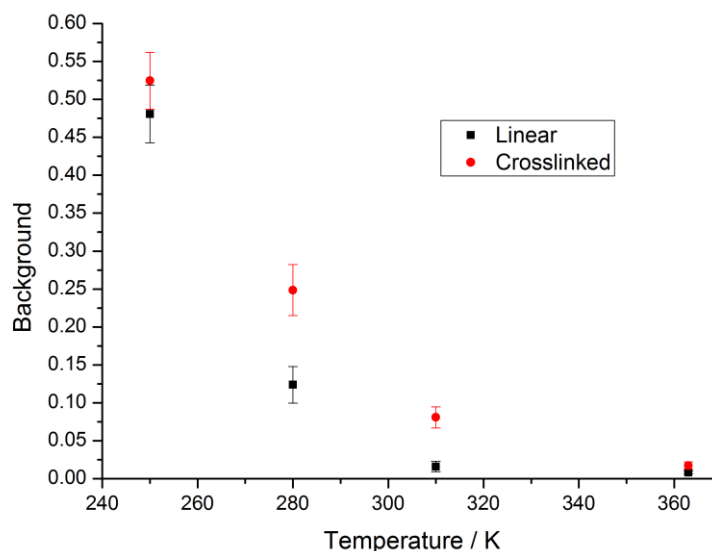
Figure 7.3: Average background over all Q of crosslinking test samples against temperature

There is a notably smaller difference at 363 K which is in agreement with the elastic scans, figure 7.1, and this implies that the hindered motions are now removed or inside the experiment window. Examination of the decay constants for 363 K finds that the cross-linked values are greater than the linear values, thus the motions are inside the instrument's range.

From this data, it can be concluded that although severe the hindering of the chain dynamics is limited to the crosslink site with the remaining chain segments unperturbed. The implication that this immobility degrades at higher temperatures suggests that the difficulty of changing chain conformation due to crosslink architecture is the cause. This result has been observed before in poly(vinyl alcohol) hydrogel systems, however to our knowledge it has not been reported in a polymer melt before.[120, 121] As the effective immobility is confined to the crosslink site, the majority of the dynamics are still comparable with free chains, allowing for reasonable comparison between non-cross-linked and cross-linked systems.

7.2 Characterisation of the glassy layer

Examination of the glassy layer phenomenon about silica filler was the focus of this investigation, which made use of isotope scattering differences and the different chain lengths of the 4OHPBd additive. Quasi elastic neutron scattering is perhaps unique in its ability to test for and examine the glassy layer, and some work has been done before to examine composite systems with QENS, with finding both for and against polymer inhibition. [68, 70, 71]

The experimental samples were composed of end functional polybutadiene, a full hydrogenous polybutadiene (PBd-300k), a per-deuterated polybutadiene (Polymer Source, M_w 138,000, PDI 1.06, P4016-dPBd), and Stöber silica (R_h: 53 nm, DLS). Cylindrical aluminium cans were used to house the samples, and the temperature was regulated with the CCR system. QENS scans were run at 3, 220, 250, 280, 310, and 363 K, for all samples. Rheological frequency sweeps on the sample material were performed after the scattering experiments (see 4.5).

Table 7.2: Composition of glassy dynamics IRIS samples by percent weight

Sample name	4OHPBd	200k PBd	dPBd	Stöber silica
IRIS GLASSY Blend	50.0	-	50.0	-
IRIS GLASSY hPBd composite	20.1	30.0	-	49.9
IRIS GLASSY 15k 4OHPBd composite	20.1	-	29.7	50.2
IRIS GLASSY 10k 4OHPBd composite	20.1	-	30.0	49.9

The QENS scattering peaks were fast Fourier transformed and fitted with KWW stretched exponential functions with a floated then averaged and fixed β coefficient according to the procedure outlined earlier in section 7.1. A sample data set is shown in figure 7.4. The decay constant appears to be similar between the samples, figure 7.4c, implying the mobile polymer fraction dynamics are constant no matter the filler content. For the dynamic behaviour, at higher Q values the dynamics appear to be homogenous, in agreement with the red line, suggesting no spatial variation in the samples; at $Q < 0.923$ Å^{-1} the behaviour appears to shift toward heterogeneity with a Q^{-2} dependence, suggesting that the polymer matrix is not uniform. The finding at higher Q is in agreement with literature QENS studies on polymer dynamics, and the shift towards heterogeneity may be a sign of a hindered polymer layer with different motions. [122]
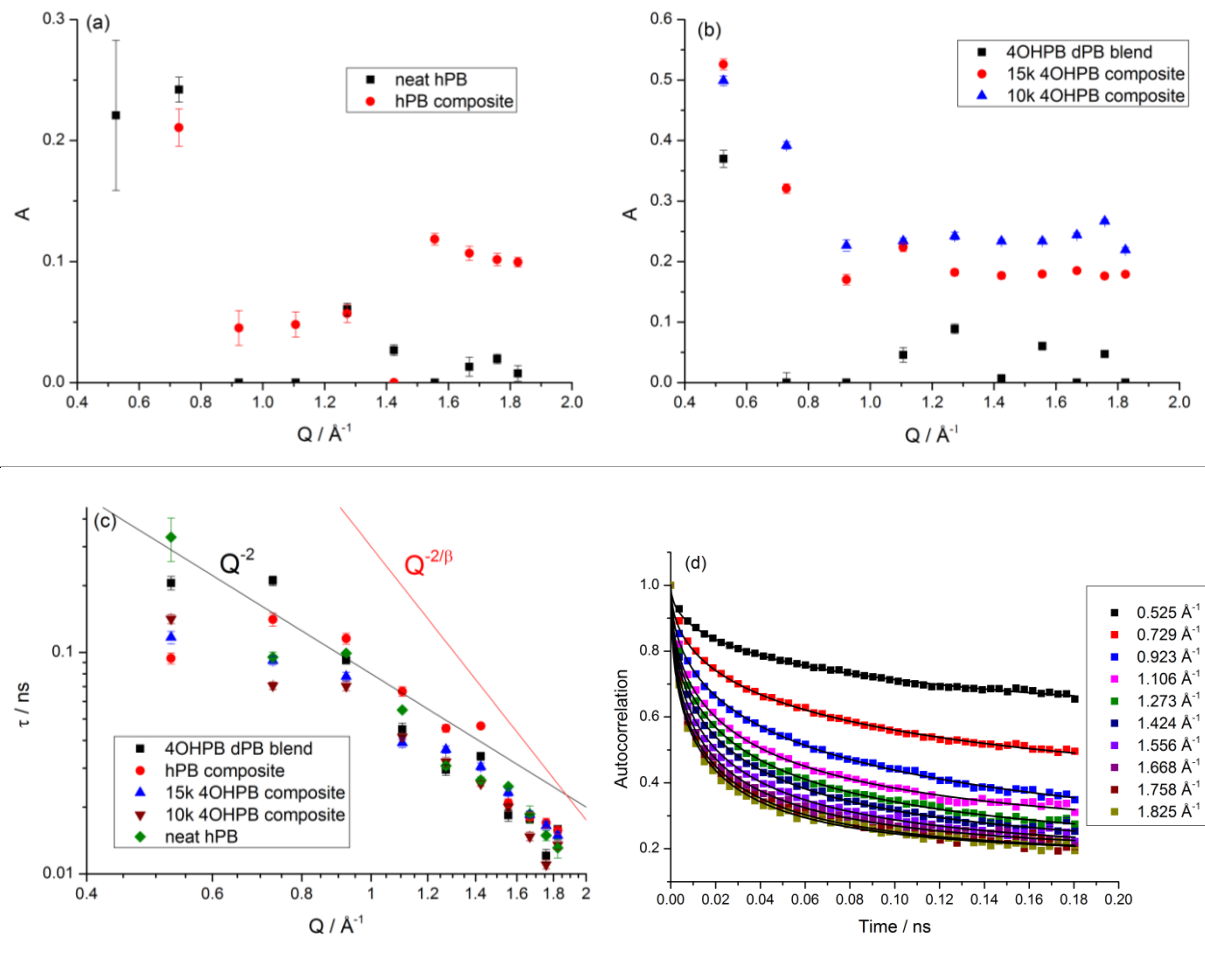
Figure 7.4: KWW (a/b) background, and (c) tau with dynamic behaviour predictions (guideline only) for polybutadiene blend and composite samples 310K, (d) 15k 4OHPBd composite at 310k autocorrelation functions, lines are fitted stretched exponential functions

Though τ is similar between the samples, the fits of the stretched exponential function yield an increased background with the presence of hydrogenated end functionalised polybutadiene composite. The increased background with the presence of silica filler particles in the matrix evidences the presence of significantly hindered dynamics; however, the similarity in tau implies the mobile polymer does not relax differently. This indicates that there is a section of greatly hindered dynamics in the system, such as a glassy layer. Although it could be suggested that the observed background increase comes from the coherent scattering of the deuterium, the pure hydrogenated linear sample and the blend of hydrogenated end functional polymer and deuterated polymer show similar background intensities, suggesting the effect is small. In fact, the calculated increase in coherent scattering from the additional deuterated polymer is only 10 percent of the total scattering, which is less than the growth observed in the background. From this it can be ascertained that the observed increased background intensity is not from coherent scattering by deuterium but instead from hindered dynamics in the samples containing silica.

Increases in background are also observed between the blend and the blend composite samples which confirm that the silica does inhibit the polymer motion.
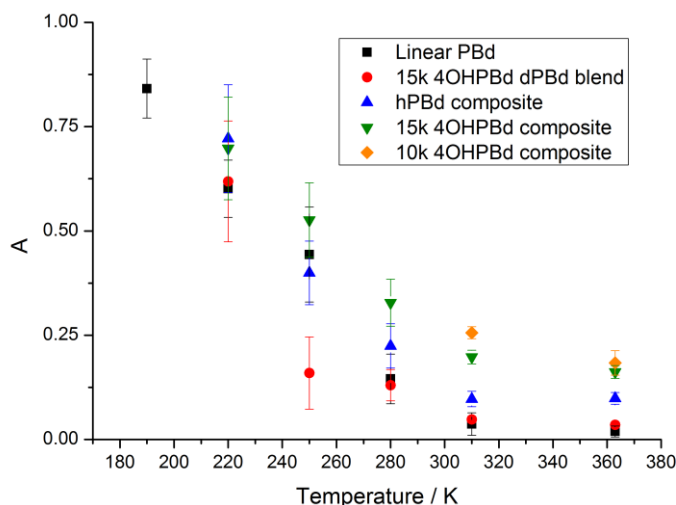
Figure 7.5: Average KWW background, Q: 0.923-1.825 Å^{-1}, against temperature for polybutadiene blends and composites

This inhibition of the dynamics is observed above 250 K, figure 7.5, with statistical uncertainty at lower temperatures due to the limited detectable motions by IRIS. A possible source of the slowed dynamics at higher temperatures is the formation of a glassy layer about the filler material. The further increased background with the removal of the bulk incoherent scattering via deuterium confirms that the inhibition is localised to the surface and supports the notion of a hindered layer. An interesting note is that this hindrance, thought to be caused by a layer, appears to persist over 100 degrees above the glass transition temperature, whereas other reports find the layer is removed at T_g + 30; this suggests that the hindered surface layer more robust than previously thought.
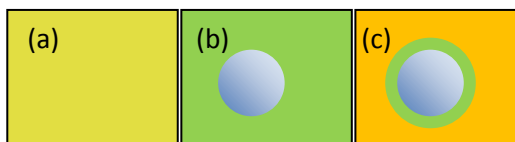
Figure 7.6: Visualisation of a silica particle with polymer layer in differing samples, (a) 4OH-PBd-15k d6-PBd-138k blend (b) PBd-280k composite (c) 4OH-PBd-15k composite; green is hydrogenous polymer, orange is deuterated polymer

The inhibition near the silica surface is highlighted as a result of the surface segregation of the 4OHPBd polymer; the different environments are illustrated in figure 7.6. In the blend (a), the hydrogenous polymer is dispersed throughout the matrix with no localisation. With the full

hydrogenous composite (b) the polymer near the silica will be dynamically inhibited, however, as there is no deuterium the entire polymer matrix motions are measured yielding an average background containing the inhibited motion. The presence of the deuterated polybutadiene and the segregation of the 4OHPBd to the surface (c) will highlight any shift in the dynamics in the near surface region. As the measured background is significantly greater in the deuterated composites, it can be concluded that the slowed dynamics are localised to the silica filler surfaces. As the hydrogenous polymer brush depth, previously characterised by Kimani et al[85] is known, further analysis can be performed to examine the nature of the hindered motion.

To analyse the dynamics of the samples, an isolated core shell model particle structure was employed as was established in the analysis of the small angle scattering data, chapter 6. It was assumed that at the silica surface the dynamics were hindered beyond the detectable range of the IRIS instrument. As such a local background value of 1 was assigned to model the polymer immediately adjacent to the filler surface and treated as a boundary condition for the model. The other boundary is at a theoretical infinite distance from the silica surface, for this the background was treated as equal to that in the absence of silica, the neat polymer blend background. To describe the glassy polymer layer quantitatively between these points, the magnitude of the measured background, $D(x)$, was treated as a simple exponential decay dependent on the distance from the surface, x,

$$D(x) = A_{blend} + (1 - A_{blend})e^{-x/d} \qquad (7.2)$$

where d is the characteristic decay length, and A_{blend} is the neat polymer background value.
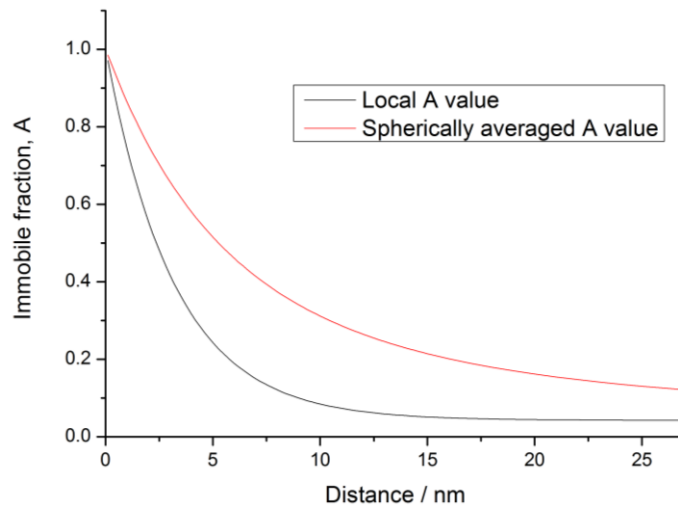
Figure 7.7: Calculated and volume average KWW background in relation to distance from silica surface, d: 2.5 nm and A: 0.027. The red curve represents the average value of A as a function of the integration limit

The values for $D(x)$ were integrated outwards from the filler surface, factoring in the increasing volume with spherical shell integration, and divided by the encompassed volume to yield an average or measured background value. From previous work the 4OHPBd chains form surface layers of known thickness; these values were used as limits for the integral as the deuterated polybutadiene bulk does not greatly contribute to the incoherent scattering of the system.[85]

In the case of the fully hydrogenated bulk, a calculated face centred cubic (FCC) average half particle separation was used as a limit to prevent double counting. While an FCC arrangement of the silica in the matrix is improbable, the large separation compared with brush thickness and the distribution's representation of volume fraction does not introduce a large error. The remaining volume in the unit cell was treated as having the neat polymer background value and incorporated into the calculation of the average value.

The characteristic decay length was varied for each temperature until a fit was obtained for the experimental background values. At 220 K only the fully hydrogenated matrix was used for fitting given uncertainty in the resolution of the dynamics near the polybutadiene glass transition temperature. Error was calculated from the fitting routine or as an average over Q of the background parameter. The exponentially decaying glassy layer was determined to be a reasonable model for the observed dynamic inhibition, evidenced by the agreement with the experimental data, figure 7.8. This simple model confirms the presence of a hindered layer as the most probable cause of the increased background observed in the composite samples.
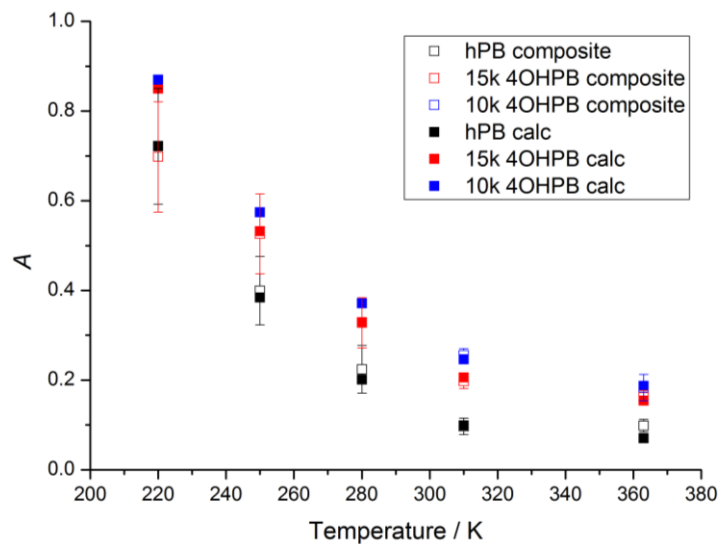
Figure 7.8: Averaged background values, Q: 0.928-1.831 Å^{-1}, against temperature, both measured (open) and calculated by model (solid)

Table 7.3: Parameters and calculated backgrounds of the glassy layer with temperature

Temperature / K	Polymer blend, A	Characteristic length, d / nm	hPBd composite	15k 4OHPBd composite	10k 4OHPBd composite	hPBd calculation	15k 4OHPBd calculation	10k 4OHPBd calculation
220	0.610 ± 0.080	15.1 ± 4.0	0.722 ± 0.129	0.698 ± 0.122	-	0.722	0.850	-
250	0.301 ± 0.071	6.39 ± 0.45	0.399 ± 0.076	0.526 ± 0.089	-	0.384	0.532	-
280	0.138 ± 0.035	4.32 ± 0.45	0.224 ± 0.053	0.328 ± 0.056	-	0.201	0.329	-
310	0.042 ± 0.014	3.24 ± 0.11	0.097 ± 0.018	0.198 ± 0.164	0.256 ± 0.014	0.099	0.206	0.246
363	0.027 ± 0.007	2.73 ± 0.32	0.099 ± 0.014	0.162 ± 0.153	0.183 ± 0.029	0.071	0.154	0.187
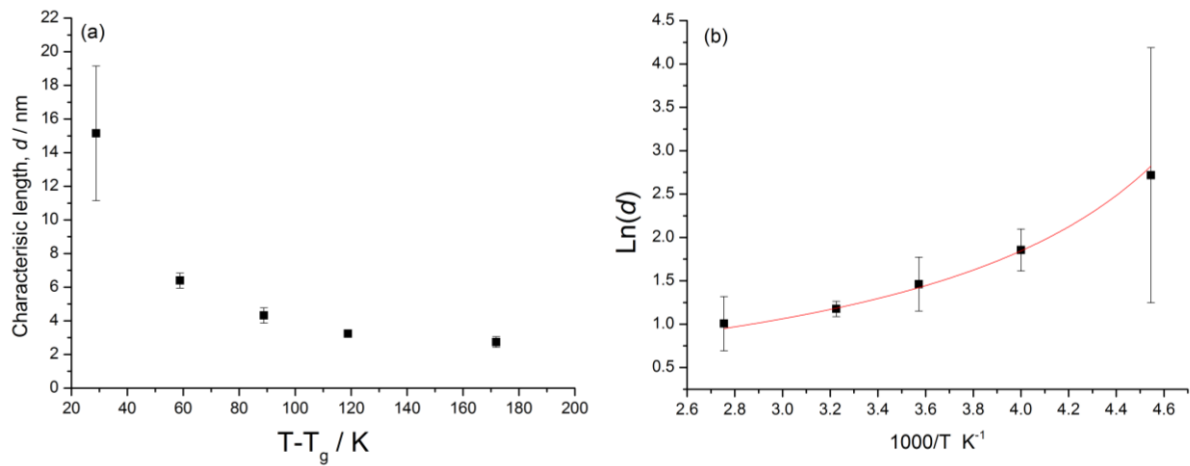
Figure 7.9: (a) Characteristic length against temperature above T_g, (b) Log characteristic length and inverse temperature data and fit for VFT relation, $T_0 = 173 \pm 15$ K

A decreasing trend in the glassy layer characteristic length with increasing temperature agrees with the consensus that chain motion is an activated thermodynamic process. Given the dominance of the α-relaxation in polymer properties above the glass transition, the choice was made to fit VFT relations to the data. This is shown in figure 7.9b, and fit over the data set. This relation is common in polymer systems and properties and is related to the glass transition, so it is not unprecedented. The T_0 value was allowed to float and was determined to be 173 ± 15 K..

The fit is in perfect agreement with the experimental data, in part this may be due to allowing the reference temperature to vary, however T_0 is often found to be below T_g. From a theoretical basis T_0 is defined as the point where melt relaxation times become infinite[15], and in an ideally cooled system ($dT/dt \sim 0$) it is postulated T_g and T_0 terms should be equal. [123] In real systems this condition is never reached and the glass transition is measured at a higher temperature because of the finite equilibration time. With this concept of a non-equilibrium system, the consideration made earlier for the reference temperature being the point at with the polymer bulk is completely glassy is valid for this system as well. [15]

Given the uncertainty in the data at lower temperatures it is not possible to be certain of the T_0 value, divergence of the VFT relation from experiment near the glass transition has been observed before, and is theorised to be from the loss of physical accuracy of the model. [124] However the VFT trends clearly demonstrate that the layer properties are related to melt polymer dynamics and in particular the transition to glassy behaviour.

7.3 Dynamics at greater timescales

A single experiment was performed to examine the effect of fillers on polymer dynamics at greater timescales. For the experiment, the IN16B setup was in its standard configuration with Si(111) analysers, yielding an energy transfer range of ±31 μeV, a resolution of 0.75 μeV, and a Q range of 0.1-1.8 Å^{-1}. The samples run were the blend, full hPBd composite, and 15k 4OHPBd composite from the glassy layer experiments on IRIS, and cylindrical aluminium sample cans were used. A single elastic window scan from 3-200 K and QENS baseline resolution at 3K was run on the blend sample. QENS measurements on the blend, full hPBd composite, and 15k 4OHPBd composite samples were run at 220, 250, 280, 310, and 363 K.
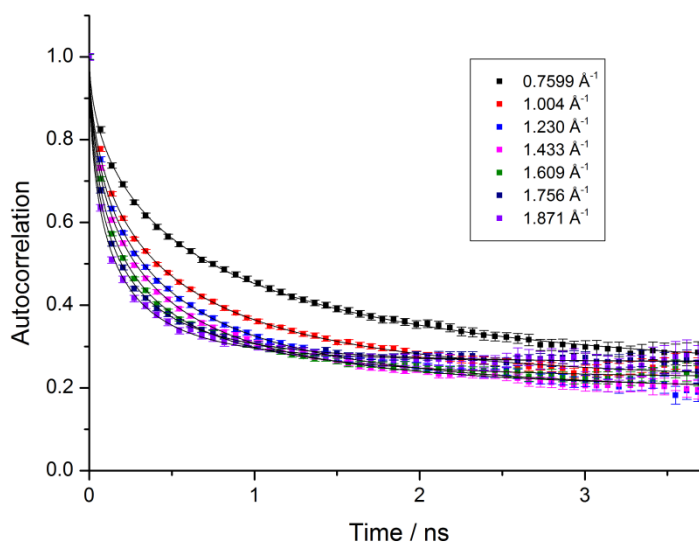
Figure 7.10: IN16B autocorrelation functions, lines are fitted stretched exponential functions, 15k 4OHPBd composite at 280 K

The KWW function previously used for the analysis of IRIS autocorrelation data, with a time range of 0-0.15 ns, was also used here. As the measurement range is significantly different between IRIS and IN16B, see chapter 3, there was a possibility that the stretched exponential relation would not provide an accurate fit to the data; however, the fitted function yields good

agreement with the data, as seen in figure 7.10. As before, to prevent over-parameterisation, the correlations were fitted with a floating β, and then β was averaged and fixed for a second fit iteration. Sample results of the fitting are shown in figure 7.11; as with the previous work examining the glassy layer of IRIS the silica composite samples have a significantly higher background value than the blend.
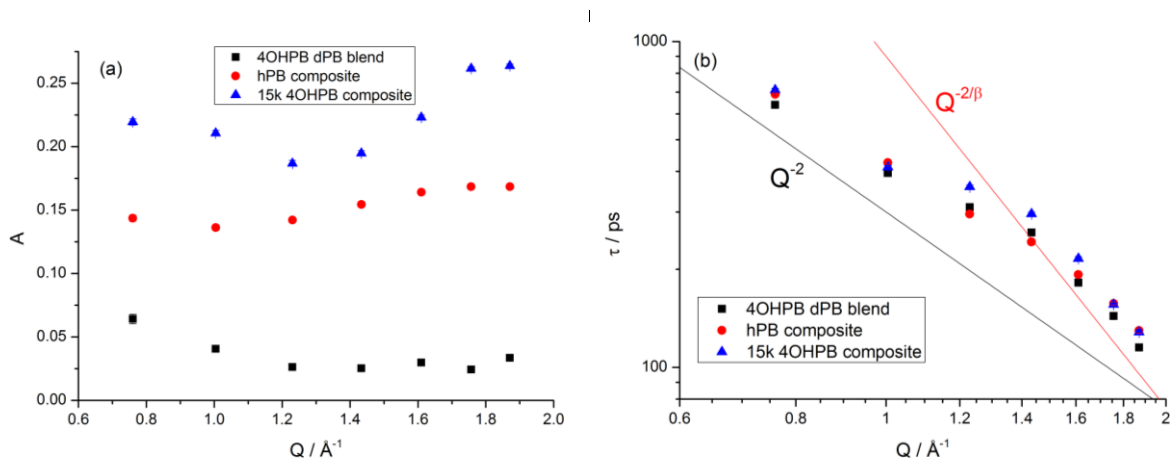
Figure 7.11: KWW equation (a) background, and (b) decay constant, τ, with dynamic behaviour predictions (guideline only) over measured Q range for all samples at 280 K on IN16B

There is a notable increase in background with Q for the composite samples relative to the blend that was not seen in the IRIS experiment. This is possibly due to issues in the reduction of the data; because of limited time only the blend could be run at 3 K and this baseline had to be used for all reductions. There appears to be a slight increase, figure 7.11b, in the decay constant for 15k 4OHPBd composite, this implies that the reduced motions are starting to feature in the experimental window. This increase does not appear in the fully hydrogenous composite because the relative proportion of material undergoing this relaxation is small and hidden by the signal of the bulk polymer. The fact that the polymer layer about the particles is still hindered at these timescales, 3.5 nanoseconds on IN16B compared with 0.15 nanoseconds on IRIS, demonstrates the severity of the dynamic inhibition, and supports the assumption made in previous analysis that the polybutadiene near the surface is immobile.

The Q dependence of the decay constant in figure 7.11b is similar to the measured behaviour with the IRIS instrument, figure 7.4c, with the high Q behaviour being homogeneous and a shift to heterogeneous behaviour at 1.2 Å^{-1}. Given that this behaviour is seen in the blend, it is not due to the filler presence, and must be part of the polybutadiene behaviour. Previous work by Doxastakis has found a greater power dependence than seen have, however this polybutadiene was primary 1,2 addition rather than the high 1,4 addition used in this experiment and a report by

Ahumada has noted similar behaviour in polypropylene, suggesting this phenomenon is not exclusive to polybutadiene. [125, 126]
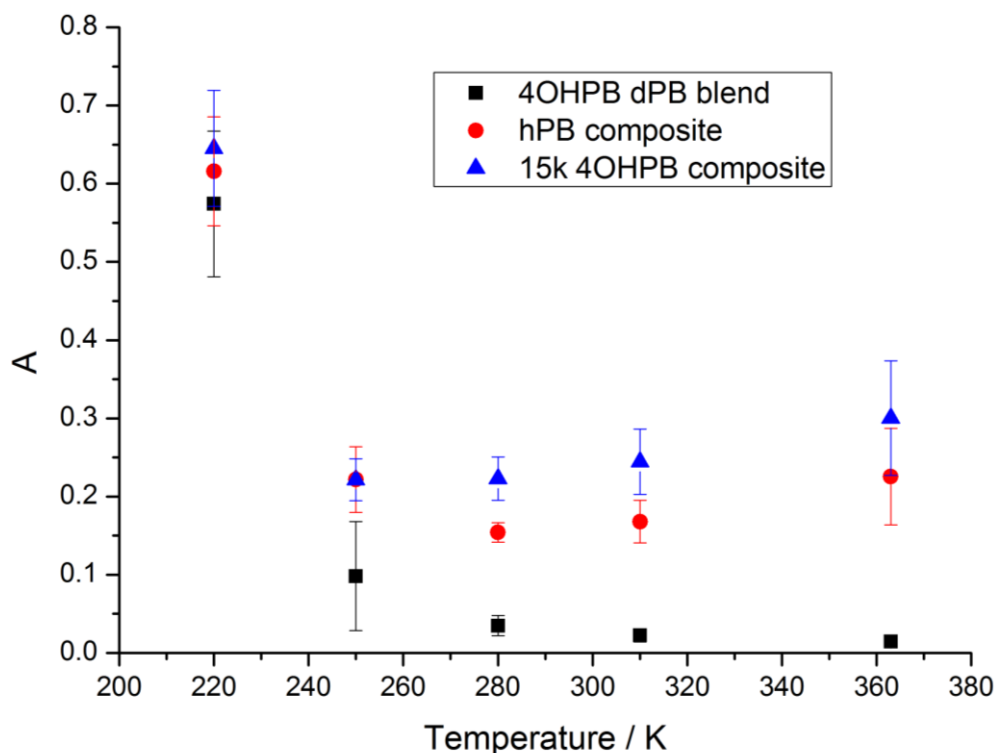
Figure 7.12: Averaged background, Q: 1.273-1.825 Å^{-1}, values against temperature for IN16B samples

The averaged background of the samples shows a similar trend to the IRIS data, with the increase in background with both silica and deuteration of the bulk in presence of silica. The cause of these effects remains unchanged, the formation of a glassy layer about the silica. One feature not present in the IRIS data, which is seen here is the increase in the background value for the composites after and including 280K, figure 7.12. This has two probable causes; the first is the noted issues with the data reduction that the blend polymer baseline had to be used for all samples. The second is the additional thermal noise in the data at higher temperatures resulting in a higher average background. Both of these factors are probably involved in the trend, and with the presence of these errors further mathematical analysis cannot be performed on the 280K, 310K, and 363K samples with certainty.

As these samples were previously examined on IRIS, section 7.2, the data was combined to yield the overall behaviour. With the IRIS data examining shorter timescales closer to t=0 ps and a better characterisation of the fast dynamics, the decision was taken to scale the IN16B data with a multiplicative factor to fit to the IRIS data. The fitted factor was found to depend on temperature and Q value, but was consistent between the samples, see appendix 10.3.
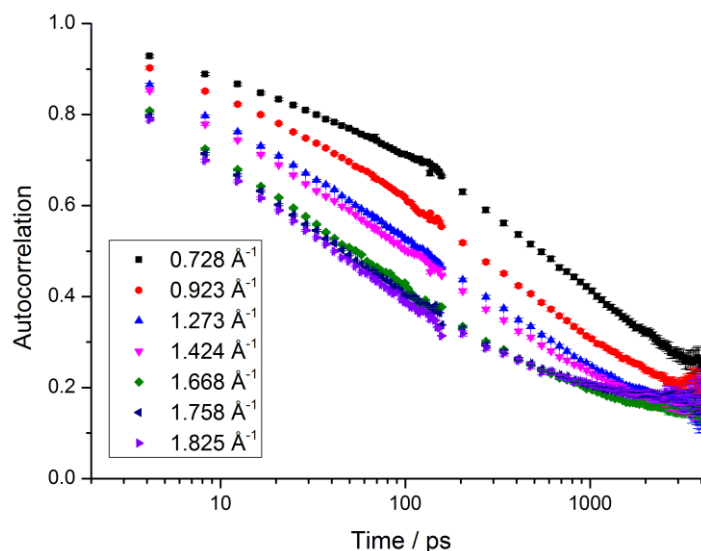
Figure 7.13: Sample autocorrelation of combined IRIS (0-150 ps) and IN16B data (68-3500 ps), 15k 4OHPBd-dPBd composite 280 K

The combined data was found to be continuous with no shifts in the observed decay at the crossover of IRIS and IN16B, as seen in figure 7.13. This suggests that the same dynamical processes occur over the timescale probed by both instruments, and that the data can be modelled with a stretched exponential function as before. The process of two iterations by averaging and fixing β was performed here.

The stretched exponential function was found to fit the combined data well, as can be seen in figure 7.14a, confirming the assumption of similar dynamic processes. As before, the decay constant τ was found to be similar between samples while the immobile background fraction increased with the addition of silica filler. Both constants are smaller than those found with the fitting of the IN16B data alone, this can be attributed to the scaling factor applied to join the two data sets.
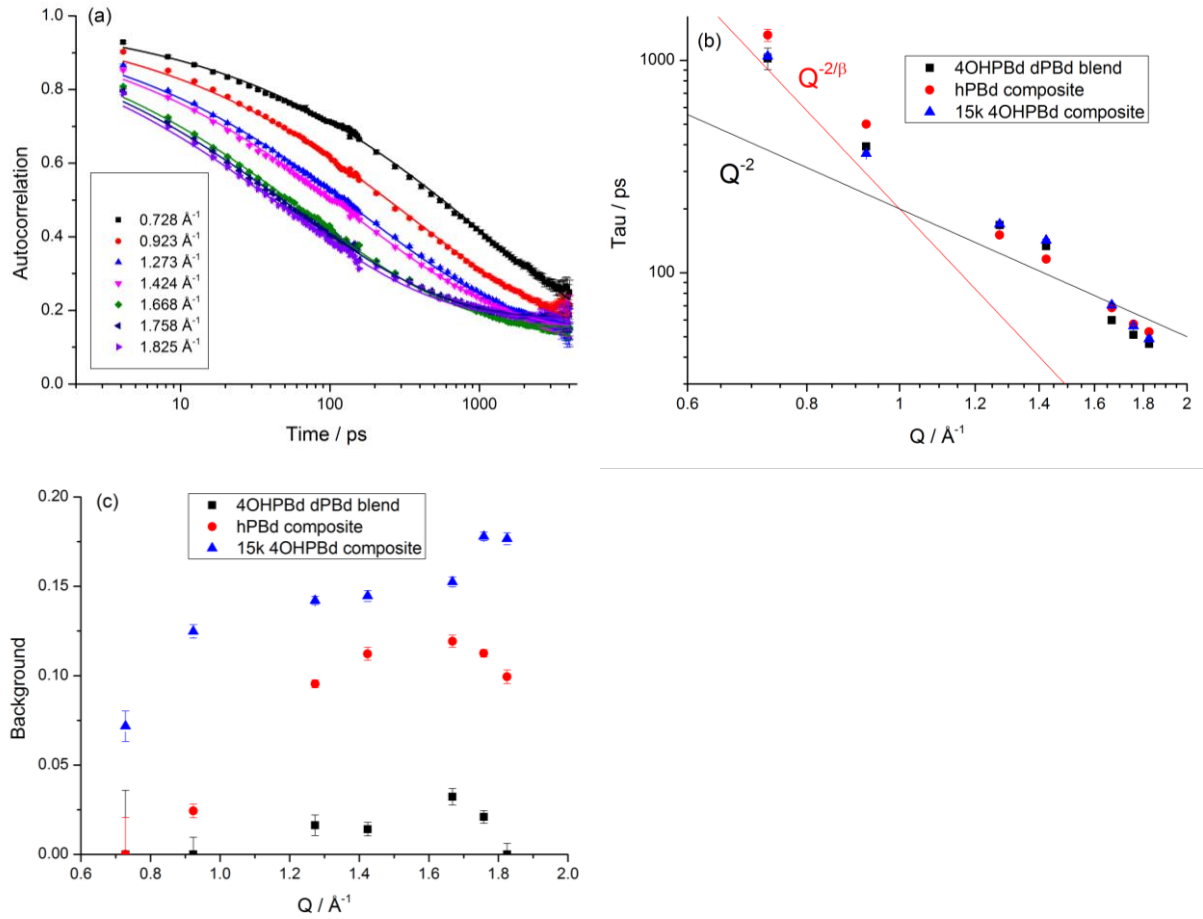
Figure 7.14: (a) Example autocorrelation of 15k 4OHPBd-dPBd composite with stretched exponential fits, (b) decay constants of stretched exponential fits with dynamic behaviour predictions (guide line only) (c) background value of stretched exponential fits; 280 K

Another notable feature is the decrease in background at low Q value; the decrease in background may be the result of the issue with reduction of the IN16B data mentioned previously. Under the assumption this is not the case, this trend is contrary to the expected trend of a decrease in background with Q due to the increase the length scale probed by the scattering which results in a greater proportion of the material being measured as immobile. Alone this implies that the polymer motions increase at greater length-scales, however, the related increase in tau, figure 7.14b, and the limits of the autocorrelation curves need to be taken into account. The dependence of the decay constant at low Q values, figure 7.14b, is higher to those seen previously and appears to follow homogeneous behaviour, which is in agreement with general polymer dynamics trends. [122] The high Q behaviour above 1.4 Å^{-1} also appears to be homogenous, implying a crossover region of heterogeneous behaviour. This has been seen before by Colmenero et al. and was theorised to be the shift from local to Rouse dynamics. [127] The higher dependence of the decay constant with Q results in greater proportions of the polymer matrix classified as mobile by the exponential fit and may yield the observed decrease in

background. While the trend in background is noteworthy it occurs primarily at low Q, thus for comparison of the average backgrounds of the composite materials these data points were excluded.

The trend in the background intensity shown in figure 7.15a is similar to those seen previously, an increased background when silica is included and with a decrease in temperature. Using the hindered polymer surface layer model, section 7.2, calculations of the layer thickness and resultant measured background were performed, figure 7.15b. The fits for the joined data were poor compared with those of the IRIS experiment, either from aforementioned issues with the IN16B data reduction or a shift in the nature of the relaxation. In the isolated IN16B data, it was noted that the decay constant was slightly higher for the 15k 4OHPBd composite sample than for the polymer blend implying that the hindered motions are almost within the experimental window. As the hindered surface layer model assumes the complete immobility of the layer over the experimental window, the breakdown of this assumption would result in poor fits of the data. This may be most visible in the characteristic length parameters, figure 7.15b, where large uncertainty is present.
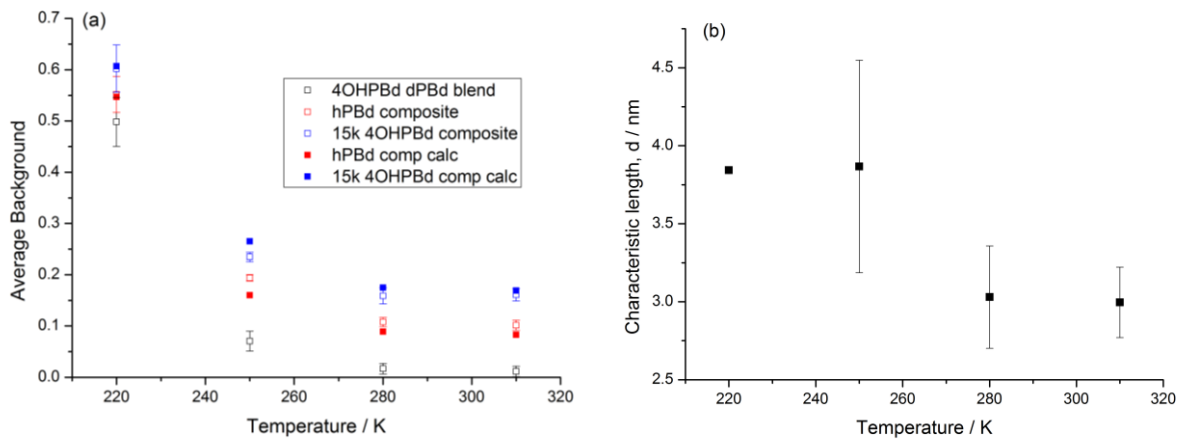
Figure 7.15: (a) Averaged background, Q: 1.273-1.825 Å^{-1}, of joined IRIS and IN16B data, along with fitted calculations of background due to immobile surface layers; (b) Characteristic length of hindered layer with temperature above T_g (191 K)

Given this uncertainty, it is impossible to determine if the trend present in the length with temperature follows a VFT relation or a stepwise decrease. A stepwise decrease would be the result of another dynamical process initiating above the glass transition temperature and increasing polymer motion, this does not have supporting evidence. A VFT relation is common in polymer systems and is in agreement with the IRIS results; this would be caused by standard polymer dynamics and is the more likely of the two scenarios. The lower length values seen in the joined data compared with those of the IRIS data can be explained by the greater range of

measured timescales over which a greater fraction of the material can move. Although no clear trend can be established, the calculated presence of the layer evidences the hindered dynamics of the polybutadiene near filler surfaces. This hindrance is severe and there may be above an order of magnitude difference in relaxation time compared with the bulk behaviour; evidenced by the increased background with silica presence and the ratio between the decay constants and the experimental window, 50-650 ps against 4000 ps respectively. The layer is also still present over 100 K above the polybutadiene glass transition temperature, again alluding to the strength and resilience of this polymer layer.

Table 7.4: Glassy layer background and characteristic length parameters for joined sample data

Temperature / K	A (Polymer blend)	Characteristic length, d / nm	A(hPBd composite)	A(15k 4OHPBd composite)	A(hPBd composite) calculation	A(15k 4OHPBd composite) calculation
220	0.498 ± 0.048	3.84 ± 0.01	0.552 ± 0.035	0.602 ± 0.046	0.547	0.607
250	0.070 ± 0.019	3.87 ± 0.68	0.194 ± 0.006	0.235 ± 0.010	0.160	0.265
280	0.017 ± 0.010	3.03 ± 0.33	0.108 ± 0.009	0.159 ± 0.016	0.089	0.175
310	0.011 ± 0.010	3.00 ± 0.23	0.101 ± 0.010	0.161 ± 0.012	0.083	0.169

7.4   Effect of strain on dynamics

Having established the presence of the glassy layer, the influence of strain on the layer was chosen to be investigated. Theories describing the reinforcement and strain softening seen in these filled rubber samples often theorise this layer is the source of the phenomena or an important component for maintaining network contacts, thus seeing if this layer is disrupted will help validate or disprove these theories. [73, 119]

Initial experiments were carried out as follows, samples were composed of end-functional polybutadiene (4OHPBd), a full hydrogenous polybutadiene (PBd-300k), a per-deuterated polybutadiene (Polymer Source, M_w 138,000, PDI 1.06, P4016-dPBd), and Stöber silica (R_h: 51 nm, DLS). Samples were crosslinked with vulcanisation in a heat press at 160 ˚C for 1 hour. The samples were placed in a stretching rig; see section 3.3.3, which was angled at 45 degrees with respect to the beam, and the CCR setup was used. QENS scans at 3 K and room temperature were performed with various strains on the samples.

A second motorized strain rig was developed to further investigate the dynamics under strain; as before, composites were made from end-functional polybutadiene, a fully hydrogenous polybutadiene, a per-deuterated polybutadiene (Polymer Source, M_w 95,000, PDI 1.05, P5899-dPBd), and Stöber silica (R_h: 19.4 nm, DLS). The samples were cross-linked using sulfur vulcanisation at 160 ˚C in inert atmosphere for 1hour. The samples were then clamped in the

motorized strain rig that was used for the SANS strain experiments. Due to the motorized components, the CCR could not be used and the experiment could only be run at room temperature.

Table 7.5: Composition of strained IRIS samples by percent weight

Sample name	4OHPBd / %(w/w)	300k PBd/ %(w/w)	dPBd/ %(w/w)	Stöber silica/ %(w/w)
IRIS STRAIN Linear	-	100	-	-
IRIS STRAIN Full hPBd composite	-	50.0	-	50.0
IRIS STRAIN 15k 4OHPBd composite	20.0	-	30.1	49.8
IRIS STRAIN 10k 4OHPBd composite	20.1	-	29.9	50.0
IRIS STRAIN MOTOR Blend	50.0	-	50.0	-
IRIS STRAIN MOTOR Full hPBd composite	20.2	30.1	-	49.7
IRIS STRAIN MOTOR 15k 4OHPBd composite	20.0	-	30.0	50.0
IRIS STRAIN MOTOR 10k 4OHPBd composite	20.2	-	29.9	49.9

The KWW fits of the initial strain samples were performed by floating, averaging, and then fixing β, to prevent over-parameterisation. The decay constant, τ, and beta, β, were found to be equivalent between the samples and in agreement with previous findings, and did not shift with applied strain. The composite sample backgrounds were found to shift with strain, figure 7.16; the hPBd sample appeared to show a minor increase in A and the deuterated samples showed a decrease, however, these changes are barely statistically significant due to the uncertainty in the measurement, but may allude to trends present in the composites. The increase in the hPBd composite sample may be the result of unrelaxed chain stretching in the matrix, and the decreases in the deuterated composites may be from the reduction in the glassy layer thought to occur with strain. While both these ideas are plausible, no certainty can be given due to the experimental nature of the equipment used for the measurement as the associated errors were substantial, seen with the standard error of the background values.
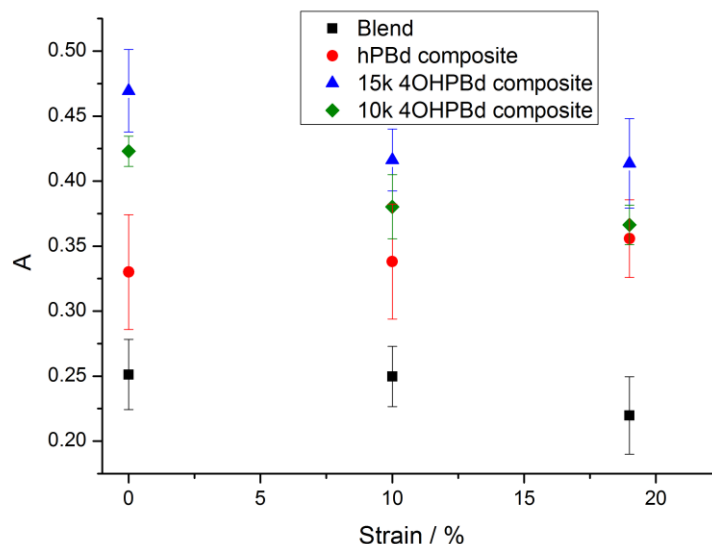
Figure 7.16: Averaged, *Q*: 0.923-1.825 Å^{-1}, KWW background values for linear PBd, silica filled hydrogenous PBd, and silica filled 4OHPBd/ d-PBd blends, under various strains.

Even though care was used straining and aligning the samples in the beam, differences between the sample environments may have been sufficient to cause the shifts in the data. An example of this issue can be seen in the relative intensity of the 10k and 15k 4OHPBd composites as unlike data in the previous examinations of these systems, the 15k sample has a notably higher background. Given the consistency of previous measurements, this is certainly from an issue in sample alignment in the beam. Shifts in sample angle from removing the sample to apply the strain would yield a change in sample thickness and scattered intensity. As such these results must be treated with care, and a second experimental system was devised to address the issues found here.

After the initial sample measurements, the development of the motorised strain setup for the second experiment allowed for the deformation of the samples without removal from the chamber as well as improved control over the deformation. As the low temperature baselines could not be run with the motor present, the baselines from the previous strain tests were used for reduction. Fitting of the autocorrelation functions was done as before with two iterations. As can be seen with the decreased uncertainty in the data, figure 7.17, compared with the previous experiment, figure 7.16, the improvements to the experimental setup were successful, with better resolution and less scatter yielding smaller standard errors.
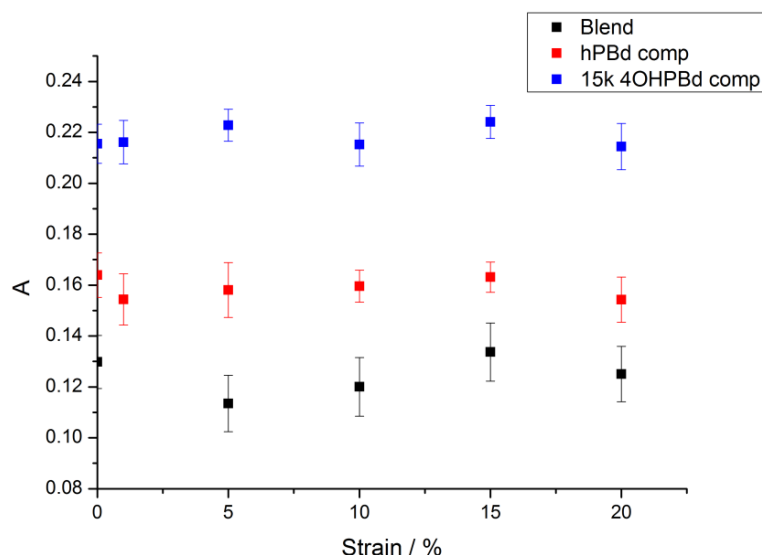
Figure 7.17: Averaged, Q: 0.923-1.825 Å^{-1}, KWW background values for linear PBd, silica filled hydrogenous PBd, and silica filled 4OHPBd/ d-PBd blends, under various strains.

With the application of strain there does not appear to be any significant change in background with any of the samples, figure 7.17. This implies the variations seen previously were not significant, and there is no discernible change in the layer structure over the strains tested. Given the finding that the hindered layer is present up to 100 K above the glass transition from previous work; the layer appears to be robust, and the proportion of polymer experiencing hindered dynamics adjacent to the silica is unaffected by strain. The range of strains tested is considered to be the approximate range of the Payne effect in most filled rubbers, as hysteresis and macroscopic material breakdown occurs at higher deformations. Combined with the clear strain softening observed for similar filler concentrations and sample deformations, chapter 5, this result is significant and does not support the polymer composite theories that ascribe the Payne effect solely to the glassy layer, implying that filler networking is more important for describing strain softening. Arguments can be made that the slowed layer may be affected at temperatures where it extends further into the bulk, or that the static nature of these measurements allowed for equilibration of the dynamics. Qualitatively, macroscopic sample creep was not observed as samples relaxed immediately after removal from the rig; however there remains the possibility that microscopic stresses to the glass layer relaxed quickly in the experiment. Given the time requirements for a QENS measurement, dynamic strains may need to be used to achieve a system where the relaxation of stress is not a possibility. Unfortunately, testing with either of these methods was not possible with the equipment available and is an avenue for further research.

7.5 Conclusions

QENS was successfully used to examine the dynamics in various polybutadiene-silica composites with different experimental setups. Changes in polymer dynamics with crosslinking were found to be limited to the crosslink sites and postulated to be caused by structural inhibition of the chain motion. Given the lack of effect on the greater chain motion at this timeframe, comparisons between cross-linked and non-cross-linked samples were deemed possible. Through use of the surface segregation properties of the end functional polybutadiene and the neutron scattering differences between hydrogen and deuterium the effect of silica filler on near-surface polymer dynamics was investigated. The presence of slowed dynamics with filler material was observed and characterised as a glassy polymer layer on the silica particle surface. This layer was found to have a VFT relation in common with other polymer properties and dynamics, and was present over 100 K above the glass transition refuting arguments that it is insubstantial in such conditions. A study of the same system at longer timescales with IN16B was able to confirm the significance of this hindrance, with only some inhibited polymer motions present with the greater range. Although initially inconclusive due to experimental errors, improvement of technique led to the observation of no change in polymer dynamics with strain. This lack of strain dependence implies that changes to the glassy layer are not responsible for strain softening in filled rubbers, and that filler networking is important, though further work can be done in this area. Overall, these experiments and the findings serve to highlight the use of quasi-elastic scattering as an investigative tool for these composite systems.

8 Combined Data Discussion

A difficulty in characterising composite systems is that complex behaviour and structures are present over several length scales, and a single experimental technique does not have the breadth to characterise a system. In filled rubber systems the rheological properties of these composites have been well documented, but fewer studies are conclusive in detail of the microscopic or nanoscale properties.[4] With examination of the same system by different experimental techniques a picture of the characteristics over various length scales can be formed, and from this improved conclusions about the system can be made.

8.1 Filler dispersion and its effect on rheological properties

The hydroxyl end functional polybutadiene used as an additive in silica composites is known to form surface layers, and from the work detailed in sections 6.1-3 it was concluded that the polymer does form a surface layer and disperse the silica filler.[85] Figure 8.1a shows the change in correlation length compared with the polymer brush density.
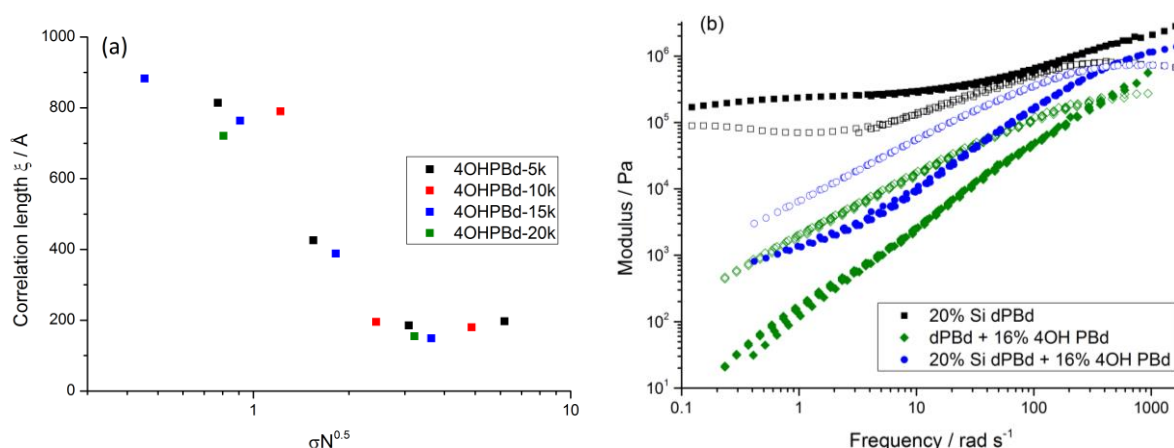
Figure 8.1: (a) Correlation length against normalised surface area for 20% w/w silica composite, section 6.3; (b) Rheology of D11 SANS experiment composites, section 4.4.1

This change in correlation length was linked to the deagglomeration and dispersion of the precipitated silica with the formation of a compact polymer brush layer. Rheological examination of the samples noted an increase of the moduli at lower frequencies with the presence of silica, figure 8.1b, and a return to viscous behaviour with the addition of end functional polymer. Given the dispersion of the silica observed by neutron scattering, figure 8.1a, it can be concluded that the trend is from the removal of filler networking by the steric stabilisation of the particles. At this silica fraction which is below the percolation threshold, the

end functional polybutadiene disperses the filler, which cannot form a permanent network and results in the decrease in the moduli.

This conclusion is backed by observations in the precipitated and Stöber silica; a precipitated silica example data set is present in figure 8.2, where the moduli and strain response of the composite samples change at higher filler fractions. The moduli (a) behaviour changes between 15 and 20% volume fraction toward being independent of the frequency, while a peak in the loss modulus appears in the strain sweep data. This peak is visible at lower precipitated silica filler concentrations in samples without the end functional polymer. A similar trend is observed in the Stöber silica, section 5.1-2, where the loss peak under strain is removed with addition of the 4OHPBd. This loss peak is thought to be caused by energy dissipation from breaking particle-particle contacts; its removal implies that the particles are dispersed and thus no contacts or network are present.
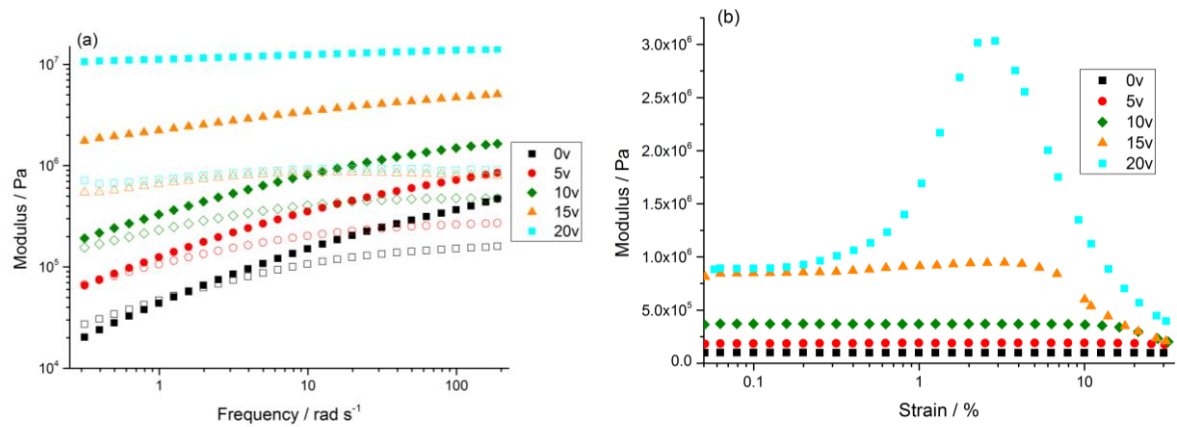
Figure 8.2: (a) Storage (full) and loss (hollow) moduli frequency sweep, section 4.2.2; (b) loss modulus strain sweep, section 5.2, for precipitated silica in 15k 4OHPBd/300k PBd blend; the concentration of silica, % volume, is in the legend

The reason for the return of the loss peak in the end-functionalised precipitated silica composites, figure 8.2b, is due to a reduced surface density of end functional polymer on the silica at higher concentrations, for the precipitated silica this density is low enough that particle contacts are able to form for the 20% silica sample. Calculations of the brush density for the cross-linked precipitated and Stöber silica samples, section 5.4, are shown in figure 8.3 along with the correlation length values from the neutron scattering on D11, section 6.3.
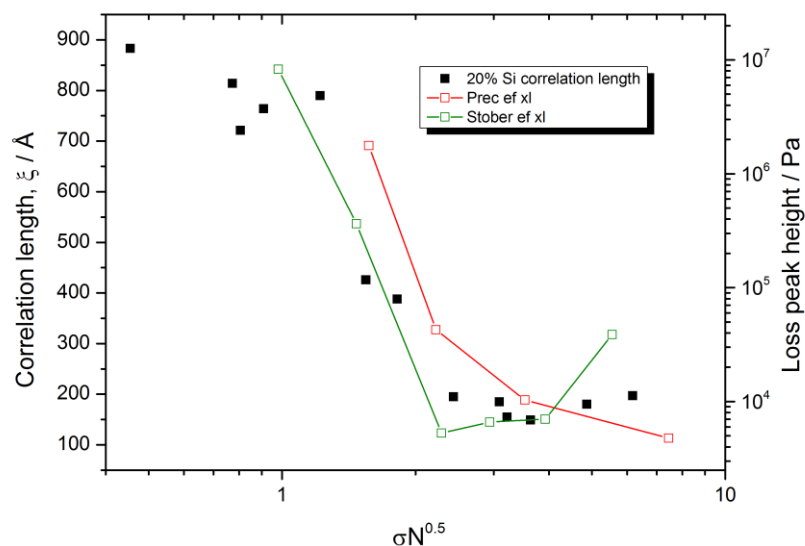
Figure 8.3: Correlation length for 20% w/w silica composite samples (solid), and loss peak height (G''_{max} − G''_0) for the cross-linked silica samples with 4OHPBd (open); against normalised surface area, lines are to guide the eye

There is a notable decrease in both the correlation length and loss peak height with improved polymer brush surface coverage, displayed in figure 8.3. As stated in section 6.3, this decrease corresponds to the chains on the filler surface experiencing deformation and elongation due to proximity with neighbouring chains. After this point, increasing surface brush density from brush overlap results in an entropic penalty and a steric stabilisation of the particles. This was noted as the cause of the decrease in correlation length attributed to the separation of the filler aggregates observed from the scattering data. In the strain softening data, the presence of the loss peak decreases once this steric stabilisation point is reached, combined with the scattering results it can be concluded that the separation and dispersion of the aggregates is cause of this. Thus the concept that the energy dissipation from filler network contact breakdown results in the loss peak is validated by this result. [29, 118]

The trends observed in the carbon black moduli and strain properties support the view that the contacts between the filler particles play an important role in the reinforcement of the rubber. Unlike the silica, the carbon black does not adsorb the hydroxyl end functional polybutadiene, thus it is not sterically stabilised and dispersed in the polymer matrix and should still yield similar composite physical properties.
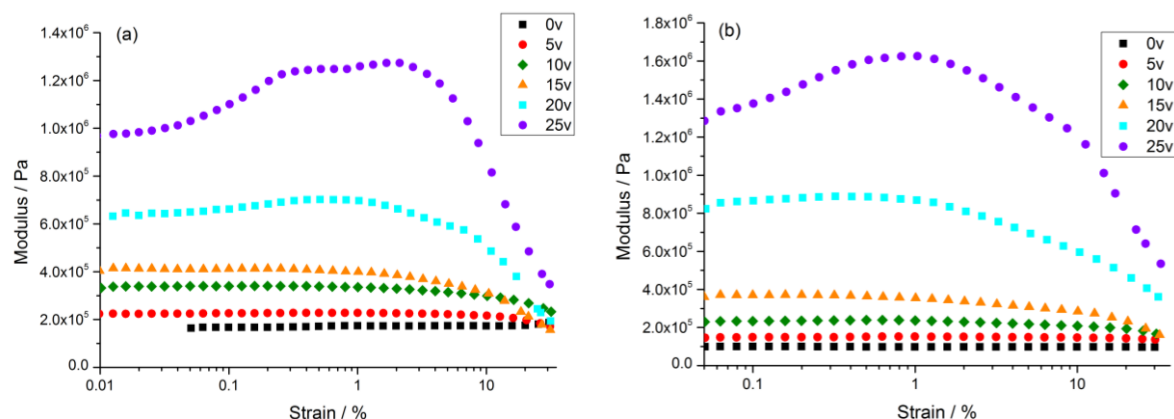
Figure 8.4: Loss moduli with strain, without (a) and with (b) 15k 4OHPBd polymer; the concentration of filler, % volume, is in the legend

The strain sweeps of the carbon black composites, figure 8.4, show little change with the presence of the polymer with the only significant change being the removal of a feature in the loss peak. This continued presence of the loss peak with the 4OHPBd in light of the lack of surface segregation for carbon black affirms the importance of particle-particle contacts for the phenomena in these systems.

Some researchers have put forward the idea that mobile chain ends may be responsible for the Payne effect; however, if this was the case the addition of the short 15k 4OHPBd polymer should have increased the observed strain softening behaviour in the carbon black composites due to proportionally greater numbers of ends, and in the case of silica given the proximity of chain ends to areas of strain amplification this increase should be even greater. The same group also noted better dispersion of the carbon black filler with the modified end groups, with postulate that this was the cause of the improvement in the material properties rather than the change to the chain end mobility. [128]

Although SANS experiments found a dispersion of silica particles with the addition of 4OHPBd, no such trend was found with the SESANS data, figure 8.5. From the increase in the gradient of the polarisation, related to the correlations in the sample; the formation of a fractal structure was observed below percolation, and developed even with the presence of the polymer brush layer. As stated in section 6.4, this is postulated to be because of the nature of the repulsion. The polymer brush provides steric hindrance but no long range repulsion for particle-particle interactions, thus particle clusters may still be present in the matrix even with local separation. Combined with significant changes to the rheology with the 4OHPBd, this implies that localised clustering does not explain the mechanical properties seen in these composites.

158
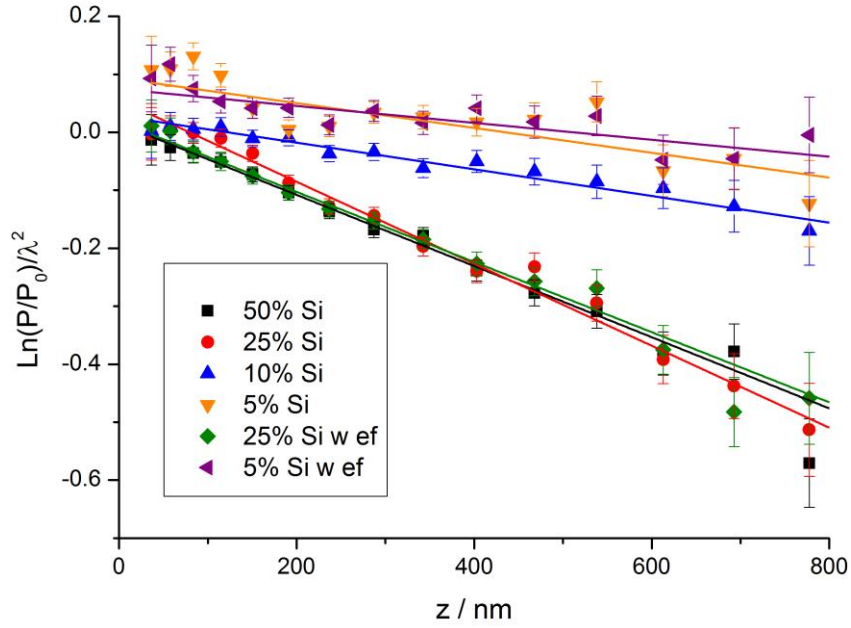
Figure 8.5: Ln of normalised polarisation over wavelength against spin echo path length for Offspec composite samples, linear least squares regression fit; the concentration of filler, % weight, and the presence of end-functional polybutadiene is listed in the legend

From these experimental observations it can be concluded that network contacts and percolation provide a significant proportion of the reinforcement in the composites, as removal of this contact by an end-functional brush layer results in changes to both the linear and non-linear rheology, most notably the strain softening behaviour and low frequency storage modulus. The removal of the contacts results in less reinforcement in the linear rheology, suggesting a fully percolating network is stiffer and able to bear greater stresses. The lack of contacts between filler particles also removes the loss peak seen in the non-linear strain softening implying network breakdown under strain is responsible for its presence. This removal is not the result of changes to the micron length scale filler dispersion, as no effect is seen in the SESANS data. This result supports the theories for composite behaviour that rely on filler networking, however, the emphasis appears to be on the filler-filler bonds rather than the overall network structure.

8.2 Crosslinking

Crosslinking is important to composite applications, such as tyres, and the effect of crosslinks on the filler and matrix needs to be resolved. Comparison of the peroxide and sulphur crosslinking through sample rheological properties was reported in section 4.1. The swelling tests conducted on the vulcanised rubber, section 4.1.3, determined the crosslink density as 211 ± 30 monomer chain units per crosslink site.

There is notable similarity of the moduli for the sulphur cross-linked sample and the equivalent peroxide cross-linked sample, figure 8.6. From this, it was concluded that the chemical nature of the crosslink site does not affect the linear rheological properties, and that the shifts in rubber behaviour with crosslinking are due to the limitation of chain diffusion and reorganisation.
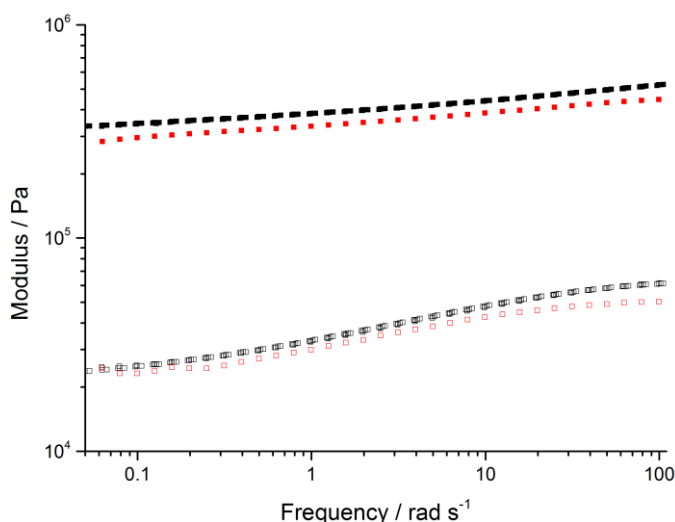
Figure 8.6: Storage (full) and loss (hollow) moduli of 200 monomers per crosslink peroxide (black) and sulphur (red) cross-linked samples

The quasi-elastic neutron scattering data, section 7.1, for the cross-linked polybutadiene consistently yielded a KWW background value greater than that of the neat linear polymer while maintaining similar decay constant values, figure 8.7. An increase in the background signifies the presence of drastically slowed dynamics for some proportion of the polymer; however there is no change in the decay constants, the measure of the motions inside the experimental window. It was determined that the crosslinking sites are greatly hindered in their motions, but this slowing is localised to the sites and does not propagate along the polymer chains and thus does not affect the majority of the polymer matrix.
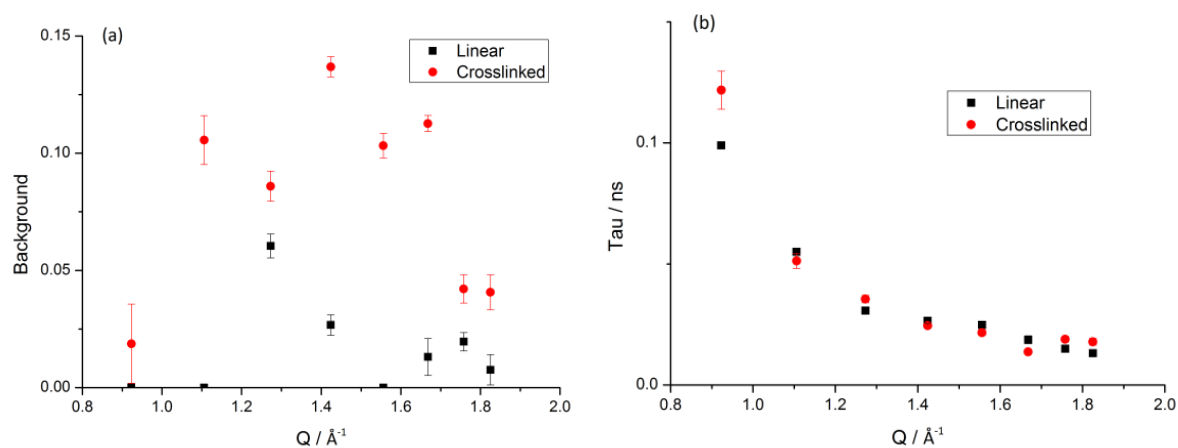
Figure 8.7: (a) second fit background and (b) tau for linear and highly cross-linked PBd, 310 K

This localised inhibition is in agreement with the rheological finding about the independence of cross-link nature. As the crosslinks only appear to affect polymer dynamics in the adjacent chain segments changes to the chemical nature of the cross-links are unlikely to affect the majority of the chain properties significantly. It may seem contradictory that a small localised inhibition and the elastic rheological properties derive from the same source; however, time and length scales need to be taken into account to understand this. The IRIS experimental instrument measures local chain motions on the picosecond time scale, before reptation and diffusion dynamics set in, while the rheology measurements at low frequency at the range tested involve these dynamics. The local polymer chain motion is not affected by distant crosslinks but the diffusion of the chains is arrested as the network sites represent permanent topological constraints. This highlights that a single dynamic timescale is not responsible for polymer and composite systems. Overall, the finding of local inhibition and independence of chemical nature allows for the contributions from crosslinking to be treated as constant for these experiments.

8.3 Presence and importance of the glassy layer

Affected dynamics of polymer chain near solid surfaces is well known and documented [47, 48, 54, 64, 71, 129, 130]; although questions still remain over these phenomena for both their presence in bulk composite materials and their effect on a material's physical properties. The glassy layer has been theorised to aid in reinforcing a composite and its removal under strain to be the cause of the Payne effect. As such the chain dynamics at interfaces needs to be characterised in order to reach a full understanding of these systems.

Selective probing the area about the Stöber silica filler particles on IRIS, section 7.2, found the presence of a layer of immobilised dynamics at all temperatures, figure 8.8. Slowed dynamics near substrates have been reported before; however the presence of such a layer over 100 K above the glass transition was thought to be unlikely. [66] Detection of this layer provides strong support for theories dependent on the glassy layer, and refutes the argument that the layer cannot exist at T_g +100 K temperatures. Further study on IN16B, section 7.3, was able to confirm this layer is immobile even on a nanosecond timescale.
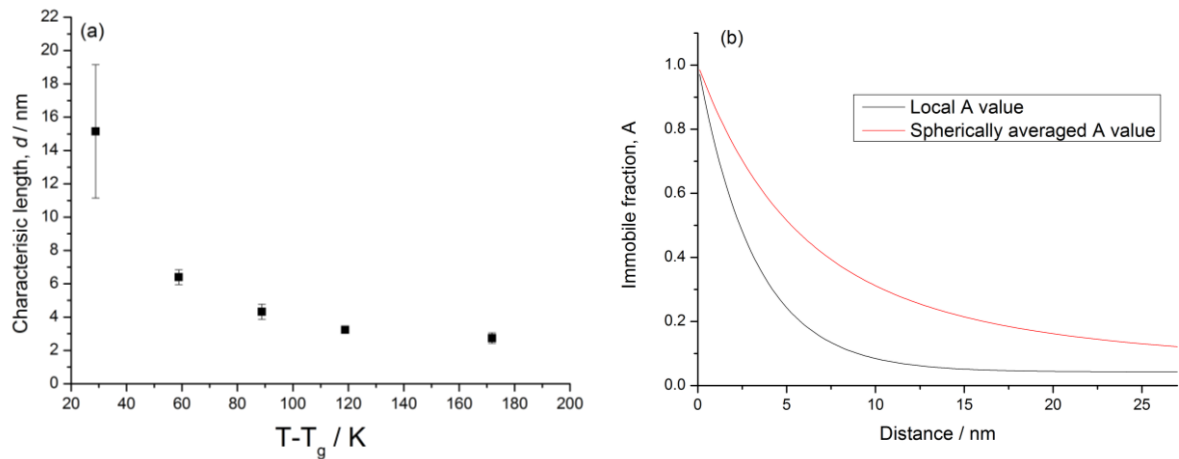
Figure 8.8: (a) Characteristic length of glassy layer against temperature above T_g (b) Calculated and volume average KWW background in relation to distance from silica surface, d: 2.5 nm and A: 0.027. The red curve represents the average value of A as a function of the integration limit

While this layer is present about the filler particles the work examining the filler dispersion and the finding that particle contacts affect the reinforcement and strain softening suggests that the glassy layer is not solely responsible for the composite reinforcement and strain softening. The layer, however, may be responsible for maintaining these particle contacts, [131] as the formation of glassy bridges between particles was put forward by Merabia *et al*. as part of a theory for composite reinforcement. [119]

In the case of close filler particle proximity, figure 8.9a, the glassy layers on each particle should overlap, resulting in an area of polymer which has a greater modulus than the surrounding material. This area between the particles will act as a bond as the increased stiffness will prevent separation of the particles. Similarly, in the case of particle contact, the polymer layer near both particle surfaces which provides extra reinforcement to the interaction. From the model and characterisation of the glassy layer, figure 8.8, at 293K dynamics of the end of the polymer brush should approach bulk behaviour, figure 8.9b. This will prevent glassy bridge formation due to steric hindrance stopping closer particle arrangements.
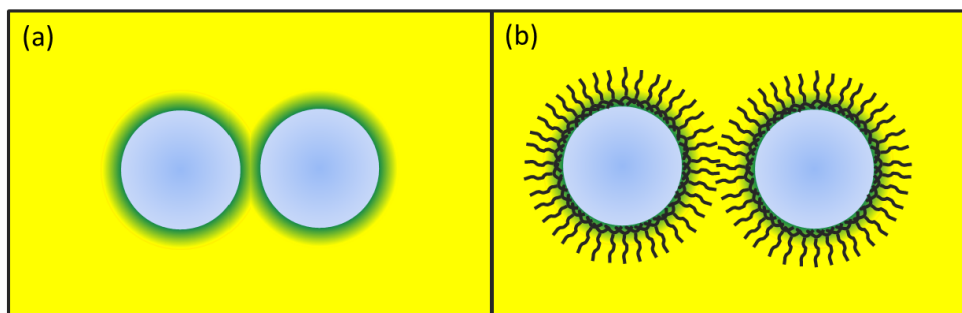
Figure 8.9: Visualisation of possible particle interactions, without (a) and with (b) end 15k 4OHPBd, polymer matrix colour represents dynamics, uninhibited (yellow) or glassy (green)

This idea is related to the dispersion and networking theories, and is supported by the same shifts in rheological behaviour. It is important to note the concept of the glassy bridge does not compete with or contradict the network theory mentioned earlier; rather it provides greater insight into the nature of the filler-filler bonds. It can be postulated that it is the glassy bridges that are broken when the composite is placed under increasing strain, with the required energy leading to the peak observed in the loss modulus. The removal of this peak with the presence of end functional polymer supports is idea, as glassy bridges would not form in these samples. Although the studies focused on silica composites, it is reasonable to assume similar behaviour for carbon black samples, as Roh et al. has reported similar hindered dynamics to those found in the reported QENS experiments.[68, 69]

Further work can be done to investigate this idea with rheological testing of samples containing short, ~5 kg mol^{-1}, end functional polymer chains or examining the current samples at temperature close to the glass transition. Unfortunately the equipment and materials necessary to carry out this work were not present at the current time and this must be continued in the future.

8.4 The effect of strain on filled rubber composites

While the reinforcement of rubber matrices beyond what would be expected from the particle volume alone is the most notable phenomenon with these composites, the strain softening of the material, first described by Payne[6, 7], is also prominent. Any complete theory of these systems needs to explain its origin, and to do so its causes must first be characterised.

Examination of the strain data for the composites characterised the Payne effect, as mentioned before. The addition of the end functional polybutadiene was found to remove the loss peak but not the strain softening. Crosslinking was observed to decrease the point of the strain softening onset, possibly from strain magnification caused by the lack of filler mobility. To further investigate the strain behaviour, the microscopic phenomena were examined in light of this information.

Examination of the Stöber silica composite under strain found no significant shift in filler or core shell organisation with strain, figure 8.10 is an example. This implies that the Payne effect is not caused by the significant reorganisation or full dispersion of the filler aggregate structure at this length scale. While this does not support full rearrangement of the filler, it implies that if the breakage of the network is important it is either not visible at this length scale or the physical change is minimal.
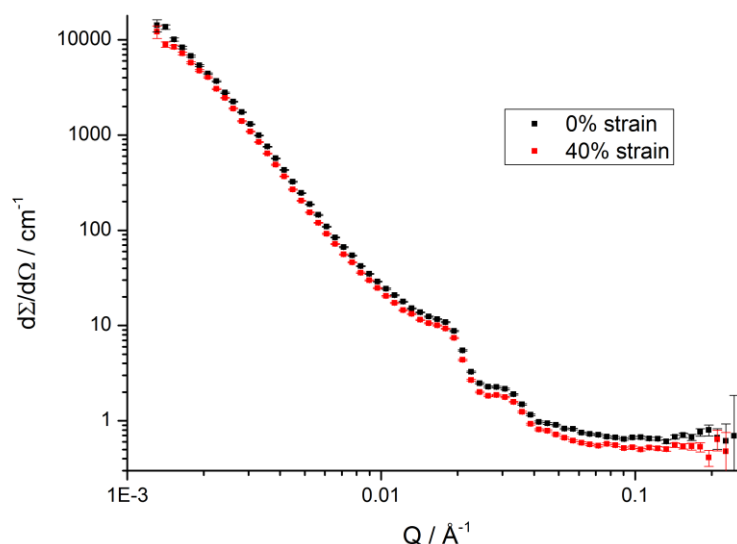
Figure 8.10: SANS2D 5% hPBd composite sample, comparison of 0 and 40% strain

Similarly, no shift was found in the immobile polymer background in QENS measurements, figure 8.11; related to the glassy layer, implying that strain does not remove a significant proportion of this hindered polymer layer.
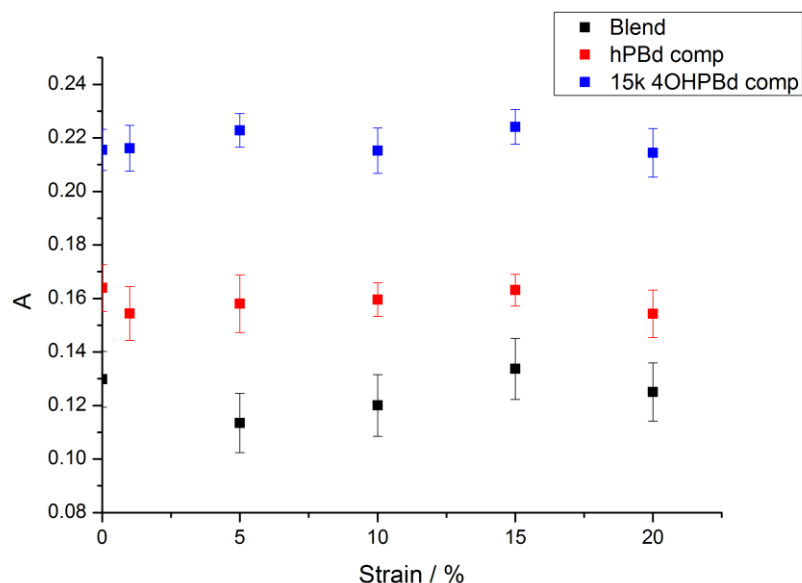
Figure 8.11: KWW background values, *A*, for linear PBd, silica filled hydrogenous PBd, and silica filled 4OHPBd/ d-PBd blends, under various strains.

Overall, there are not significant shifts in the filler structure or the glassy layer with application of strain. This result appears to be at odds with the strain softening seen with the rheological testing, as network breakdown and removal of the glassy layer are the two most prominent theories of rubber composite reinforcement and strain softening. The lack of shifts in the data implies whatever is causing the strain softening behaviour is a small section of the overall composite structure as it is unable to be detected by either system.

It was documented in previous sections that dispersing the filler and preventing particle contacts, either direct or through a glassy bridge, changes both the reinforcement and strain softening behaviour; most notably the removal of the loss peak, however, the Payne effect is not removed completely with this polymer brush layer. Without the brush layer, the onset of the decrease in the storage modulus is accompanied by the rise in the loss modulus, suggesting a common origin. Some change in filler aggregate behaviour may explain the softening while keeping the lack of structural or chain dynamics shifts observed in the SANS and QENS.

8.5 Towards an improved theory

These experiments and their analyses have found several notable features of the microscopic structure, polymer dynamics, and rheological properties of these rubber composites at both low and significant deformations. From the results, a theory for the reinforcement and strain softening observed in filled rubbers can be determined.

Aggregated filler structures are the most probable cause of reinforcement of these rubber matrixes, as the dispersion of the filler material through steric hindrance reduced the storage moduli; however, this dispersion did not completely remove the reinforcement of the polymer or the strain softening effects. This suggests some other influence or that some correlation is left in the filler positions. It was observed that although the hydroxyl end functional polybutadiene dispersed the silica filler and prevented particle contact, nanoscale aggregates and fractal structures were still present. While these structures do not contain filler contacts, the close proximity of the particles may allow for the bearing of stress in the composite and provide reinforcement, as has been mentioned in literature. [32] This effect would be improved with the presence of a cross-linked matrix, which would prevent the diffusion of the filler particles. The two different correlation states, the fully percolating network and the dispersed aggregates, are illustrated in figure 8.12 left.
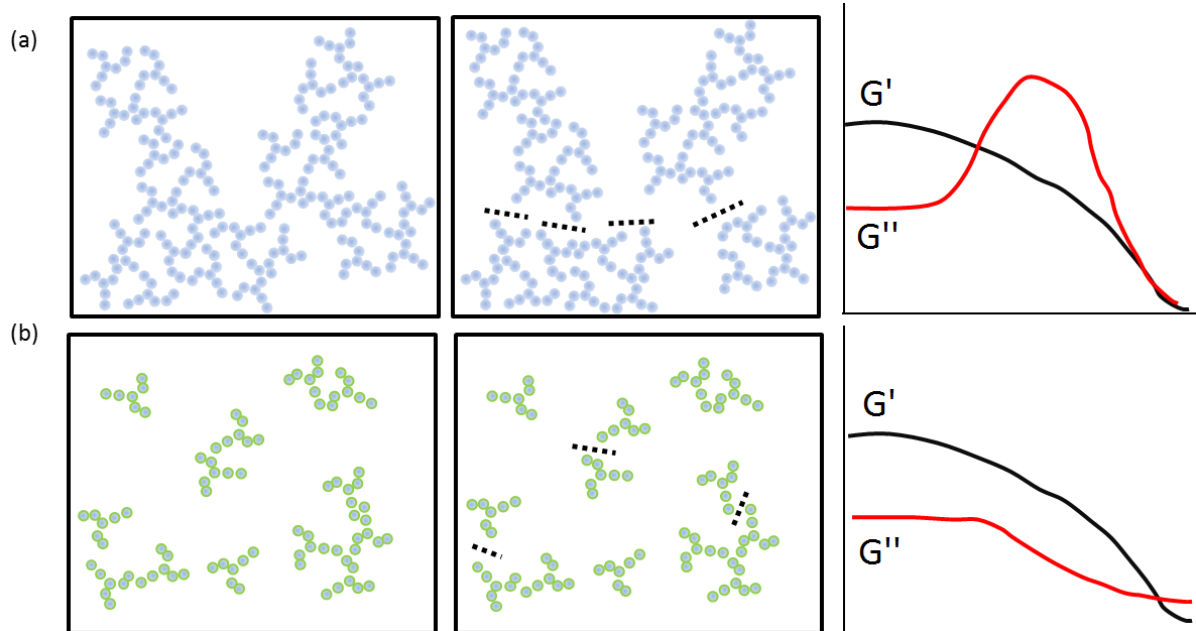
Figure 8.12: Left to right, depiction of filler structure without strain, under strain, and theoretical strain-modulus curves (G' black, G'' red); (a) percolating filler network (b) dispersed aggregates

Both systems contain filler structures that support the polymer matrix by bearing stress, however, in an undispersed and fully percolating structure, figure 8.12a, the network is continuous and able to provide increased support resulting in a greater storage modulus than in the dispersed

166

case (b). Under significant strain, the filler structures may yield and deform resulting in a decrease in the storage modulus as the aggregates no longer stiffen the material.

Key areas for these deformations is the bridges between local particles or particle structures, which transfer the stress and require less energy to break or deform than the large scale structure. The breakdown of these bridges is likely to be small, figure 8.12 centre, and does not change the characteristic structure of the aggregates, meaning that such a change is not detectable with small angle scattering; however the breakages of these bridges would result in the strain softening behaviour as the supporting network is removed.

A similar effect would be observed in quasi-elastic scattering, where the breakage of these contacts would require the dissolution of the inhibited polymer and energy input which would be dissipated into the matrix. While particle bridges bound by a glassy layer may break with strain, there is no universal decrease in the glassy layer thickness as the proportion of the material involved is small.

The presence and the removal of the loss peak are also describable by this theoretical system. The loss peak that occurs during strain softening is thought to arise from additional energy dissipation with the breaking of filler contact bonds. In both dispersion cases network bridges are broken, however the difference in behaviour arises from the presence of percolation.

With the percolating structure the stress is distributed throughout the network, when the stress is substantial enough to cause a particle bridge to yield, the interconnectedness results in the remainder of the bridges supporting the stress and an increase in stress per bridge, figure 8.12a centre. Under the circumstance that this increase results in further breaks, this pattern continues until the network does not percolate. Thus with this structure there is a critical stress were a significant proportion of the network bridges yield leading to the formation of a loss peak, figure 8.12a right.

The dispersed aggregates do not distribute stress, and the behaviour is localised to each cluster of particles. Thus when significant stress results in the breakdown of a contact bridge, no stress is transferred to the other aggregates. This results in a weaker but more flexible structure, and a lack of a critical strain at which most contacts are broken, hence no loss peak with strain is observed, figure 8.12b right.

This model is consistent with that put forward by Merabia et al., whom suggested that the filler network was maintained by glass polymer bridges between the particles, and that strain softening was the result of breaking these bridges. [119] It also bears similarity to the cluster-cluster aggregation model in which aggregate structures are broken down under applied strain, and

Payne's initial proposal for the cause of the softening as network breakdown. [6, 27] The current findings may be considered to be a partial validation of these models, as filler networking was found to be the primary cause of reinforcement and its breakdown under strain the reason for softening of the material. The results of both the SANS and QENS experiments have allowed for refinement of these ideas and location of the primary source of network breakdown in the composites tested. Further improvement with this model will be to advance it beyond a conceptual level and apply mathematical or computational models. This would provide confirmation of the ideas stated here and allow for predictive capacities.

8.6 Conclusions

Combination of the small angle scattering and rheological results was used to determine that removal of a percolating filler network not only decreases reinforcement of the material but also yields the removal of the loss peak as seen in the strain sweeps. The work examining the effect of cross-linking with QENS and rheology found that the crosslinking sites only inhibit local chain dynamics; however chain diffusion is arrested by topological constraints and results in the elastic behaviour of cross-linked systems. It was determined that cross-links would not have significant effects on the results of other experiments. While strain softening was found to occur in composite samples, no effect on the filler structure or the hindered dynamics with strain was observed, suggesting small localised changes were responsible for the softening. From these conclusions a model for the behaviour of the filled rubbers was devised for cases with and without percolation of the filler particles. The localised changes leading to strain softening were postulated to be from the breakdown of bridges between particle clusters, and the presence of the loss modulus peak was explained by the connectivity of the clusters.

9 Conclusions and future work

This work set out to characterise the behaviour of filled polybutadiene rubber nanocomposites of carbon black and silica using both rheology and neutron scatting in order to illuminate the underlying processes and devise a model of the composite system. These aims have been met; however there is room for further investigation and improvement of the results, the experimental techniques, and the devised model.

Composites containing quantities of unmodified polybutadiene, hydroxyl end-functionalised polybutadiene, and a type of filler material were rheologically tested to characterise their behaviour. Work with linear rheology found the addition of end-functionalised polybutadiene to silica containing composites reduced the effective reinforcement of the filler particles, while no changes in behaviour were found for the carbon black composites. From the non-linear strain sweeps, the removal of the loss modulus peak with the presence of the end-functionalised polybutadiene was observed for the silica composite samples, but no significant shifts were seen for the carbon black composites. Given previous work that found adsorption of the end-functionalised polybutadiene onto silica surfaces, it was postulated that the formation of a brush layer on the silica particles affected the composite properties.[85]

Small angle neutron scattering experiments were performed on silica composites similar to those characterised with rheology to examine the filler structure. Surface segregation of the end-functionalised polybutadiene to silica surfaces was observed, in agreement with the published literature, and a core-shell particle structure was noted. This brush layer was found to disperse the silica aggregates and prevent a percolating network structure from forming; however examination of the filler structure at micron length scales with spin echo small angle neutron scattering noted no change in filler correlations. Thus it was concluded that while the brush layer prevented particle contacts it did not prevent clustering. Finally, small angle neutron scattering on strained composite samples found that there was no change visible in the silica network when compared to unstrained material.

To examine the dynamics of the polymer and test for the presence of an inhibited polymer layer, quasi-elastic neutron scattering experiments were carried out on silica composite samples. Cross-linking was found to have little effect on the majority of the chain dynamics, and inhibited motion was limited to the cross-link sites. Scattering studies of the silica composites containing end-functional polybutadiene was able to note and characterise the presence of a dynamically inhibited polymer layer about the silica particles. This hindrance was found to be severe, and to occur at temperatures significantly above the glass transition temperature of polybutadiene.

Experiments on strained composite samples found no change in the hindered polymer layer with any level of strain. These results suggested that the layer is robust and not affected by the deformations applied to the composite filler networks.

The conclusions from each experimental method were analysed together to provide additional insight into the composite behaviour. While the strain softening was present, there were no corresponding changes to the nanoscale filler structure or the polymer layer dynamics. This suggested that the cause for the softening did not involve significant fractions of the material. The contact bridges between fillers were determined to result in the observed effects, and a conceptual model was devised. This model was able to provide an explanation for both the observed rheological and scattering results.

While this work has successfully investigated the processes responsible for composite reinforcement and strain softening, there are areas for improvement. The linear rheology is mature and well documented, and as a technique there are no clear developments to be made, though characterisation of further composite systems will aid in developing and verifying models of composite behaviour. The strain softening effects are well known and documented, with Payne providing the earliest literature; however to our knowledge no significant work has been done to measure the harmonics beyond the first with large amplitude oscillatory shear.[6, 7] Analysis of this data may provide additional insight into the composite behaviour, particularly the strain softening.

In regards to the scattering experiments, the use of surface segregation along with isotopic labelling allows for the development of new quasi elastic scattering experiments and the ability to selectively measure fractions of a material. Significant improvements can still be made to the devices used to strain the polymer samples in-situ. In particular, development to apply a dynamic strain to sample materials would be of use and open new avenues of research on soft materials to be explored. Other techniques may be viable to study these composites, although TEM lacks the penetration needed, SEM measurements on cryo-fractured samples could provide an image of the network. In regards to dynamic strain measurements, use of fluorescent markers to map particle positions may be able to observe the theorised breakages and fractures in the composites.

Overall, this work gives insight into the behaviour of filled rubber composites, and provides methods to expand and develop knowledge of composites. Given the importance of such composites in daily life, this field will continue to develop and improve for the foreseeable future.

10 Appendices

10.1 Krieger fit parameters

Table 10.1: Krieger fit parameters, chapter 4, storage modulus

Filler type	Parameters				
	Prefactor, C	C uncertainty	Numerical factor, B	B uncertainty	Critical volume fraction, φ_c
CB	1.00	± 0.07	6.68	± 0.47	0.64
Prec.	0.85	± 0.14	14.18	± 1.66	0.64
Stöber	1.05	± 0.05	4.00	± 0.14	0.64
CB ef	1.05	± 0.05	10.43	± 0.33	0.64
Prec. ef	1.06	± 0.05	15.48	± 0.48	0.64
Stöber ef	1.04	± 0.07	3.92	± 0.20	0.64
CB xl	0.46	± 0.03	13.16	± 0.41	0.64
Prec. xl	0.89	± 0.13	10.08	± 1.57	0.64
Stöber xl	0.30	± 0.04	8.17	± 0.38	0.64
CB ef xl	0.46	± 0.11	19.82	± 1.42	0.64
Prec. ef xl	1.05	± 0.05	10.79	± 0.53	0.64
Stöber ef xl	1.26	± 0.26	6.38	± 0.56	0.64

Table 10.2: Krieger fit parameters, chapter 4, loss modulus

Filler type	Parameters				
	Prefactor, C	C uncertainty	Numerical factor, B	B uncertainty	Critical volume fraction, φ_c
CB	1.04	± 0.10	4.64	± 0.72	0.64
Prec.	0.87	± 0.14	11.64	± 1.62	0.64
Stöber	1.07	± 0.05	3.53	± 0.14	0.64
CB ef	1.04	± 0.04	7.66	± 0.27	0.64
Prec. ef	1.01	± 0.01	12.67	± 0.09	0.64
Stöber ef	0.90	± 0.08	3.73	± 0.27	0.64
CB xl	0.89	± 0.16	10.20	± 1.20	0.64
Prec. xl	1.18	± 0.18	13.23	± 1.52	0.64
Stöber xl	0.70	± 0.09	7.22	± 0.33	0.64
CB ef xl	0.80	± 0.17	15.17	± 1.34	0.64
Prec. ef xl	0.89	± 0.11	13.81	± 1.22	0.64
Stöber ef xl	1.00	± 0.00	7.93	± 0.12	0.64

10.2 Kraus strain softening fits

Figure 10.1: Kraus fits for composite samples, (a) carbon black, (b) precipitated silica, (c) low content Stöber silica, (d) high content Stöber silica; filler content in the legend

Figure 10.2: Kraus fits for composite samples with end-functional polybutadiene, (a) carbon black, (b) precipitated silica, (c) low content Stöber silica, (d) high content Stöber silica; filler content in the legend

173
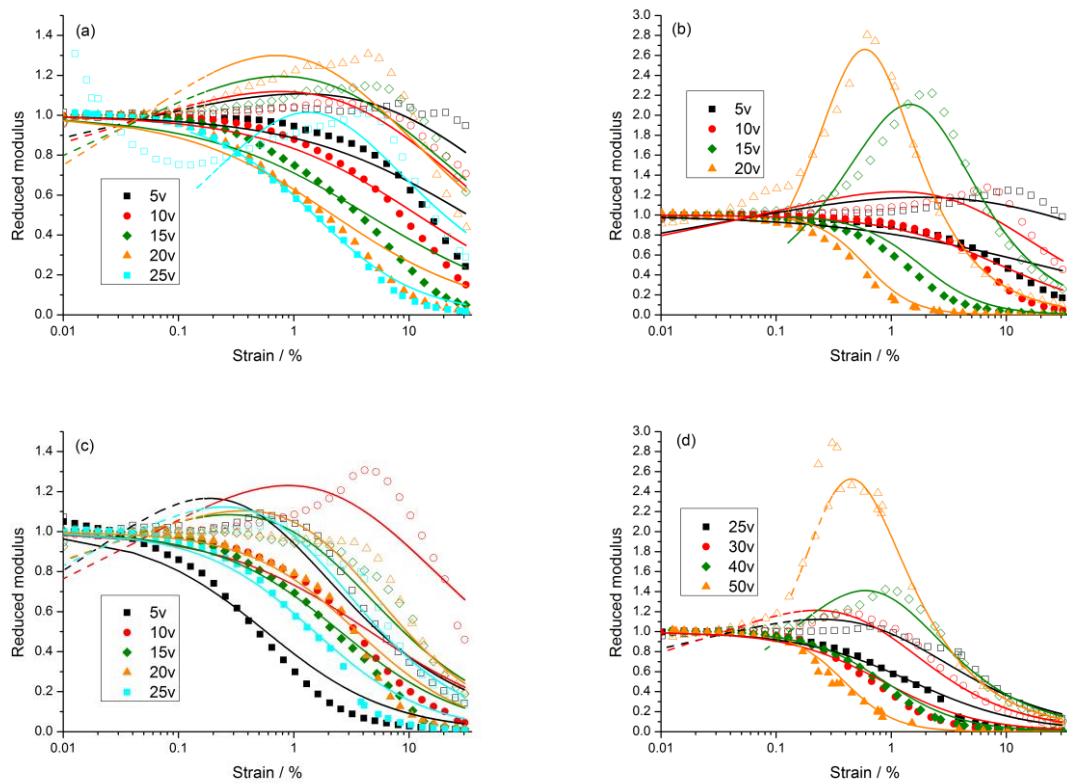
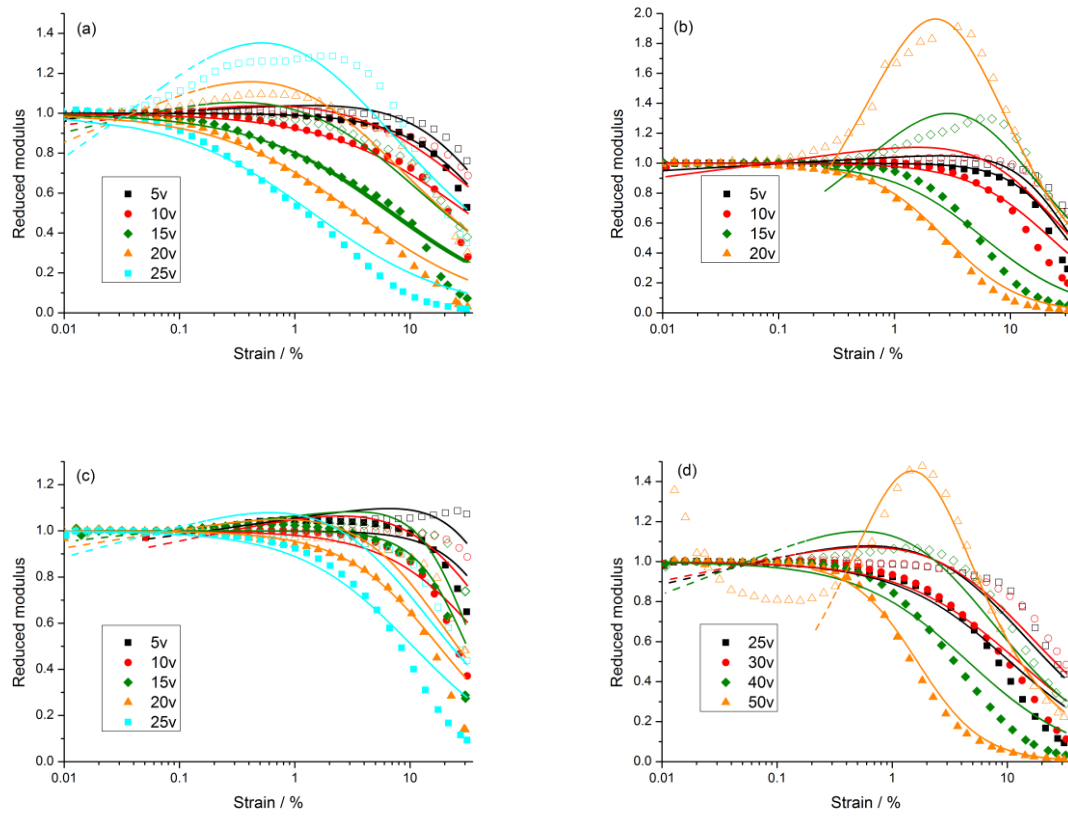Figure 10.3: Kraus fits for cross-linked composite samples, (a) carbon black, (b) precipitated silica, (c) low content Stöber silica, (d) high content Stöber silica; filler content in the legend
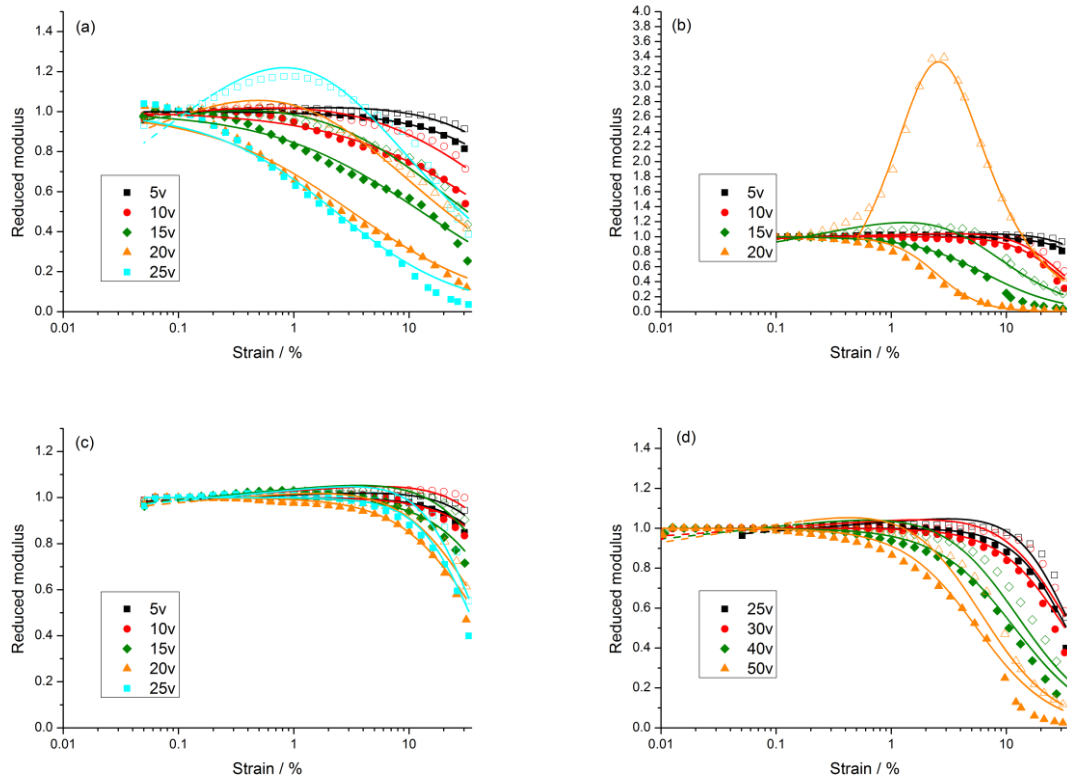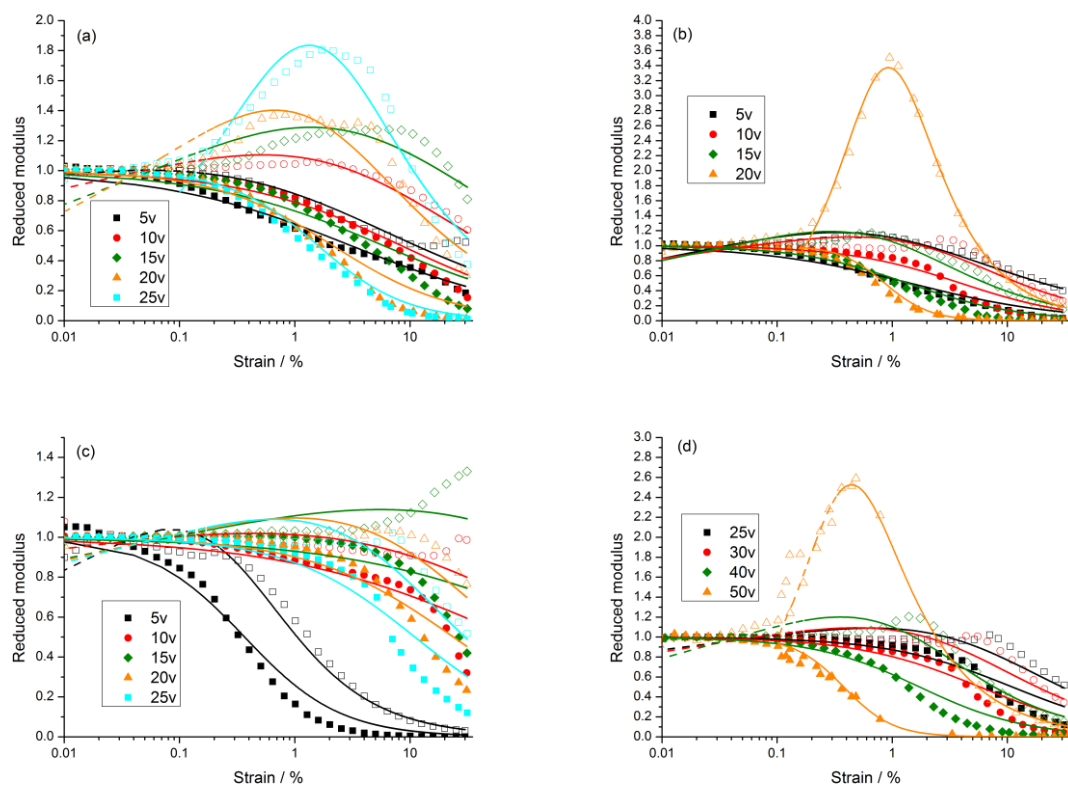
Figure 10.4: Kraus fits for cross-linked composite samples with end-functional polybutadiene, (a) carbon black, (b) precipitated silica, (c) low content Stöber silica, (d) high content Stöber silica; filler content in the legend

10.3 QENS KWW fit parameters

Table 10.3: Crosslinking experiment KWW average beta and background, section 7.1

Sample	Average β	Background, A									
		0.525/ Å^{-1}	0.729/ Å^{-1}	0.923/ Å^{-1}	1.106/ Å^{-1}	1.273/ Å^{-1}	1.424/ Å^{-1}	1.556/ Å^{-1}	1.668/ Å^{-1}	1.758/ Å^{-1}	1.825/ Å^{-1}
Linear 220K	0.476 ± 0.048	0.90 ± 0.01	0.44 ± 0.65	0.80 ± 0.03	0.82 ± 0.01	0.81 ± 0.01	0.74 ± 0.01	0.74 ± 0.01	0.60 ± 0.05	0.72 ± 0.01	0.71 ± 0.01
Linear 250K	0.497 ± 0.061	0.00 ± 0.69	0.79 ± 0.01	0.68 ± 0.01	0.55 ± 0.01	0.52 ± 0.01	0.47 ± 0.01	0.46 ± 0.01	0.47 ± 0.01	0.41 ± 0.01	0.29 ± 0.02
Linear 280K	0.464 ± 0.039	0.00 ± 0.20	0.35 ± 0.04	0.00 ± 0.04	0.25 ± 0.01	0.10 ± 0.01	0.12 ± 0.01	0.14 ± 0.01	0.16 ± 0.01	0.15 ± 0.01	0.07 ± 0.01
Linear 310K	0.501 ± 0.041	0.22 ± 0.06	0.24 ± 0.01	0.00 ± 0.01	0.00 ± 0.01	0.06 ± 0.01	0.03 ± 0.01	0.00 ± 0.01	0.01 ± 0.01	0.02 ± 0.01	0.01 ± 0.01
Linear 363K	0.590 ± 0.054	0.08 ± 0.02	0.08 ± 0.01	0.04 ± 0.01	0.01 ± 0.01	0.02 ± 0.01	0.01 ± 0.01	0.02 ± 0.01	0.02 ± 0.01	0.00 ± 0.01	0.01 ± 0.01
Cross-linked 220K	0.461 ± 0.053	0.92 ± 0.01	0.86 ± 0.02	0.86 ± 0.01	0.83 ± 0.01	0.68 ± 0.06	0.61 ± 0.09	0.71 ± 0.02	0.56 ± 0.06	0.72 ± 0.01	0.67 ± 0.02
Cross-linked 250K	0.471 ± 0.067	0.00 ± 3.6	0.61 ± 0.01	0.73 ± 0.01	0.69 ± 0.04	0.48 ± 0.02	0.52 ± 0.01	0.57 ± 0.01	0.48 ± 0.01	0.02 ± 0.25	0.33 ± 0.04
Cross-linked 280K	0.470 ± 0.037	0.60 ± 0.01	0.00 ± 0.01	0.42 ± 0.01	0.33 ± 0.01	0.28 ± 0.01	0.26 ± 0.01	0.24 ± 0.01	0.12 ± 0.01	0.20 ± 0.01	0.13 ± 0.01
Cross-linked 310K	0.476 ± 0.007	0.07 ± 0.06	0.15 ± 0.02	0.02 ± 0.01	0.11 ± 0.01	0.09 ± 0.01	0.14 ± 0.01	0.10 ± 0.01	0.11 ± 0.01	0.04 ± 0.01	0.04 ± 0.01
Cross-linked 363K	0.465 ± 0.110	0.00 ± 0.06	0.00 ± 0.02	0.00 ± 0.01	0.00 ± 0.01	0.00 ± 0.01	0.02 ± 0.01	0.03 ± 0.01	0.03 ± 0.01	0.03 ± 0.01	0.02 ± 0.01

Table 10.4: Characterisation of the glassy layer experiment, KWW average beta and background, section 7.2, larger detector groupings were run at 250 K

Sample	Average β	Background, A									
		0.525/ Å^{-1}	0.729/ Å^{-1}	0.923/ Å^{-1}	1.106/ Å^{-1}	1.273/ Å^{-1}	1.424/ Å^{-1}	1.556/ Å^{-1}	1.668/ Å^{-1}	1.758/ Å^{-1}	1.825/ Å^{-1}
220K Blend	0.476 ± 0.029	0.00 ± 10	0.91 ± 0.01	0.88 ± 0.01	0.71 ± 0.06	0.71 ± 0.04	0.79 ± 0.01	0.76 ± 0.01	0.73 ± 0.01	0.00 ± 0.01	0.38 ± 0.19
220K hPBd composite	0.472 ± 0.022	0.95 ± 0.01	0.81 ± 0.07	0.85 ± 0.01	0.78 ± 0.03	0.81 ± 0.01	0.78 ± 0.01	0.76 ± 0.01	0.76 ± 0.01	0.44 ± 0.12	0.59 ± 0.03
220K 15k 4OHPBd composite	0.480 ± 0.031	0.96 ± 0.01	0.91 ± 0.01	0.00 ± 0.01	0.00 ± 0.01	0.00 ± 0.01	0.79 ± 0.01	0.78 ± 0.01	0.74 ± 0.01	0.00 ± 0.30	0.49 ± 0.08
250K Blend	0.41 ± 0.02	0.49 ± 0.13	-	0.08 ± 0.12	-	0.58 ± 0.02	-	0.10 ± 0.04	-	0.28 ± 0.02	0.20 ± 0.02
250K hPBd composite	0.45 ± 0.06	0.87 ± 0.01	-	0.71 ± 0.01	-	0.42 ± 0.02	-	0.51 ± 0.01	-	0.36 ± 0.02	0.30 ± 0.02
250K 15k 4OHPBd composite	0.52 ± 0.04	0.87 ± 0.01	-	0.71 ± 0.01	-	0.62 ± 0.01	-	0.58 ± 0.01	-	0.39 ± 0.02	0.51 ± 0.01
280K Blend	0.465 ± 0.014	0.56 ± 0.03	0.36± 0.02	0.22 ± 0.02	0.12 ± 0.01	0.24 ± 0.01	0.17 ± 0.01	0.09 ± 0.01	0.14 ± 0.01	0.10 ± 0.01	0.00 ± 0.01
280K hPBd composite	0.466 ± 0.019	0.76 ± 0.01	0.51 ± 0.01	0.27 ± 0.01	0.31 ± 0.01	0.20 ± 0.01	0.27 ± 0.01	0.18 ± 0.01	0.23 ± 0.01	0.20 ± 0.01	0.15 ± 0.01
280K 15k 4OHPBd composite	0.500 ± 0.014	0.75 ± 0.01	0.54 ± 0.01	0.33 ± 0.01	0.36 ± 0.01	0.33 ± 0.01	0.34 ± 0.01	0.34 ± 0.01	0.26 ± 0.01	0.27 ± 0.01	0.24 ± 0.01
310K Blend	0.476 ± 0.008	0.37 ± 0.01	0.00 ± 0.02	0.00 ± 0.01	0.05 ± 0.01	0.09 ± 0.01	0.01 ± 0.01	0.06 ± 0.01	0.00 ± 0.01	0.05 ± 0.01	0.00 ± 0.01
310K hPBd composite	0.461 ± 0.010	0.55 ± 0.01	0.21 ± 0.02	0.05 ± 0.01	0.05 ± 0.01	0.06 ± 0.01	0.00 ± 0.01	0.12 ± 0.01	0.11 ± 0.01	0.10 ± 0.01	0.10 ± 0.01
310K 15k 4OHPBd composite	0.484 ± 0.008	0.53 ± 0.01	0.32 ± 0.01	0.17 ± 0.01	0.22 ± 0.01	0.18 ± 0.01	0.18 ± 0.01	0.18 ± 0.01	0.18 ± 0.01	0.18 ± 0.01	0.18 ± 0.01
310K 10k 4OHPBd composite	0.514 ± 0.010	0.50 ± 0.01	0.39 ± 0.01	0.23 ± 0.01	0.23 ± 0.01	0.24 ± 0.01	0.23 ± 0.01	0.23 ± 0.01	0.24 ± 0.01	0.27 ± 0.01	0.22 ± 0.01
363K Blend	0.555 ± 0.024	0.00 ± 0.01	0.02 ± 0.01	0.03 ± 0.01	0.04 ± 0.01	0.04 ± 0.01	0.02 ± 0.01	0.02 ± 0.01	0.04 ± 0.01	0.04 ± 0.01	0.03 ± 0.01
363K hPBd composite	0.471 ± 0.025	0.06 ± 0.11	0.00 ± 0.01	0.10 ± 0.01	0.13 ± 0.01	0.10 ± 0.01	0.08 ± 0.01	0.08 ± 0.01	0.10 ± 0.01	0.10 ± 0.01	0.12 ± 0.01
363K 15k 4OHPBd composite	0.502 ± 0.029	0.18 ± 0.02	0.15 ± 0.01	0.14 ± 0.01	0.16 ± 0.01	0.13 ± 0.01	0.14 ± 0.01	0.17 ± 0.01	0.19 ± 0.01	0.17 ± 0.01	0.17 ± 0.01
363K 10k 4OHPBd composite	0.534 ± 0.020	0.04 ± 0.05	0.21 ± 0.01	0.18 ± 0.01	0.16 ± 0.01	0.13 ± 0.01	0.17 ± 0.01	0.20 ± 0.01	0.22 ± 0.01	0.22 ± 0.01	0.21 ± 0.01

Table 10.5: IN16B glassy layer characterisation, KWW average beta and background, section 7.3

| Sample | Average β | Background, A | | | | | | |
		0.760/ Å^{-1}	1.004/ Å^{-1}	1.230/ Å^{-1}	1.433/ Å^{-1}	1.610/ Å^{-1}	1.757/ Å^{-1}	1.871/ Å^{-1}
220K Blend	0.458 ± 0.009	0.72 ± 0.01	0.68 ± 0.01	0.62 ± 0.01	0.56 ± 0.01	0.50 ± 0.01	0.49 ± 0.01	0.45 ± 0.01
220K hPBd composite	0.444 ± 0.010	0.73 ± 0.01	0.69 ± 0.01	0.66 ± 0.01	0.59 ± 0.01	0.55 ± 0.01	0.55 ± 0.01	0.55 ± 0.01
220K 15k 4OHPBd composite	0.462 ± 0.015	0.76 ± 0.01	0.70 ± 0.01	0.69 ± 0.01	0.66 ± 0.01	0.57 ± 0.01	0.56 ± 0.01	0.56 ± 0.01
250K Blend	0.472 ± 0.005	0.25 ± 0.01	0.12 ± 0.01	0.10 ± 0.01	0.10 ± 0.01	0.03 ± 0.01	0.04 ± 0.01	0.05 ± 0.01
250K hPBd composite	0.464 ± 0.005	0.31 ± 0.01	0.23 ± 0.01	0.24 ± 0.01	0.17 ± 0.01	0.20 ± 0.01	0.20 ± 0.01	0.20 ± 0.01
250K 15k 4OHPBd composite	0.460 ± 0.009	0.26 ± 0.01	0.20 ± 0.01	0.21 ± 0.01	0.19 ± 0.01	0.20 ± 0.01	0.23 ± 0.01	0.26 ± 0.01
280K Blend	0.572 ± 0.005	0.06 ± 0.01	0.04 ± 0.01	0.03 ± 0.01	0.03 ± 0.01	0.03 ± 0.01	0.02 ± 0.01	0.03 ± 0.01
280K hPBd composite	0.558 ± 0.004	0.14 ± 0.01	0.14 ± 0.01	0.14 ± 0.01	0.15 ± 0.01	0.16 ± 0.01	0.17 ± 0.01	0.17 ± 0.01
280K 15k 4OHPBd composite	0.555 ± 0.005	0.22 ± 0.01	0.21 ± 0.01	0.19 ± 0.01	0.19 ± 0.01	0.22 ± 0.01	0.26 ± 0.01	0.26 ± 0.01
310K Blend	0.649 ± 0.013	0.04 ± 0.01	0.02 ± 0.01	0.01 ± 0.01	0.02 ± 0.01	0.02 ± 0.01	0.02 ± 0.01	0.02 ± 0.01
310K hPBd composite	0.598 ± 0.017	0.13 ± 0.01	0.13 ± 0.01	0.15 ± 0.01	0.17 ± 0.01	0.19 ± 0.01	0.21 ± 0.01	0.19 ± 0.01
310K 15k 4OHPBd composite	0.592 ± 0.016	0.21 ± 0.01	0.20 ± 0.01	0.21 ± 0.01	0.22 ± 0.01	0.27 ± 0.01	0.30 ± 0.01	0.30 ± 0.01
363K Blend	0.634 ± 0.068	0.01 ± 0.01	0.01 ± 0.01	0.01 ± 0.01	0.01 ± 0.01	0.01 ± 0.01	0.02 ± 0.01	0.02 ± 0.01
363K hPBd composite	0.437 ± 0.053	0.13 ± 0.01	0.16 ± 0.01	0.19 ± 0.01	0.24 ± 0.01	0.28 ± 0.01	0.31 ± 0.01	0.27 ± 0.01
363K 15k 4OHPBd composite	0.378 ± 0.049	0.19 ± 0.01	0.23 ± 0.01	0.25 ± 0.01	0.30 ± 0.01	0.36 ± 0.01	0.40 ± 0.01	0.36 ± 0.01

Table 10.6: Stitched IRIS and IN16B data, KWW average beta and background, section 7.3

Sample	Average β	Background, A						
		0.760/ $Å^{-1}$	1.004/ $Å^{-1}$	1.230/ $Å^{-1}$	1.433/ $Å^{-1}$	1.610/ $Å^{-1}$	1.757/ $Å^{-1}$	1.871/ $Å^{-1}$
220K Blend	0.371 ± 0.010	0.55 ± 0.02	0.59 ± 0.01	0.57 ± 0.01	0.52 ± 0.01	0.51 ± 0.01	0.46 ± 0.01	0.43 ± 0.01
220K hPBd composite	0.368 ± 0.006	0.64 ± 0.01	0.60 ± 0.01	0.61 ± 0.01	0.56 ± 0.01	0.55 ± 0.01	0.53 ± 0.01	0.51 ± 0.01
220K 15k 4OHPBd composite	0.399 ± 0.010	0.69 ± 0.01	0.68 ± 0.01	0.66 ± 0.01	0.65 ± 0.01	0.59 ± 0.01	0.56 ± 0.01	0.55 ± 0.01
250K Blend	0.372 ± 0.008	0.00 ± 0.05	0.00 ± 0.02	0.06 ± 0.01	0.08 ± 0.01	0.10 ± 0.01	0.07 ± 0.01	0.05 ± 0.01
250K hPBd composite	0.371 ± 0.007	-	0.00 ± 0.02	0.20 ± 0.01	0.19 ± 0.01	0.20 ± 0.01	0.18 ± 0.01	-
250K 15k 4OHPBd composite	0.390 ± 0.005	-	0.00 ± 0.03	0.23 ± 0.01	0.20 ± 0.01	0.23 ± 0.01	0.25 ± 0.01	-
280K Blend	0.426 ± 0.010	0.00 ± 0.04	0.00 ± 0.01	0.02 ± 0.01	0.01 ± 0.01	0.03 ± 0.01	0.02 ± 0.01	0.00 ± 0.01
280K hPBd composite	0.418 ± 0.008	0.00 ± 0.02	0.02 ± 0.01	0.10 ± 0.01	0.11 ± 0.01	0.12 ± 0.01	0.11 ± 0.01	0.10 ± 0.01
280K 15k 4OHPBd composite	0.422 ± 0.006	0.07 ± 0.01	0.12 ± 0.01	0.14 ± 0.01	0.14 ± 0.01	0.15 ± 0.01	0.18 ± 0.01	0.18 ± 0.01
310K Blend	0.457 ± 0.005	0.00 ± 0.01	0.00 ± 0.01	0.02 ± 0.01	0.00 ± 0.01	0.00 ± 0.01	0.03 ± 0.01	0.01 ± 0.01
310K hPBd composite	0.455 ± 0.007	0.06 ± 0.01	0.09 ± 0.01	0.09 ± 0.01	0.09 ± 0.01	0.11 ± 0.01	0.11 ± 0.01	0.11 ± 0.01
310K 15k 4OHPBd composite	0.452 ± 0.005	0.15 ± 0.01	0.15 ± 0.01	0.14 ± 0.01	0.14 ± 0.01	0.17 ± 0.01	0.16 ± 0.01	0.17 ± 0.01

Table 10.7: Stitched IRIS and IN16B data, scaling factor, section 7.3

Sample	Scaling factor						
	$0.760/\text{ Å}^{-1}$	$1.004/\text{ Å}^{-1}$	$1.230/\text{ Å}^{-1}$	$1.433/\text{ Å}^{-1}$	$1.610/\text{ Å}^{-1}$	$1.757/\text{ Å}^{-1}$	$1.871/\text{ Å}^{-1}$
220K Blend	0.99	0.975	0.93	0.94	0.9	0.89	0.9
220K hPBd composite	0.985	0.98	0.94	0.93	0.91	0.895	0.91
220K 15k 4OHPBd composite	0.985	0.965	0.94	0.945	0.915	0.905	0.92
250K Blend	0.95	0.93	0.86	0.84	0.77	0.77	0.78
250K hPBd composite	-	0.95	0.88	0.86	0.82	0.78	-
250K 15k 4OHPBd composite	-	0.95	0.9	0.88	0.84	0.84	-
280K Blend	0.93	0.88	0.77	0.75	0.6	0.6	0.6
280K hPBd composite	0.95	0.88	0.75	0.74	0.67	0.65	0.66
280K 15k 4OHPBd composite	0.91	0.85	0.76	0.75	0.65	0.67	0.69
310K Blend	0.93	0.87	0.67	0.6	0.47	0.6	0.6
310K hPBd composite	0.93	0.85	0.62	0.58	0.5	0.5	0.53
310K 15k 4OHPBd composite	0.9	0.8	0.67	0.63	0.57	0.53	0.55

Table 10.8: IRIS stretching first experiment, KWW average beta and background, section 7.4

Sample	Average β	Background, A									
		0.525 / Å^{-1}	0.729 / Å^{-1}	0.923 / Å^{-1}	1.106 / Å^{-1}	1.273 / Å^{-1}	1.424 / Å^{-1}	1.556 / Å^{-1}	1.668 / Å^{-1}	1.758 / Å^{-1}	1.825 / Å^{-1}
Blend 0%	0.467 ± 0.013	0.50 ± 0.10	0.20 ± 0.27	0.28 ± 0.08	0.49 ± 0.01	0.22 ± 0.06	0.00 ± 0.18	0.21 ± 0.04	0.22 ± 0.04	0.00 ± 0.10	0.00 ± 0.10
Blend 10%	0.499 ± 0.013	0.19 ± 0.35	0.00 ± 0.01	0.33 ± 0.06	0.34 ± 0.03	0.29 ± 0.03	0.31 ± 0.02	0.27 ± 0.02	0.23 ± 0.02	0.20 ± 0.02	0.23 ± 0.02
Blend 20%	0.472 ± 0.007	0.42 ± 0.11	0.35 ± 0.10	0.00 ± 0.01	0.24 ± 0.05	0.00 ± 0.10	0.26 ± 0.04	0.17 ± 0.04	0.22 ± 0.02	0.16 ± 0.03	0.00 ± 0.10
hPBd composite 0%	0.504 ± 0.018	0.00 ± 0.10	0.63 ± 0.01	0.00 ± 0.10	0.37 ± 0.04	0.47 ± 0.01	0.38 ± 0.01	0.23 ± 0.03	0.19 ± 0.04	0.24 ± 0.02	0.06 ± 0.07
hPBd composite 10%	0.491 ± 0.018	0.69 ± 0.02	0.64 ± 0.02	0.00 ± 0.10	0.42 ± 0.03	0.43 ± 0.02	0.22 ± 0.05	0.39 ± 0.01	0.34 ± 0.02	0.00 ± 0.10	0.00 ± 0.10
hPBd composite 20%	0.514 ± 0.022	0.55 ± 0.11	0.28 ± 0.18	0.51 ± 0.02	0.53 ± 0.01	0.45 ± 0.01	0.26 ± 0.04	0.35 ± 0.02	0.35 ± 0.01	0.21 ± 0.03	0.13 ± 0.03
15k 4OHPBd composite 0%	0.518 ± 0.009	0.76 ± 0.01	0.66 ± 0.01	0.60 ± 0.02	0.53 ± 0.02	0.44 ± 0.03	0.48 ± 0.02	0.30 ± 0.09	0.39 ± 0.02	0.40 ± 0.02	0.34 ± 0.02
15k 4OHPBd composite 10%	0.519 ± 0.018	0.66 ± 0.04	0.57 ± 0.05	0.43 ± 0.05	0.57 ± 0.01	0.44 ± 0.02	0.48 ± 0.01	0.45 ± 0.01	0.43 ± 0.01	0.32 ± 0.03	0.33 ± 0.02
15k 4OHPBd composite 20%	0.496 ± 0.027	0.00 ± 0.10	0.00 ± 0.63	0.68 ± 0.01	0.57 ± 0.01	0.00 ± 0.10	0.49 ± 0.02	0.25 ± 0.09	0.37 ± 0.02	0.17 ± 0.09	0.31 ± 0.02
10k 4OHPBd composite 0%	0.526 ± 0.017	0.76 ± 0.01	0.00 ± 0.01	0.29 ± 0.16	0.44 ± 0.04	0.49 ± 0.01	0.44 ± 0.02	0.37 ± 0.02	0.36 ± 0.04	0.42 ± 0.01	0.41 ± 0.01
10k 4OHPBd composite 10%	0.506 ± 0.024	0.74 ± 0.01	0.00 ± 0.01	0.50 ± 0.04	0.25 ± 0.14	0.47 ± 0.02	0.48 ± 0.01	0.38 ± 0.02	0.00 ± 0.10	0.31 ± 0.02	0.00 ± 0.1
10k 4OHPBd composite 20%	0.495 ± 0.015	0.71 ± 0.02	0.00 ± 0.10	0.47 ± 0.03	0.14 ± 0.28	0.43 ± 0.03	0.34 ± 0.03	0.24 ± 0.05	0.40 ± 0.02	0.27 ± 0.03	0.28 ± 0.02

Table 10.9: IRIS stretching second experiment, KWW average beta and background, section 7.4

Sample	Average β	Background, A									
		0.525/ Å^{-1}	0.729/ Å^{-1}	0.923/ Å^{-1}	1.106/ Å^{-1}	1.273/ Å^{-1}	1.424/ Å^{-1}	1.556/ Å^{-1}	1.668/ Å^{-1}	1.758/ Å^{-1}	1.825/ Å^{-1}
Blend 0%	0.472 ± 0.013	0.15 ± 0.02	0.41 ± 0.01	0.26 ± 0.01	0.10 ± 0.01	0.14 ± 0.01	0.13 ± 0.01	0.16 ± 0.01	0.15 ± 0.01	0.12 ± 0.01	0.15 ± 0.01
Blend 5%	0.481 ± 0.018	0.16 ± 0.02	0.30 ± 0.01	0.19 ± 0.01	0.20 ± 0.01	0.10 ± 0.01	0.11 ± 0.01	0.15 ± 0.01	0.14 ± 0.01	0.11 ± 0.01	0.16 ± 0.01
Blend 10%	0.485 ± 0.009	0.00 ± 0.07	0.21 ± 0.01	0.19 ± 0.01	0.18 ± 0.01	0.10 ± 0.01	0.13 ± 0.01	0.16 ± 0.01	0.15 ± 0.01	0.11 ± 0.01	0.00 ± 0.01
Blend 15%	0.448 ± 0.016	0.13 ± 0.02	0.37 ± 0.01	0.28 ± 0.01	0.17 ± 0.01	0.17 ± 0.01	0.14 ± 0.01	0.15 ± 0.01	0.14 ± 0.01	0.12 ± 0.01	0.13 ± 0.01
Blend 20%	0.490 ± 0.013	0.00 ± 0.07	0.24 ± 0.01	0.11 ± 0.01	0.19 ± 0.01	0.11 ± 0.01	0.12 ± 0.01	0.16 ± 0.01	0.15 ± 0.01	0.12 ± 0.01	0.08 ± 0.01
hPBd composite 0%	0.474 ± 0.008	0.00 ± 0.08	0.23 ± 0.01	0.16 ± 0.01	0.08 ± 0.01	0.12 ± 0.01	0.16 ± 0.01	0.16 ± 0.01	0.18 ± 0.01	0.19 ± 0.01	0.18 ± 0.01
hPBd composite 1%	0.446 ± 0.010	0.00 ± 0.04	0.33 ± 0.01	0.16 ± 0.01	0.06 ± 0.01	0.11 ± 0.01	0.13 ± 0.01	0.15 ± 0.01	0.17 ± 0.01	0.18 ± 0.01	0.17 ± 0.01
hPBd composite 5%	0.464 ± 0.008	0.00 ± 0.02	0.24 ± 0.01	0.14 ± 0.01	0.11 ± 0.01	0.11 ± 0.01	0.14 ± 0.01	0.16 ± 0.01	0.17 ± 0.01	0.19 ± 0.01	0.17 ± 0.01
hPBd composite 10%	0.462 ± 0.007	0.00 ± 0.06	0.26 ± 0.01	0.10 ± 0.01	0.13 ± 0.01	0.14 ± 0.01	0.15 ± 0.01	0.15 ± 0.01	0.16 ± 0.01	0.18 ± 0.01	0.18 ± 0.01
hPBd composite 15%	0.460 ± 0.008	0.00 ± 0.07	0.26 ± 0.01	0.10 ± 0.01	0.12 ± 0.01	0.14 ± 0.01	0.15 ± 0.01	0.17 ± 0.01	0.16 ± 0.01	0.18 ± 0.01	0.17 ± 0.01
hPBd composite 20%	0.465 ± 0.009	0.00 ± 0.06	0.22 ± 0.01	0.15 ± 0.01	0.08 ± 0.01	0.12 ± 0.01	0.14 ± 0.01	0.15 ± 0.01	0.17 ± 0.01	0.18 ± 0.01	0.16 ± 0.01
15k 4OHPBd composite 0%	0.454 ± 0.008	0.16 ± 0.01	0.18 ± 0.01	0.14 ± 0.01	0.19 ± 0.01	0.21 ± 0.01	0.11 ± 0.01	0.21 ± 0.01	0.21 ± 0.01	0.20 ± 0.01	0.25 ± 0.01
15k 4OHPBd composite 1%	0.453 ± 0.007	0.20 ± 0.02	0.26 ± 0.01	0.05 ± 0.01	0.17 ± 0.01	0.23 ± 0.01	0.10 ± 0.01	0.19 ± 0.01	0.20 ± 0.01	0.21 ± 0.01	0.25 ± 0.01
15k 4OHPBd composite 5%	0.451 ± 0.011	0.01 ± 0.03	0.19 ± 0.02	0.04 ± 0.01	0.21 ± 0.01	0.24 ± 0.01	0.14 ± 0.01	0.20 ± 0.01	0.22 ± 0.01	0.21 ± 0.01	0.25 ± 0.01
15k 4OHPBd composite 10%	0.438 ± 0.010	0.37 ± 0.01	0.26 ± 0.01	0.10 ± 0.01	0.20 ± 0.01	0.22 ± 0.01	0.12 ± 0.01	0.19 ± 0.01	0.21 ± 0.01	0.20 ± 0.01	0.25 ± 0.01
15k 4OHPBd composite 15%	0.450 ± 0.011	0.00 ± 0.03	0.21 ± 0.01	0.17 ± 0.01	0.16 ± 0.01	0.23 ± 0.01	0.10 ± 0.01	0.21 ± 0.01	0.21 ± 0.01	0.22 ± 0.01	0.25 ± 0.01
15k 4OHPBd composite 20%	0.468 ± 0.007	0.00 ± 0.02	0.18 ± 0.01	0.02 ± 0.01	0.21 ± 0.01	0.22 ± 0.01	0.13 ± 0.01	0.19 ± 0.01	0.19 ± 0.01	0.21 ± 0.01	0.25 ± 0.01

11 References

1. Hosler, D., Burkett, S. L. and Tarkanian, M. J., *Science*, 1999, 284, 1988-1991.
2. Guth, E., *Journal of Applied Physics*, 1945, 16, 20-25.
3. Giannelis, E. P., Krishnamoorti, R. and Manias, E., *Polymers in Confined Environments*, eds. Granick, S., Binder, K., de Gennes, P. G., Giannelis, E. P., Grest, G. S., Hervet, H., Krishnamoorti, R., Léger, L., Manias, E., Raphaël, E. and Wang, S. Q., Springer Berlin Heidelberg, Berlin, Heidelberg, 1999, DOI: 10.1007/3-540-69711-x_3, pp. 107-147.
4. Kumar, S. K., Benicewicz, B. C., Vaia, R. A. and Winey, K. I., *Macromolecules*, 2017, 50, 714-731.
5. *Rolling out the Changes*, The Economist Newspaper Limited, London, 2010, vol. Technology Quarterly Q1.
6. Payne, A. R., *Journal of Applied Polymer Science*, 1962, 6, 57-63.
7. Payne, A. R., *Journal of Applied Polymer Science*, 1963, 7, 873-885.
8. Rouse, P. E., *The Journal of Chemical Physics*, 1953, 21, 1272-1280.
9. Doi, M. and Edwards, S. F., *The Theory of Polymer Dynamics*, Clarendon Press, Oxford, 1986.
10. Bueche, F., *The Journal of Chemical Physics*, 1952, 20, 1959-1964.
11. Ferry, J. D., *Viscoelastic Properties of Polymers* Wiley, New York :, 2d ed. edn., 1970.
12. de Gennes, P. G., *The Journal of Chemical Physics*, 1971, 55, 572-579.
13. Pethrick, R. A., *Polymer Structure Characterization : From Nano to Macro Organization*, Cambridge, Royal Society of Chemistry, Cambridge, 2007.
14. Sperling, L. H., *Introduction to Physical Polymer Science*, Hoboken, New Jersey : Wiley-Interscience, Hoboken, New Jersey, 4th ed. edn., 2006.
15. Garca-Coln, L. S., del Castillo, L. F. and Goldstein, P., *Physical Review B*, 1989, 40, 7040-7044.
16. Reding, F. P., Faucher, J. A. and Whitman, R. D., *Journal of Polymer Science*, 1962, 57, 483-498.
17. Frick, B., Alba-Simionesco, C., Hendricks, J. and Willner, L., *Progress of Theoretical Physics Supplement*, 1997, 126, 213-218.
18. Zorn, R., Arbe, A., Colmenero, J., Frick, B., Richter, D. and Buchenau, U., *Physical Review E*, 1995, 52, 781-795.
19. Frick, B. and Richter, D., *Science*, 1995, 267, 1939.
20. Einstein, A., *Annalen der Physik*, 1911, 339, 591-592.
21. Mooney, M., *Journal of Colloid Science*, 1951, 6, 162-170.
22. Krieger, I. M. and Dougherty, T. J., *Transactions of the Society of Rheology*, 1959, 3, 137-152.
23. Krieger, I. M., *Advances in Colloid and Interface Science*, 1972, 3, 111-136.
24. Pabst, W., Gregorová, E. and Berthold, C., *Journal of the European Ceramic Society*, 2006, 26, 149-160.
25. Lin, M. Y., Lindsay, H. M., Weitz, D. A., Ball, R. C., Klein, R. and Meakin, P., *Nature*, 1989, 339, 360-362.
26. Rintoul, M. D. and Torquato, S., *Journal of Physics A: Mathematical and General*, 1997, 30, L585.
27. Heinrich, G., Klüppel, M. and Vilgis, T. A., *Current Opinion in Solid State and Materials Science*, 2002, 6, 195-203.
28. Wang, Z., Liu, J., Wu, S., Wang, W. and Zhang, L., *Physical Chemistry Chemical Physics*, 2010, 12, 3014-3030.
29. Heinrich, G. and Klüppel, M., *Filled Elastomers Drug Delivery Systems*, Springer Berlin Heidelberg, 2002, vol. 160, ch. 1, pp. 1-44.
30. Cassagnau, P., *Polymer*, 2003, 44, 2455-2462.
31. Karasek, L., Meissner, B., Asai, S. and Sumita, M., *Polym J*, 1996, 28, 121-126.
32. Akcora, P., Kumar, S. K., Moll, J., Lewis, S., Schadler, L. S., Li, Y., Benicewicz, B. C., Sandy, A., Narayanan, S., Ilavsky, J., Thiyagarajan, P., Colby, R. H. and Douglas, J. F., *Macromolecules*, 2009, 43, 1003-1010.

33. Maillard, D., Kumar, S. K., Fragneaud, B., Kysar, J. W., Rungta, A., Benicewicz, B. C., Deng, H., Brinson, L. C. and Douglas, J. F., *Nano Letters*, 2012, 12, 3909-3914.
34. Kraus, G., *Applied Polymer Symposia*, 1984, 75-92.
35. Vilgis, T. A., Heinrich, G. and Kluppel, M., *Reinforcement of Polymer Nano-Composites: Theory, Experiments, and Applications*, Cambridge University Press, Cambridge, 2009, ch. 10.
36. Buscall, R., Mills, P. D. A., Goodwin, J. W. and Lawson, D. W., *Journal of the Chemical Society, Faraday Transactions 1: Physical Chemistry in Condensed Phases*, 1988, 84, 4249-4260.
37. Klüppel, M., Schuster, R. H. and Heinrich, G., *Rubber Chemistry and Technology*, 1997, 70, 243-255.
38. van de Walle, A., Tricot, C. and Gerspacher, M., *Kautsch. Gummi Kunstst.*, 1996, 49, 172-179.
39. Lin, C. R. and Lee, Y. D., *Macromol. Theory Simul.*, 1996, 5, 1075-1104.
40. Baeza, G. P., Genix, A.-C., Degrandcourt, C., Petitjean, L., Gummel, J., Couty, M. and Oberdisse, J., *Macromolecules*, 2012, 46, 317-329.
41. Oberdisse, J., El Harrak, A., Carrot, G., Jestin, J. and Boué, F., *Polymer*, 2005, 46, 6695-6705.
42. Dorigato, A., Dzenis, Y. and Pegoretti, A., *Mechanics of Materials*, 2013, 61, 79-90.
43. Oberdisse, J., *Soft Matter*, 2006, 2, 29-36.
44. Jouault, N., Vallat, P., Dalmas, F., Said, S. r., Jestin, J. and Boué, F. o., *Macromolecules*, 2009, 42, 2031-2040.
45. Yatsuyanagi, F., Kaidou, H. and Ito, M., *Rubber Chemistry and Technology*, 1999, 72, 657-672.
46. Sternstein, S. S. and Zhu, A.-J., *Macromolecules*, 2002, 35, 7262-7273.
47. Forrest, J. A., Dalnoki-Veress, K. and Dutcher, J. R., *Physical Review E*, 1997, 56, 5705-5716.
48. Forrest, J. A. and Mattsson, J., *Physical Review E*, 2000, 61, R53-R56.
49. Kawana, S. and Jones, R. A. L., *Physical Review E*, 2001, 63, 021501.
50. Li, X. and McKenna, G. B., *Macromolecules*, 2015, 48, 6329-6336.
51. Grohens, Y., Brogly, M., Labbe, C., David, M.-O. and Schultz, J., *Langmuir*, 1998, 14, 2929-2932.
52. Wallace, W. E., van Zanten, J. H. and Wu, W. L., *Physical Review E*, 1995, 52, R3329-R3332.
53. Fryer, D. S., Peters, R. D., Kim, E. J., Tomaszewski, J. E., de Pablo, J. J., Nealey, P. F., White, C. C. and Wu, W.-l., *Macromolecules*, 2001, 34, 5627-5634.
54. Berriot, J., Montes, H., Lequeux, F., Long, D. and Sotta, P., *Macromolecules*, 2002, 35, 9756-9762.
55. Robertson, C. G., Bogoslovov, R. and Roland, C. M., *Physical Review E*, 2007, 75, 051403.
56. Montes, H., Lequeux, F. and Berriot, J., *Macromolecules*, 2003, 36, 8107-8118.
57. Kim, D., Srivastava, S., Narayanan, S. and Archer, L. A., *Soft Matter*, 2012, 8, 10813-10818.
58. Carretero-Gonzalez, J., Retsos, H., Giannelis, E. P., Ezquerra, T. A., Hernandez, M. and Lopez-Manchado, M. A., *Soft Matter*, 2009, 5, 3481-3486.
59. Berriot, J., Lequeux, F., Monnerie, L., Montes, H., Long, D. and Sotta, P., *Journal of Non-Crystalline Solids*, 2002, 307–310, 719-724.
60. Leu, G., Liu, Y., Werstler, D. D. and Cory, D. G., *Macromolecules*, 2004, 37, 6883-6891.
61. Holt, A. P., Griffin, P. J., Bocharova, V., Agapov, A. L., Imel, A. E., Dadmun, M. D., Sangoro, J. R. and Sokolov, A. P., *Macromolecules*, 2014, 47, 1837-1843.
62. Vo, L. T., Anastasiadis, S. H. and Giannelis, E. P., *Macromolecules*, 2011, 44, 6162-6171.
63. Vladkov, M. and Barrat, J.-L., *Macromolecules*, 2007, 40, 3797-3804.
64. Bogoslovov, R. B., Roland, C. M., Ellis, A. R., Randall, A. M. and Robertson, C. G., *Macromolecules*, 2008, 41, 1289-1296.
65. Robertson, C. G., Lin, C. J., Rackaitis, M. and Roland, C. M., *Macromolecules*, 2008, 41, 2727-2731.
66. Zhu, Z., Thompson, T., Wang, S.-Q., von Meerwall, E. D. and Halasa, A., *Macromolecules*, 2005, 38, 8816-8824.
67. Moll, J. F., Akcora, P., Rungta, A., Gong, S., Colby, R. H., Benicewicz, B. C. and Kumar, S. K., *Macromolecules*, 2011, 44, 7473-7477.
68. Roh, J. H., Tyagi, M., Hogan, T. E. and Roland, C. M., *Macromolecules*, 2013, 46, 6667-6669.
69. Roh, J. H., Tyagi, M., Hogan, T. E. and Roland, C. M., *The Journal of Chemical Physics*, 2013, 139, 134905.

70. Akcora, P., Kumar, S. K., García Sakai, V., Li, Y., Benicewicz, B. C. and Schadler, L. S., *Macromolecules*, 2010, 43, 8275-8281.
71. Glomann, T., Schneider, G. J., Allgaier, J., Radulescu, A., Lohstroh, W., Farago, B. and Richter, D., *Physical Review Letters*, 2013, 110, 178001.
72. Sodhani, D. and Reese, S., *Macromolecules*, 2014, 47, 3161-3169.
73. Papon, A., Merabia, S., Guy, L., Lequeux, F., Montes, H., Sotta, P. and Long, D. R., *Macromolecules*, 2012, 45, 2891-2904.
74. Mujtaba, A., Keller, M., Ilisch, S., Radusch, H. J., Beiner, M., Thurn-Albrecht, T. and Saalwächter, K., *ACS Macro Letters*, 2014, 3, 481-485.
75. Mujtaba, A., Keller, M., Ilisch, S., Radusch, H. J., Thurn-Albrecht, T., Saalwächter, K. and Beiner, M., *Macromolecules*, 2012, 45, 6504-6515.
76. Yang, J. and Han, C.-R., *The Journal of Physical Chemistry C*, 2013, 117, 20236-20243.
77. Stöckelhuber, K. W., Svistkov, A. S., Pelevin, A. G. and Heinrich, G., *Macromolecules*, 2011, 44, 4366-4381.
78. Litvinov, V. M., Orza, R. A., Klüppel, M., van Duin, M. and Magusin, P. C. M. M., *Macromolecules*, 2011, 44, 4887-4900.
79. Mortazavian, H., Fennell, C. J. and Blum, F. D., *Macromolecules*, 2016, 49, 298-307.
80. Jouault, N., Moll, J. F., Meng, D., Windsor, K., Ramcharan, S., Kearney, C. and Kumar, S. K., *ACS Macro Letters*, 2013, 2, 371-374.
81. Robertson, C. G. and Rackaitis, M., *Macromolecules*, 2011, 44, 1177-1181.
82. Pérez-Aparicio, R., Schiewek, M., Valentín, J. L., Schneider, H., Long, D. R., Saphiannikova, M., Sotta, P., Saalwächter, K. and Ott, M., *Macromolecules*, 2013, 46, 5549-5560.
83. Gavrilov, A. A., Chertovich, A. V., Khalatur, P. G. and Khokhlov, A. R., *Macromolecules*, 2014, 47, 5400-5408.
84. *Rubber Technology*, Van Nostrand Reinhold, 3rd edn., 1987.
85. Kimani, S. M., Hardman, S. J., Hutchings, L. R., Clarke, N. and Thompson, R. L., *Soft Matter*, 2012, 8, 3487-3496.
86. Schach, R., personal communication.
87. Pecora, R., *Dynamic Light Scattering : Applications of Photon Correlation Spectroscopy*, New York : Plenum, New York, 1985.
88. Provencher, S. W., *Computer Physics Communications*, 1982, 27, 229-242.
89. Ju, R. T. C., Frank, C. W. and Gast, A. P., *Langmuir*, 1992, 8, 2165-2171.
90. Stöber, W., Fink, A. and Bohn, E., *Journal of Colloid and Interface Science*, 1968, 26, 62-69.
91. Lindberg, R., Sjöblom, J. and Sundholm, G., *Colloids and Surfaces A: Physicochemical and Engineering Aspects*, 1995, 99, 79-88.
92. Stöckelhuber, K. W., Das, A., Jurk, R. and Heinrich, G., *Polymer*, 2010, 51, 1954-1963.
93. Sears, V. F., *Neutron News*, 1992, 3, 26-37.
94. *Mantid*, Mantid Project, 2013, DOI: 10.5286.
95. *Sasview*, 3.1.2 edn., 2015.
96. Plomp, J., PhD, Delft University of Technology, 2009.
97. Khintchine, A., *Mathematische Annalen*, 1934, 109, 604-615.
98. McLeish, T. C. B., *Macromolecules*, 1988, 21, 1062-1070.
99. Flory, P. J. and Rehner, J., *The Journal of Chemical Physics*, 1943, 11, 521-526.
100. Alger, M., *Polymer Science Dictonary*, Chapman & Hall, London, 1997.
101. Coran, A. Y., *Rubber Chemistry and Technology*, 1964, 37, 689-697.
102. Ding, R. and Leonov, A. I., *Journal of Applied Polymer Science*, 1996, 61, 455-463.
103. Zhao, D., Ge, S. F., Senses, E., Akcora, P., Jestin, J. and Kumar, S. K., *Macromolecules*, 2015, 48, 5433-5438.
104. Brenner, H., *Annu. Rev. Fluid Mech.*, 1970, 2, 137-&.
105. Piau, J.-M., Dorget, M., Palierne, J.-F. and Pouchelon, A., *Journal of Rheology*, 1999, 43, 305-314.
106. Kendall, J. and Monroe, K. P., *Journal of the American Chemical Society*, 1917, 39, 1802-1806.
107. Song, Y. and Zheng, Q., *Progress in Materials Science*, 2016, 84, 1-58.
108. Pavlov, A. S. and Khalatur, P. G., *Soft Matter*, 2016, 12, 5402-5419.

109. Williams, M. L., Landel, R. F. and Ferry, J. D., *Journal of the American Chemical Society*, 1955, 77, 3701-3707.
110. Ramirez, J. and Likhtman, A., Reptate http://reptate.com/.
111. Solomon, M. J., Almusallam, A. S., Seefeldt, K. F., Somwangthanaroj, A. and Varadan, P., *Macromolecules*, 2001, 34, 1864-1872.
112. Knauert, S. T., Douglas, J. F. and Starr, F. W., *Journal of Polymer Science Part B: Polymer Physics*, 2007, 45, 1882-1897.
113. Edwards, D. C., *Journal of Materials Science*, 1990, 25, 4175-4185.
114. Bates, F. S., Wignall, G. D. and Dierker, S. B., *Macromolecules*, 1986, 19, 1938-1945.
115. Teixeira, J., *Journal of Applied Crystallography*, 1988, 21, 781-785.
116. Lin, M. Y., Lindsay, H. M., Weitz, D. A., Ball, R. C., Klein, R. and Meakin, P., *Physical Review A*, 1990, 41, 2005-2020.
117. Aharoni, S. M., *Macromolecules*, 1983, 16, 1722-1728.
118. Aubouy, M., Fredrickson, G. H., Pincus, P. and Raphaeel, E., *Macromolecules*, 1995, 28, 2979-2981.
119. Merabia, S., Sotta, P. and Long, D. R., *Macromolecules*, 2008, 41, 8252-8266.
120. Paradossi, G., Cavalieri, F., Chiessi, E. and Telling, M. T. F., *The Journal of Physical Chemistry B*, 2003, 107, 8363-8371.
121. Chiessi, E., Cavalieri, F. and Paradossi, G., *The Journal of Physical Chemistry B*, 2007, 111, 2820-2827.
122. Arbe, A., Colmenero, J., Monkenbusch, M. and Richter, D., *Physical Review Letters*, 1998, 81, 590-593.
123. Gibbs, J. H. and DiMarzio, E. A., *The Journal of Chemical Physics*, 1958, 28, 373-383.
124. McKenna, G. B., *Nat Phys*, 2008, 4, 673-673.
125. Doxastakis, M., Kitsiou, M., Fytas, G., Theodorou, D. N., Hadjichristidis, N., Meier, G. and Frick, B., *The Journal of Chemical Physics*, 2000, 112, 8687-8694.
126. Ahumada, O., Theodorou, D. N., Triolo, A., Arrighi, V., Karatasos, C. and Ryckaert, J.-P., *Macromolecules*, 2002, 35, 7110-7124.
127. Colmenero, J., Arbe, A. A., Alegría, A. and Ngai, K. L., *Journal of Non-Crystalline Solids*, 1994, 172, 229-233.
128. Wang, L., Zhao, S., Li, A. and Zhang, X., *Polymer*, 2010, 51, 2084-2090.
129. Xia, W. J., Song, J. K., Hsu, D. D. and Keten, S., *Macromolecules*, 2016, 49, 3810-3817.
130. Ye, C. H., Wiener, C. G., Tyagi, M., Uhrig, D., Orski, S. V., Soles, C. L., Vogt, B. D. and Simmons, D. S., *Macromolecules*, 2015, 48, 801-808.
131. Montes, H., Chaussée, T., Papon, A., Lequeux, F. and Guy, L., *The European Physical Journal E*, 2010, 31, 263-268.